June 1988

HYDROGEOLOGY OF FORMATIONS USED FOR DEEP-WELL INJECTION, TEXAS GULF COAST

by

Charles W. Kreitler
M. Saleem Akhter
Andrew C. A. Donnelly
Warren T. Wood

Prepared for the
U.S. Environmental Protection Agency under
Cooperative Agreement ID No. CR812786-01-0

Bureau of Economic Geology
W. L. Fisher, Director
The University of Texas at Austin
Austin, Texas 78713

CONTENTS

ILLUSTRATIONS

Figures

Tables

1. ABSTRACT

This research program was conducted to investigate fluid migration potential and fluid direction and velocities in the regional hydrologic environment of the Texas Gulf Coast Tertiary formations in the context of deep-well injection of hazardous chemical wastes. The study has focused on the Frio Formation because it is the target of massive waste injection and because a large data base exists on formation pressures and water chemistry in the Frio.

Pressure data gathered from drill-stem tests and bottomhole pressure measurements in onshore oil and gas wells were used in evaluating pressure regimes. Pressure-depth profiles and potentiometric surfaces constructed from the pressure data reflect existence of three hydrologic regimes: a shallow fresh to moderately saline water section in the upper 3,000-4,000 ft, an underlying 4,000- to 5,000-ft-thick, essentially saline hydrostatic section, and a deeper overpressured section with moderate to high salinities. The complexity of the hydrologic environment is enhanced by extensive depressurization in the 4,000- to 8,000-ft depth interval. This presumably results from the estimated production of more than 10 billion barrels of oil equivalent and associated brines from this interval alone in the past 50 years. A composite potentiometric surface of the entire Frio to determine "natural" flow gradients or "natural" points of discharge cannot be constructed.

Potentiometric surfaces representing discrete depth intervals were mapped. These values and the flow gradients determined from potentiometric surfaces and published permeability and porosity data were used to compute linear fluid flow velocities ranging from 0.01 ft/year to 105 ft/year in the lateral direction.

Potential for vertical fluid migration was investigated with equivalent environmental hydraulic head maps. The presence of widespread pockets of depressured formations significantly affects the direction and value of fluid gradients, inasmuch as these depressured oil and gas fields may become potential sinks for the injected chemical wastes.

Published water chemistry data were supplemented by field sampling of waters from 32 oil fields. Active recharge of Frio by continental waters does not appear to be occurring. All waters sampled appear to be in isotopic equilibrium with the rock

matrix. In the northern section salt dome dissolution is the primary reaction controlling water chemistry in this region. Brines from the deeper geopressured section may be leaking into the hydrostatic section of the central and southern Gulf Coast Frio.

The lack of organic acids and the alteration of Frio oils from samples shallower than approximately 7,000 ft suggest biodegradation. This has a useful implication for degradation of injected chemical wastes.

A detailed analysis of the localized hydrodynamics in Victoria County, Texas, as a case study shows the applicability of the developed techniques to injection facility siting and monitoring process, where depressurization was observed on a local, county-size scale.

2. INTRODUCTION

Within the past 30 years, subsurface disposal of liquid industrial wastes generated by chemical and manufacturing industries into deep formations has become an acceptable and increasingly conventional technology. More than twenty states in the continental United States now allow this form of industrial waste disposal. In Texas, deep-well injection is the major method of chemical waste disposal, with projected volumes of 2.2 billion gallons (9.1 billion kilograms) in 1988 (Carpenter, 1987). Since this is a geological method of disposal, it is regulated by federal and state agencies and laws similar to the ones governing the oil and gas and other extractive industries. These laws have evolved in response to environmental concerns, to prevent contamination of ground-water resources from unsafe underground injection practices. The U.S. Congress passed the Safe Drinking Water Act, Public Law 93-523, in 1974, to ensure protection of underground sources of drinking water by subsurface injection of industrial wastes. The Environmental Protection Agency (EPA) has been mandated through this law to develop regulations for underground injection control.

The proposed rule-changes for the U.S. Environmental Protection Agency's Underground Injection Control Program (Federal Register, August 27, 1987) require a Class I injection well operator to show through a permit application that either the injected hazardous wastes will degrade to nontoxic materials or these wastes will not migrate to a point of discharge in 10,000 years. This report provides an approach in which Class I injection well operators can characterize the original injection zone hydrology that surrounds an injection well being considered for a permit. Using this methodology and with greater integration of regional geologic information such as depositional facies and fault distributions, it is possible to build a hydrodynamic model to describe the injection fluid pathways and velocities and its hydrologic interaction with formation fluids.

2.1 Scope of Work

The objective of the overall study is to evaluate regional trends in pressure regimes and the potential, direction, and velocity of fluid migration in the Texas Gulf Coast Tertiary formations. To complement this hydrologic investigation, we also studied the chemical composition of the brines. The preliminary activity plan for this study outlined the following topics for investigation:

A. Basin Hydrology: Map potentiometric surfaces of major injection zones in Texas Gulf Coast to assess horizontal directions and velocities of saline ground-water flow.

1. Injection zones to be studied with data availability- Frio/Catahoula, Wilcox, Undifferentiated Miocene, Oakville, Yegua.
2. Data sources- Petroleum Information Corp. (PI Corp.) data files, Railroad Commission of Texas files, available oil company files.
3. Evaluate data quality prior to mapping.
4. Mapping methods to be considered => fresh-water head equivalent, salt-water heads, pressure surfaces, bond surfaces, kriging.
5. Map cross sections of hydraulic potential to assess vertical flow potential.
6. Assess available permeability and porosity data from injection zones for integration into velocity calculations.

B. Basin Geology: Evaluate available geologic information.

1. Collect relevant geologic maps of Texas Gulf Coast onshore Tertiary formations.
2. Develop base maps for fresh-water, saline hydrostatic, and geopressured sections.

C. Integrate Geologic and Hydrologic Data: Synthesis of geologic and hydrologic information for regional characterization.

1. Investigate influence of facies change, existence of faults and salt domes.
2. Regional generic and site-specific modeling of ground-water flow.

D. Basin Geochemistry: Enhance our understanding of the hydrochemical environment of Gulf Coast brine aquifers used for deep-well injection.

1. Review available water-chemistry data to describe regional trends.
2. Obtain and analyze water samples from selected oil fields.
3. Integrate hydrochemical and hydrologic interpretation of regional and local features.

This report focuses on the Frio Formation, which has a large data base and which is the target of most of the hazardous chemical waste disposed of by deep-well injection. It summarizes the methodology and results and includes a discussion of a hydrologic study based on the analysis of formation-pressure data. As a sample case, an in-depth evaluation of hydrologic investigations in Victoria County, Texas, is presented here. Victoria County was chosen because of its large pressure data base and because of the presence of a large injection facility for which pressure data were available in the literature.

Results of the hydrologic investigation are presented in the form of pressure-depth profiles reflecting the pressure regimes in the Frio Formation and as potentiometric and residual surfaces defining regional trends and migration potential for formation fluids. Potentiometric surfaces were based on either fresh-water or salt-water head equivalent corresponding to the prevalent brine densities in the formation. These potentiometric surfaces were further utilized to evaluate flow patterns, to estimate flow velocities, and to compile a generic hydrodynamic model of the Gulf Coast aquifer system. Integration of faults and salt domes in the model and analysis of transient pressure data for delineation of oil field depressurization has been deferred pending additional data acquisition. Detailed discussion of the chemical composition of formation brines is contained in Sections 1 through 10 of this report.

2.2 Previous Work on Geohydrologic Description of the Gulf Coast

The regional hydrologic and geochemical environment of the saline sections of the Gulf Coast sedimentary basin controls the transport and ultimate fate of the injected liquid wastes. In Texas, the Gulf of Mexico basin is a relatively young (Tertiary-age) compacting basin. In the deeper brine sections, fluid movement is driven by shale compaction and is up the stratigraphic dip or up fault zones. The basin is still being filled with fine-grained clastic sediments (mud) and has undergone extensive growth faulting that may have restricted lateral fluid movement but could provide likely pathways for upward migration of waters (Kreitler, 1986). An earlier report by Kreitler and Richter (1986) reviewed previously published data on the hydrochemistry of Gulf Coast formation brines.

3. THE TEXAS GULF COAST HYDROGEOLOGIC ENVIRONMENT

The unconsolidated Tertiary sandstones designated for chemical waste disposal are part of a larger Gulf of Mexico sedimentary basin, deposited continuously for nearly 70 million years. The Frio Formation of Oligocene-Miocene age is one of the major progradational wedges of the Texas Gulf Coastal Plain and contains prolific hydrocarbon-producing plays. This wedge, which consists of interfingering marine and nonmarine sands and shales, extends in a band that is as much as 50 mi wide and in places more than 12,000 ft thick along the Texas Gulf Coast (Galloway and others, 1982).

Ground waters in the Coastal Plain aquifers are considered to have two origins: meteoric waters, introduced into shallow aquifers by precipitation, and formation

waters, from original depositional environments (Kreitler, 1979). These two types of waters coexist in the basin in the following three hydrologic regimes:

(1) The uppermost permeable strata are continuously recharged by meteoric waters, forming a fresh to moderately saline water regime, where flow is directed toward the Gulf of Mexico. This regime may extend to a depth of 3,000 to 4,000 ft below land surface.

(2) A brine hydrostatic section lies beneath the fresh to moderately saline section. Waters within this essentially saline section are assumed to be original formation waters or at least several million years old, or they may be meteoric in origin (Kreitler and Richter, 1986). Hydraulic connection between the hydrostatic and the overlying meteoric sections prevents excessive pressure buildup within the hydrostatic zone.

(3) Deeper, the underlying strata represent the overpressured or geopressured zone where abnormally high fluid pressures exist due to restricted drainage conditions. Figure 1 schematically delineates these three hydrologic regimes and identifies the possible migratory pathways for deep waters.

Various researchers have found evidence of deep penetration of fresh meteoric waters into the saline sections of the Gulf Coast Basin (Bachman, 1979; Carothers and Kharaka, 1978; Lundegard, 1985). Deep basinal ground water from the geopressured zone is presumed to be leaking upward into shallower aquifer systems (Jones, 1968; Fisher, 1982). Downward flow of fresh meteoric water, upward movement of deep basinal brines, and the possible presence of original depositional waters suggest existence of a hydrologically dynamic system. However, flow rates within this environment need to be considered in the context of geologic time--that is, millions of years. The existence of complex fault systems and literally hundreds of thousands of oil- and gas-related holes adds a new dimension to the consideration of potential pathways for the movement of the various types of waters. Within this context, the injection and long-time confinement of toxic chemical wastes present an interesting topic of study.

The Texas Gulf Coast sedimentary basin can be classified into three hydrologic units: a shallow fresh to moderately saline hydropressured section, a brine hydrostatic section, and a deep overpressured section. The following paragraphs briefly describe the hydrology of each of these units.

3.1 Shallow Fresh to Moderately Saline Section

This near-surface to 4,000-ft-deep section is characterized by water of less than 10,000 parts per million total dissolved solids, with fluid pressure gradient of

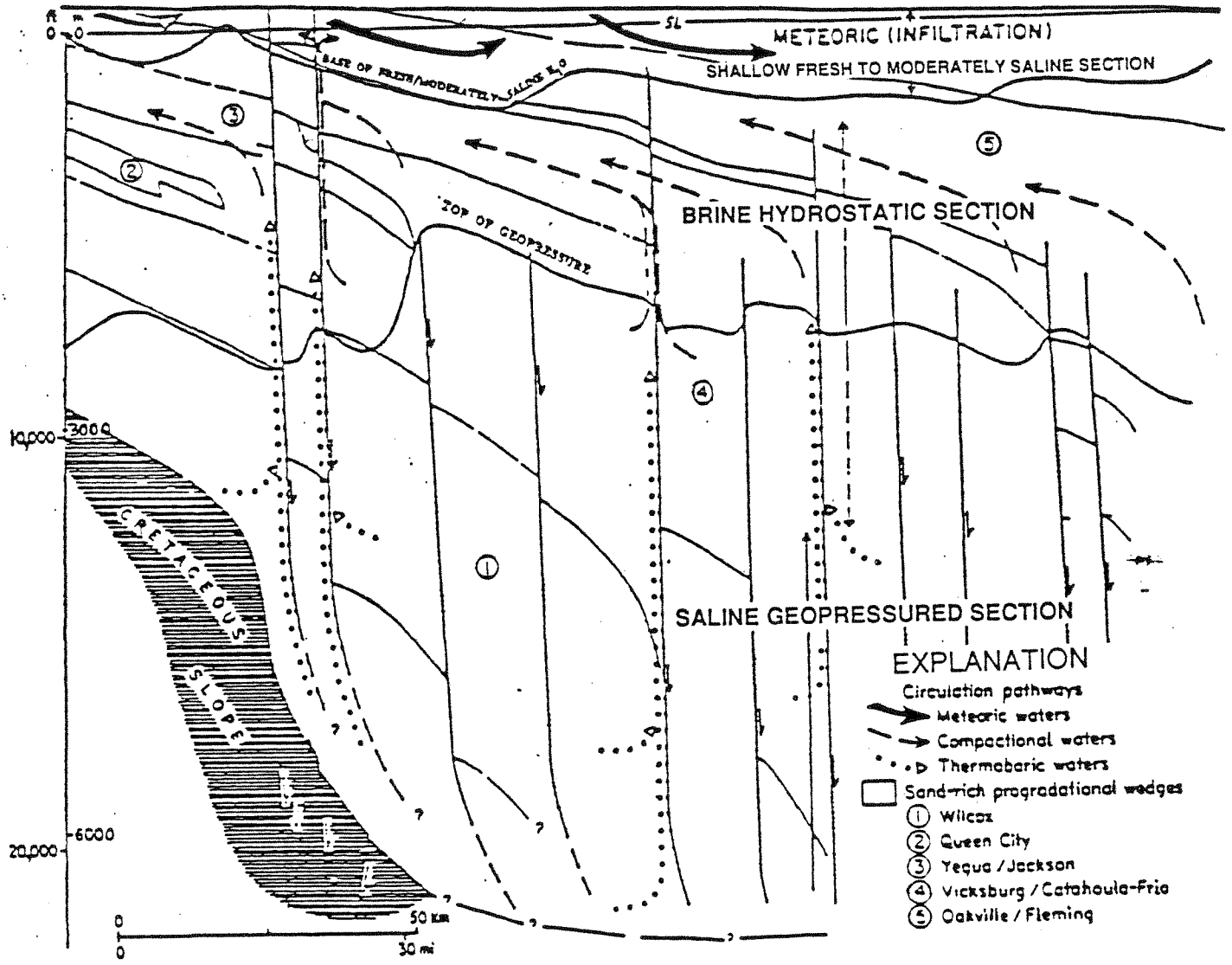

Figure 1. Ground-water regimes and circulation pathways within the Tertiary basin fill of the northwestern Gulf Coast Basin (modified from Galloway, 1982).

0.433 psi/ft. Within this regime, surface waters penetrate permeable strata and ground-water flow is directed toward the Gulf of Mexico (Kreitler and Richter, 1986). Figure 2 (Kreitler and Richter, 1986) outlines the base of the fresh to moderately saline section in the Texas Gulf Coast. The hydraulic heads in this section rise to near land surface and vertical hydraulic gradients are +0.01 or less.

3.2 Brine Hydrostatic Section

From about 4,000 to 10,000 ft deep, this essentially brine hydrostatic section underlies the fresh to moderately saline section. Hydraulic communication between the two sections prevents buildup of excessive pressures within the brine hydrostatic section. The upper part of this section is a transition zone characterized by mixing of meteoric water with in situ formation water. Salinities vary laterally and vertically, ranging from 10,000 ppm to 50,000 ppm TDS. In the lower parts of the brine hydrostatic section, waters are assumed to be original formation waters and several million years old, and salinity values range from 80,000 to 150,000 ppm TDS. The hydrology of this section is very complex due to the presence of divergent pressure regimes. Numerous hydrocarbon plays found in this section have been extensively developed and exhibit a large degree of depressurization. At the same time, a transition zone of weakly overpressured sediments is interspersed within and underlies this section.

3.3 Geopressured Section

At 7,000 to 10,000-14,000 ft in depth, the overpressured zone extends from onshore beyond the coast into the continental shelf. Previous researchers (such as Galloway and Hobday, 1983) reported top of the overpressured sediments between 9,500 and 11,000 ft, whereas the current research encounters a transition to overpressured gradients as shallow as 6,000 ft. The overpressured regime is not confined to any single hydrostratigraphic unit, but cuts across most of them. Fisher (1982) described a relationship between formation lithology and the top to this zone. Numerous investigators have also suggested release of ground water from overpressured zone into shallower regional aquifer systems. These hypotheses were based on the study of thermal maturity of hydrocarbons, studies of organic acids in deep-basin brines, and the tracking of isotherms in the deep formations. Traditionally, top of geopressured zone has been delineated using either drilling engineering criteria, that is, from a need to increase mud weight to control oil/gas kicks, or from shale resistivity measurements with electrical logs, or by using an arbitrary 0.7 psi/ft

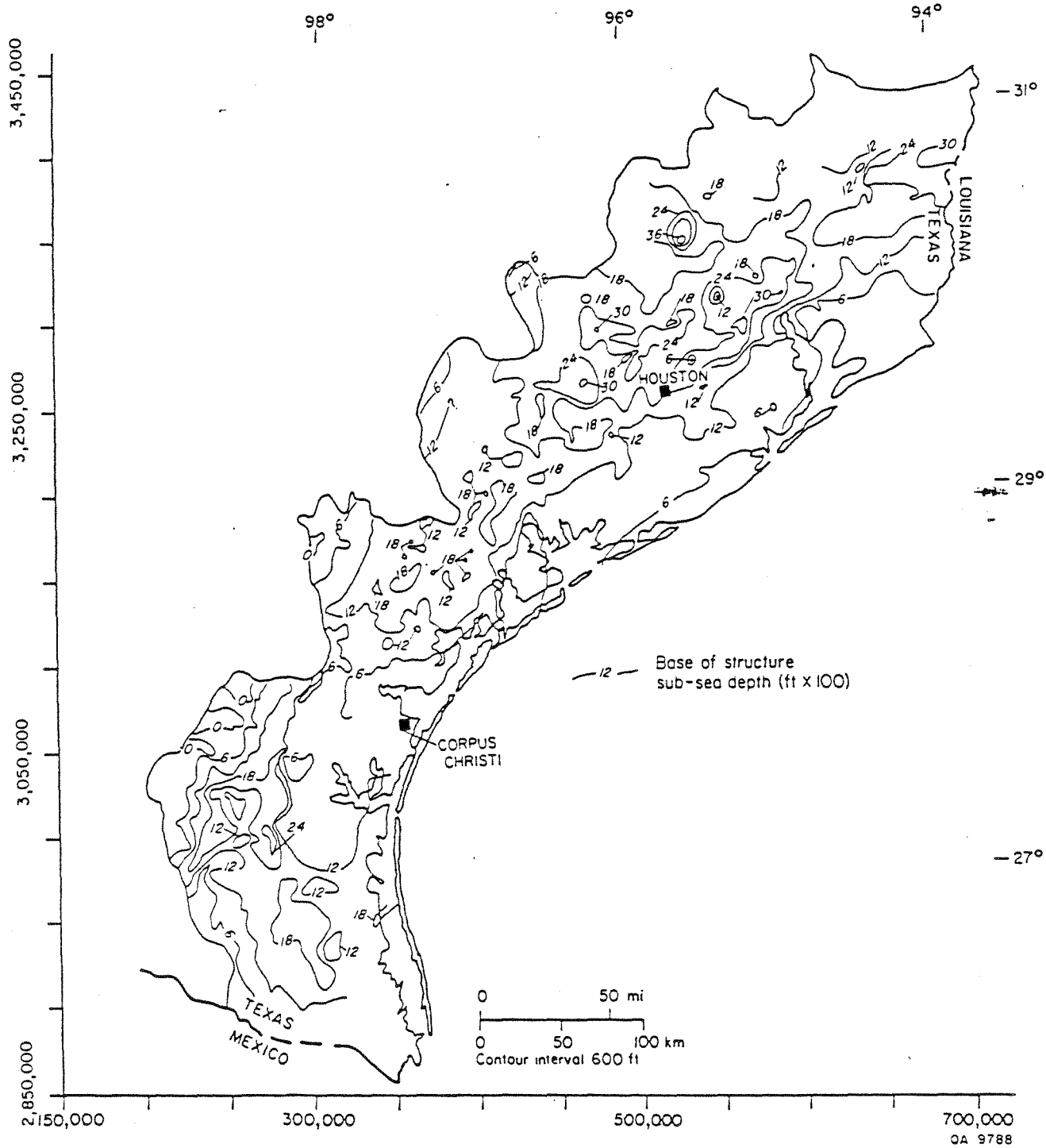

Figure 2. Base of fresh to moderately saline water along the Texas Gulf Coast (after Wood and others, 1963)

pressure gradient. These definitions did not necessarily correlate to the in situ fluid pressures. This report departs from the often used "soft" and "hard" geopressure concept and proposes that very similar processes control the formation of overpressures in both previously defined regions. Thus, for the purpose of differentiating the brine hydrostatic regime from the overpressured regime, a hydrologic criteria of fluid pressures is applied, whereby fluid pressure gradients in excess of 0.465 psi/ft are considered overpressured.

3.4 The Injection Zones

Tertiary saline formations of the Texas Gulf Coast have been used for more than 20 years for deep-well disposal of chemical wastes. The depths of waste disposal range from 2,000 to 8,250 ft below land surface in the Oakville, Catahoula, Yegua, and Frio Formations, the undifferentiated Miocene formations, and the Wilcox Group. Most injection operations are concentrated in the Miocene, Frio, Yegua, and Catahoula aquifers. To date, more than 80 billion gallons (10.7 billion ft^3) of industrial waste have been injected in these zones (Kreitler and Richter, 1986). In Victoria County, large volumes of chemical waste (nearly 16 billion gallons) have been injected since 1953 at the E. I. Du Pont de Nemours facility in selected intervals between 3,800 and 4,900 ft below land surface (Texas Water Commission, 1987). Figure 3 reflects the overall area of investigation covered by this regional study, identifies the location of major concentrations of deep-well injection facilities, and delineates the regions A, B, and C into which the data were separated for convenience in handling the large computer data base.

3.4.1 Structure

The Frio and its updip equivalent, the Catahoula Formation, consist of deposits of two large fluvial and associated deltaic systems, centered in the Houston and Rio Grande Embayments (Galloway and others, 1982). Structural history in the Houston Embayment is dominated by syndepositional deformation of underlying Jurassic salt. Mobilization of thick, undercompacted prodelta and slope muds characterized the tectonic evolution of the deltaic sequence in the Rio Grande Embayment. These two major deltaic depocenters are separated by a vertically stacked, strike-parallel coastal barrier and strandplain system, called the San Marcos Arch. The Houston Embayment of East Texas is characterized by salt diapirism and associated faulting and large salt withdrawal subbasins (Bebout and others, 1978). Across the San Marcos Arch and southward toward the Rio Grande Embayment, underlying salt is thin or absent, and long linear belts of growth faults and deep-seated shale ridges and

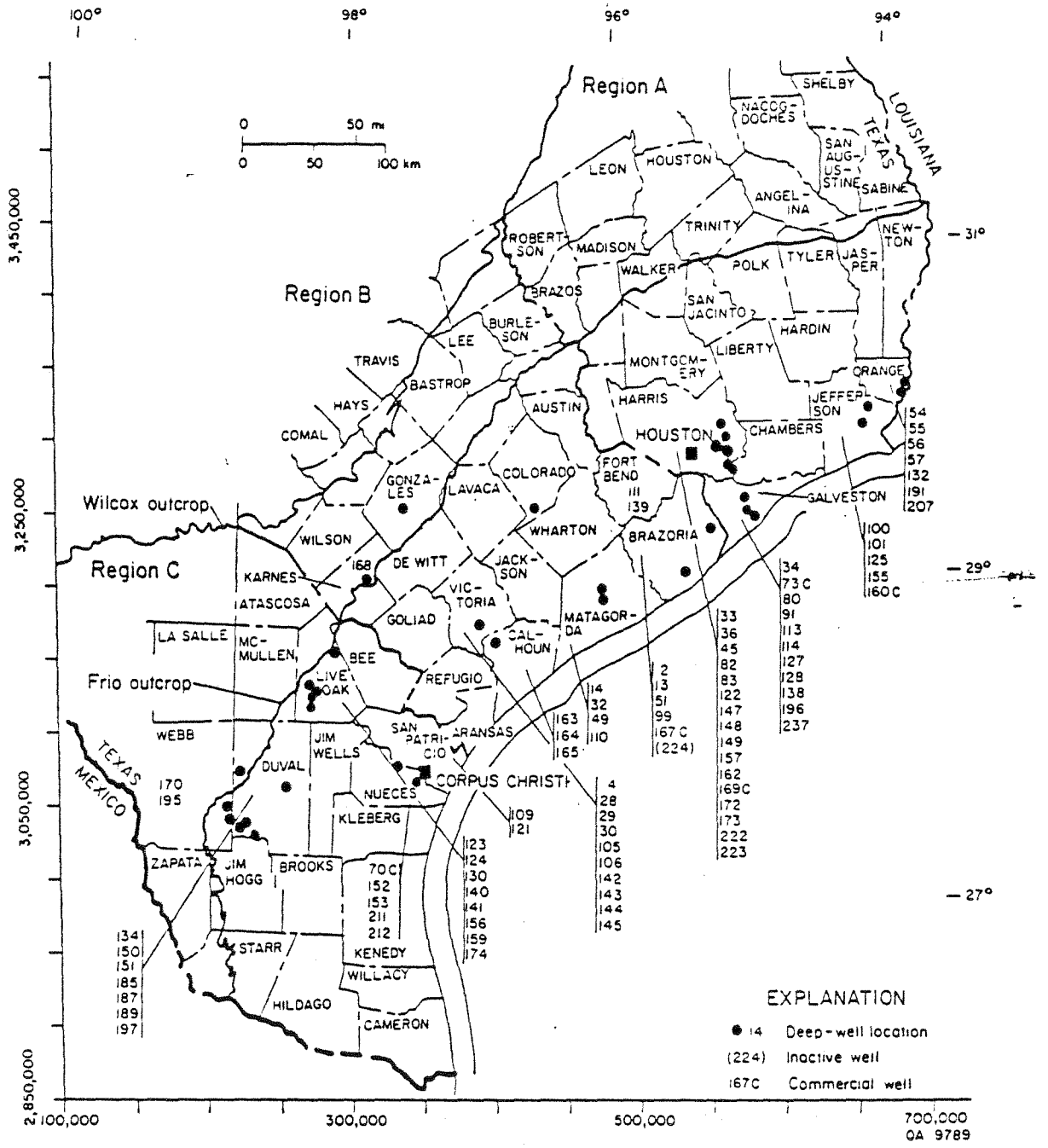

Figure 3. County map with deep-well injection locations, Texas Gulf Coast.

massifs occur. The frequency of faulting gradually decreases in updip portions of the Frio. But in the thick gulfward sections, major faulting and increasingly complex and segmented structure are encountered. The Vicksburg flexure forms the updip limit of significant structural deformation of the Frio. It is a continuous, narrow band of faults characterized by extreme vertical displacement of the underlying section. Figure 4 outlines the major structural elements on a structural map of the Frio. Structure contours for the Miocene and Wilcox are presented in figures 5 and 6.

All Frio depositional systems contain major, geologically defined, hydrocarbon-producing plays (Galloway and others, 1982). Extensive development and production over the past 55 years has yielded nearly 20 billion barrels of oil equivalent and has presumably caused widespread disequilibrium in the hydrodynamic system through depressurization. These depressured zones are encompassed by negative hydraulic contours on the potentiometric surfaces.

3.4.2 Geologic and Hydrologic Description

As a means of consolidating the available geologic information on the Gulf Coast saline formations, earlier published and unpublished maps, including structure, isopach, and net-sand-thickness maps done by various investigators, were acquired. The structure maps were digitized and reproduced using a computerized contouring program. These computer-generated structure maps were used for verifying the formation codes of test wells in the PI data base, as well as for assigning formation codes to test intervals where such information was missing in the data base. Figure 7 is a generalized cross section representing the various stratigraphic units of the Gulf Coast saline formations. A steep thickening of the Frio below the 2,000-ft subsea depth is evident (fig. 7). Stratigraphic and hydrogeologic dip section FF', through the middle section of the Texas Gulf Coast including Victoria County, is represented in figure 8. Major hydrologic units including the Frio and its updip equivalent, the Catahoula Formation, are delineated in figure 8. Exclusion of faulting from the dip section in figure 8 presents a simplistic picture of hydraulic continuity. In reality, the faults may either act as barriers to fluid flow or provide pathways for vertical communication.

3.4.3 Geochemistry

Kreitler and Richter (1986) have provided a detailed description of the chemical composition of Gulf Coast formation fluids. Most of the brines are NaCl type, with salinities varying vertically and laterally, ranging from less than 10,000 mg/L to greater than 250,000 mg/L; most values lie between 30,000 and 80,000 mg/L. Salt

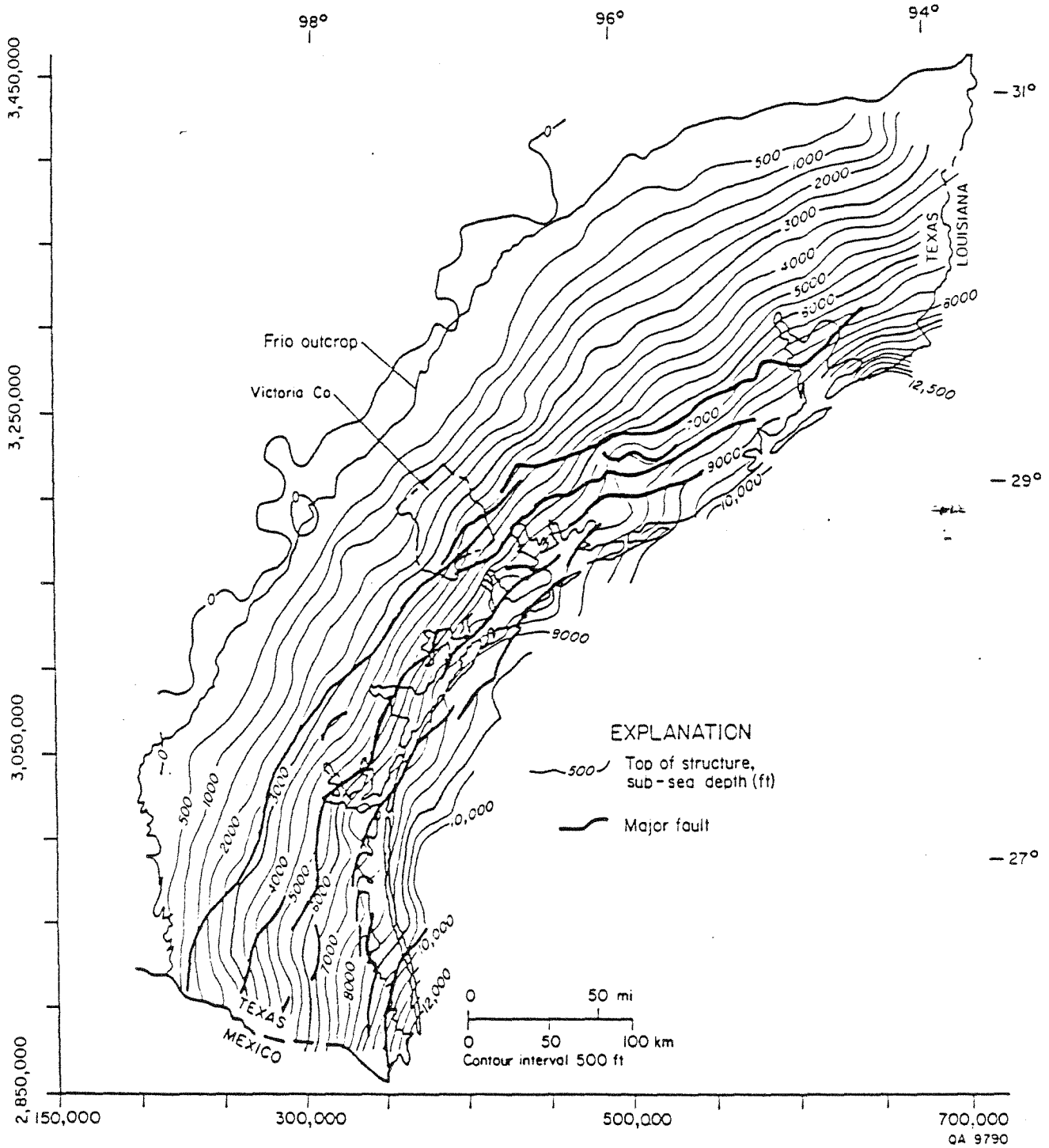

Figure 4. Computer generated structure map of the top of Frio Formation, with major fault features (after Dodge and Posey, 1981; Galloway and others, 1982).

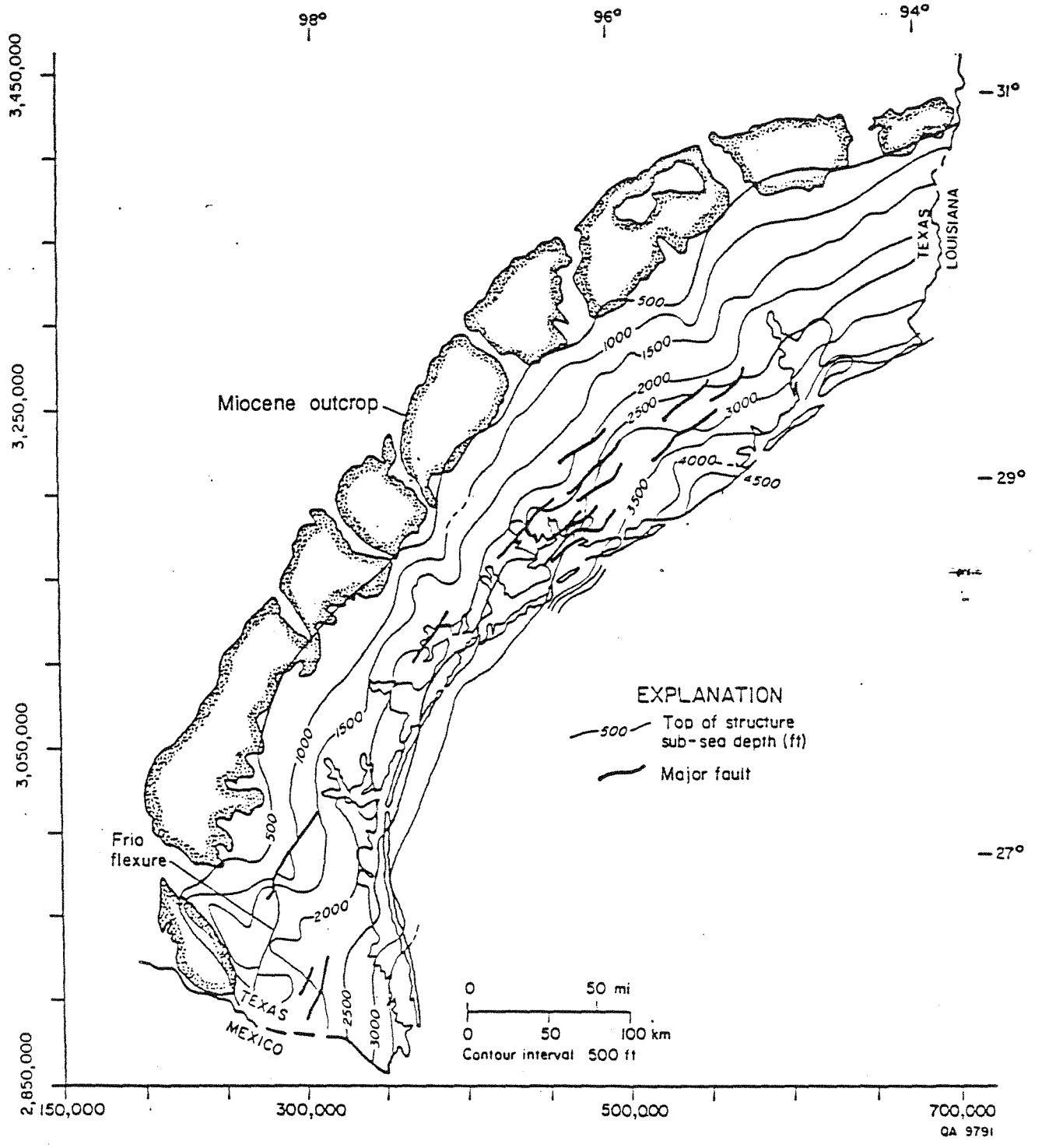

Figure 5. Structure map of the top of Miocene Formation (from DuBar, 1982).

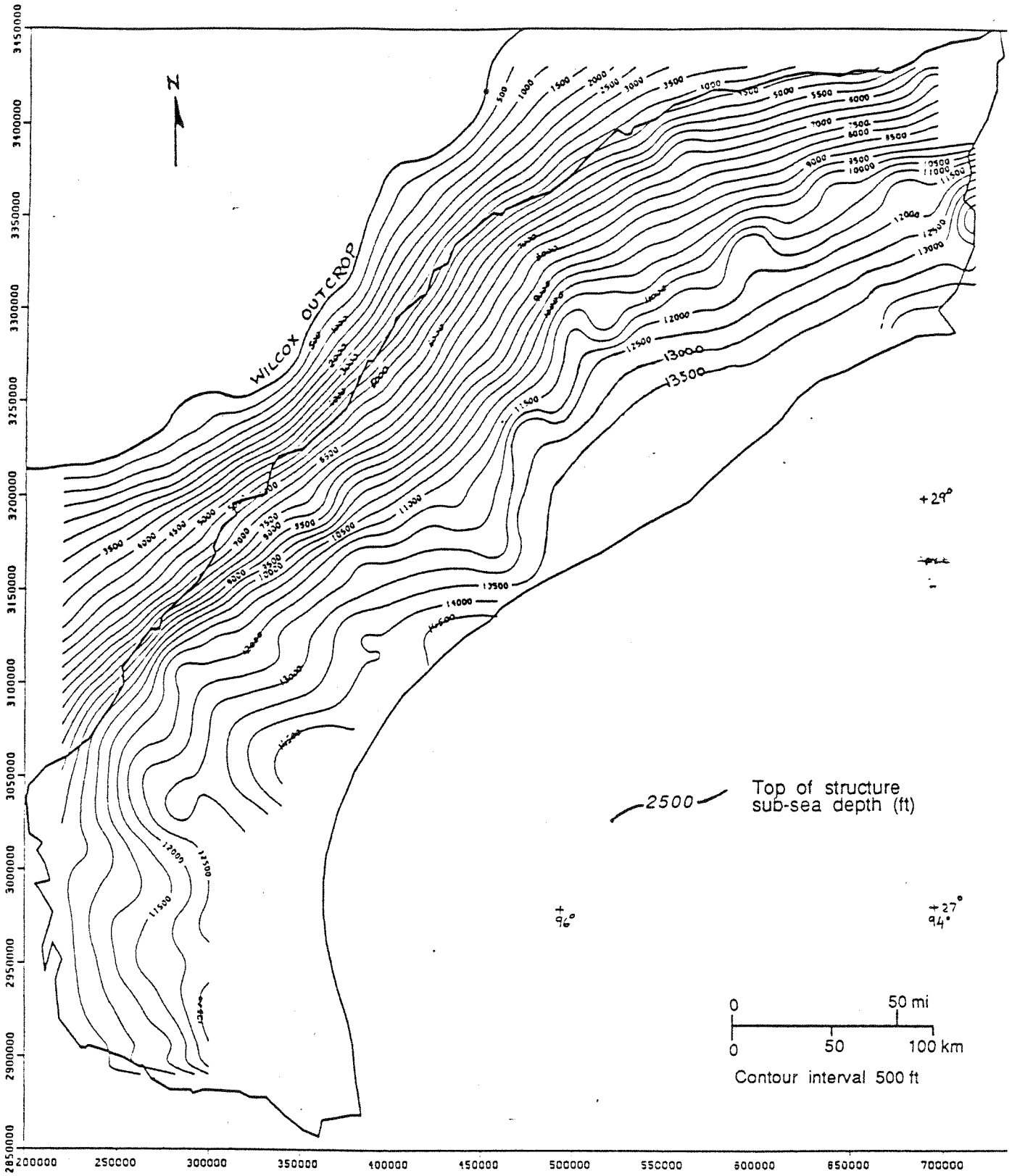

Figure 6. Computer generated structural configuration on top of middle Wilcox Formation (after Dodge and Posey, 1981).

dissolution in northern Gulf Coast causes higher salinities in that region. However, mixing of fresh water and brines may cause some of the low salinities at depths ranging from 4,000 ft to 9,000 ft along the southern Gulf Coast. High alkalinity values are contributed from organic acids as well as by bicarbonates. Estimates of pH range between 4 and 6. Deep-basin brines reflect a preponderance of reducing conditions. Detailed geochemistry of the formation waters is discussed in the second section of this report.

4. PHYSICAL HYDROLOGY

4.1 Data Acquisition and Sources

Pressure data used for the investigation of the pressure regimes and the hydrology in this project were acquired from the Petroleum Information Corporation (PI Corp.), Denver, Colorado, under a cooperative agreement with the U.S. Geological Survey and the Environmental Protection Agency. The data base, obtained on magnetic tapes, consists of drilling, completion, and testing information on nearly 147,000 new and worked-over wells. Originally compiled by PI Corp. from well-data records of the Railroad Commission of Texas and private oil companies, the data base includes bottomhole-pressure information gathered during drill-stem tests, and initial flow-potential tests, and by other bottomhole-pressure-measuring techniques. Hydrologic parameters (porosity and permeability values) were gathered from reports submitted by the injection facility operators to the regulating authorities (the Texas Water Commission and the Railroad Commission of Texas).

4.2 Logistics of Data Processing

Due to the size and complexity of the acquired pressure data, significant time and computing resources were expended in sorting, screening and processing. The following sections describe the data manipulation.

4.2.1 Data Description

The large data base acquired from the Petroleum Information Corporation (PI Corp.), Denver, Colorado, was contained on three magnetic tapes. In-house computer programs developed at the Bureau of Economic Geology (BEG) were utilized for reading the magnetic tapes and for retrieving the relevant information from them. Figure 9 is a flow chart that was used for processing the data base. A major part of the data manipulation was executed on the Dual-Cyber system at The University of Texas, and the subsequent graphics plotting was done on the BEG's VAX 11/780

FLOWCHART FOR PROCESSING OF P.I. DATA TAPES

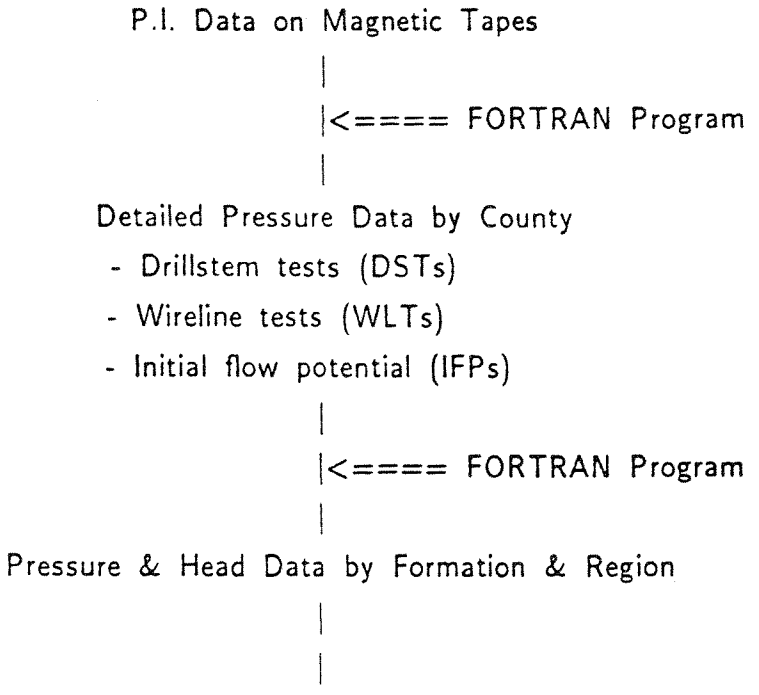

Figure 9. Schematic flow diagram for data processing.

computer. A commercially available contouring package, CPS-1 by Radian Corporation, Austin, was used for plotting the potentiometric surfaces. Although the data base spanned the years 1940 through 1985, scant pressure information was available for the years 1940-44, and wells included after 1984 lacked geographical location coordinates; hence, data from 1945 through 1984 were used for this research. A total of 64,400 pressure values pertaining to some 25,500 wells were retrieved from the PI files. Many wells had multiple pressure values for different test intervals. Thus, a data base of nearly 38,700 pressure values for the Tertiary formations spanning 81 counties along the Texas Gulf Coast was compiled for use in this research. Out of these, about 17,400 pressure values were assigned to the Frio Formation.

4.2.2 Methodology

The formation pressures used to construct the pressure-depth profiles and the potentiometric surfaces are predominantly final shut-in pressures (FSIPs) from DST records and static bottomhole pressures taken with wireline testers during the initial completion or initial production-potential testing of oil and gas wells. A small percentage (<10%) of data are from wells recompleted during a workover. In the case of DSTs where two pressures, the initial and final shut-in pressures (ISIP and FSIP), were available, the higher of the two values was used. The pressures were converted to equivalent fresh-water heads; thus, the potentiometric surface represents the elevation from a datum (sea-level), to which an equivalent fresh-water head would rise in a well completed to the midpoint depth of the DST interval.

Thus,

$$\text{hydraulic head (ft)} = \text{subsea depth (ft)} + \frac{\text{measured fluid pressure (psi)}}{\text{fresh-water pressure gradient (psi/ft)}}$$

The subsea depth is calculated as the difference of the well elevation and the midpoint of the measured test-depth. Initially, a fresh-water pressure gradient of 0.433 psi/ft was used for computing the equivalent hydraulic heads. The use of fresh-water heads is commonly accepted for determining heads in aquifers with variable fluid density. On a regional scale, such application provides good results for evaluation of flow directions and flow gradients in a lateral direction. Brine chemistry data gathered by Kreitler and Richter (1986) exhibit higher salinity values in the deeper sections of the brine hydrostatic zone (fig. 10). Hence, potentiometric maps with equivalent salt-water heads (gradient of 0.465 psi/ft) were also compiled for the Frio.

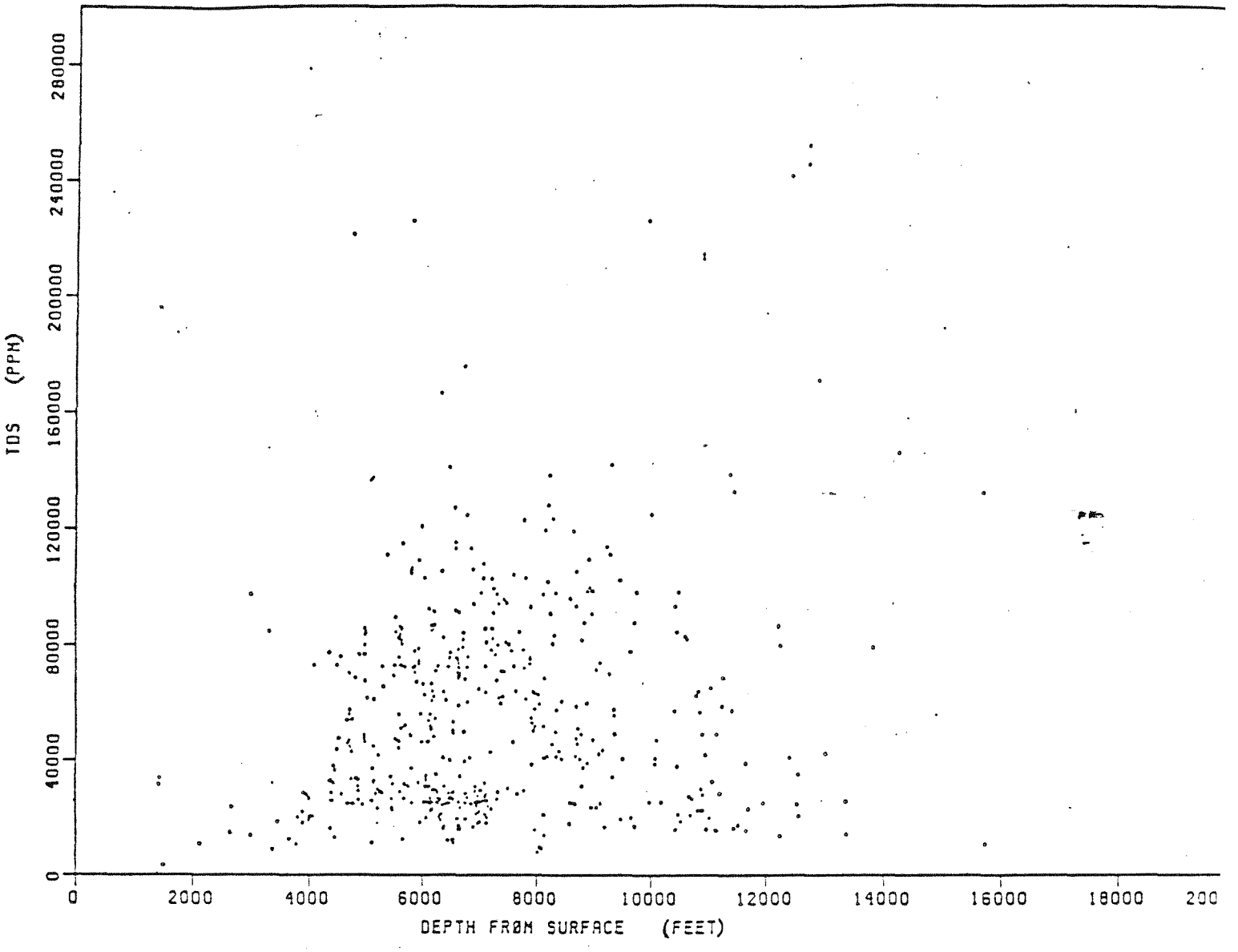

Figure 10. Salinity (total dissolved solids)-depth plot for Texas Gulf Coast Tertiary formations (from Kreitler and Richter, 1986).

These brine head potentiometric surfaces were utilized for mapping residual flow potential in the vertical direction.

Choice of fresh-water or salt-water heads is based on hydrochemistry and applicability. Strictly speaking, in fluids of variable density it is very difficult to construct potentiometric surfaces (Hubbert, 1957; Bond, 1972), due to existence of vertical flow gradient. Vertical components of potential gradients cannot be identified from the potentiometric contours. Moreover, the fresh-water head is a function of pressure, which itself depends on the local density of the formation fluid (Toth, 1978). By differentiating the Frio Formation in separate hydrologic sections (fresh to moderately saline hydropressured, brine hydrostatic), on the basis of brine chemistry, and through the use of horizontal slices, a generic model was created. Thus, the potentiometric surface of a thick slice within a relatively homogeneous hydrologic section is a valid representation of the average energy distribution. Also, the use of fresh-water or brine heads within each corresponding hydrologic environment provides reasonably accurate lateral potential gradients. This technique is also valid for estimation of vertical flow potential by mapping residual potential surfaces.

Figure 11 is a pressure-depth plot of the Frio data from regions A, B, and C. A careful look identifies two distinct trends on figure 11 that seem to match the gradient trends for 0.433 and 0.465 psi/ft, corresponding to fresh-water and brine densities. Figure 12 reflects the geographical distribution of Frio data from surface down to a depth of about 14,000 ft (datum: sea level). This is a representative sample of the overall dataset and indicates the high data density in regions B and C. Data density in region A is relatively lower.

4.2.3 Quality Control

An important initial step was to evaluate the reliability of pressure measurements contained in the PI data base. Pressure-depth plots were used as a diagnostic tool to assess the range and variability of pressure data, as well as an interpretive technique to delineate major trends for hydrologic regimes in the Frio.

DST pressures comprised nearly 6,000 data points and were culled to obtain about 1,000 data values, each having a minimum of two pressures: an initial shut-in pressure (ISIP) and a final shut-in pressure (FSIP). An assessment of reliability of the drillstem test pressures was performed at this stage. Histograms for the ratio FSIP/ISIP exhibited a very high degree of convergence between the two pressures. The mean value was 0.975. Nearly 82% of the ratio values ranged between 0.9 and 1.1, and an additional 10% of the values ranged within 30 percent of a

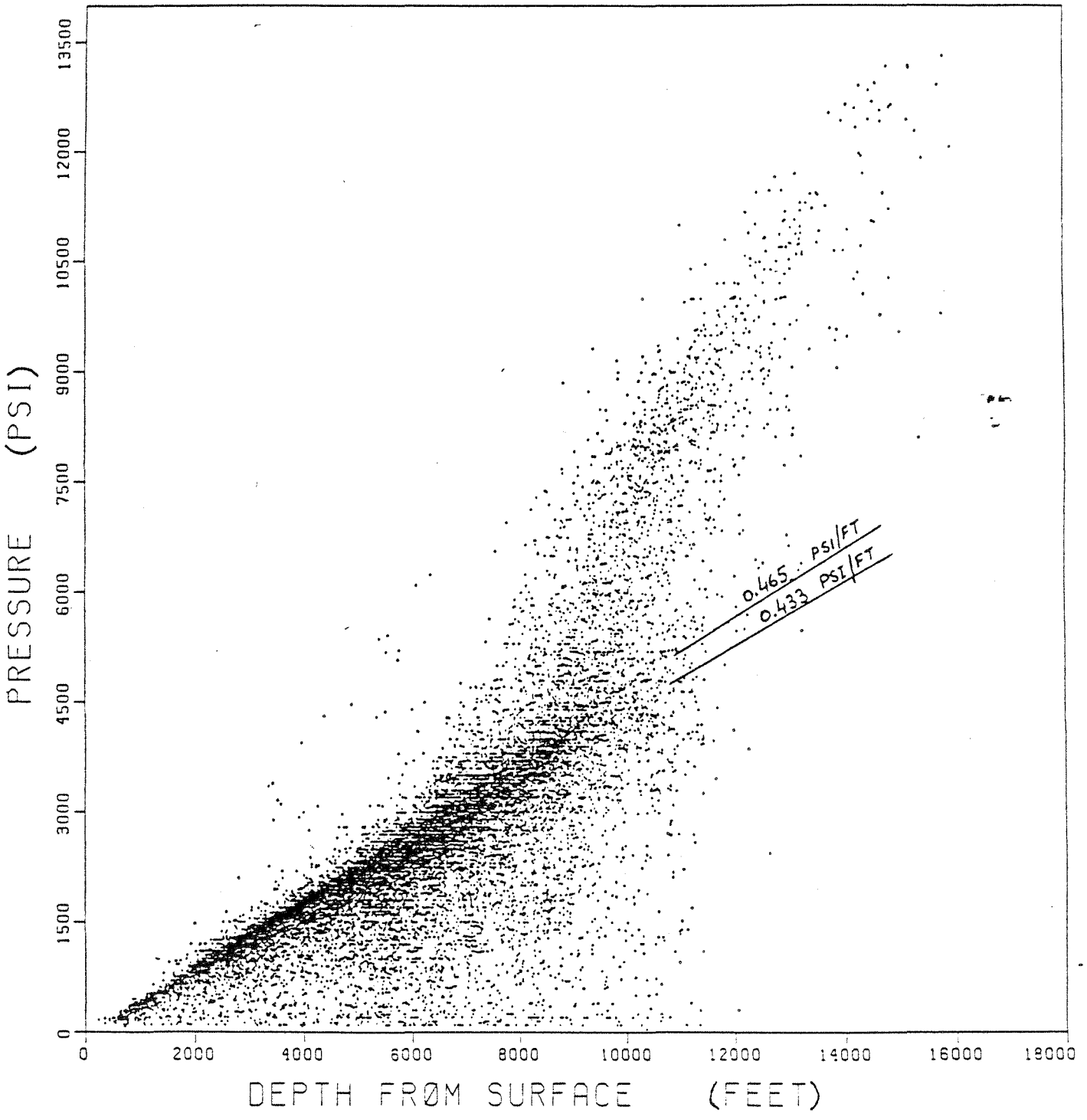

Figure 11. Pressure-depth diagram for Frio regions A, B, and C data.

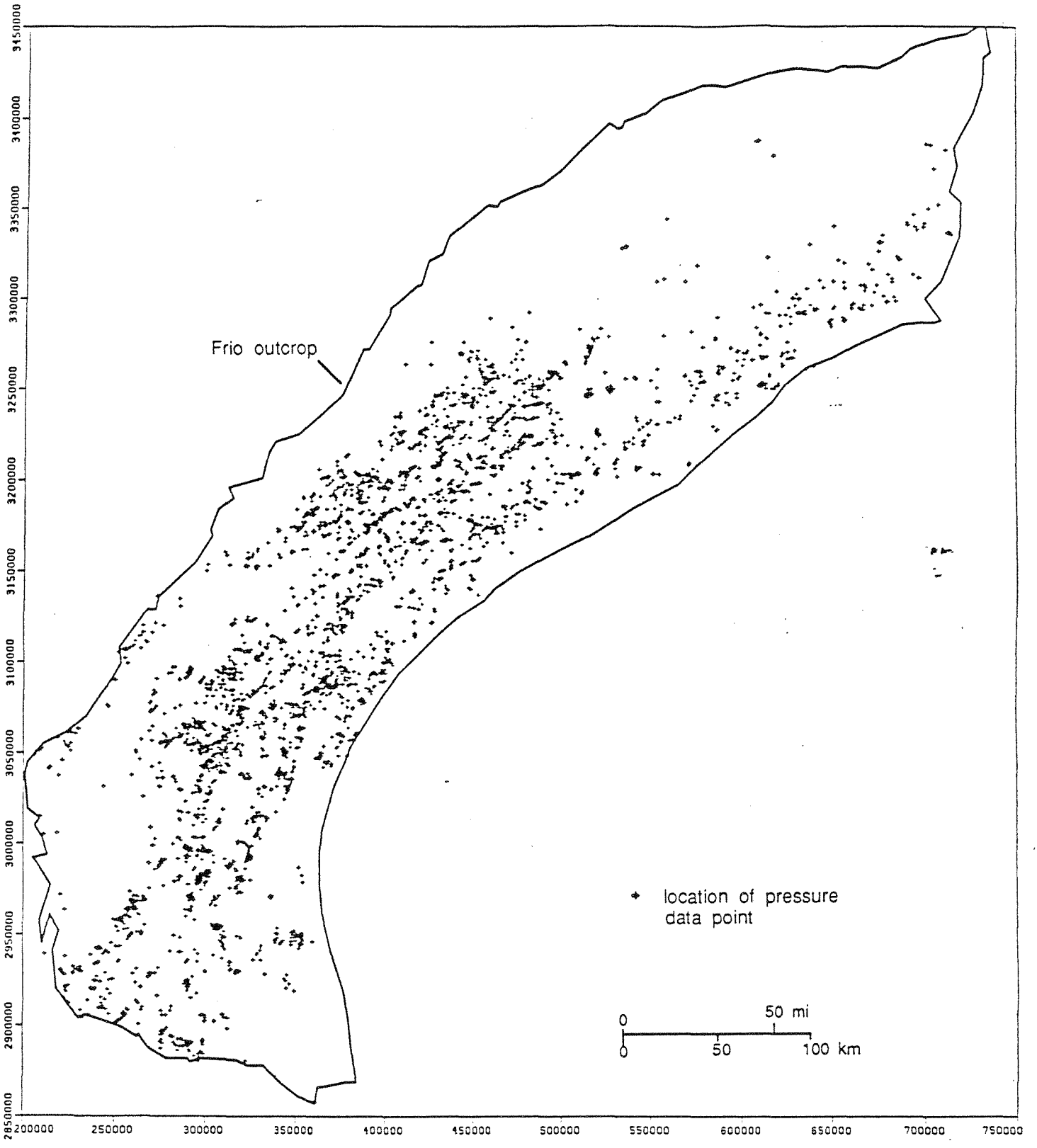

Figure 12. Geographical distribution of Frio data, from 0 to 14,000 ft subsea depth.

1.0 ratio. Figure 13 is a histogram showing the convergence of the two shut-in pressures for DSTs. The formation pressure gradient (psi/ft) was plotted versus the FSIP/ISIP ratio, in order to identify any possible correlation between different pressure levels and their frequency of convergence. Figure 14 confirms that a close convergence (ratio = ~1.0) of pressures is prevalent in all pressure levels, moreso in the 0.3-0.5 psi/ft range, where most of the data lie. This enhances the level of confidence in the DST pressures and in the entire pressure data base from which the DST pressures are drawn. To promote further quality assurance, a classification and screening scheme for the entire data base was applied:

Data Classification

Class A data: Tests in which ISIP and FSIP agree within 10%
Class B data: Tests in which ISIP and FSIP diverge by more than 10%
Class C data: Tests where only one pressure (ISIP or FSIP) is available
Class D data: Pressures that convert to equivalent fresh-water heads higher than ground elevation (flowing wells)
Class Z data: Class A data within class D

The data were sorted according to aquifer (undifferentiated Miocene, Catahoula, Vicksburg, Jackson, Frio, and Wilcox).

Data Screening

1. Nonrepresentative pressures: data with pressure gradients greater than 2.0 or less than 0.05 were deleted
2. Multiple pressure points: in case of multiple pressure data for a single well in one formation-depth interval, only the highest class and the highest pressure from the same class were retained.

Additionally, at various stages, data were also sorted by well types (wildcat, oil, and gas) and by timespan intervals for definition of trends. Identified as wildcat were wells drilled for exploration purposes in new productive zones. Development wells drilled for production were classified as oil and gas wells. During the posting of head values for contouring, anomalous data that drastically differed from local surrounding values were culled. The data classification scheme served a useful purpose in this culling process, since during comparison, the higher class (class A) was preferentially retained against the lower class (class B or C).

One of the limitations of the PI Corp. data base was a large number of missing formation codes for the pressure-test intervals. This problem was partly resolved by

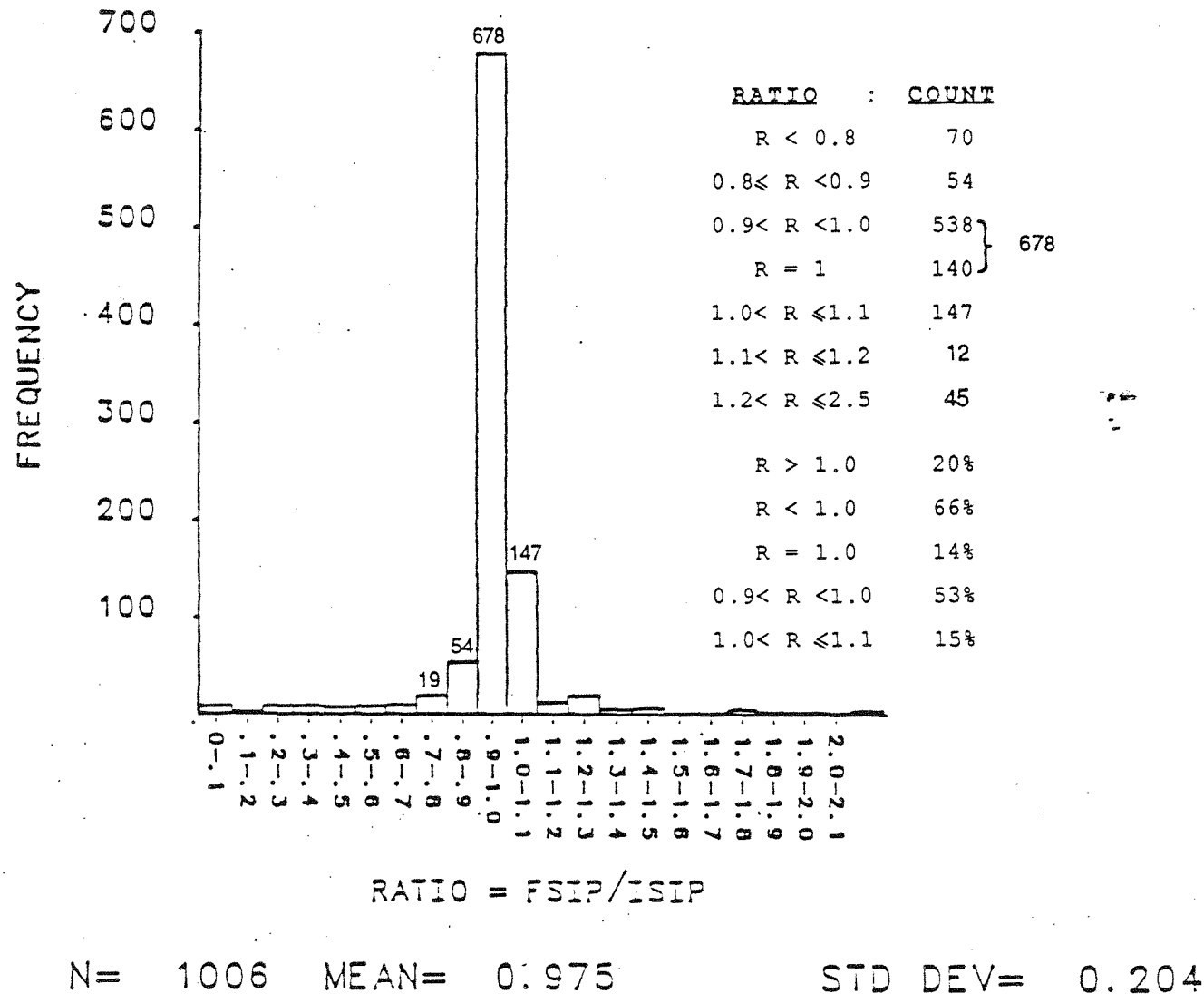

Figure 13. Histogram for FSIP/ISIP ratio, Frio regions A, B, & C data. A, B, and Z class data included.

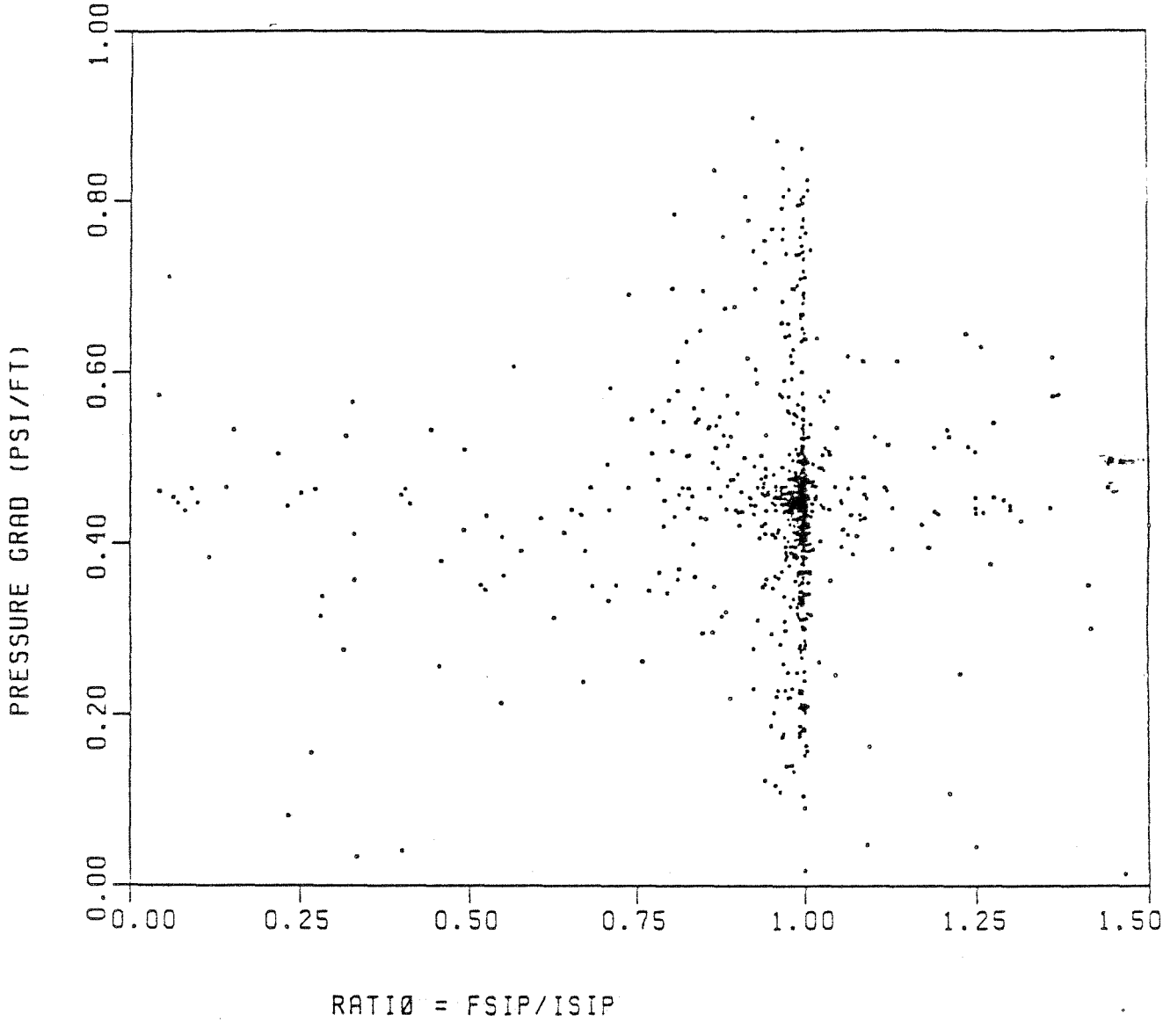

Figure 14. Pressure gradient (psi/ft) versus convergence ratio (FSIP/ISIP) for DST data, Frio regions A, B, C.

assigning interpolated formation codes in such missing cases, with the help of the contouring program CPS-1. The structure tops for the Tertiary formations were digitized and transformed into a grid network. Then the tested depths were correlated to these interpolated stratigraphic picks and their values assigned reasonable formation codes. Where no reliable match was obtained between the tested intervals and the computerized structure contour surfaces, the data were culled from the data base.

The contouring program CPS-1 used for mapping the potentiometric surfaces requires careful handling. The continuous contour lines are defined by the irregularly spaced head data, which are transformed to a regular X-Y grid mesh. The density of data in each grid cell is different, and the program averages all the data from each cell to determine the values at the nodes (corners) of the grid cells. Thus, the data density and grid-cell size influence the value of the averaged contour line passing through that cell. The size of the grid cells and the averaging algorithm were carefully selected in this study to produce representative surfaces. This data averaging approach is necessary because of the high density of data. Contouring of individual data points is impossible. This technique does, however, provide an averaged surface. Moreover, mapping of potentiometric surfaces on a county-size scale facilitated a closer scrutiny of the data.

4.3 Pressure-Depth Plots

The fluid pressures retrieved from the PI data were plotted versus the corresponding depths to obtain a pressure-depth profile for the entire Frio Formation. This P-D profile (fig. 11) was used as a diagnostic tool to scan the complete range of fluid pressures existing in the Frio, as well as an interpretive technique for evaluating the presence of different hydrologic regimes. Two trend lines are drawn on the P-D plot; one with a 0.433 psi/ft slope, and the other with a 0.465 psi/ft slope. These slopes were not computed from any regression analysis, but merely represent the dominant trends visible on the P-D plot. These slopes also delineate the fresh-water and brine hydrostatic gradients in the Gulf Coast. Additionally, the following observations are relevant to the P-D profile:

1. a significant volume of data lie along the fresh-water gradient line
2. the overpressured regime is represented by data above the brine hydrostatic line
3. a large body of data lies in the underpressured zone below the 0.433 psi/ft gradient line.

The pressure data were then plotted separately for the three regions (A, B, and C), and similar trends were observed. Figure 15 is the pressure-depth profile for region C. A histogram of the pressure gradients in region C (fig. 16) reveals the larger groupings into which the pressure measurements are differentiated, and once again it reinforces the significance of the 0.433 and 0.465 gradient trends.

For investigating the variability in the pressure-depth profiles as a function of well type and time, several P-D plots were compiled for region C for various well categories; wildcat, oil, and gas (figs. 17, 18, and 19, respectively). There are basic similarities between these plots and the integrated plot shown in figure 11. Figure 20 is the gradient versus time plot for region C. No distinguishing trends can be observed from this plot. Thus, the influence of time on the nature of hydrologic regimes can be isolated only indirectly, and it has been addressed in the context of potentiometric surfaces compiled for different time segments.

4.4 Regional Potentiometric Surfaces, Frio Formation

Regional potentiometric surfaces of the Frio were constructed using equivalent fresh-water and salt-water heads calculated from the highest available shut-in pressures. The initial surface was generated from the screened class A, B, and Z data. This surface contained several localized highs and lows (bulls-eyes) and represented complex variations in flow trends. The enormous thickness of the Frio and the variability in hydraulic gradients as reflected on the stratigraphic cross section (fig. 7) and the pressure-depth plot (fig. 11) made it difficult to discern any specific flow trends in this regional surface. Consequently, potentiometric surfaces were generated for separate slices through the Frio. This allowed a rough delineation between the top fresh to moderately saline hydropressured zone, the next lower brine hydrostatic zone, and the deep overpressured formations. As part of the preliminary investigations, potentiometric surfaces were generated for 2,000-ft-thick horizontal slices of the Frio, from land surface down to a 14,000-ft depth. These surfaces are presented in figures 21 through 26. Outlined on these maps are the boundaries of reliable data regions, beyond which sparseness and boundary effects make any viable interpretation difficult. Most of these surfaces cover regions B and C, and only partially extend into region A, due to scarcity of data in region A. Data from years 1975-84, within classes A, B, C, and D were selected for constructing these potentiometric surfaces.

The large pressure dataset provides good areal coverage on a regional scale, and reliable regional potentiometric surfaces can be generated. Kriging, a geostatistical analysis method used for minimizing variance in a regionalized variable such as

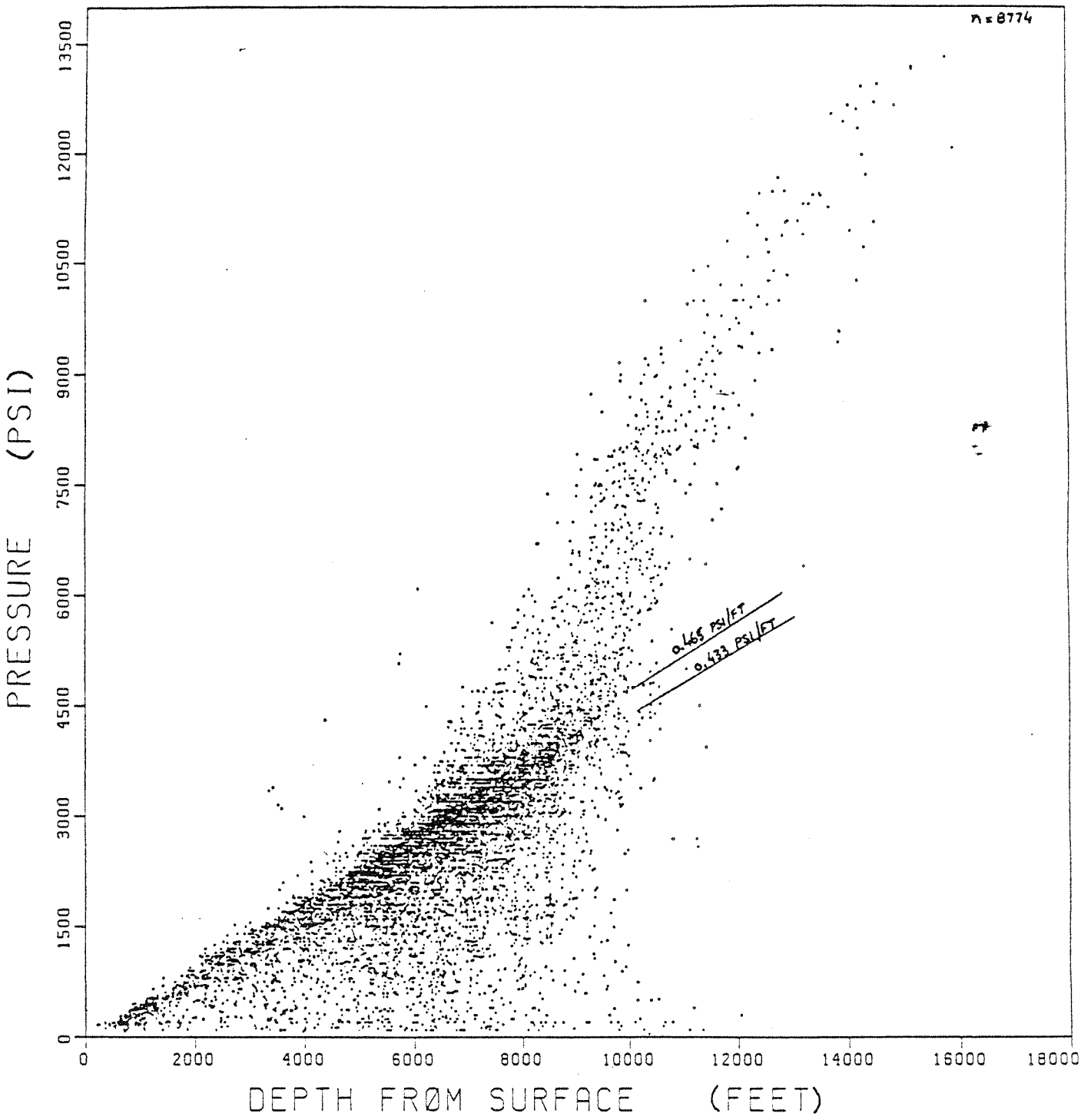

Figure 15. Pressure-depth diagram for Frio region C data.

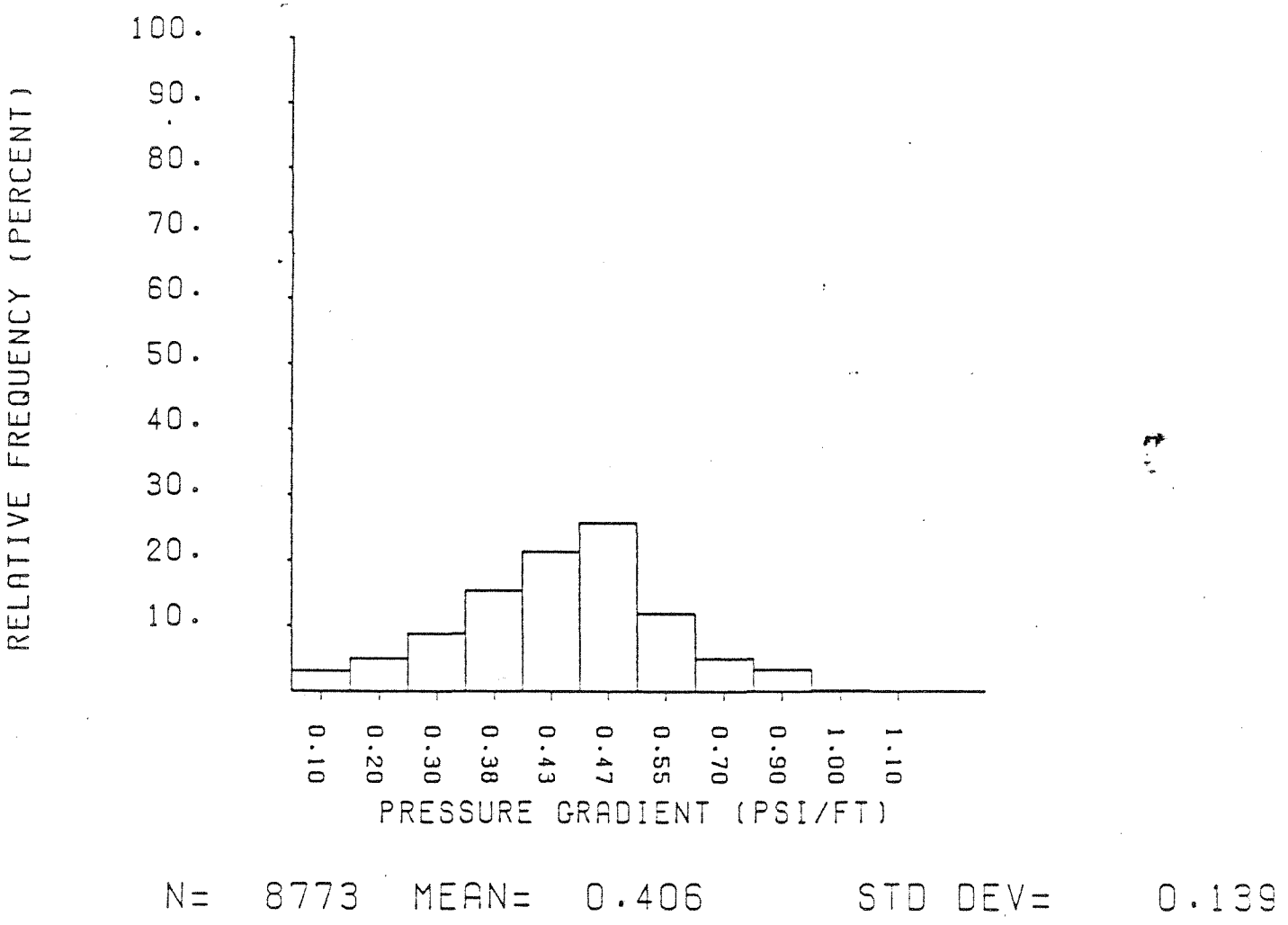

Figure 16. Histogram of formation fluid pressure gradients (psi/ft), region C data.

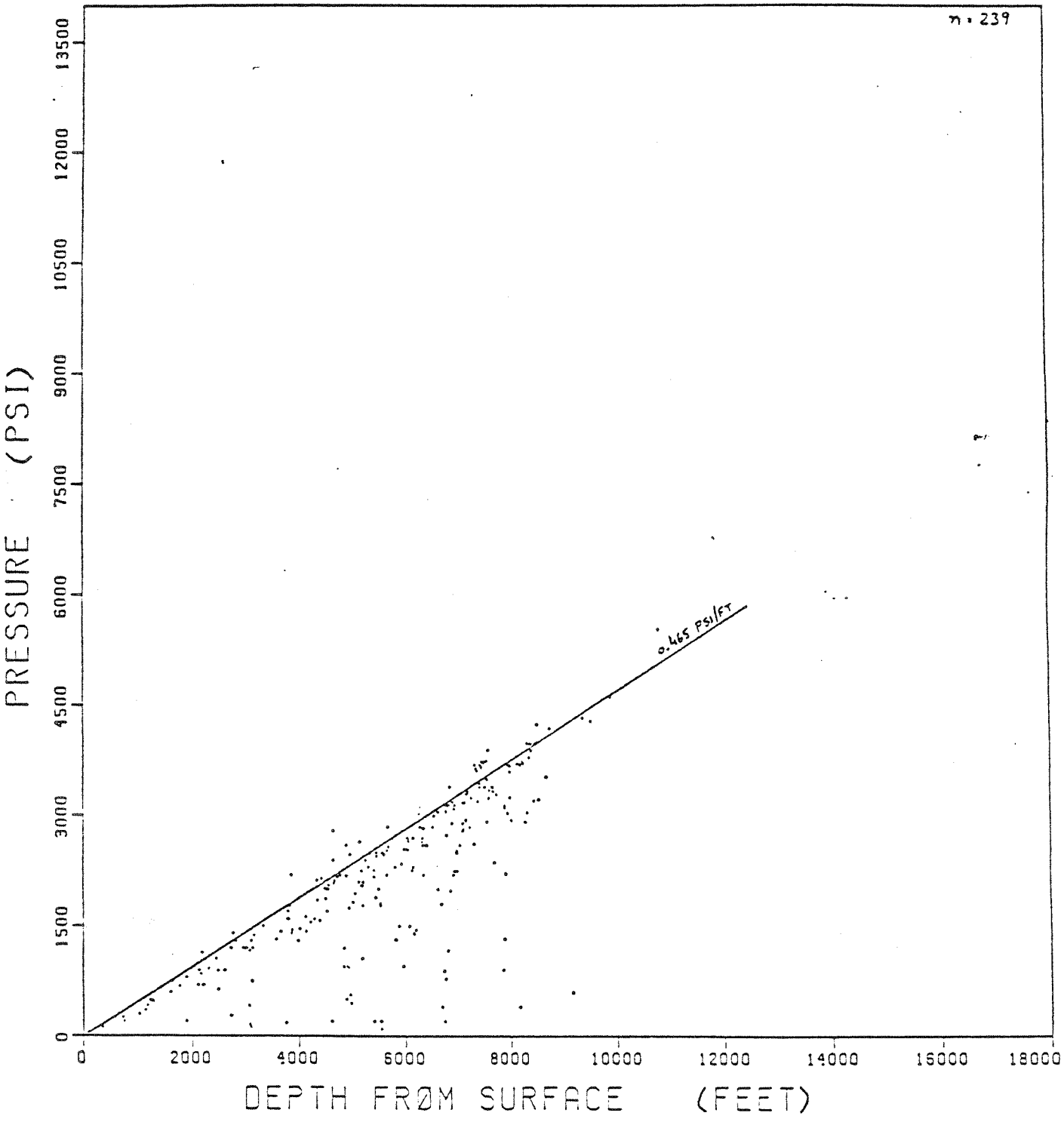

Figure 17. Pressure-depth diagram for Frio region C, wildcat wells.

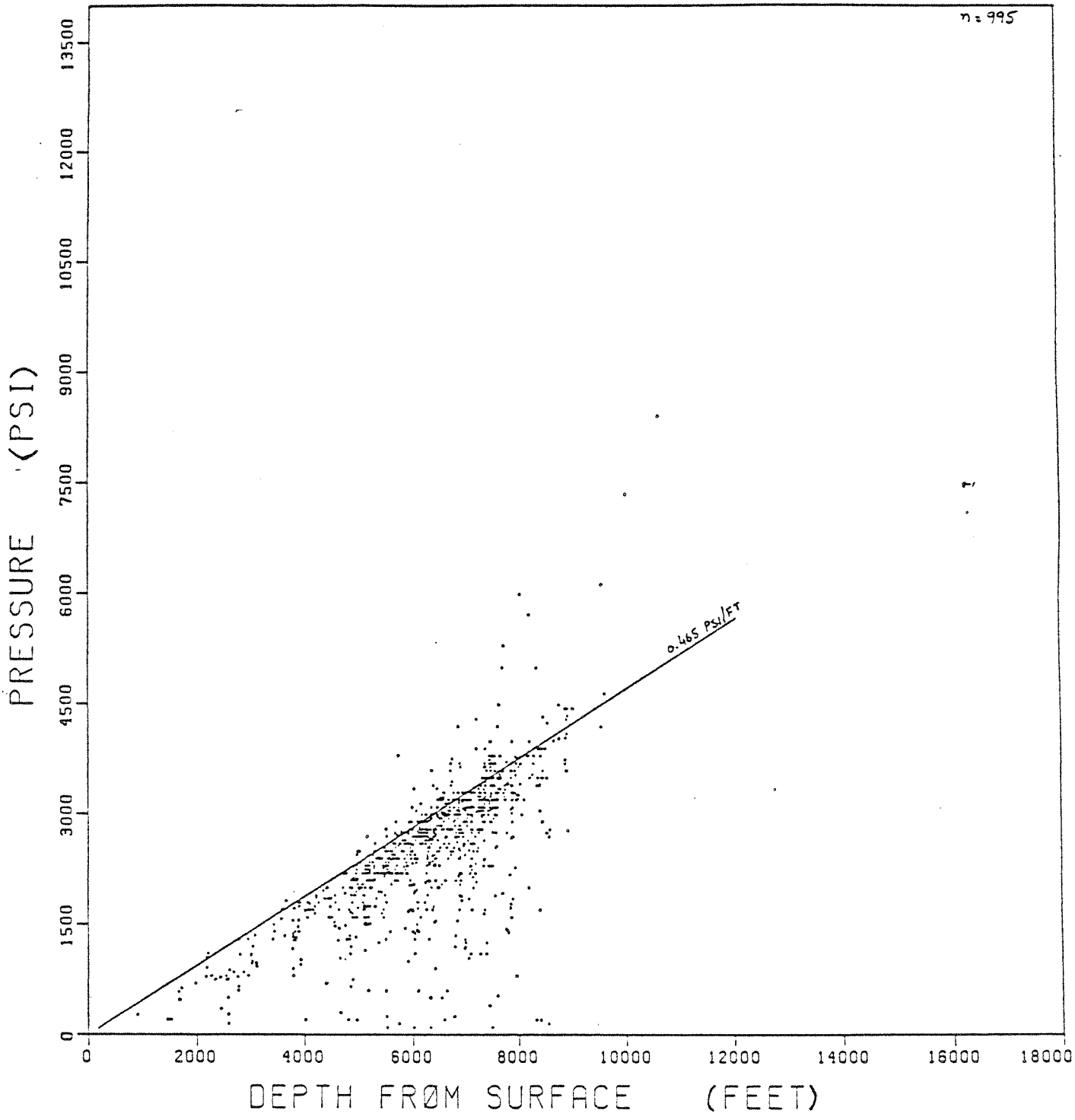

Figure 18. Pressure-depth diagram for Frio region C, oil wells.

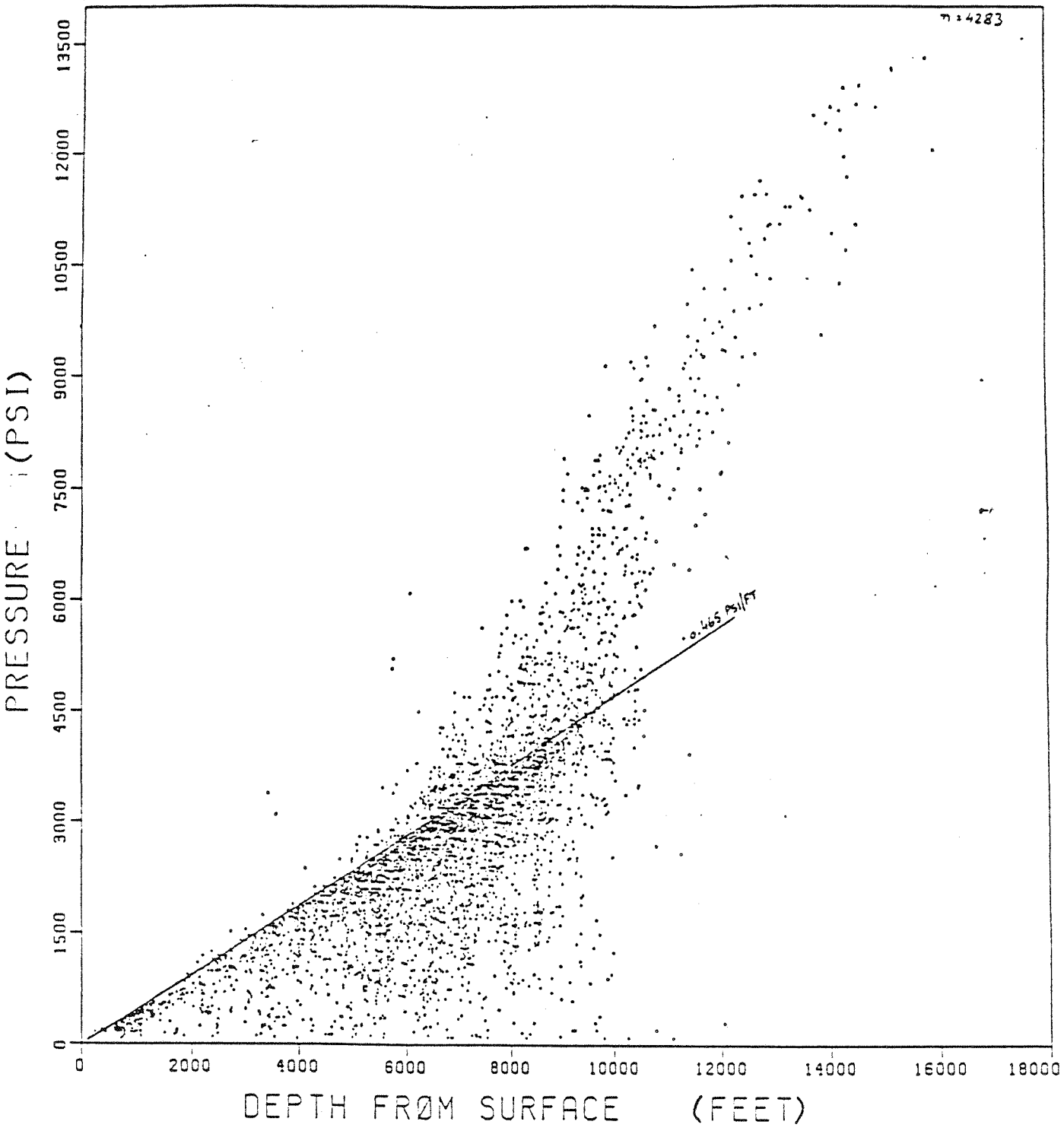

Figure 19. Pressure-depth diagram for Frio region C, gas wells.

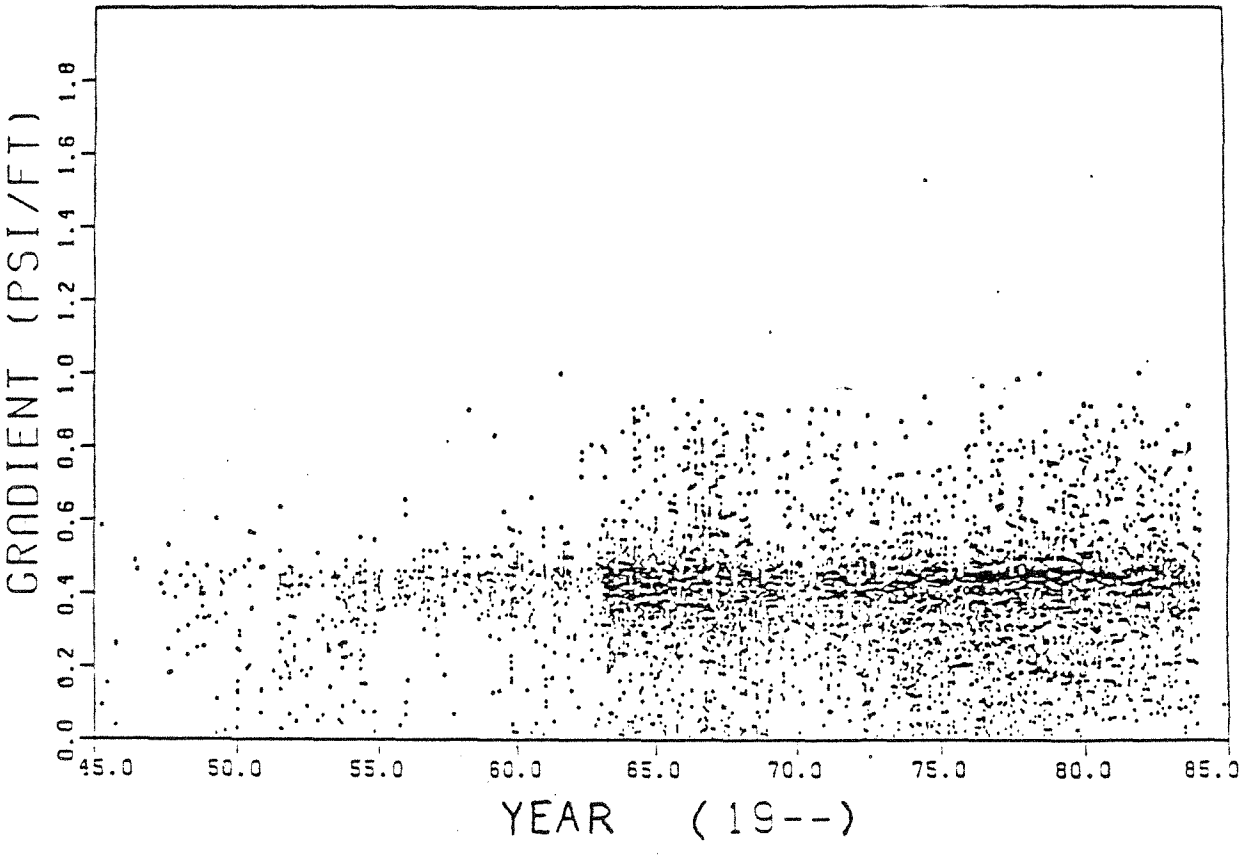

Figure 20. Pressure gradient versus time plot for Frio region C.

potentiometric level, may be needed when data are sparse. High data density, separation of data by horizontal slices, and the capability of analyzing county-size maps combined to make kriging unnecessary. As discussed earlier, equivalent fresh-water and salt-water heads proved adequate for characterizing the lateral flow potentials. Lack of continuous data along the vertical prevents determination of environmental heads. But, within the bounds of the horizontal slices, variations of formation water salinities are small enough so that fresh-water and salt-water heads result in representative surfaces for the corresponding hydrologic regimes. Therefore, at less than a 4,000-ft depth, a fresh-water gradient (0.433 psi/ft) was used to compute hydraulic heads, and in the deeper intervals, a salt-water gradient (0.465 psi/ft) was used.

Following is a brief discussion of the salient features of each of these surfaces.

(a). 0-2,000 ft interval (fig. 21): Most of the surface is flat with hydraulic heads near land elevation (-250- to +250-ft contours). There is a cone of depression in the middle of the map (in north region C) that corresponds to extreme negative contours in Jim Wells County. Individual pressure values for wells in this area reveal a cluster of producing gas wells that presumably have caused the depletion.

(b). 2,000-4,000 ft interval (fig. 22): A majority of hydraulic heads are near land elevation; however, the area covered by depressured contours has expanded. But there are no extreme contrasts in flow gradient. The depressured areas are confined by negative contours, in the central and southern parts of the study area. Normally pressured areas are represented by mildly positive and zero-contour lines and are located on the western flank. Due to coexistence of normally pressured and underpressured areas side-by-side, localized reversals of flow direction are observed.

(c). 4,000-6,000 ft interval (fig. 23): This represents the average potentiometric surface for pressures in the 4,000-6,000-ft slice. Negative depressured contours envelope almost the entire surface. The lower bound of the negative contours (-2000 ft) corresponds to depressurization to the extent of 930 psi below hydrostatic pressure. The large volume of pressure data also reflects extensive hydrocarbon development in this horizon.

(d). 6,000-8,000 ft interval (fig. 24): This surface has a character similar to that of the overlying interval. Underpressured regime occupies a significant part of the surface. The surface becomes positive near the shoreline in the north-central part, which reflects a gradual transition to overpressures. Reversal of flow direction is also observed. Adequate hydraulic communication over a large overlapping segment of the two slices probably exists there.

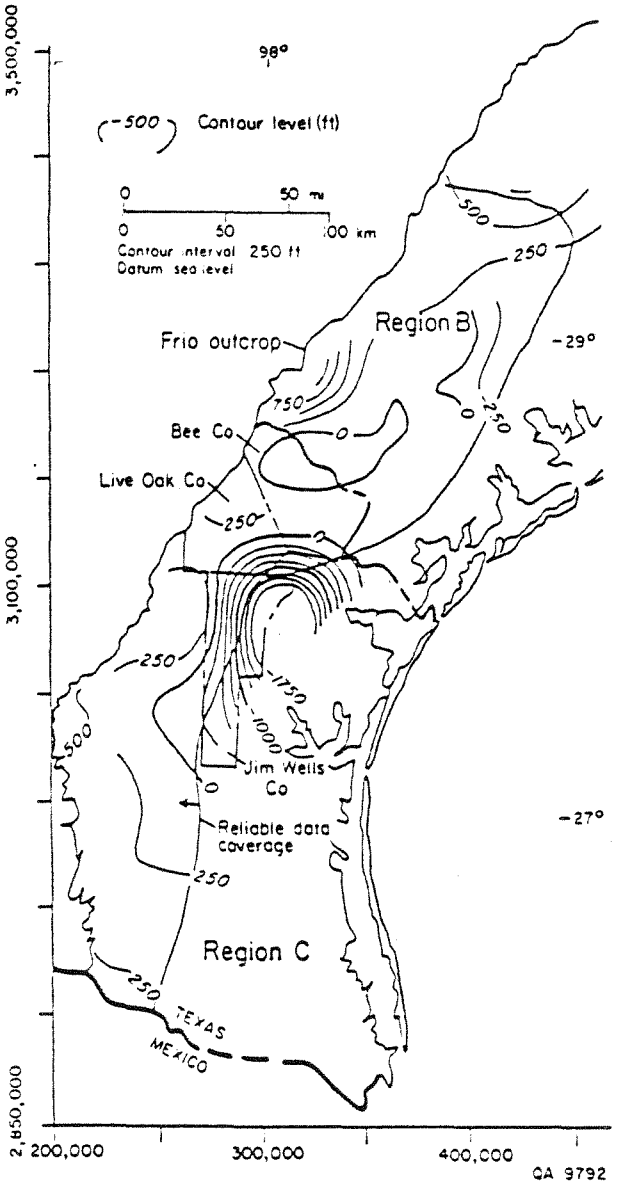

Figure 21. Regional potentiometric surface, Frio regions A-B-C, all class data, years 1975-84, 0-2,000 ft horizontal slice. Equivalent fresh-water heads.

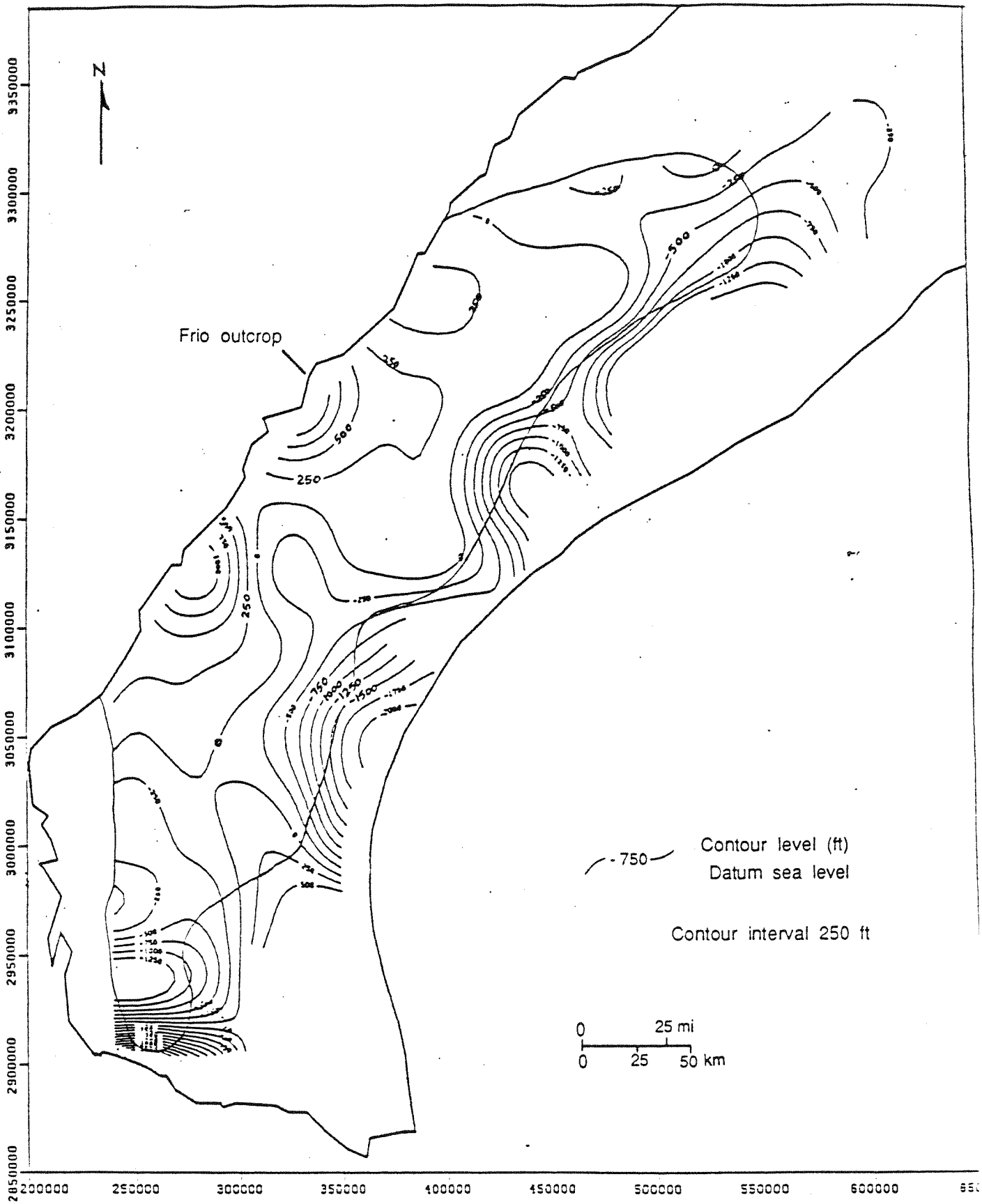

Figure 22. Regional potentiometric surface, Frio regions A-B-C, all class data, years 1975-84, 2,000-4,000 ft horizontal slice. Equivalent fresh-water heads.

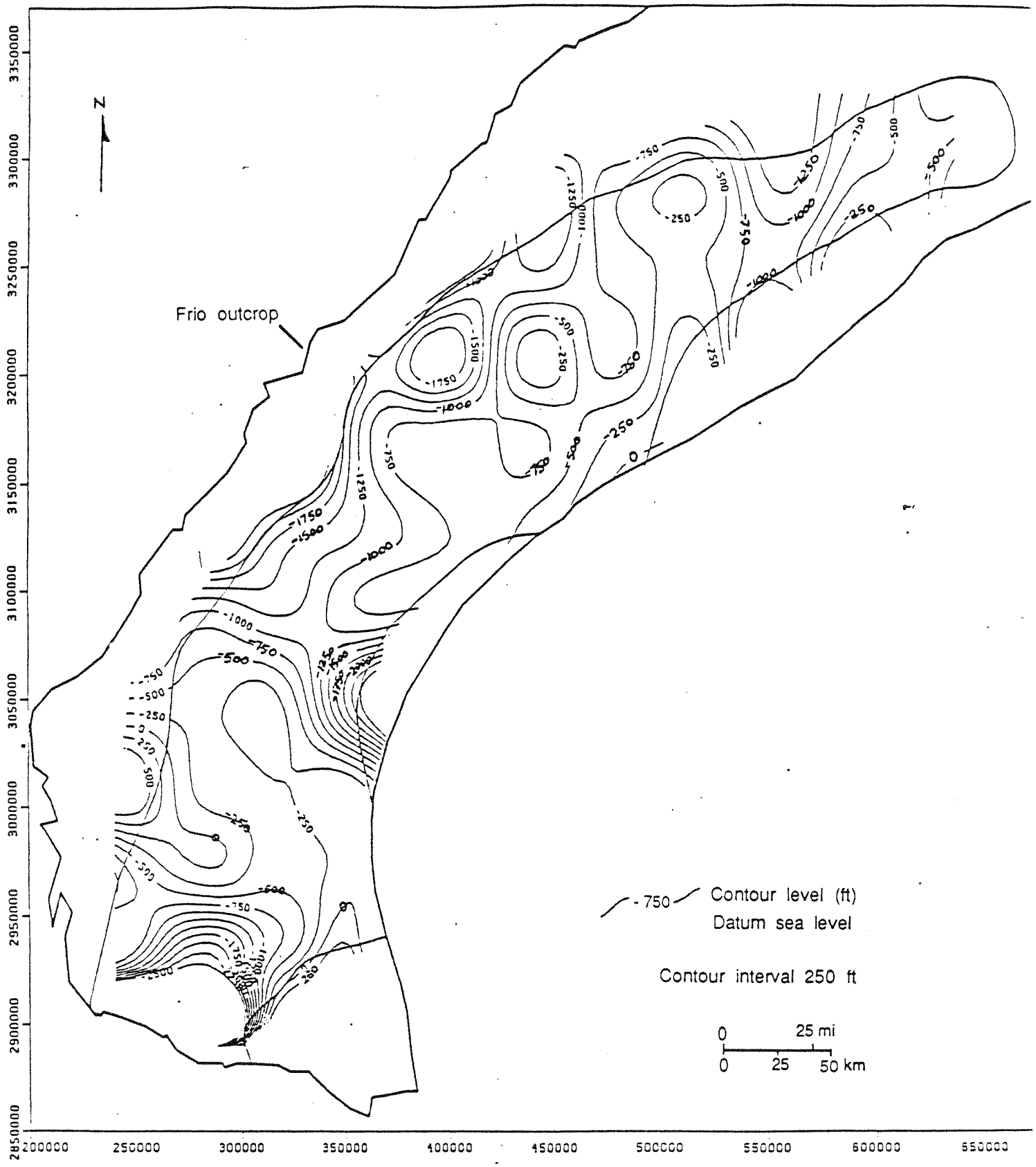

Figure 23. Regional potentiometric surface, Frio regions A-B-C, all class data, years 1975-84, 4,000-6,000 ft horizontal slice. Equivalent brine heads.

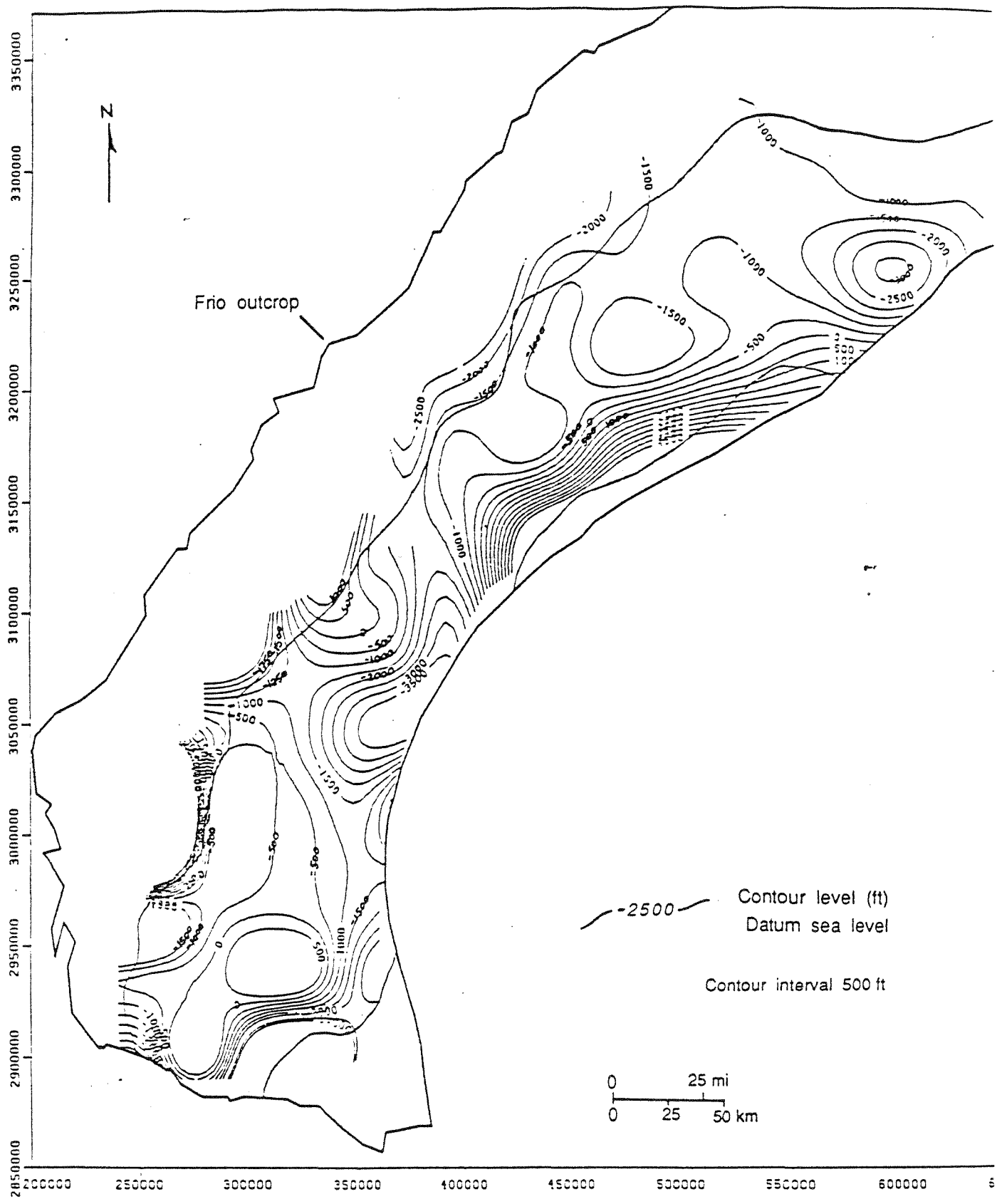

Figure 24. Regional potentiometric surface, Frio regions A-B-C, all class data, years 1975-84, 6,000-8,000 ft horizontal slice. Equivalent brine heads.

(e). 8,000-10,000 ft interval (fig. 25): A large part of the surface is encompassed by positive contours, especially closer to the coast line. This reflects a transition to overpressured gradients in the predominantly gas wells in this slice.
(f). 10,000-12,000 ft interval (fig. 26): The hydraulic heads in this surface are all positive, ranging from 2,000 to 10,000 ft above sea level. All the pressure gradients are above 0.465 psi/ft and reflect overpressured conditions.

The geographic position of these discrete thickness slices moves toward the coastline with each successively lower interval. Thus, each structurally lower horizon dips toward the Gulf Coast and thickens. There is sufficient lateral heterogeneity within each slice of the hydrologic system for it to exhibit a complex potentiometric surface. Hydraulic communication is inferred in the central part of each slice, where pressures seem to have uniformly declined due to oil and gas exploration.

Furthermore, residual surfaces that compare the potentiometric surfaces in the shallow and deeper intervals were created for better definition of vertical flow potential. Figures 27 through 32 are the residual surfaces between depth intervals 0-2,000, 2,000-4,000, 4,000-6,000, and 6,000-8,000 ft. Constructing a residual potential surface involves subtracting the potentiometric surface for one (shallower) depth interval from the other (deeper) depth interval. The shallow potentiometric surfaces (down to 4,000 ft) were constructed with fresh-water equivalent heads (0.433 psi/ft gradient), whereas deeper surfaces were generated by using brine hydrostatic gradient (0.465 psi/ft). This is considered more logical for evaluating the vertical flow gradient in view of the predominantly brine densities encountered in the deep Frio sediments.

(a). 4K-2K Residual Surface (fig. 27): This surface results from subtracting the potentiometric surface for the 0-2,000-ft slice from the surface for the 2,000-4,000-ft slice. In the center of the map, a large area defined by positive contours represents potential for upflow from the deeper to the shallower horizon, whereas the negative contours in the upper and lower flanks outline potential for downward flow toward the deeper zone. Quantitatively, except in the center of the map (area of Jim Wells County), no extreme vertical gradient exists in either direction, given the fact that both slices are predominantly in the fresh to moderately saline hydrostatic environment. The negative contours in the lower section of the map confirm the depressured part of the 2,000-4,000-ft slice.
(b). 6K-4K Residual Surface (fig. 28): This surface is generated by subtracting the 2,000-4,000-ft slice potentiometric surface from the 4,000-6,000-ft slice potentiometric

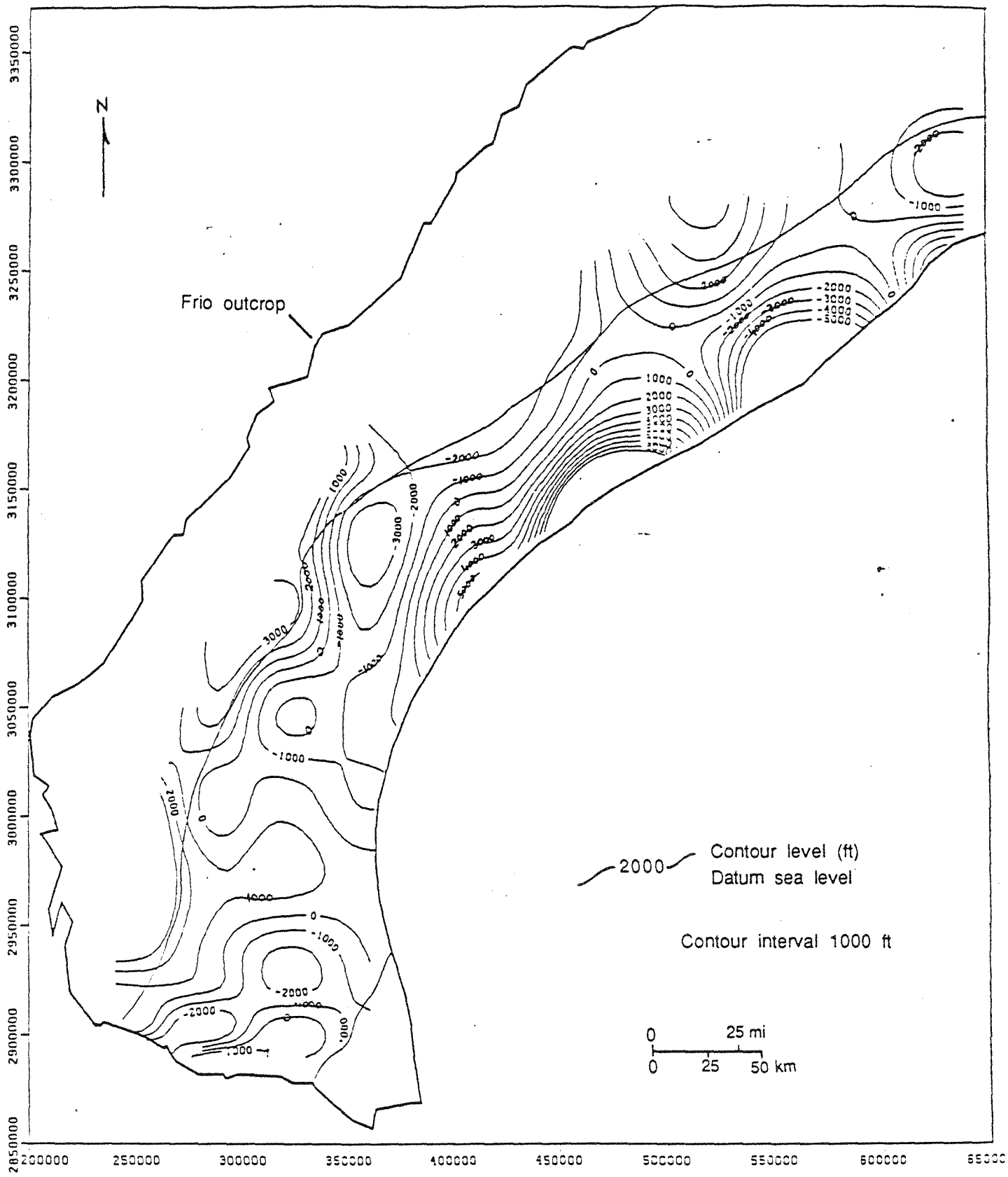

Figure 25. Regional potentiometric surface, Frio regions A-B-C, all class data, years 1975-84, 8,000-10,000 ft horizontal slice. Equivalent brine heads.

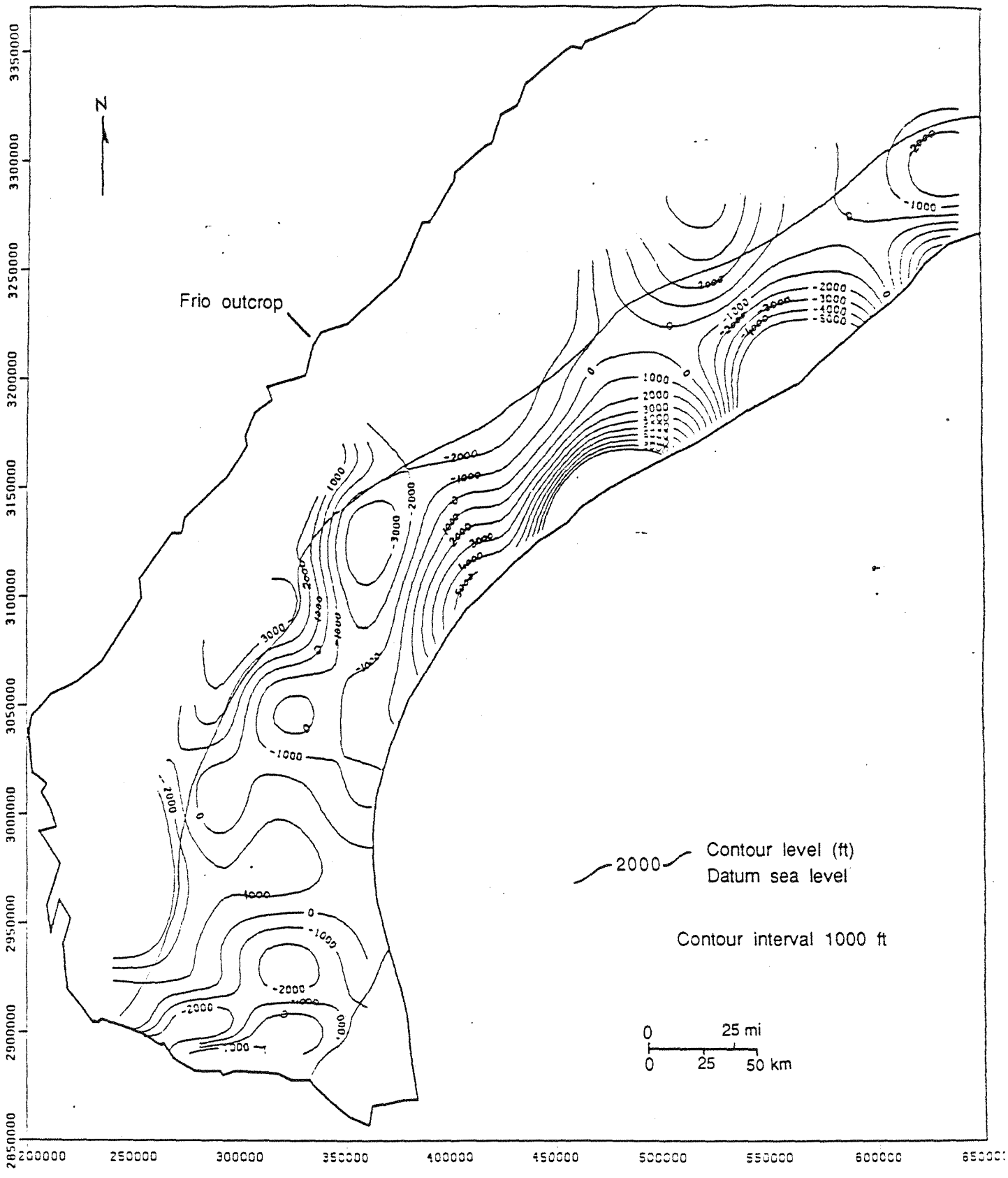

Figure 25. Regional potentiometric surface, Frio regions A-B-C, all class data, years 1975-84, 8,000-10,000 ft horizontal slice. Equivalent brine heads.

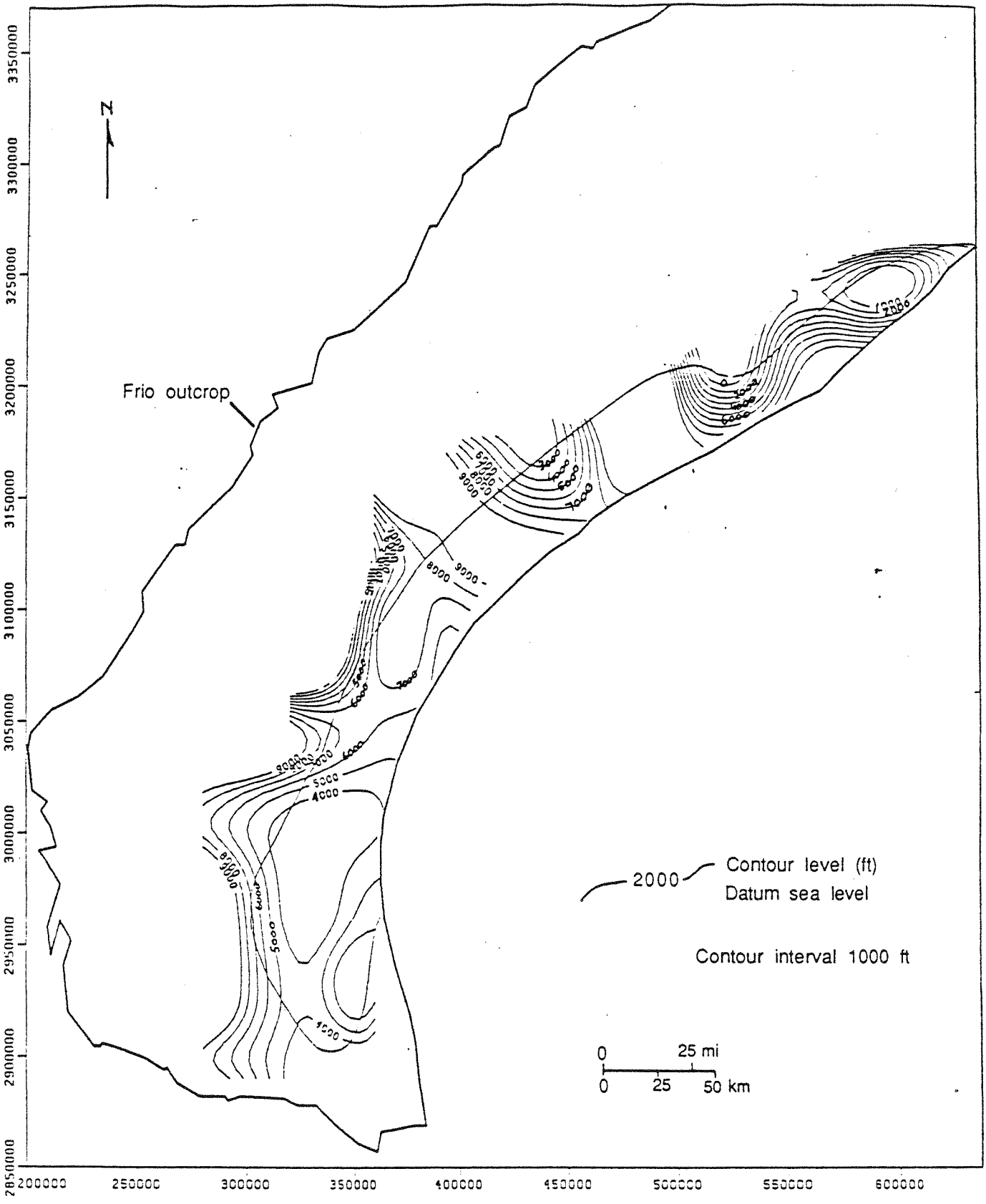

Figure 26. Regional potentiometric surface, Frio regions A-B-C, all class data, years 1975-84, 10,000-12,000 ft horizontal slice. Equivalent brine heads.

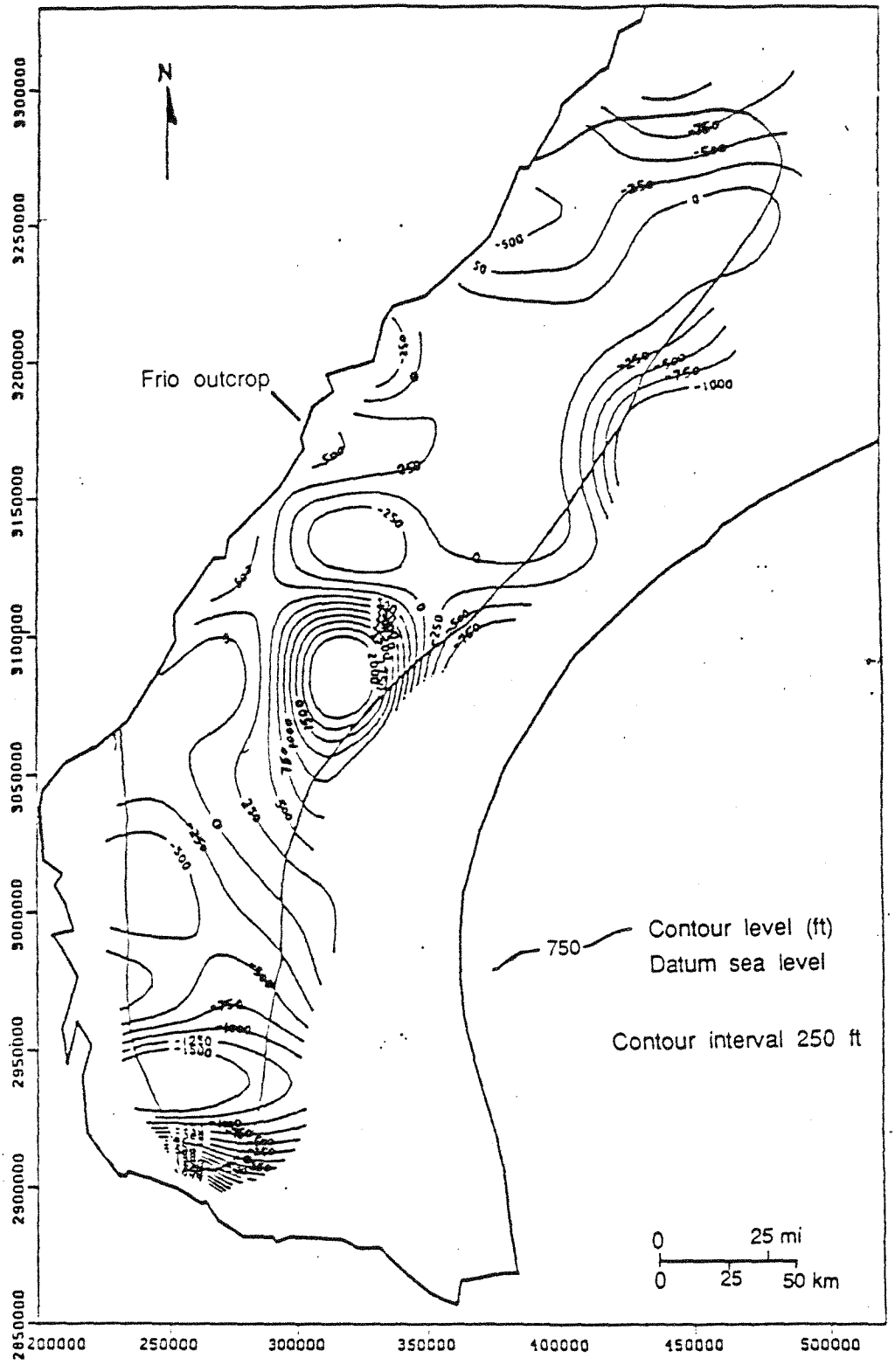

Figure 27. Frio residual potential surface, 2,000-4,000 ft minus 0-2,000 ft slice (4K-2K), all classes, 1975-84 data. Positive contours indicate upward flow, and negative contours indicate downward flow. Heads for both surfaces computed with fresh water gradient.

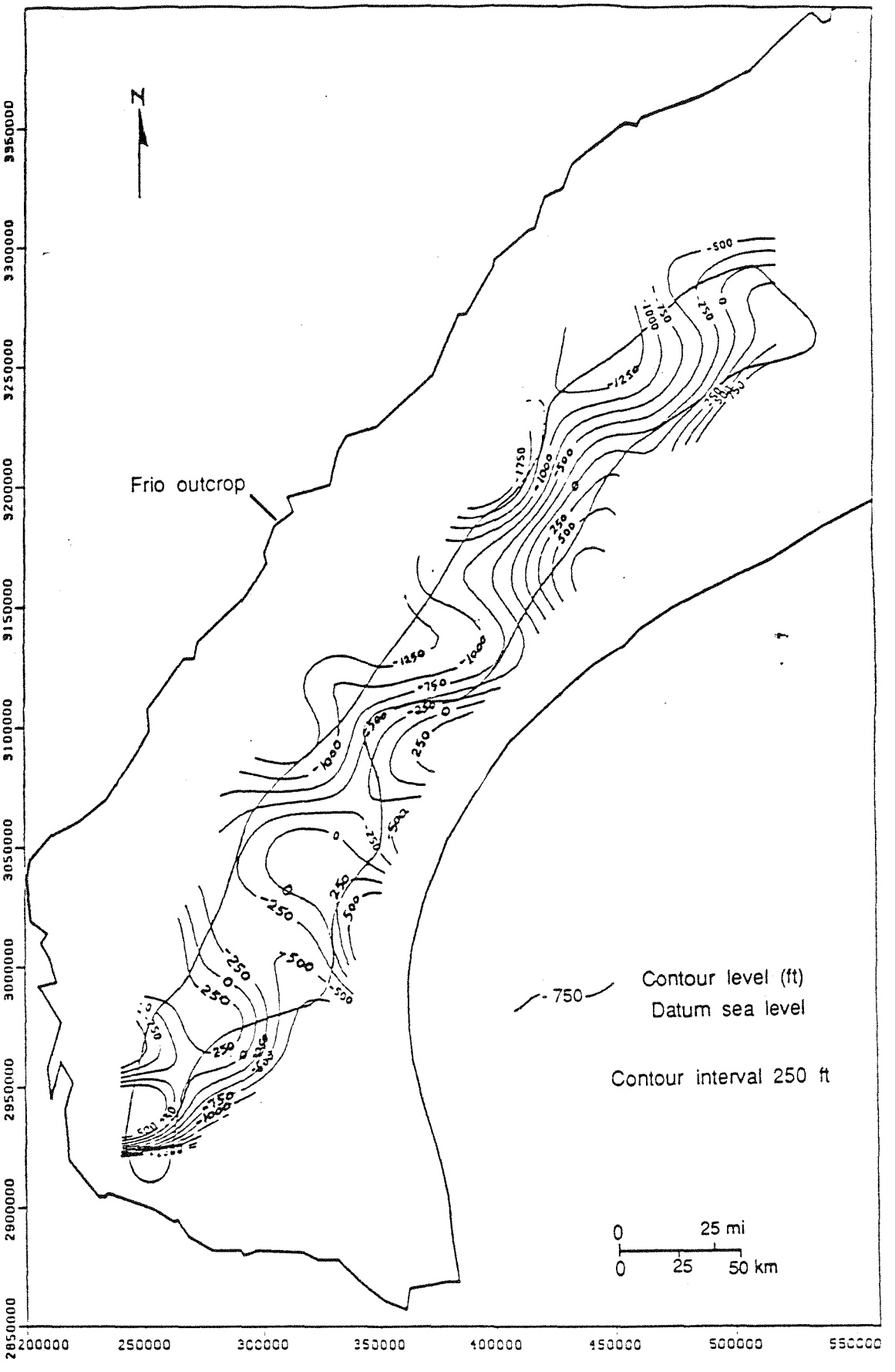

Figure 28. Frio residual potential surface, 4,000-6,000 ft minus 2,000-4,000 ft slice (6K-4K), all classes, 1975-84 data. Positive contours indicate upward flow, and negative contours indicate downward flow. Heads for 6K surface computed with environmental brine gradier

surface. The residual surface is characterized by negative contours in most of the regions, except positive contours in the east flanks and southern area. This reflects a large area of downflow potential. The steep downward gradient results from a great degree of depressurization that has occurred in the 4,000-6,000-ft slice.

(c). 6K-2K Residual Surface (fig. 29): Due to the relative lateral displacement of these two slices, only a narrow section of the two surfaces overlaps. Most of the residual surface exhibits potential downflow (negative contours) due to the depressured condition in the deeper slice. The objective of mapping this surface is to determine whether fluid from a deeper slice could bypass the intermediate horizon and still rise to the topmost zone.

(d). 8K-2K Residual Surface (fig. 30): A very narrow band of overlapping sections from the two surfaces results in residuals that are bunched together and exhibit reversals of flow direction. The maximum residual head is about -2,000 feet in the downward direction.

(e). 8K-4K Residual Surface (fig. 31): The dominating trend in the central and southern part is upflow to the shallower (2,000-4,000 ft) slice, and in the rest of the region is downward to the deeper (6,000-8,000 ft) slice.

(f). 8K-6K Residual Surface (fig. 32): The configuration of this residual surface is similar to the previous surface. Low residual values suggest good hydrologic continuity and pressure equilibrium between the two slices (6,000-8,000 ft and 4,000-6,000 ft).

A common characteristic of the residual surfaces is an upward flow trend through all the slices in the south-central part (confluence of Nueces, San Patricio, Jim Wells Counties). In other regions, the gradient is a function of the depressurization in the slice.

It must be reiterated that these horizontal slices are merely a qualitative interpretation of the variability in pressure and the resulting fluid flow potential in the different layers of the extremely heterogeneous Frio Formation. In reality, no discrete 2,000-ft thick slices exist, and the hydrologic continuity within the Frio is very difficult to map on a large (regional) scale.

This regional approach provides fundamental information on the hydrology of the Frio Formation. Incorporating so much data from a large area into a single map, however, smooths trends and prevents a detailed picture of smaller areas. To understand the "regional" flow and its interaction with an injection facility, county-size maps are needed. The next section describes the detailed mapping of the hydrologic system in Victoria County.

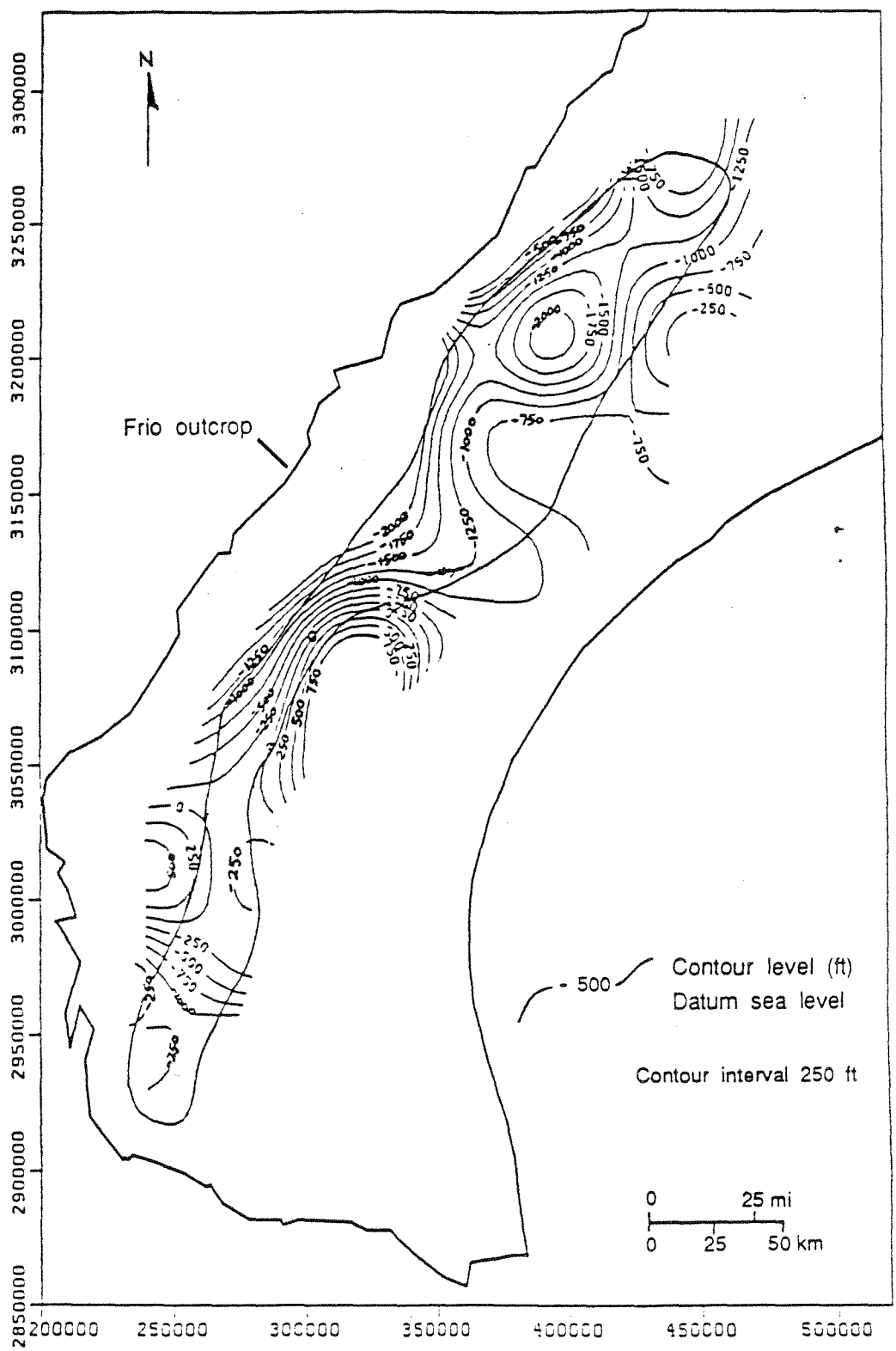

Figure 29. Frio residual potential surface, 4,000-6,000 ft minus 0-2,000 ft slice (6K-2K), all classes, 1975-84 data. Positive contours indicate upward flow, and negative contours indicate downward flow. Heads for 6K surface computed with environmental brine gradient.

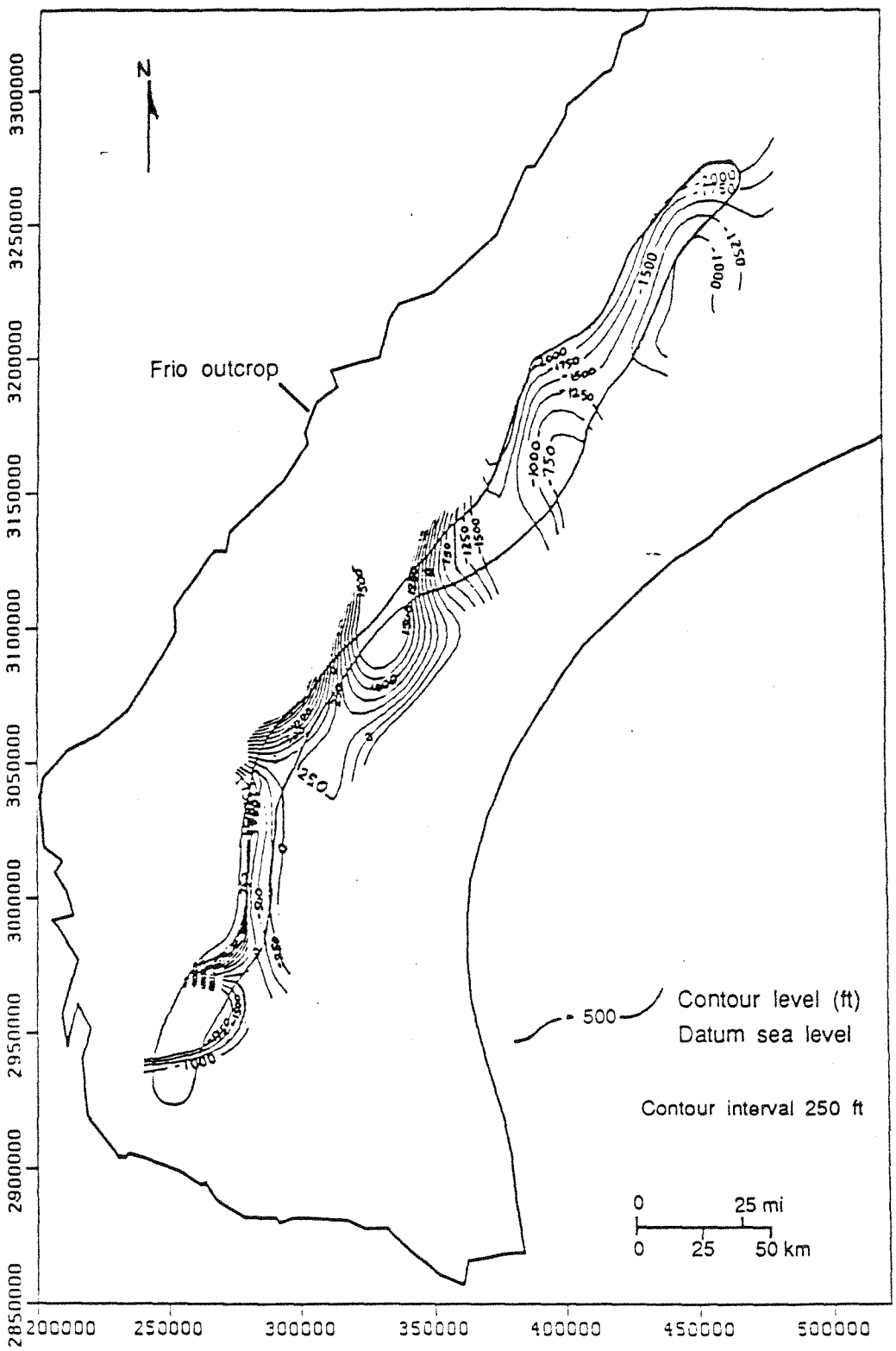

Figure 30. Frio residual potential surface, 6,000-8,000 ft minus 0-2,000 ft slice (8K-2K), all classes, 1975-84 data. Positive contours indicate upward flow, and negative contours indicate downward flow. Heads for 8K surface computed with environmental brine gradient.

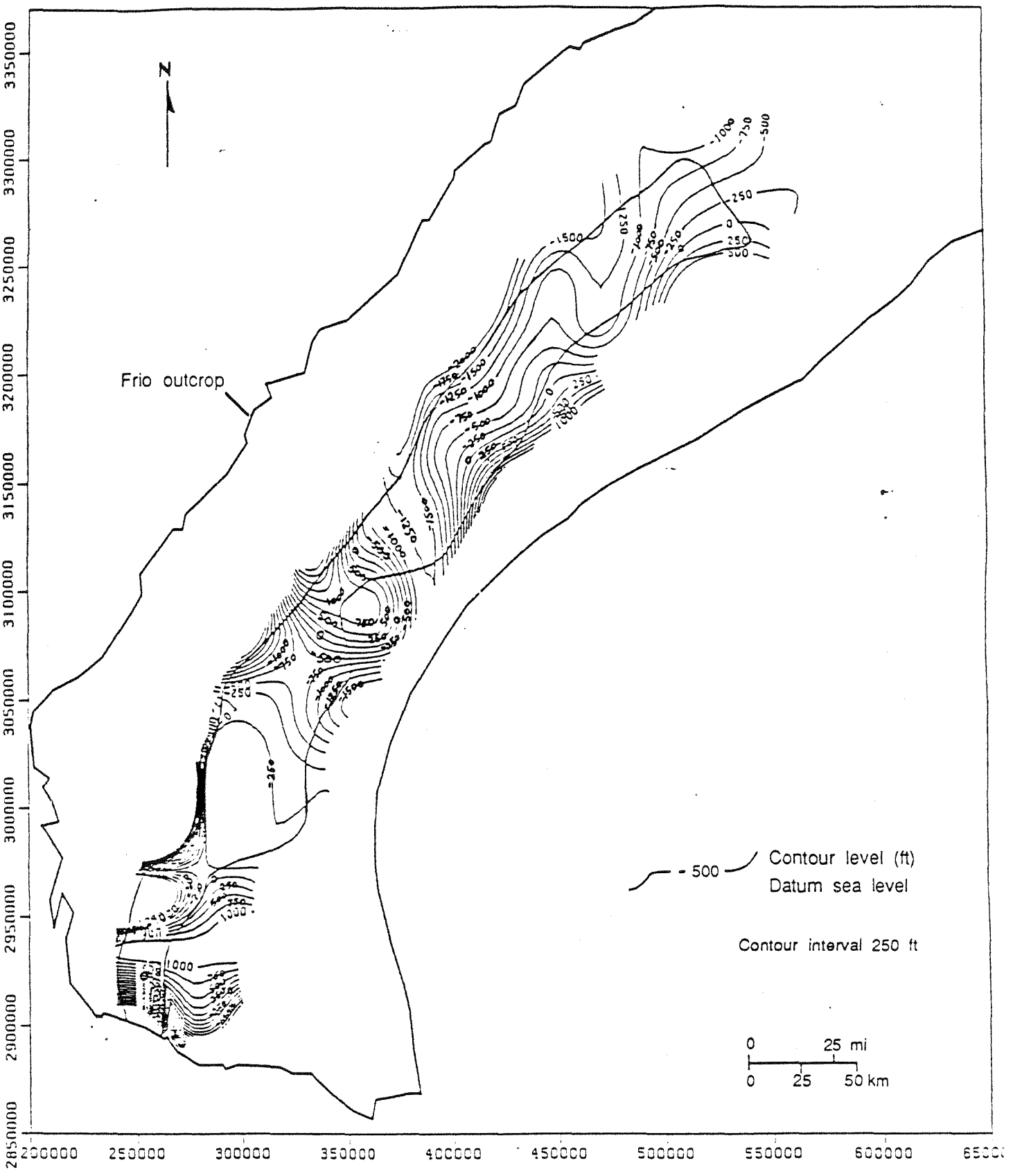

Figure 31. Frio residual potential surface, 6,000-8,000 ft minus 2,000-4,000 ft slice (8K-4K), all classes, 1975-84 data. Positive contours indicate upward flow, and negative contours indicate downward flow. Heads for 8K surface computed with environmental brine gradient.

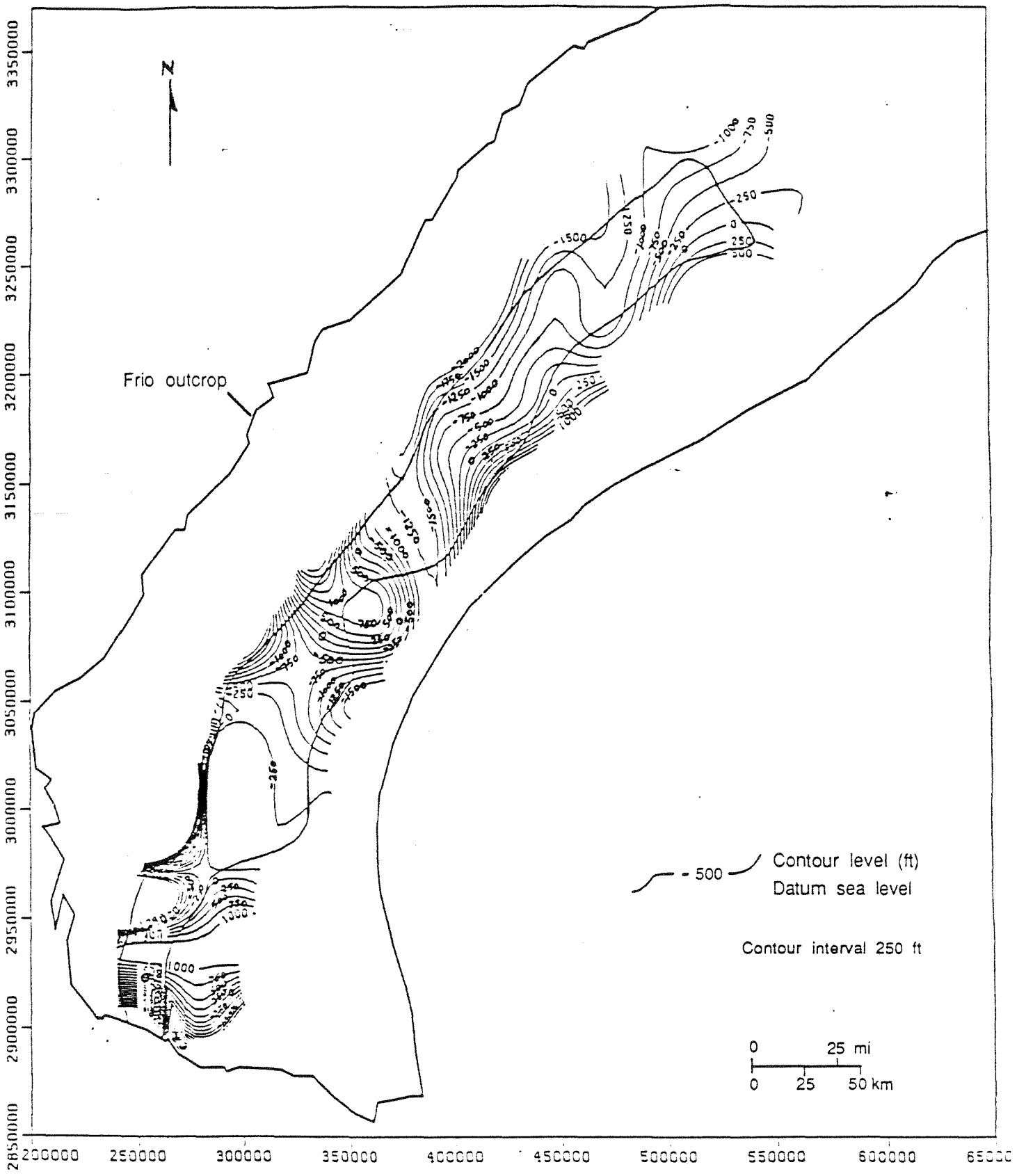

Figure 31. Frio residual potential surface, 6,000-8,000 ft minus 2,000-4,000 ft slice (8K-4K), all classes, 1975-84 data. Positive contours indicate upward flow, and negative contours indicate downward flow. Heads for 8K surface computed with environmental brine gradient.

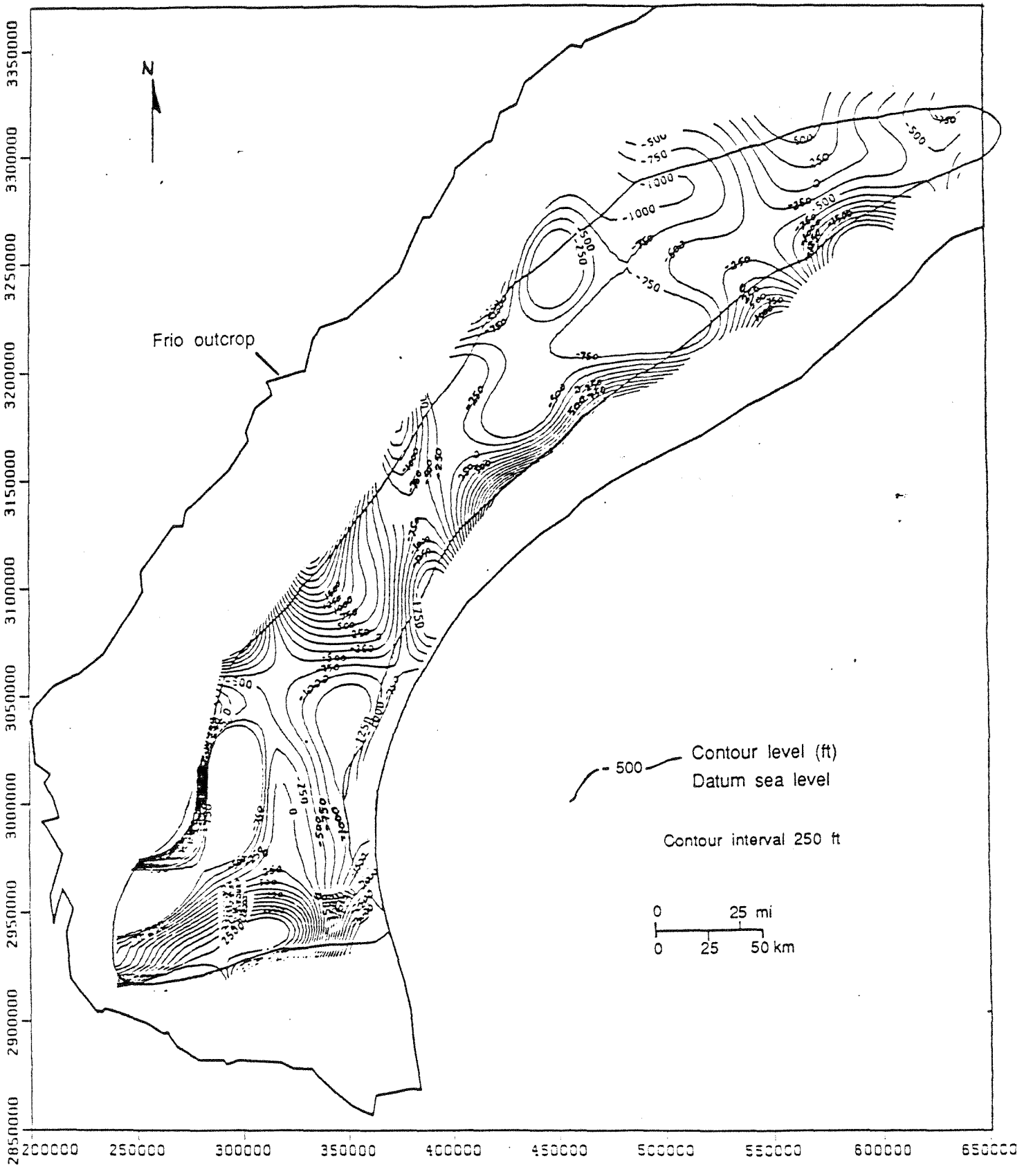

Figure 32. Frio residual potential surface, 6,000-8,000 ft minus 4,000-6,000 ft slice (8K-6K), all classes, 1975-84 data. Positive contours indicate upward flow, and negative contours indicate downward flow. Heads for 8K surface computed with environmental brine gradient.

5. CASE ANALYSIS, VICTORIA COUNTY, TEXAS

As a representative study on a county scale, the pressure data in Victoria County were used for developing pressure-depth plot and potentiometric surfaces.

5.1 Pressure-Depth Plot

All the available pressures in Victoria County were plotted on a pressure-depth plot. The resulting profile in figure 33 is similar in character to the integrated Frio pressure-depth profile (fig. 11). Two trend lines, one for 0.433 psi/ft fresh-water gradient and the other for 0.465 psi/ft brine (with 80,000 ppm salinity), are drawn on the Victoria County plot. Additionally, a scatter of overpressured data and an extended area of depressured conditions are visible on the plot. Figure 34 is a formation brine salinity-depth plot for Victoria County based on data from Kreitler and Richter (1986). It indicates relatively consistent salinities between 60,000 and 80,000 ppm below 4,000 ft. Although salinities from depths shallower than 4,000 ft in Victoria County are not directly available, other data from the middle Gulf Coast Frio Formation reflect values closer to fresh-water environments (Kreitler and Richter, 1986). This observation is also confirmed by the gradient (psi/ft) values computed from individual bottomhole pressures in the PI pressure file. Thus, a correlation of pressure-depth and salinity-depth profiles formed the basis for use of fresh-water gradient in shallow depths and brine gradient in deeper intervals for calculation of equivalent hydraulic heads.

5.2 Potentiometric Surfaces

An integrated potentiometric surface of the entire Frio thickness in Victoria County would presumably be too complex due to the steep gulfward dip of the various components of the Tertiary system. Figure 35 is a simplified isometric view of the structure tops of the Frio, Vicksburg-Jackson, Claiborne, and Wilcox Formations. Analogous to the regional Frio surfaces, horizontal slices were used for constructing potentiometric surfaces in Victoria County. Figures 36 and 37 consist of the posted hydraulic-head values and the resulting potentiometric surface in the 0-2,000-ft depth interval. Pressure data from all Tertiary formations through the years 1965-84 were included in this surface. Relative paucity of Frio data and a need to maintain integrity of the surface necessitated use of the other Tertiary data. Moreover, available formation brine salinity data in this depth interval for all formations suggest a predominantly fresh-water environment; hence, pooling all the pressures and using a 0.433 psi/ft pressure gradient for hydraulic head conversion were considered justifiable.

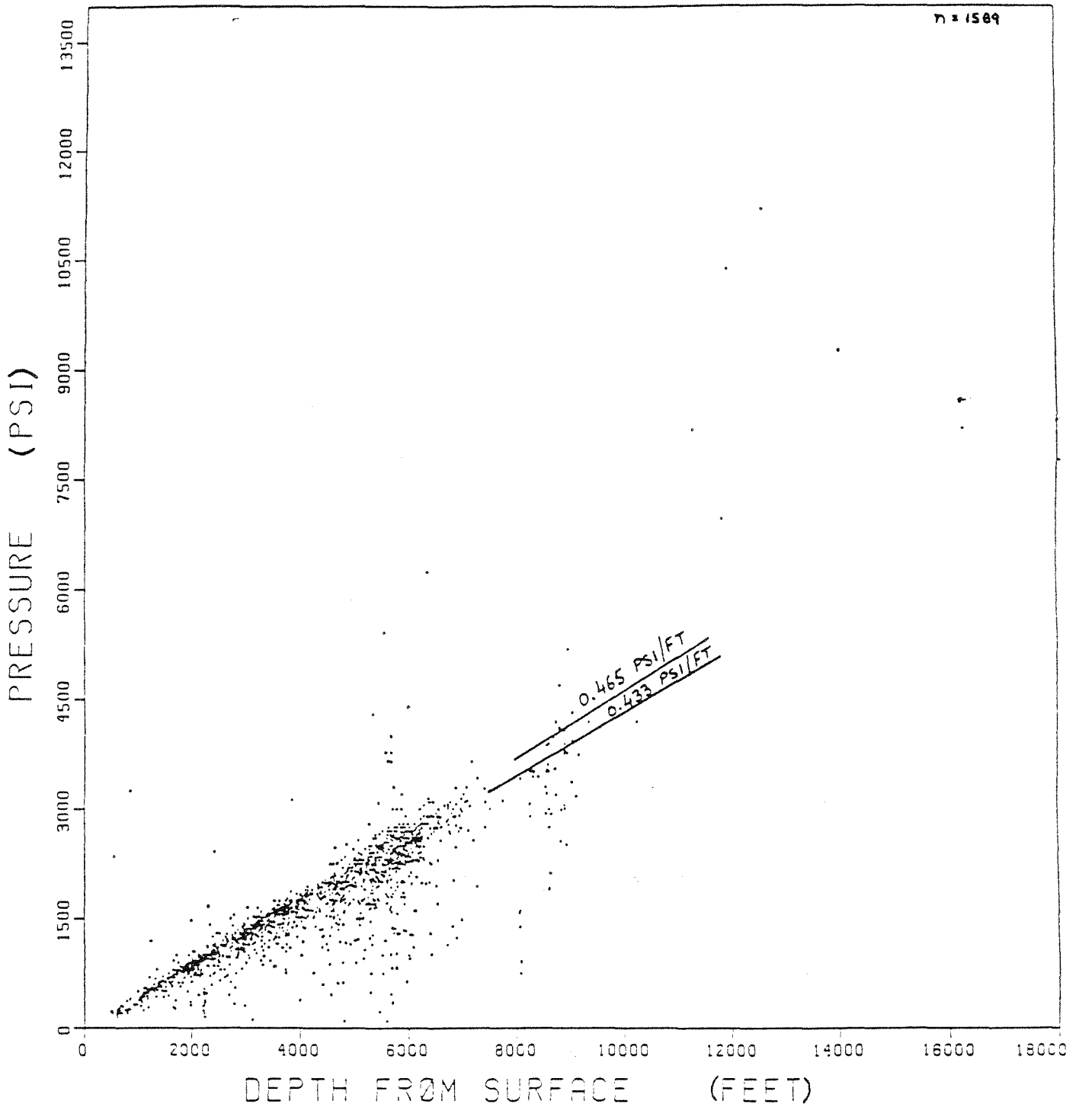

Figure 33. Pressure-depth diagram, Victoria County data.

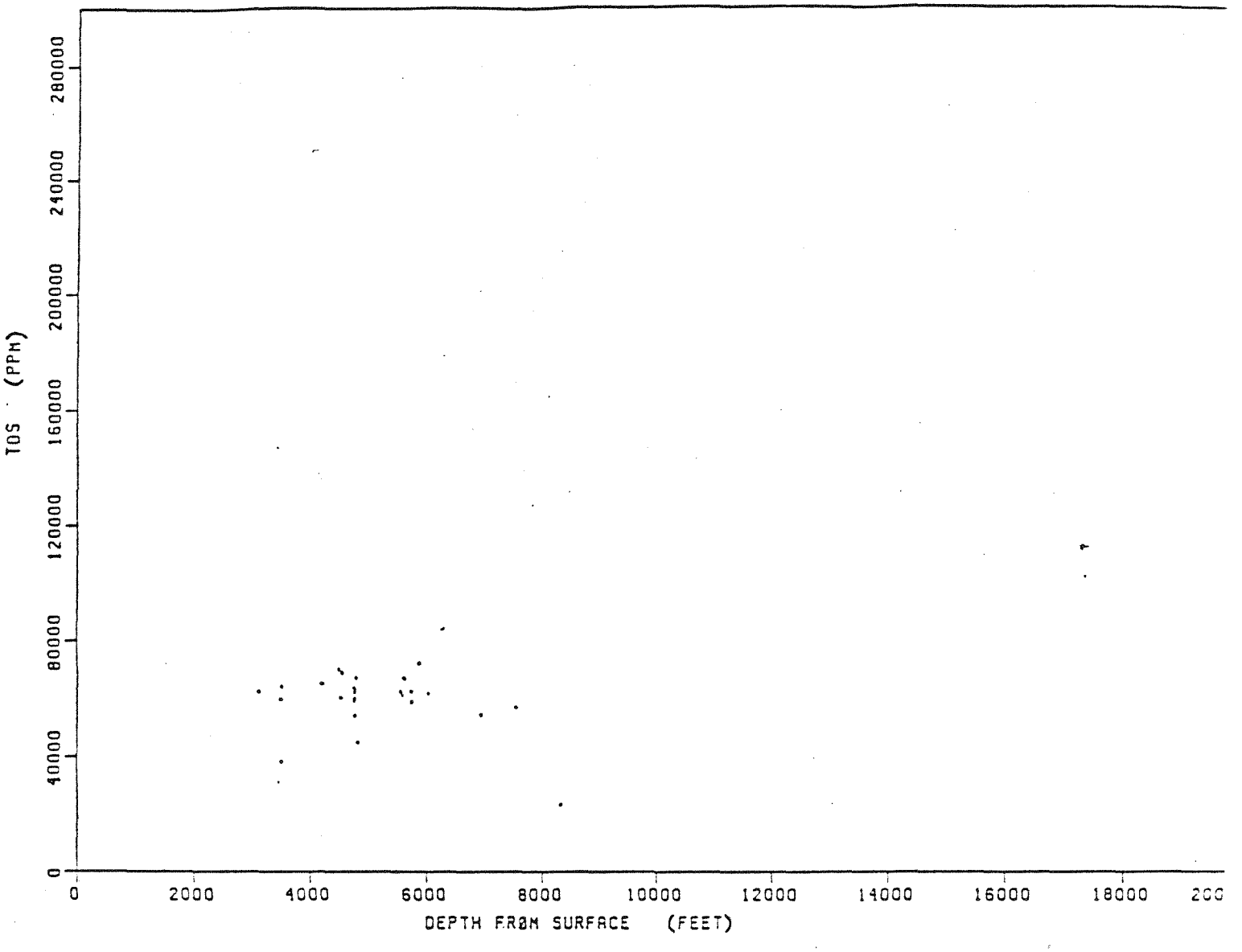

Figure 34. Salinity (total dissolved solids)-depth plot for Tertiary formations in Victoria County (from Kreitler and Richter, 1986).

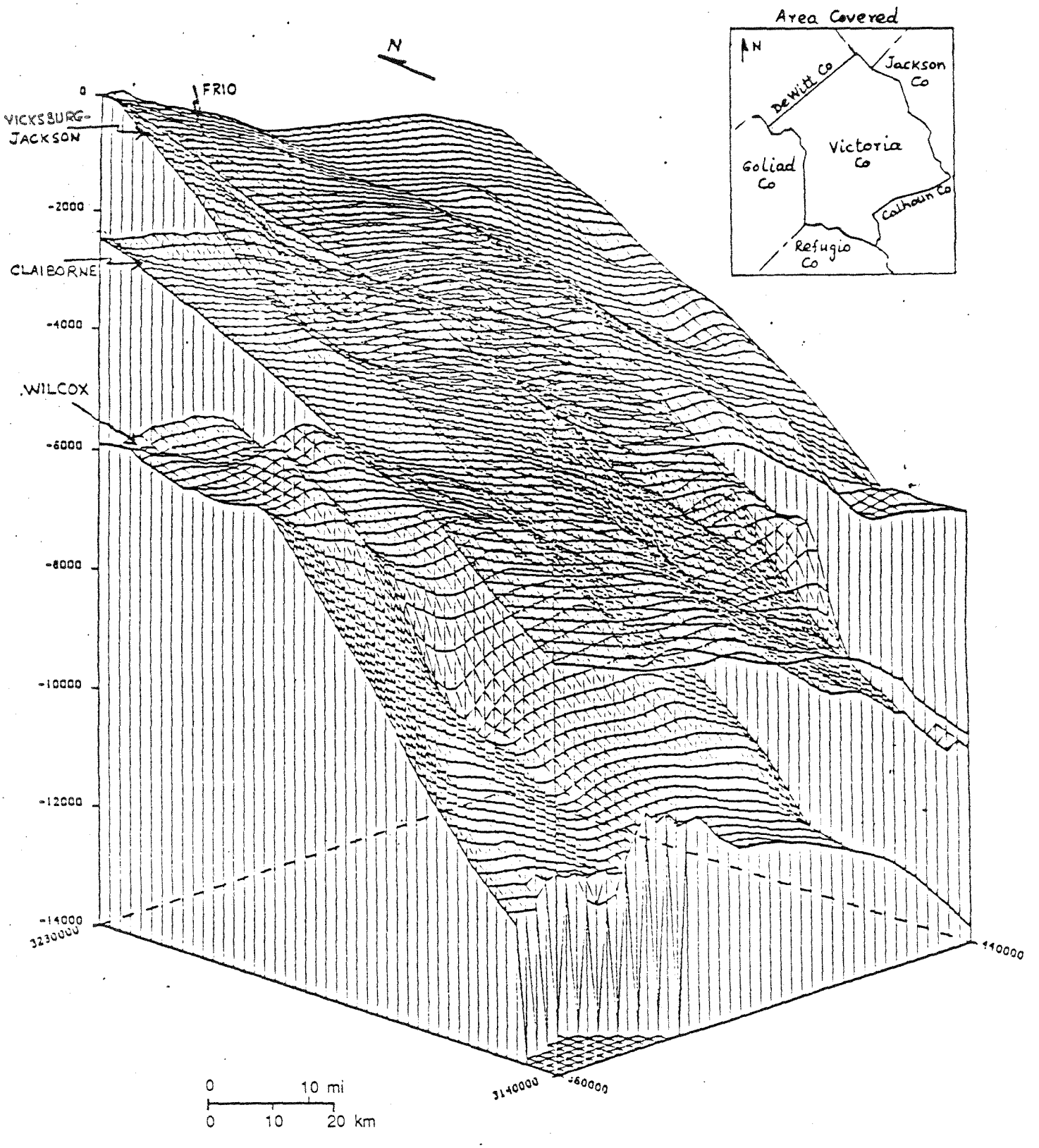

Figure 35. Isometric view of structure tops, Tertiary system, Victoria County. Tops of Frio, Vicksburg-Jackson, Claiborne, and Wilcox Formations (after Dodge and Posey, 1981).

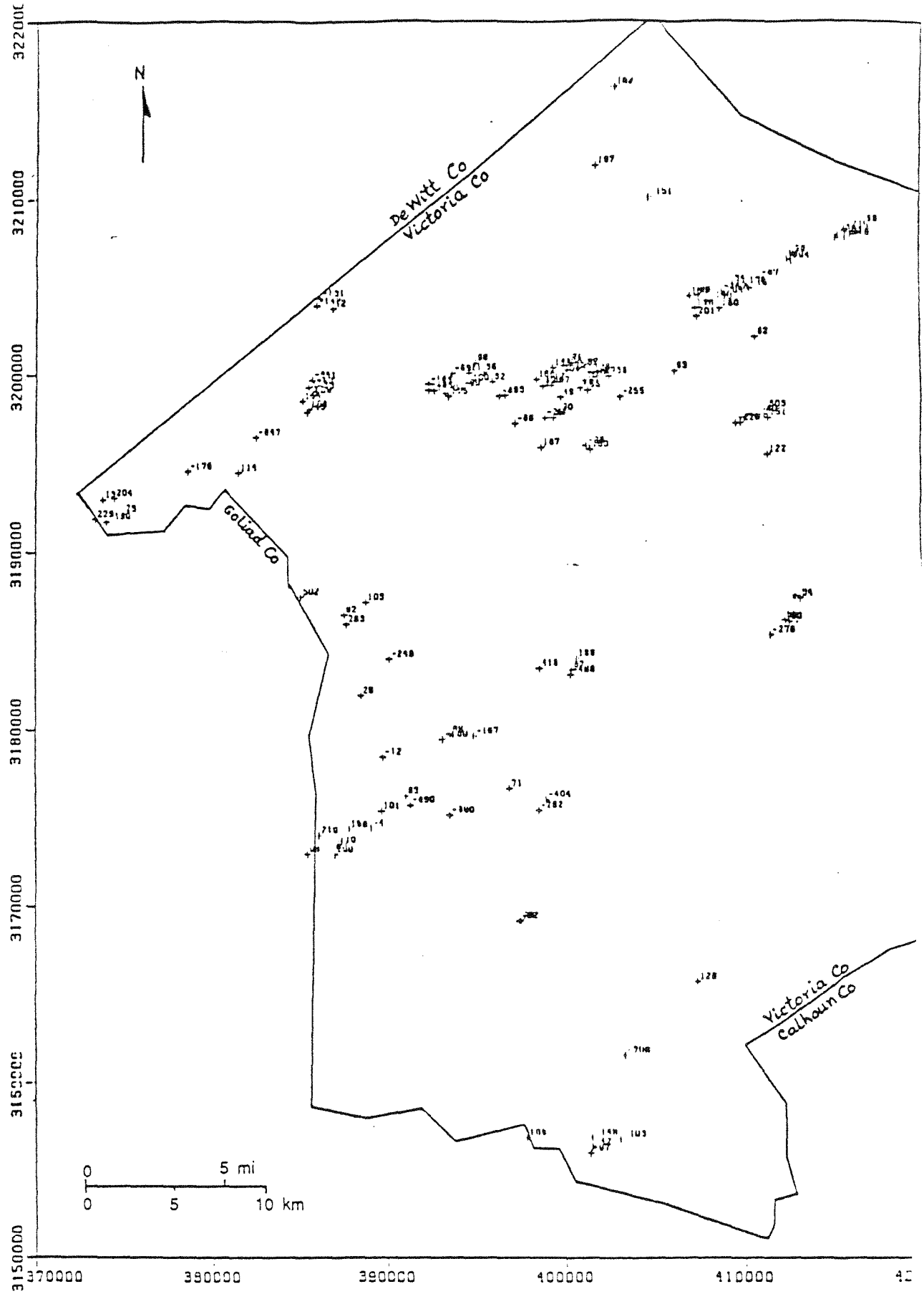

Figure 36. Hydraulic head values, 0-2000 ft horizontal slice, Victoria Co., all formations, all classes, 1965-84 data. Equivalent fresh-water heads.

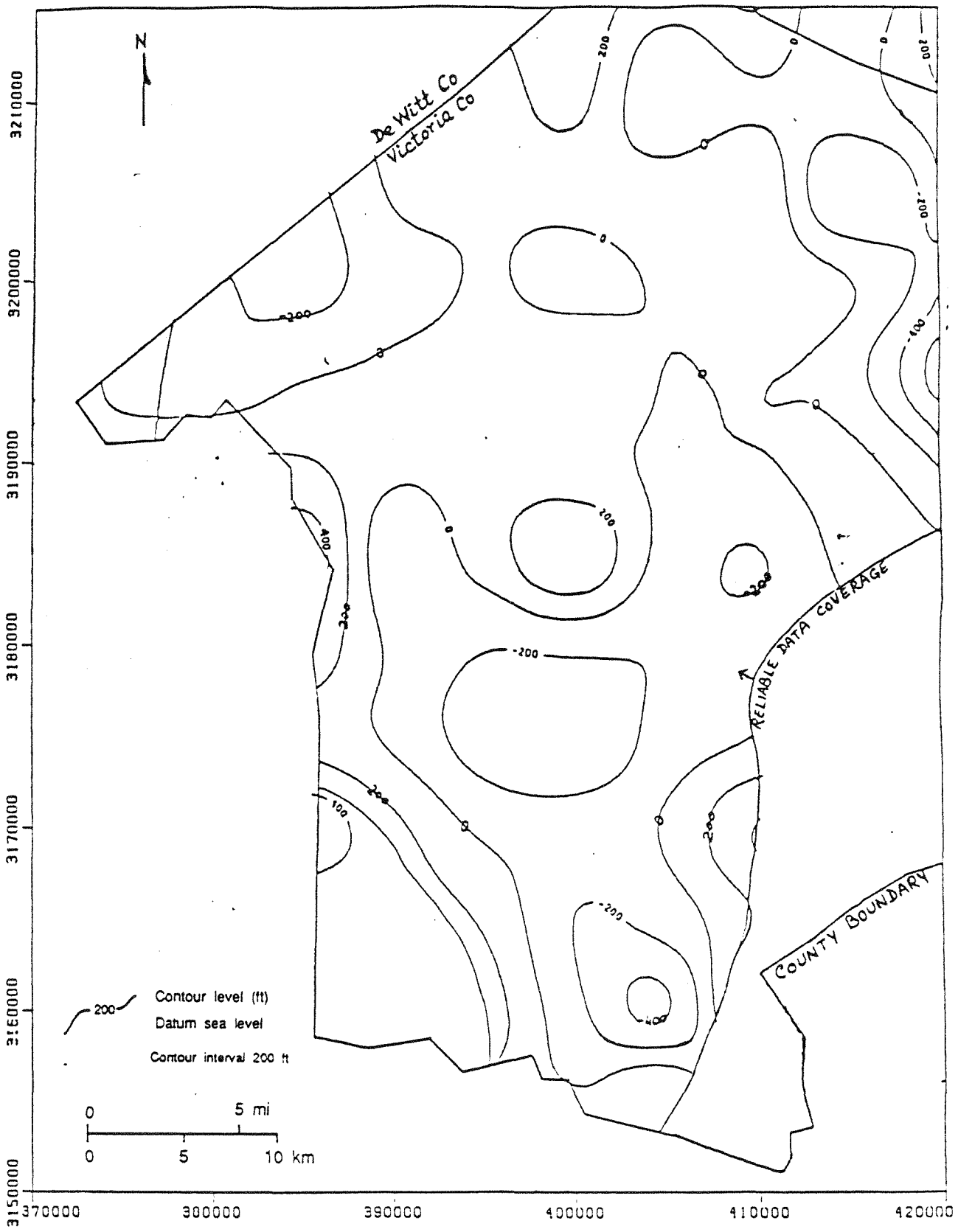

Figure 37. Potentiometric surface, 0-2000 ft slice, Victoria Co., all formations, all classes, 1965-84 data. Equivalent fresh-water heads.

The potentiometric surface for this slice is quite flat, with near-land-surface head values. The county boundary (thick border) and confines of reliable data coverage (thin inner line) are marked in figure 37.

Figures 38 and 39 represent, respectively, the hydraulic head values and the potentiometric surface for the 2,000-4,000-ft depth interval. Pressures from Frio and its updip equivalent, the Catahoula Formation, were screened from the time interval 1965-84, and converted to fresh-water equivalent hydraulic heads. The head values are near land surface, although some depressurization is observed in the central part of the county.

Figure 40 reflects the posted head values for the horizontal slice through the 4,000-6,000-ft depth interval. The corresponding potentiometric surface for this dataset is plotted in figure 41. This dataset encompasses pressures in Frio and Catahoula Formations in 1965-84. A general feature of this plot is the mostly negative contours reflecting depressured conditions. The negative depression is slightly enhanced toward the southeast. Pressure data from the injection wells operated by Du Pont de Nemours (Frank, 1986) were included in this dataset for constructing the potentiometric surface.

Figures 42 and 43 consist of the posted hydraulic-head values and the corresponding potentiometric surface in the 4,000-4,900-ft depth interval, a more restrictive depth range that encompasses the depths of injection by Du Pont. For greater areal coverage this dataset was expanded to include pressures in the Frio and Catahoula Formations in the Tertiary for the years 1945-84. Negative contours are more enhanced in the lower half of this surface. The outline of major oil and gas fields producing from the 4,000-5,000-ft depth range and the location of Du Pont's major deep well injection facility are marked in figure 43. A regional flow trend toward the south and southwest is indicated on this figure. Flow from the injection facility would be south or southwest. Inadequate data control in the immediate vicinity of the injection facility makes it difficult to better define the potentiometric surface in that area. An isometric view of this surface from the southeast is presented in figure 44. This dataset includes the injection formation pressure at Du Pont's facility.

5.3 Residual Surface

For a qualitative definition of vertical flow potential, residual surfaces were created whereby the potentiometric surface in the uppermost interval (0-2,000-ft) was subtracted from the average potentiometric surface in the deeper (4,000-6,000-ft) interval. The 0-2,000-ft potentiometric surface was generated with fresh-water (0.433 psi/ft) equivalent heads, and the 4,000-6,000-ft surface was based on

The potentiometric surface for this slice is quite flat, with near-land-surface head values. The county boundary (thick border) and confines of reliable data coverage (thin inner line) are marked in figure 37.

Figures 38 and 39 represent, respectively, the hydraulic head values and the potentiometric surface for the 2,000-4,000-ft depth interval. Pressures from Frio and its updip equivalent, the Catahoula Formation, were screened from the time interval 1965-84, and converted to fresh-water equivalent hydraulic heads. The head values are near land surface, although some depressurization is observed in the central part of the county.

Figure 40 reflects the posted head values for the horizontal slice through the 4,000-6,000-ft depth interval. The corresponding potentiometric surface for this dataset is plotted in figure 41. This dataset encompasses pressures in Frio and Catahoula Formations in 1965-84. A general feature of this plot is the mostly negative contours reflecting depressured conditions. The negative depression is slightly enhanced toward the southeast. Pressure data from the injection wells operated by Du Pont de Nemours (Frank, 1986) were included in this dataset for constructing the potentiometric surface.

Figures 42 and 43 consist of the posted hydraulic-head values and the corresponding potentiometric surface in the 4,000-4,900-ft depth interval, a more restrictive depth range that encompasses the depths of injection by Du Pont. For greater areal coverage this dataset was expanded to include pressures in the Frio and Catahoula Formations in the Tertiary for the years 1945-84. Negative contours are more enhanced in the lower half of this surface. The outline of major oil and gas fields producing from the 4,000-5,000-ft depth range and the location of Du Pont's major deep well injection facility are marked in figure 43. A regional flow trend toward the south and southwest is indicated on this figure. Flow from the injection facility would be south or southwest. Inadequate data control in the immediate vicinity of the injection facility makes it difficult to better define the potentiometric surface in that area. An isometric view of this surface from the southeast is presented in figure 44. This dataset includes the injection formation pressure at Du Pont's facility.

5.3 Residual Surface

For a qualitative definition of vertical flow potential, residual surfaces were created whereby the potentiometric surface in the uppermost interval (0-2,000-ft) was subtracted from the average potentiometric surface in the deeper (4,000-6,000-ft) interval. The 0-2,000-ft potentiometric surface was generated with fresh-water (0.433 psi/ft) equivalent heads, and the 4,000-6,000-ft surface was based on

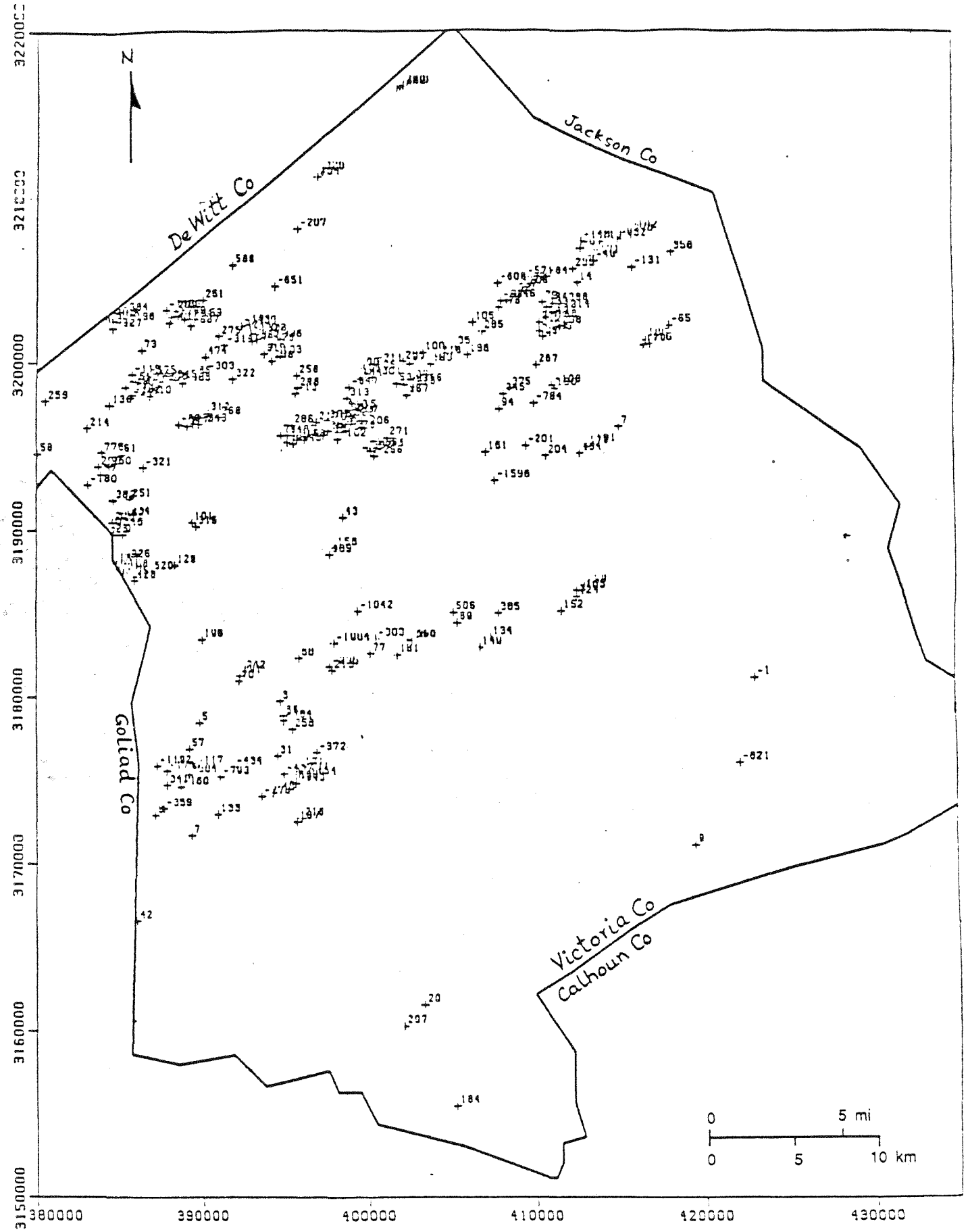

Figure 38. Hydraulic head values, 2,000-4,000 ft horizontal slice, Victoria Co., Frio and Catahoula, all classes, 1965-84 data. equivalent fresh-water heads.

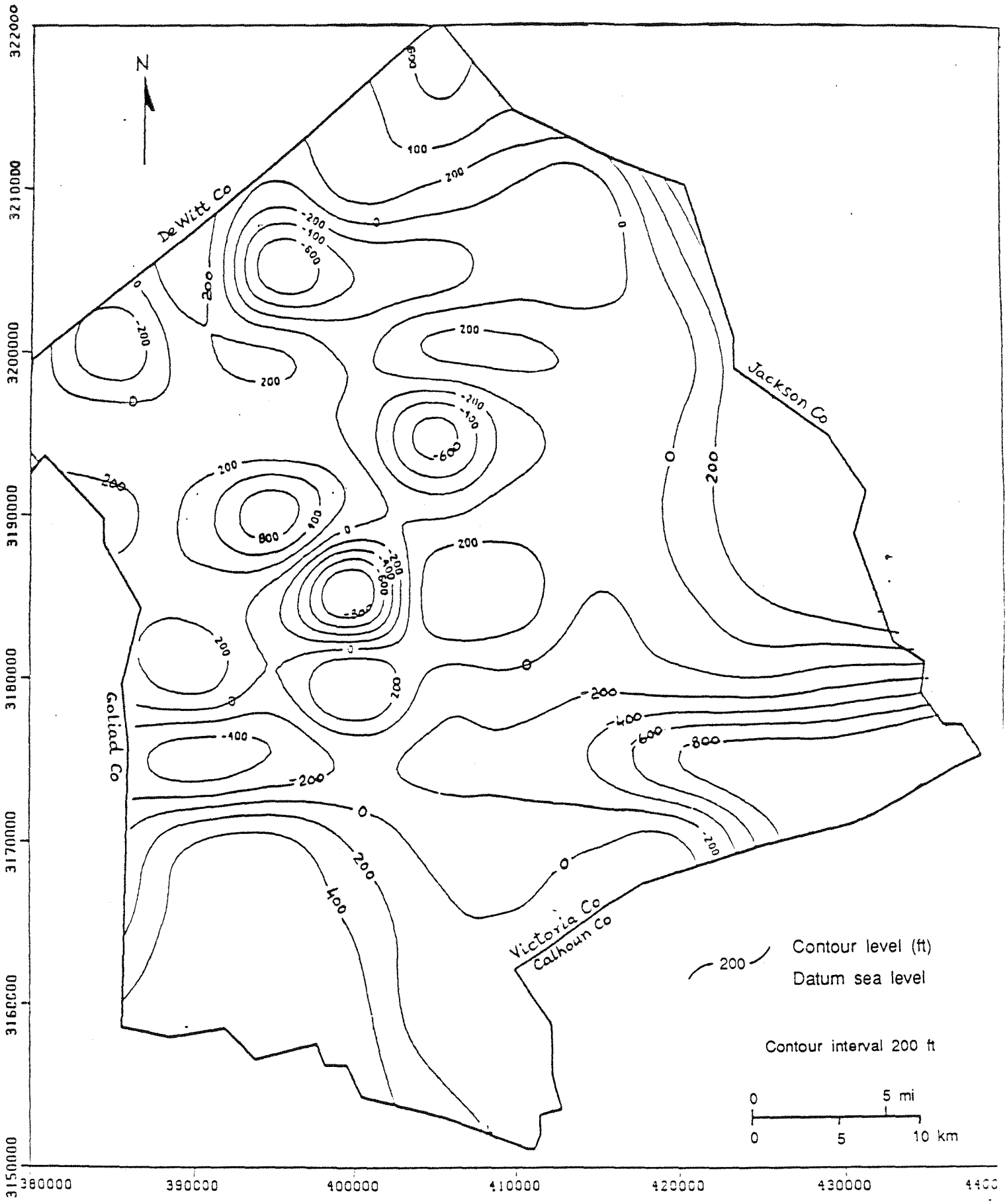

Figure 39. Potentiometric surface, 2,000-4,000 ft horizontal slice, Victoria Co., Frio and Catahoula, all classes, 1965-84 data. Equivalent fresh-water heads.

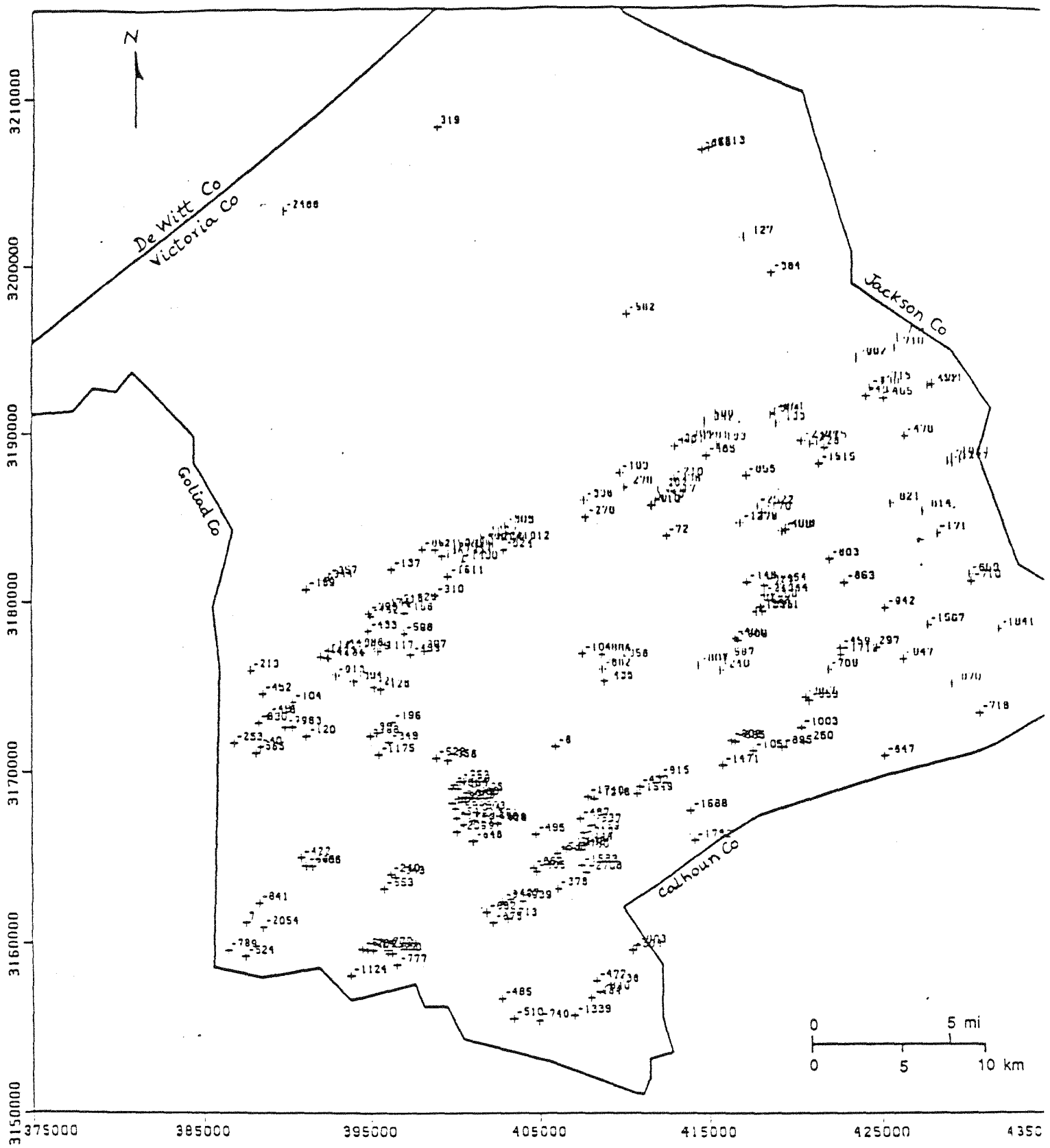

Figure 40. Hydraulic head values, 4,000-6,000 ft horizontal slice, Victoria Co., Frio Formation, all classes, 1965-84 data. Include formation pressure at Du Pont facility. Equivalent brine heads.

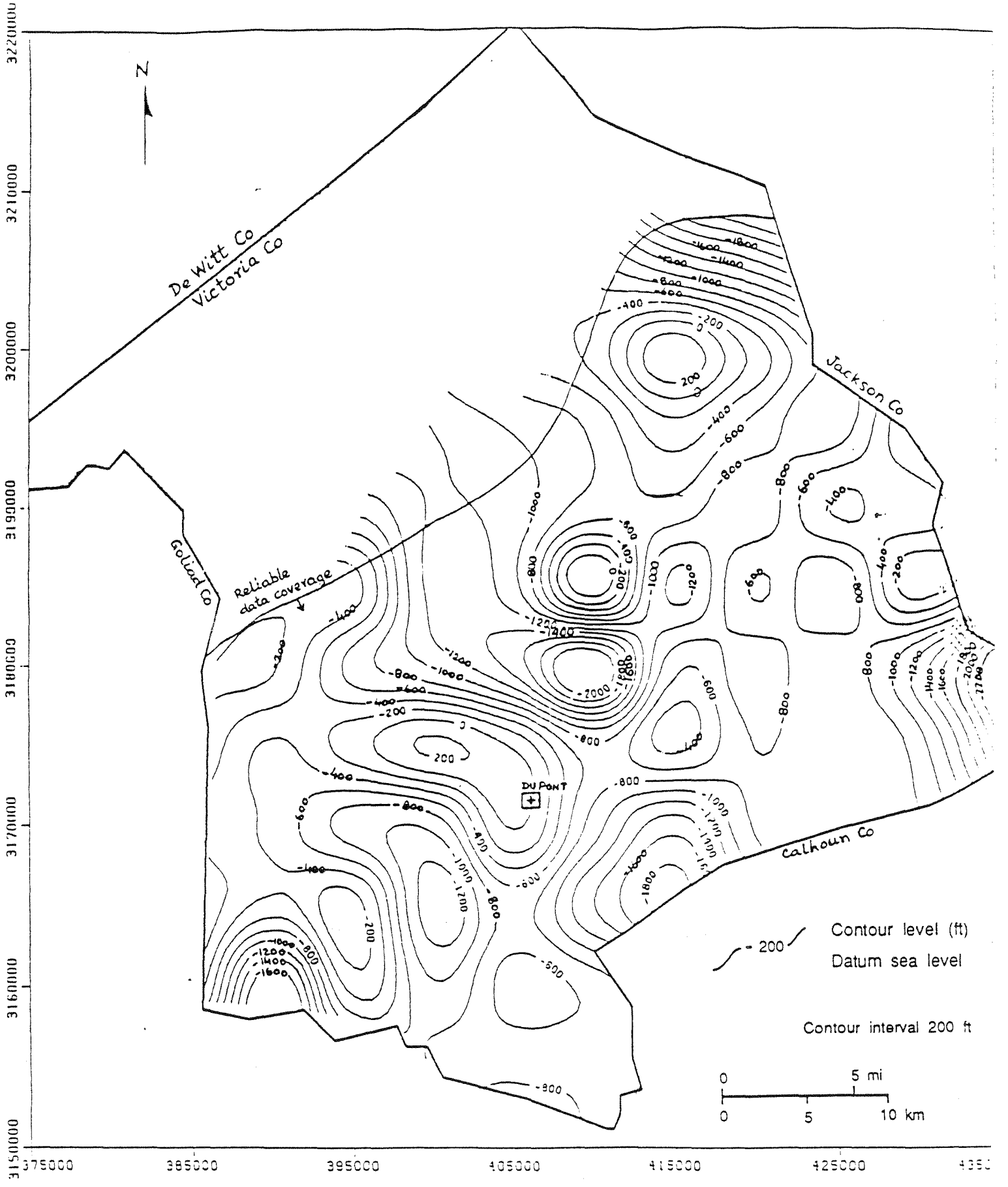

Figure 41. Potentiometric surface, 4,000-6,000 ft slice, Victoria Co., Frio Formation, all classes, 1965-84 data. Includes formation pressure at Du Pont facility. Equivalent brine heads.

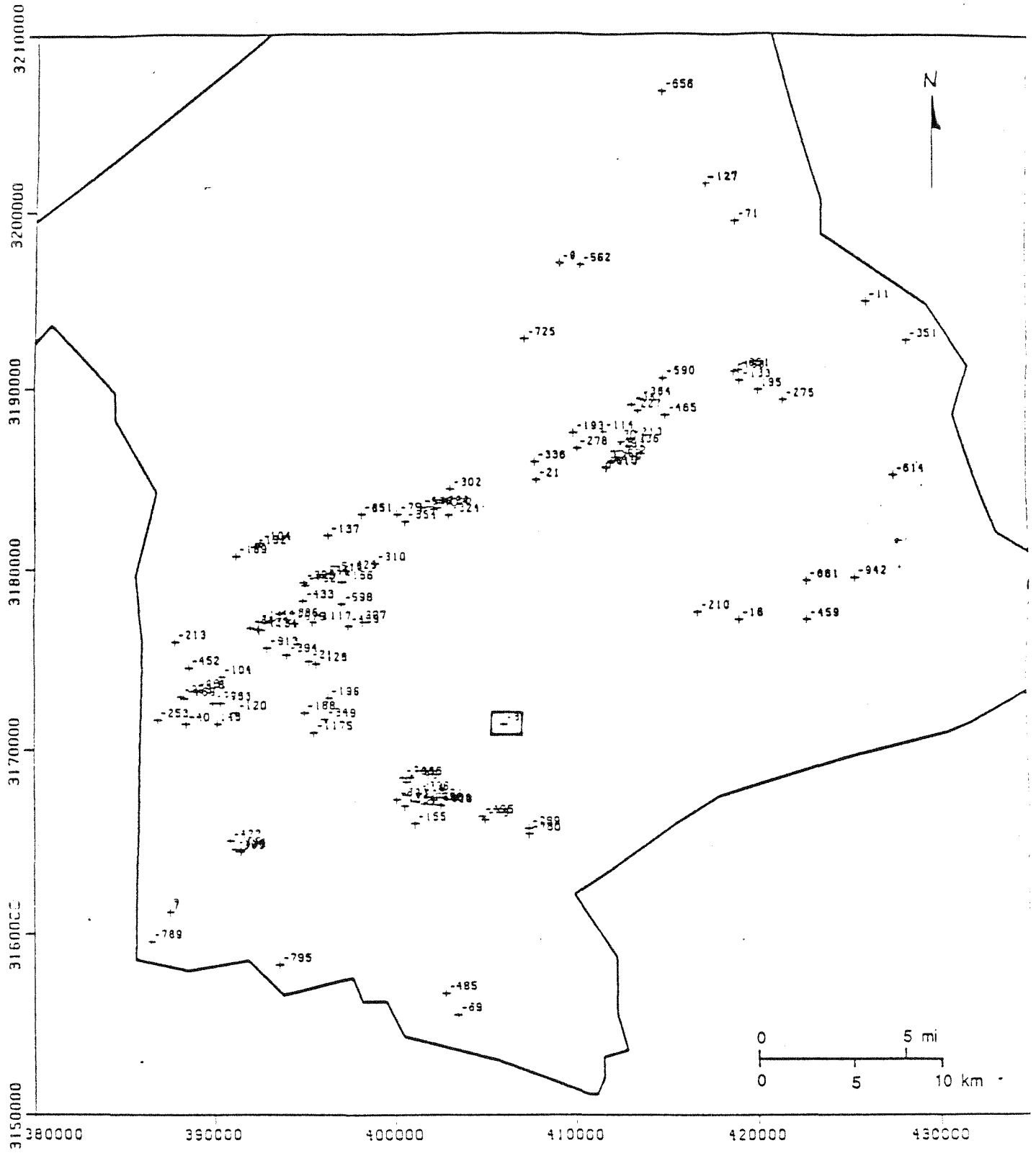

Figure 42. Hydraulic head values, 4,000-4,900 ft slice, Victoria Co., Frio and Catahoula, all classes, 1945-84 data. Includes formation pressure at Du Pont facility. Equivalent brine heads.

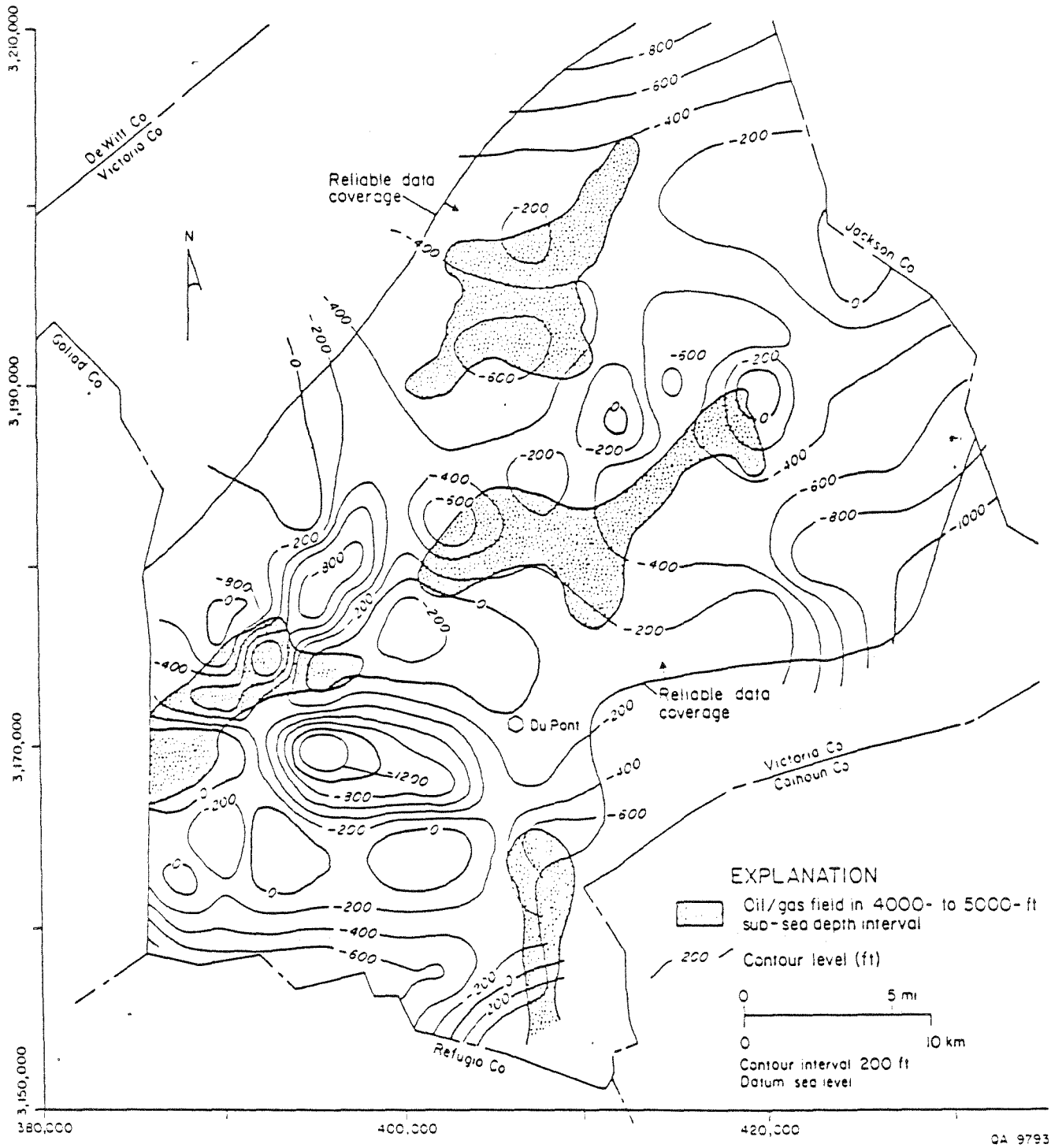

Figure 43. Potentiometric surface, 4,000-4,900 ft slice, Victoria Co., Frio and Catahoula, all classes, 1945-84 data. Includes formation pressure at Du Pont facility. Equivalent brine heads.

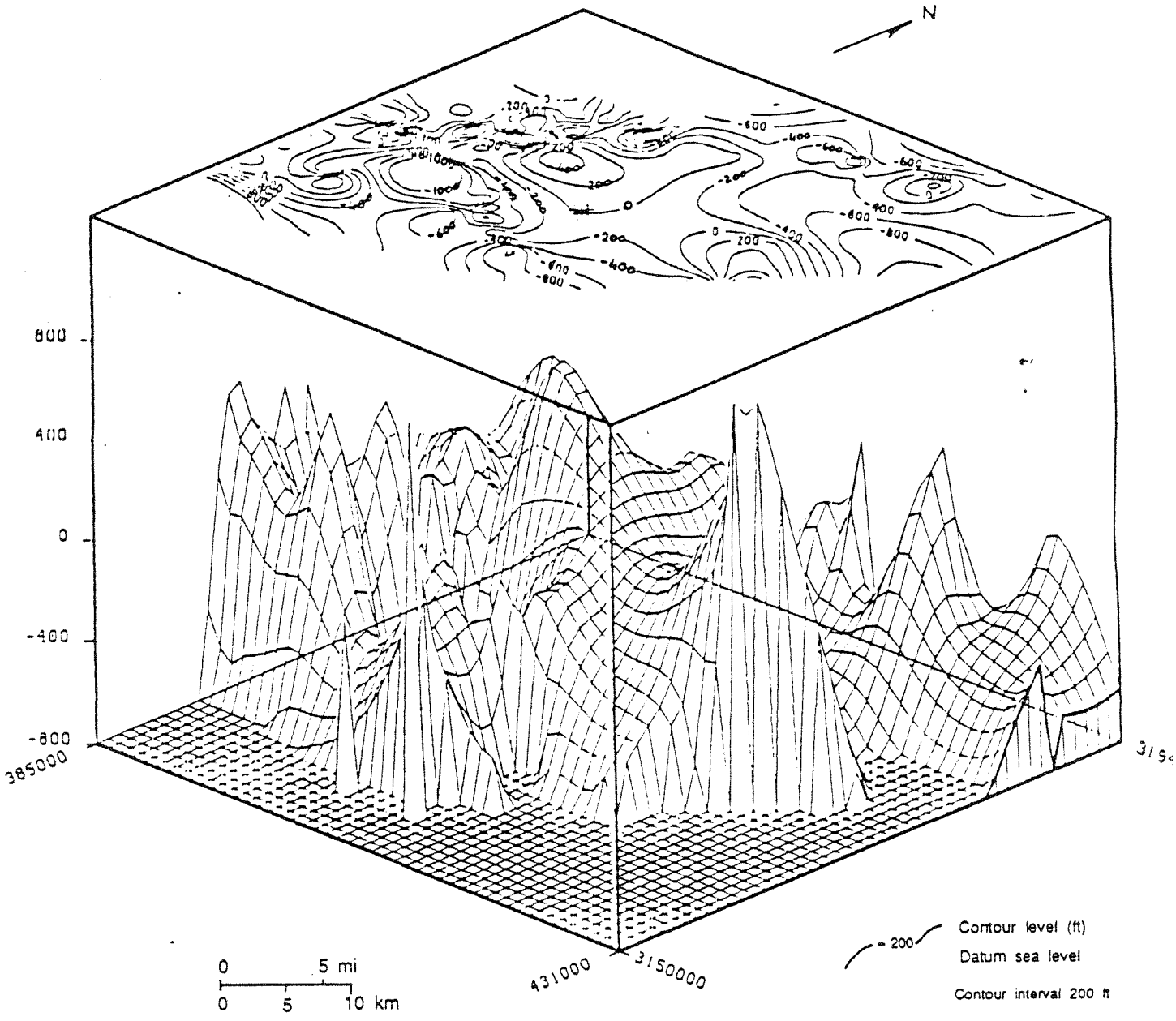

Figure 44. Isometric view of potentiometric surface, 4,000-4,900 ft slice, Victoria Co., Frio and Catahoula, all classes, 1945-84 data. Includes formation pressure at Du Pont facility. Equivalent brine heads.

equivalent brine heads (0.465 psi/ft). This residual surface is plotted in figure 45 in the plan view and in figure 46 in an isometric view. The residuals are all negative, implying a flow potential in the downward direction, that is, toward the deeper interval. This logically follows from the underpressured environment in the deeper zone. The 4,000-6,000-ft interval has historically been the target of the most oil and gas development.

6. DISCUSSION--PHYSICAL HYDROLOGY

6.1 Regional Trends

The pressure-depth profiles reflect the existence of two hydrologic systems in the Frio. Hydrostatic and subhydrostatic pressures exist in the depth interval above 10,000 ft. This is overlapped by an overpressured system observed as shallow as 6,000 ft. Extensive oil and gas development seems to have caused large-scale depressurization and resulted in subhydrostatic pressures within the productive plays of the Frio. The overpressures at shallow depths indicate two possibilities: (1) there is compactional disequilibrium in an environment of restricted drainage in the shallow depth range of the hydrostatic system, and/or (2) brines from deeper geopressured zones are leaking upward into the shallower hydrostatic section.

Grossly overpressured and underpressured aberrant data that did not match surrounding values were culled to refine the potentiometric surfaces. Still, within regional context there are numerous depressured areas and frequent reversals of flow direction to make definition of regional flow trends very difficult. Identifying flow potential on a local scale with better definition of pressures in the vicinity of injection sites is made possible by using the county maps.

6.2 Victoria County Hydrologic Trends

The potentiometric surfaces in the predominantly fresh to moderately saline environment (0-4,000-ft interval) are quite flat. Effect of depressurization is felt in the deeper intervals. In the context of chemical waste injection, this implies that injected fluids in the deep subsurface under existing hydrologic regimes would be constrained from migrating upward, but they possess a greater potential for lateral migration. Alteration of hydrologic conditions, however, could change this scenario. For example, massive localized fluid injection could raise the formation pressures and hydraulic heads sharply and develop vertically upward potential gradients.

The Victoria County residual surface map needs to be integrated with a structure map that locates faults and salt domes, and with a deep-well/abandoned-borehole

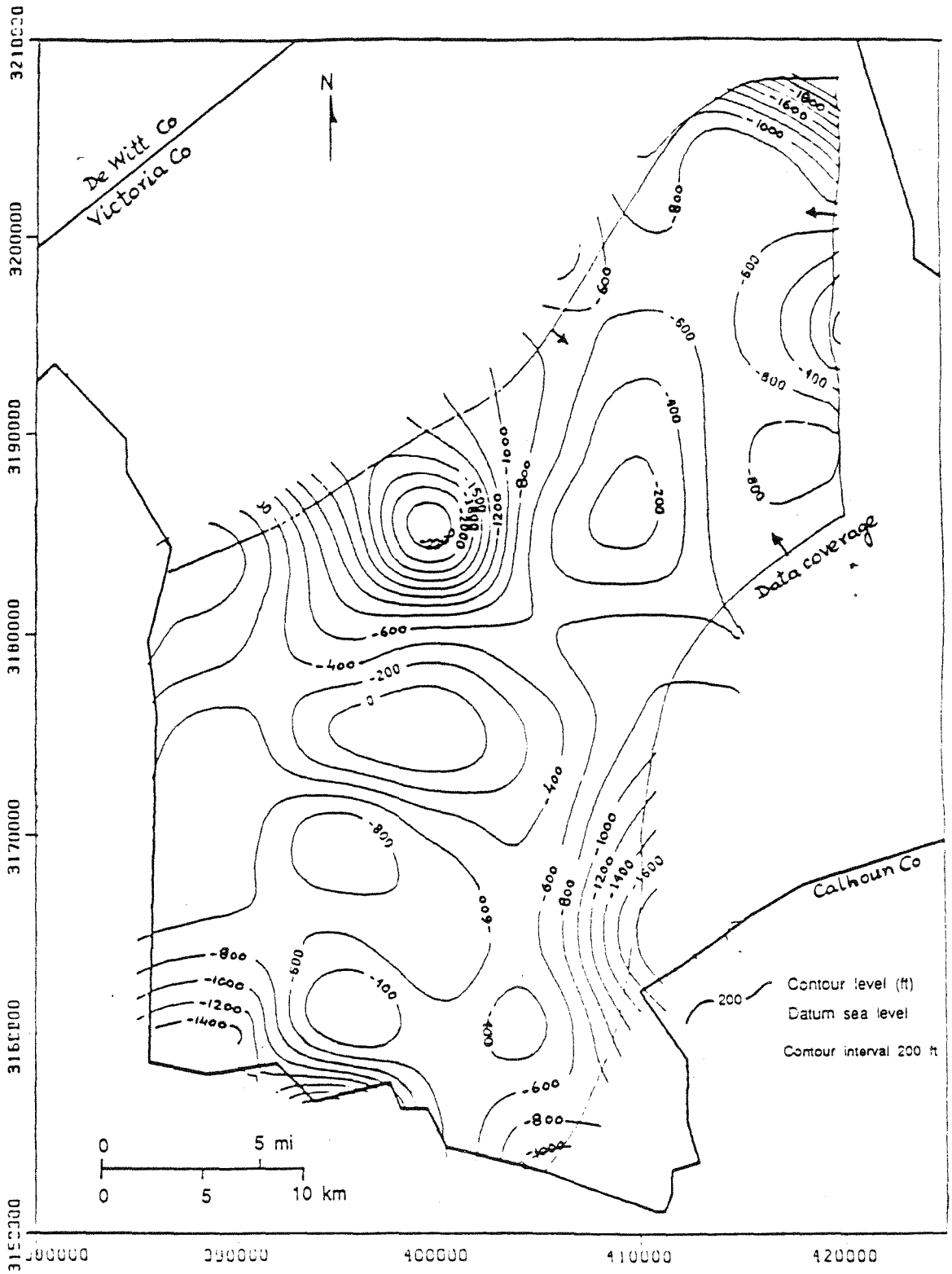

Figure 45. Residual potential surface, 4,000-6,000 ft (Frio) minus 0-2,000 ft (Miocene) slice, Victoria Co., all classes, 1965-84 data. Negative contours indicate downward flow. The 4,000-6,000 ft surface generated with equivalent brine heads.

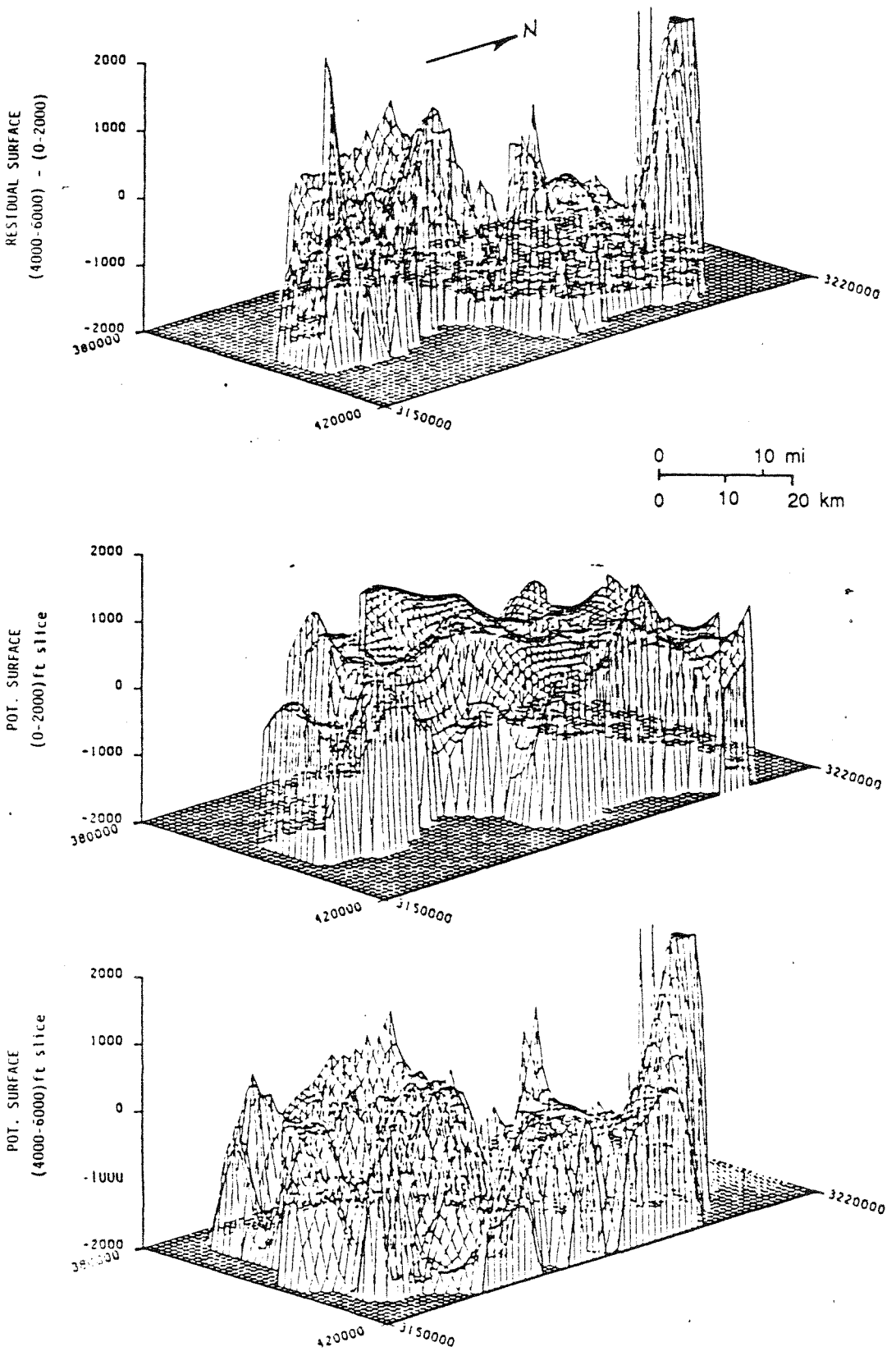

Figure 46. Isometric view of residual potential surface, 4,000-6,000 ft minus 0-2,000 ft slice, Victoria Co., all formations, all classes, 1965-85 data. Positive contours indicate upward flow, and negative contours indicate downward flow. The 4,000-6,000 ft surface generated with equivalent brine heads.

map. Such integrated maps will present a comprehensive picture of permeability pathways as well as the direction for potential flow.

6.3 Reservoir Parameters and Fluid Velocities

Table 1 summarizes some of the hydrologic parameters of the Texas Gulf Coast Tertiary formations, retrieved from various hydrologic reports submitted by injectors of hazardous chemical wastes to regulatory authorities during the permitting process.

Table 1: Hydrologic properties of Tertiary formations in injection zones (from Knape, 1984; PI Corp. data).

Aquifer	Average injection depth (ft)	Average porosity (%)	Permeability (md)
Undifferent. Miocene	5,100	31	300-1,800
Frio	6,700	31	200-1,200
Yegua	4,200	26	200-500
Catahoula	4,450	30	400-800
Oakville	3,850	30	500-1,300
Wilcox	6,500	25	100-600

Figure 47 represents the permeability distribution in the 4,000-6,000-ft-depth interval for Texas Gulf Coast Tertiary formations. These values (included in square brackets) reflect results of core analyses or pressure tests conducted by well operators in the injection intervals, and mostly lie in the 200-2000 millidarcy (md) range. Other values marked on figure 47 were computed from drillstem test pressure data retrieved from the PI file, and are predominantly from the oil and gas bearing sands. Figure 48 locates flow gradients in the 4000-6000-ft Frio interval in different regions used for calculating fluid flow velocities. The average linear flow velocities in horizontal direction (product of average permeability and flow gradient, divided by average porosity) were computed in three different regions (A, B, and C) in the 4000-6000-ft interval and are summarized in table 2.

map. Such integrated maps will present a comprehensive picture of permeability pathways as well as the direction for potential flow.

6.3 Reservoir Parameters and Fluid Velocities

Table 1 summarizes some of the hydrologic parameters of the Texas Gulf Coast Tertiary formations, retrieved from various hydrologic reports submitted by injectors of hazardous chemical wastes to regulatory authorities during the permitting process.

Table 1: Hydrologic properties of Tertiary formations in injection zones (from Knape, 1984; PI Corp. data).

Aquifer	Average injection depth (ft)	Average porosity (%)	Permeability (md)
Undifferent. Miocene	5,100	31	300-1,800
Frio	6,700	31	200-1,200
Yegua	4,200	26	200-500
Catahoula	4,450	30	400-800
Oakville	3,850	30	500-1,300
Wilcox	6,500	25	100-600

Figure 47 represents the permeability distribution in the 4,000-6,000-ft-depth interval for Texas Gulf Coast Tertiary formations. These values (included in square brackets) reflect results of core analyses or pressure tests conducted by well operators in the injection intervals, and mostly lie in the 200-2000 millidarcy (md) range. Other values marked on figure 47 were computed from drillstem test pressure data retrieved from the PI file, and are predominantly from the oil and gas bearing sands. Figure 48 locates flow gradients in the 4000-6000-ft Frio interval in different regions used for calculating fluid flow velocities. The average linear flow velocities in horizontal direction (product of average permeability and flow gradient, divided by average porosity) were computed in three different regions (A, B, and C) in the 4000-6000-ft interval and are summarized in table 2.

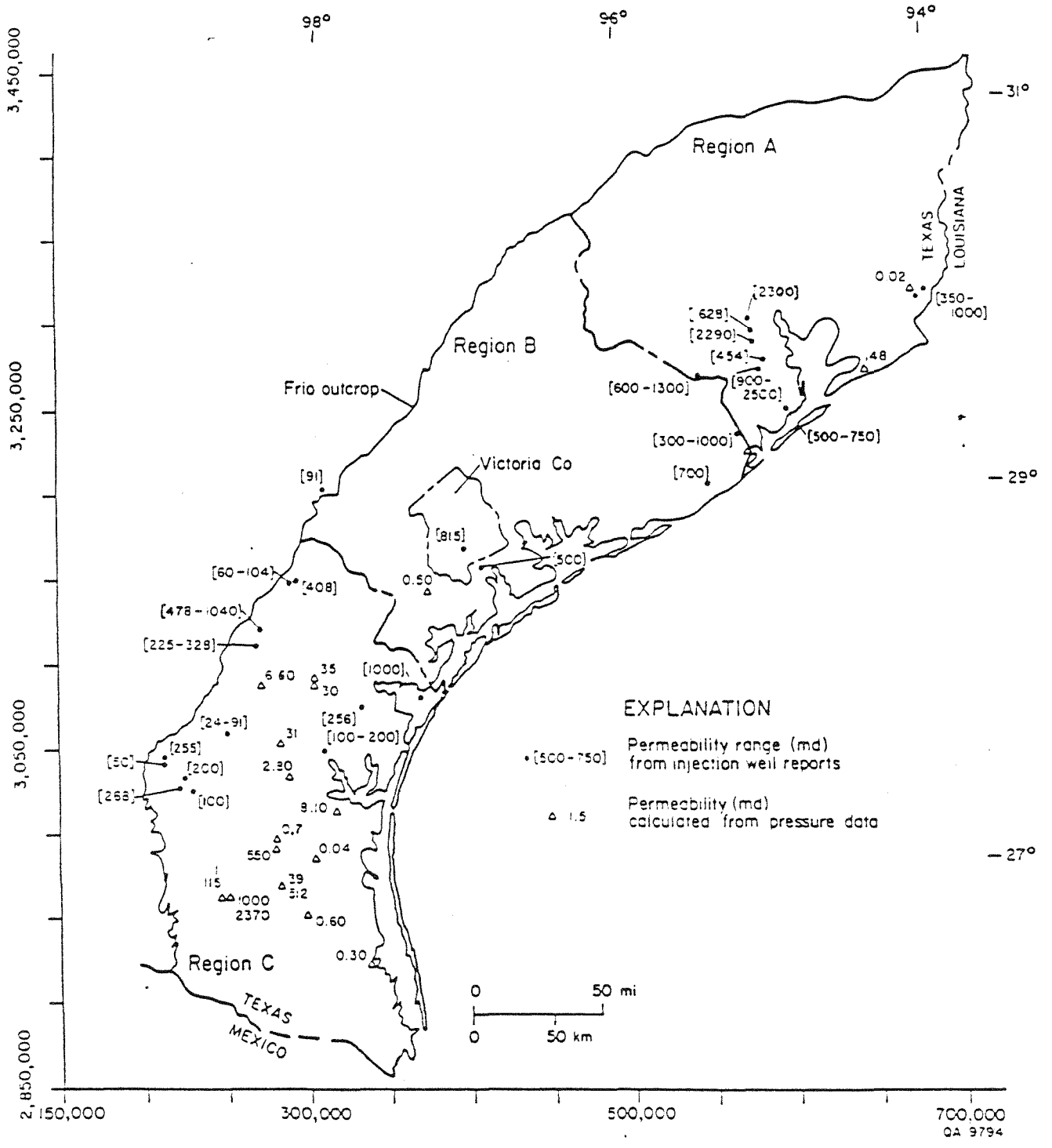

Figure 47. Permeability distribution in Texas Gulf Coast Tertiary formations, 4,000-6,000 ft interval, summarized from injection-well completion reports and computed from PI Corp. pressure data.

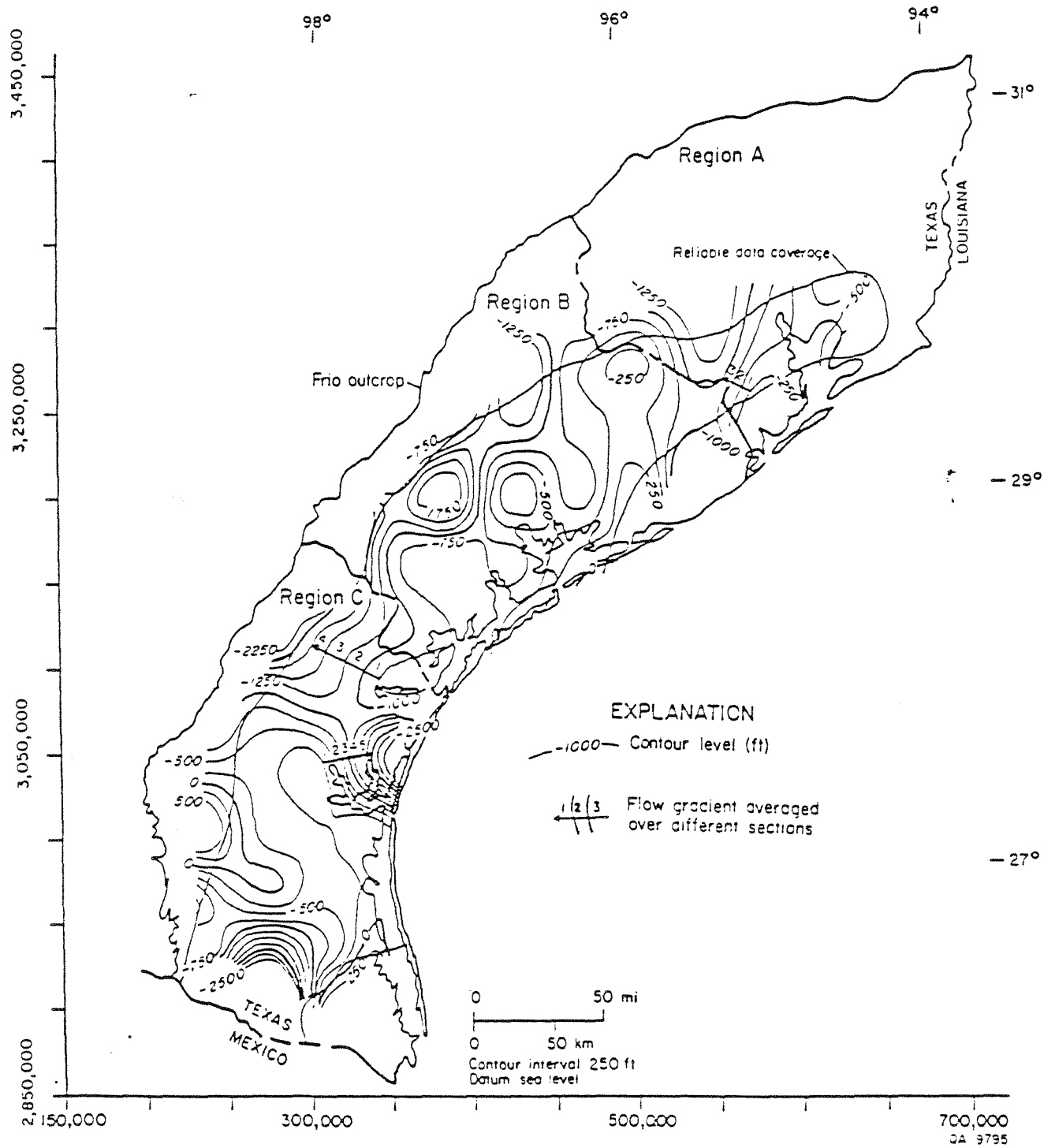

Figure 48. Location of average flow gradients in the 4,000-6,000 ft interval, Frio Formation, Texas Gulf Coast. Potentiometric surface generated with equivalent brine heads.

Table 2. Average horizontal linear velocities in 4,000-6,000-ft depth interval.

Region	Flow gradient (dimensionless)	Porosity (%)	Permeability (ft/yr)	Avg. linear velocity (ft/yr)
A	0.0141	31	300	13.7
	0.0141	31	2300	104.6
B	0.0063	31	0.5	0.01
	0.0063	31	800	16.3
C	0.0167	31	3.0	0.2
	0.0167	31	1000	53.9

Thus, the average horizontal linear velocities range from 0.01 ft/yr to 105 ft/yr in regions with moderate flow gradients. These values are based on oil and gas formation pressures and reflect more realistically the flow potential toward moderately depressurized fields. In instances of extreme depressurization, these velocities can be several times higher. For a better estimate of flow velocities from an injection zone toward an oil field, additional pressure distribution in the injection area is required.

6.4 Sensitivity of Potentiometric Surfaces to Data Selection and Fluid Density

The classification and screening system applied to the dataset allowed a more objective evaluation of the potentiometric surfaces. Surfaces were constructed with the highest confidence data (classes A, B, and Z) and were compared with surfaces for the same depth range and area resulting from all the pooled data (classes A, B, C, and D). The differences in these surfaces were analyzed and attributed to intra-class variance for a better explanation of some of the local variations in flow trends. This was helpful in culling some aberrant data from the dataset. Depressured and overpressured data introduce localized reversals in flow direction that do not fit a smooth regional trend but that must be considered a realistic reflection of existing conditions. Elimination of exceptionally high or low hydraulic heads relative to the surrounding values from the dataset resulted in more realistic regional surfaces. In instances of multiple head values for the same well location, the highest class and highest head value were retained. Averaging of data values is an artifact of the contouring software CPS-1, and the resultant contours reflect the dominating trend from a group of high and low values within a selected grid cell. The potentiometric surfaces for horizontal slices are considered representative of the regional trends because, on the one hand, they are not complicated by the extremes of highs and

lows resulting from a mixing of depressured and overpressured data from different depths, and on the other hand they preserve the local variations in flow directions and hydraulic gradients.

A good example of the sensitivity of potentiometric surfaces to data screening is the 4,000-4,900-ft slice in Victoria County. The surface in figure 43 was constructed after eliminating some extreme high and low heads and including data for only the Frio and Catahoula Formations. This surface is mostly flat and has near-land-surface head values, except in the south and southwest parts where cones of depression exist. The data in figure 49 include these extreme head values (identified within circled areas) and also include heads for other Tertiary formations. The resulting potentiometric surface in figure 50 exhibits greater localized highs and lows. Both these surfaces were constructed with brine equivalent heads (0.465 psi/ft gradient) and include an estimated pressure at Du Pont's injection site (Frank, 1986). Inclusion of non-Frio data is not as critical as the extreme values that are aberrant to local pressures. These extremes represent localized conditions without extensive lateral and vertical equilibration, and their exclusion results in a more average representative potentiometric surface.

Sensitivity of the potentiometric surface to fluid density is demonstrated in figure 51 in the 4,000-4,900-ft slice, Victoria County. This surface is based on equivalent hydraulic heads computed with a fluid gradient of 0.433 psi/ft (fresh water). The surface in figure 51 exhibits characteristics similar to those of the surface in figure 43 (both are for the 4,000-4,900-ft slice), except that the contours in the 0.433 gradient surface (fig. 51) are higher by 150-200 ft than the corresponding contours in the 0.465 gradient surface (fig. 43). Use of correct gradient (0.433 or 0.465) is critical to mapping potentiometric and residual surfaces and is based on availability of formation-brine-chemistry data.

This discussion of the sensitivity of the potentiometric surfaces highlights the need to examine the dataset very carefully, bearing in mind all the local variations possible within the context of the various pressure regimes.

6.5 Implications of Depressurization

The Frio Formation in the Gulf Coast has produced over 20 billion boe (barrels of oil equivalent) of hydrocarbons in the past 50 years of exploration and development. This appears to have led to extensive depressurization. In the 4,000-8,000-ft-depth interval, pressures have declined in some areas by as much as 1,000 psi from the original hydrostatic level. This is equivalent to a decline of more than 2,000 ft in the hydraulic heads. Depressurization may be beneficial in that the leakage of injected fluids up faults into shallow aquifers may be impeded. However,

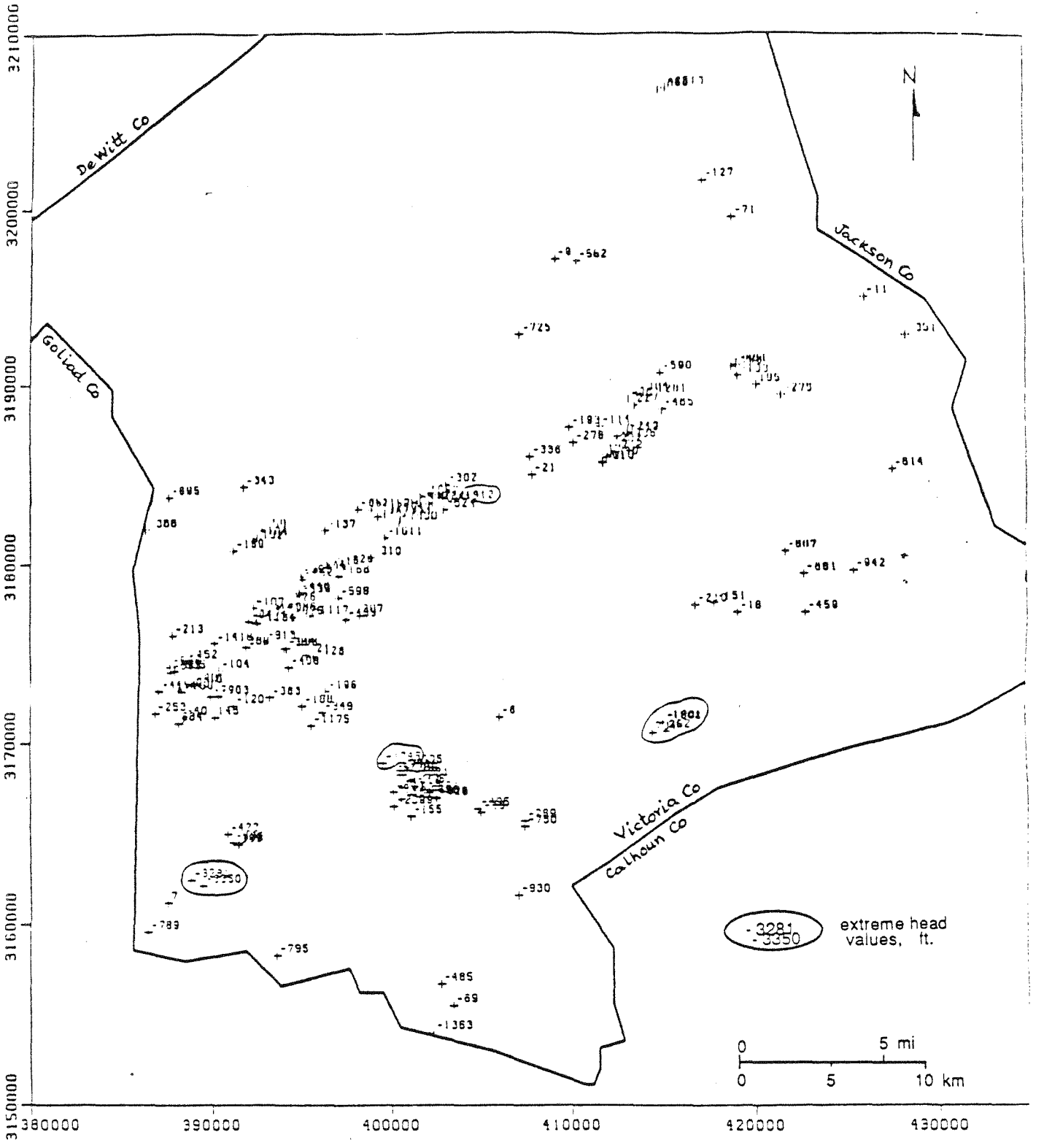

Figure 49. Hydraulic head values, 4,000-4,900 ft slice, Victoria Co., with 0.465 gradient, include extreme head values, all classes, Frio and Catahoula, 1945-84 data. Includes formation pressure at Du Pont facility.

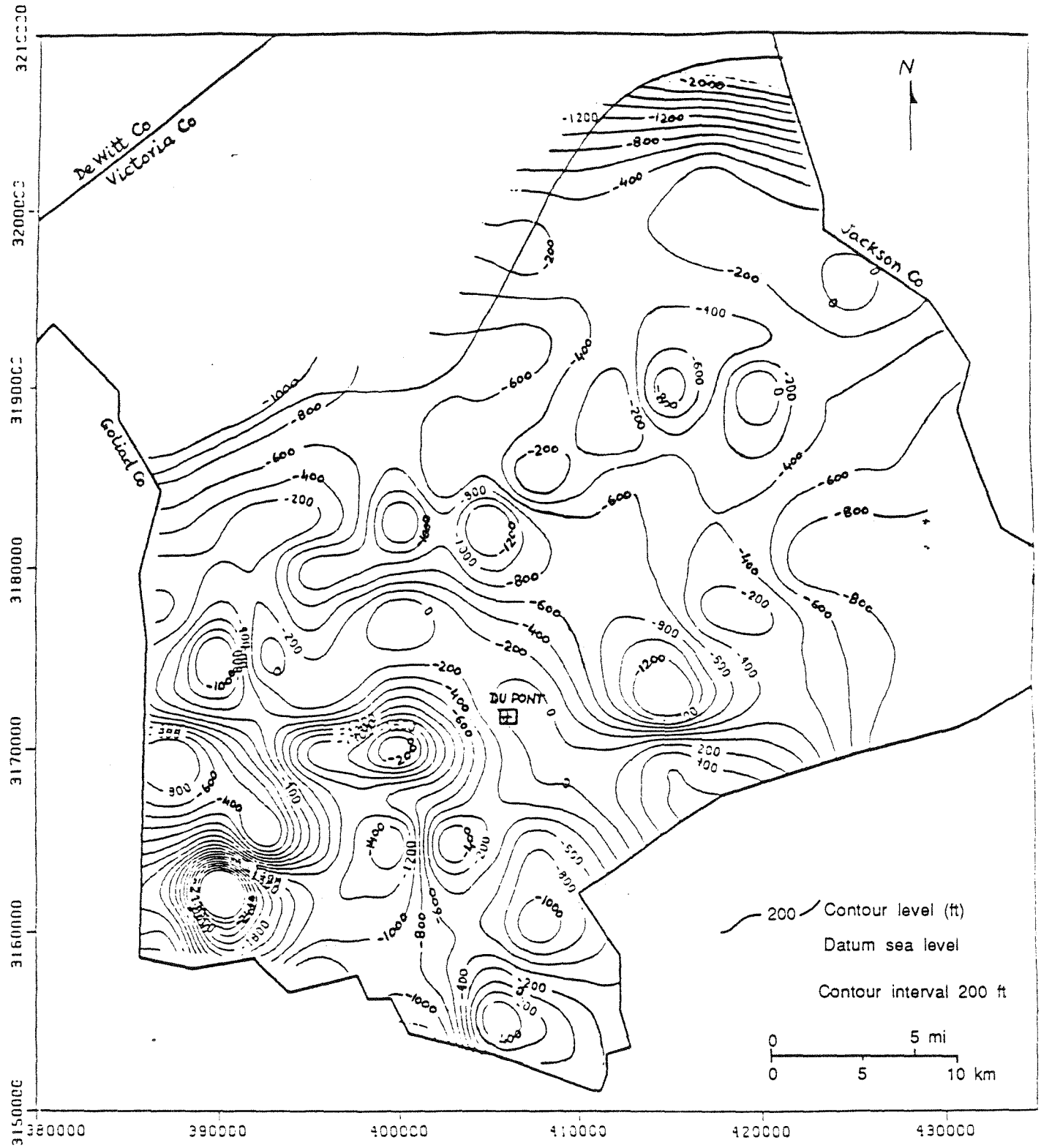

Figure 50. Potentiometric surface, 4,000-4,900 ft slice, Victoria Co., with 0.465 gradient, includes extreme heads, all classes, all formations, 1945-84 data. Includes formation pressure at Du Pont facility.

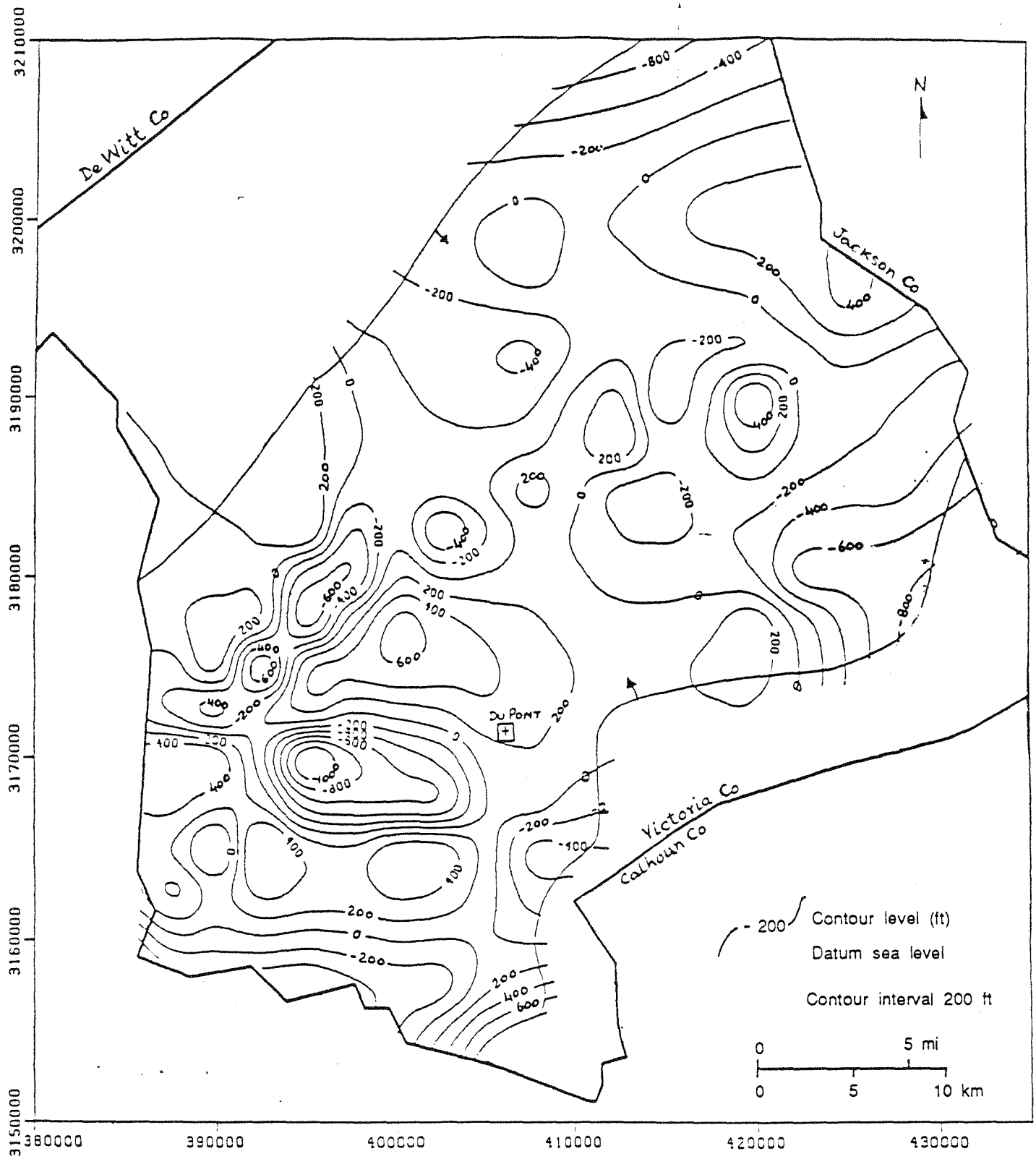

Figure 51. Potentiometric surface, 4,000-4,900 ft slice, Victoria Co., with 0.433 gradient, Frio and Catahoula, all classes, 1945-84 data. Includes formation pressure at Du Pont facility.

the negative effect could be that oil fields may become the ultimate sinks for these wastes. This problem could be compounded by the presence of numerous improperly abandoned wells in old depleted fields. The steep hydraulic gradients and high permeability of Frio sands may enable the migration of injected fluids to an oil field within a time period significantly less than the 10,000 years stipulated by EPA regulations. Fluid velocities (between 0.01 and 100 ft/yr) could accelerate by an order of magnitude owing to the presence of high-permeability streaks in the injected formations.

The depressurization phenomenon is reflected in localized depressions and negative contours on the potentiometric surfaces. Although some of these depressions may be temporal, they have serious implications for the regional trend in flow potential, in that the possibility for fluid flow toward the oil and gas fields is enhanced. A reasonable degree of hydraulic continuity, high permeability, and a steep hydraulic gradient could result in the flow of injected chemical wastes toward a depressured abandoned or producing field. At present we do not know how far the depressurized zone from an oil field may migrate laterally. Pressure declines may only be confined within a field, or they may migrate significantly far from the field, depending upon permeability, storativity, and presence of hydrologic barriers. Attempts to correlate potentiometric cones of depression to location of oil and gas fields reveal that not all depressions center on such fields. Reasons for this mismatch could be (1) factors other than hydrocarbon production contributing to depressuring, (2) contouring of potentiometric surfaces with localized temporal depressured data skewing the potential gradients and offsetting the cones of depression. The areal extent of depressurization is better determined by means of transient pressure analyses. This requires formation injectivity and productivity tests. More detailed investigations of the depressurization phenomenon are needed.

6.6 Implications of Overpressurization

Pressure-depth profiles have helped identify the top of geopressured sediments as significantly shallower than previously recognized. Top of geopressure in the Frio and Wilcox may be as shallow as 6,000 to 8,000 ft. The hydrostatic regime may bottom out at about 10,000 ft. Formation pressures from the PI data base were used with 0.465 psi/ft gradient as the marker to contour and delineate the hydrostatic and geopressured hydrologic regimes. Figure 52 represents the structure contours at the base of the saline hydrostatic section mapped for the deepest occurrence of fluid gradients less than or equal to 0.465 psi/ft. Shallowest occurrences of gradients greater than 0.465 psi/ft were used to delineate the top of geopressure structure in

the negative effect could be that oil fields may become the ultimate sinks for these wastes. This problem could be compounded by the presence of numerous improperly abandoned wells in old depleted fields. The steep hydraulic gradients and high permeability of Frio sands may enable the migration of injected fluids to an oil field within a time period significantly less than the 10,000 years stipulated by EPA regulations. Fluid velocities (between 0.01 and 100 ft/yr) could accelerate by an order of magnitude owing to the presence of high-permeability streaks in the injected formations.

The depressurization phenomenon is reflected in localized depressions and negative contours on the potentiometric surfaces. Although some of these depressions may be temporal, they have serious implications for the regional trend in flow potential, in that the possibility for fluid flow toward the oil and gas fields is enhanced. A reasonable degree of hydraulic continuity, high permeability, and a steep hydraulic gradient could result in the flow of injected chemical wastes toward a depressured abandoned or producing field. At present we do not know how far the depressurized zone from an oil field may migrate laterally. Pressure declines may only be confined within a field, or they may migrate significantly far from the field, depending upon permeability, storativity, and presence of hydrologic barriers. Attempts to correlate potentiometric cones of depression to location of oil and gas fields reveal that not all depressions center on such fields. Reasons for this mismatch could be (1) factors other than hydrocarbon production contributing to depressuring, (2) contouring of potentiometric surfaces with localized temporal depressured data skewing the potential gradients and offsetting the cones of depression. The areal extent of depressurization is better determined by means of transient pressure analyses. This requires formation injectivity and productivity tests. More detailed investigations of the depressurization phenomenon are needed.

6.6 Implications of Overpressurization

Pressure-depth profiles have helped identify the top of geopressured sediments as significantly shallower than previously recognized. Top of geopressure in the Frio and Wilcox may be as shallow as 6,000 to 8,000 ft. The hydrostatic regime may bottom out at about 10,000 ft. Formation pressures from the PI data base were used with 0.465 psi/ft gradient as the marker to contour and delineate the hydrostatic and geopressured hydrologic regimes. Figure 52 represents the structure contours at the base of the saline hydrostatic section mapped for the deepest occurrence of fluid gradients less than or equal to 0.465 psi/ft. Shallowest occurrences of gradients greater than 0.465 psi/ft were used to delineate the top of geopressure structure in

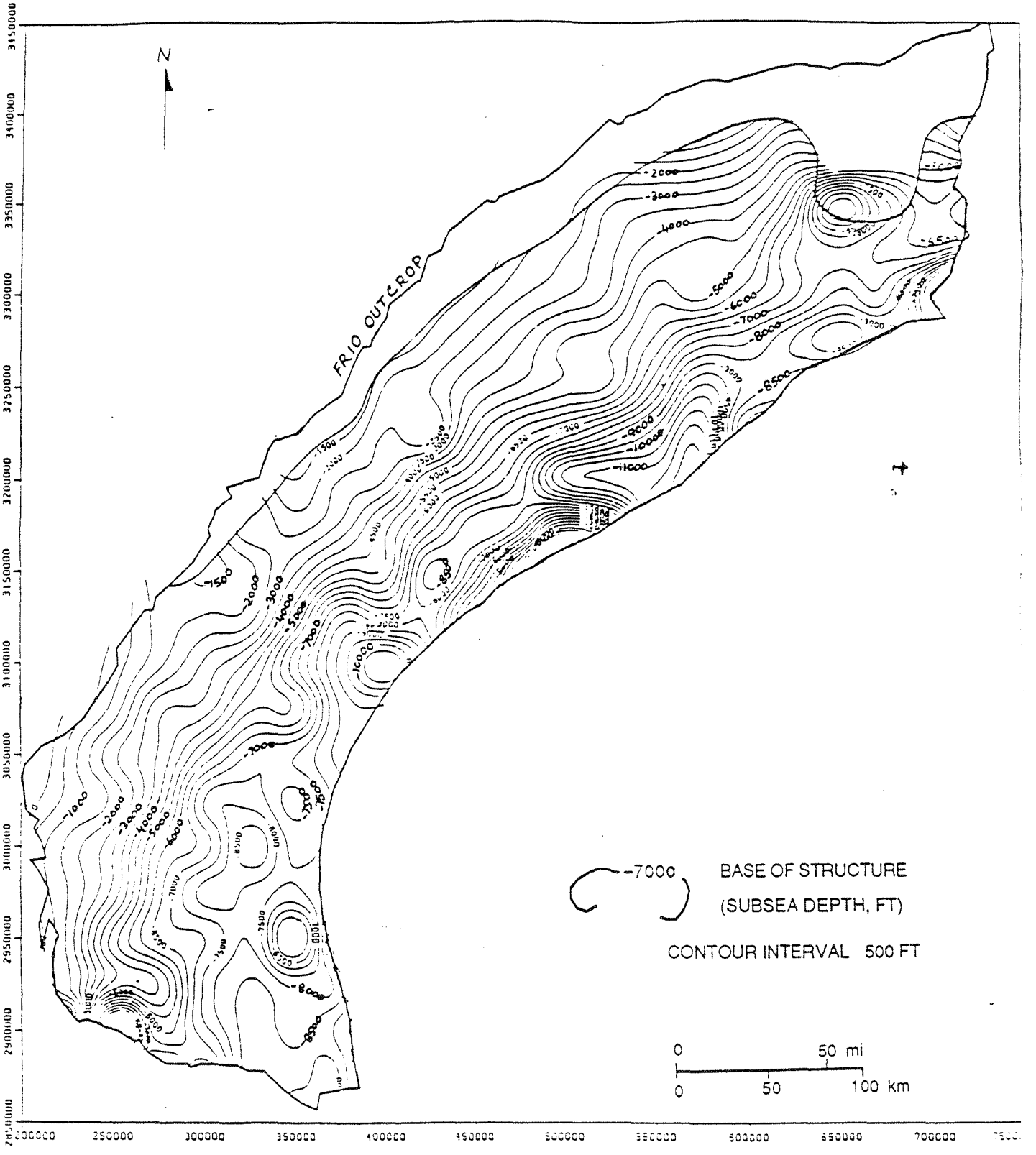

Figure 52. Base of saline hydrostatic section along the Texas Gulf Coast (mapped for deepest occurrence of $\leq$ 0.465 psi/ft fluid gradient).

figure 53. The outlined areas in figure 53 identify counties where the hydrostatic and overpressured surfaces may overlap. The overlap of top of geopressure (fig. 53) and base of hydrostatic (fig. 52), both contoured with 0.465 psi/ft gradient marker, is shown in figure 54. Contours in figure 54 reflect the interval thickness in which geopressured sediments either overlie or are interspersed within normally pressured sands; there are only isolated pockets of overlap. Pressure-depth profiles of counties (Kenedy, Brazoria, and parts of Brooks and Refugio) (figs. 55 through 58) within the overlapping segments are included in the appendix, and they confirm the shallow transition to overpressures. The apparent overlap of normally pressured and geopressured regimes, as seen in pressure-depth plot (fig. 11), is exaggerated due to the pooling of all data from different geographical areas. When individual counties are examined, it can be seen that the overlap is much smaller and is more a reflection of some overpressured sands interspersed in the hydrostatically pressured formations. Top of geopressure from the shallowest occurrence of 0.7 psi/ft gradient is contoured in figure 59. The fluid pressure gradient of 0.7 psi/ft is traditionally considered to be the marker for top of geopressured sediments (Powers, 1967; Jones, 1975). The difference between top of geopressure based on > 0.7 gradient and top of geopressure based on > 0.465 gradient is mapped in figure 60. This figure indicates how much shallower top of geopressure is encountered if it is delineated using the 0.465 gradient marker. Correct identification of top of geopressure may be important for safe siting of hazardous waste facilities.

Figures 61 and 62 are the pressure-depth profiles for the middle-Wilcox and the undifferentiated Miocene formations. The transition to overpressured sediments is observed on both plots and bears strong resemblance to Frio pressure-depth profiles. Similar processes may control formation of geopressuring in all Tertiary formations. Most of the overpressured Miocene data lie offshore. Since offshore pressure data were not available for this study, relatively few overpressured values are included in the Miocene data.

The phenomenon of overpressured conditions existing at relatively shallow depths is complex and is linked to occurrence of shales and faults (Dickey and others, 1968). The presence of hydrostatic and overpressured conditions in the same depth range suggests compartmentalization that may be fault controlled. This compartmentalization may be important in locating future injection facilities. If faults indeed act as barriers to flow, then they may be advantageous to confinement of injected chemical wastes. Conversely, if they act as pathways for upward migration of deep overpressured brines, injection wells should be drilled away from such locations.

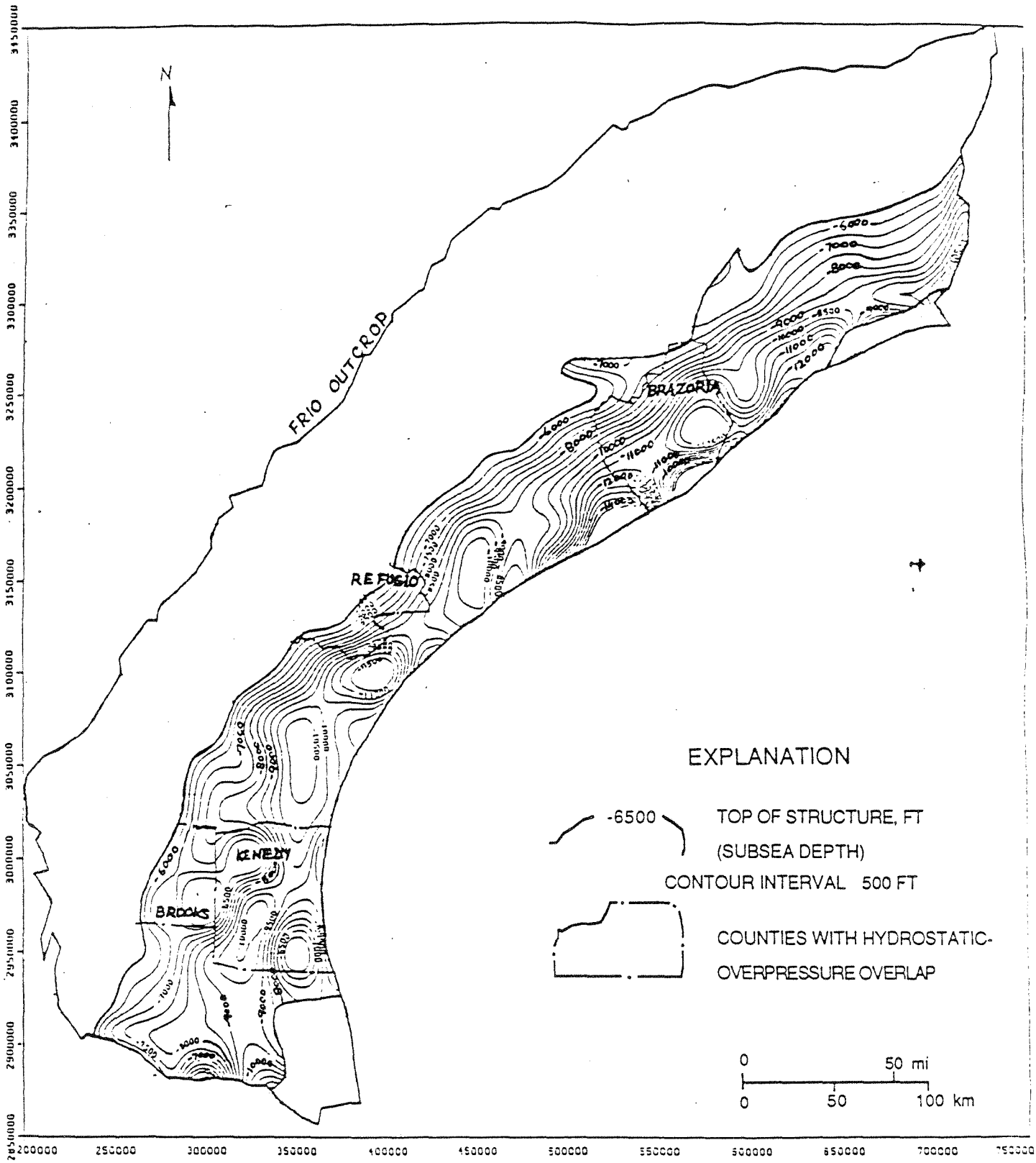

Figure 53. Top of geopressured section along the Texas Gulf Coast (mapped for shallowest occurrence of > 0.465 psi/ft fluid gradient).

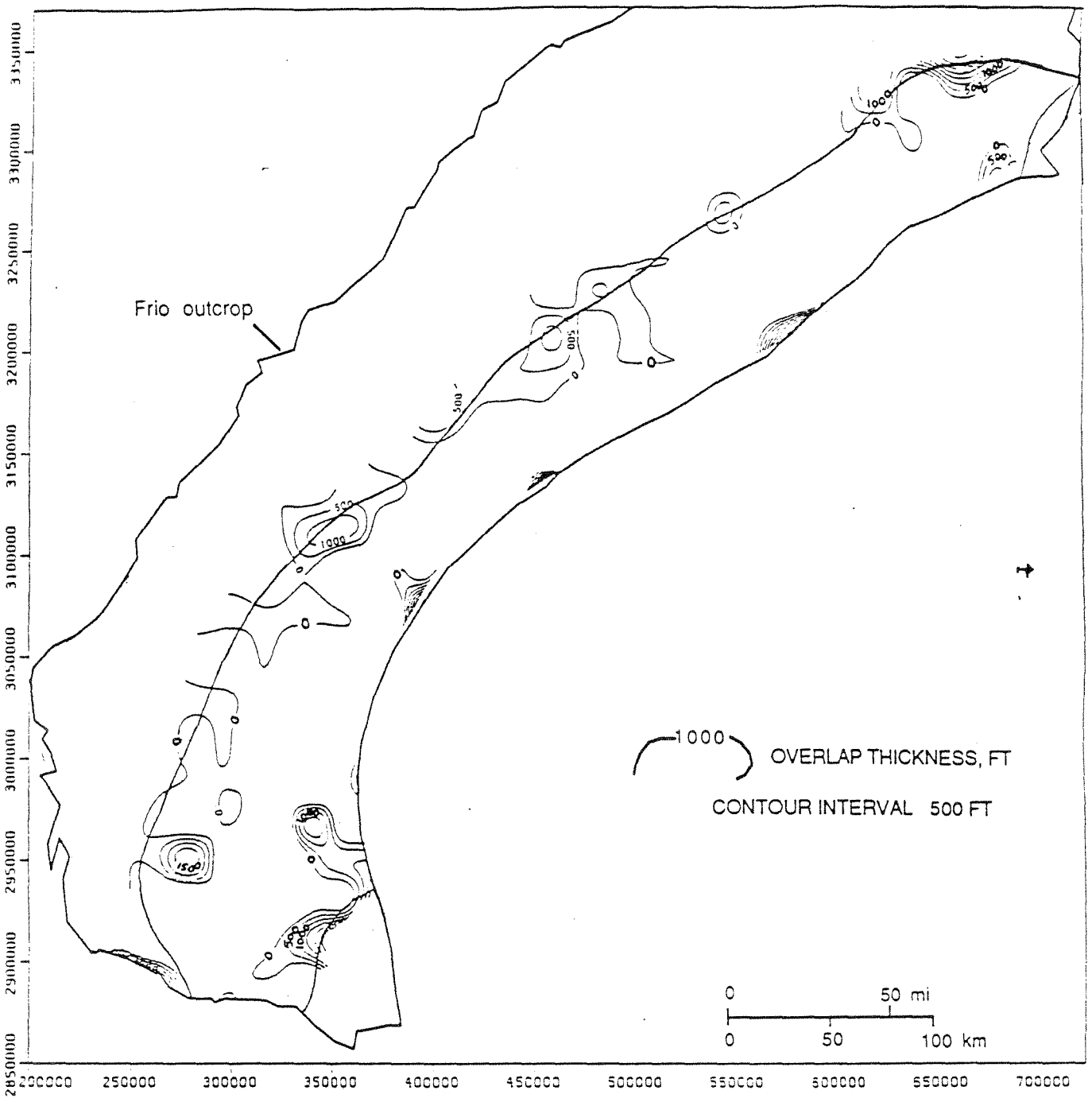

Figure 54. Overlap between base of hydrostatic and top of geopressured sections (figs. 53 and 52). Base of hydrostatic contoured for deepest occurrence of ≤ 0.465 psi/ft gradient, and top of geopressured contoured for shallowest occurrence of > 0.465 psi/ft gradient.

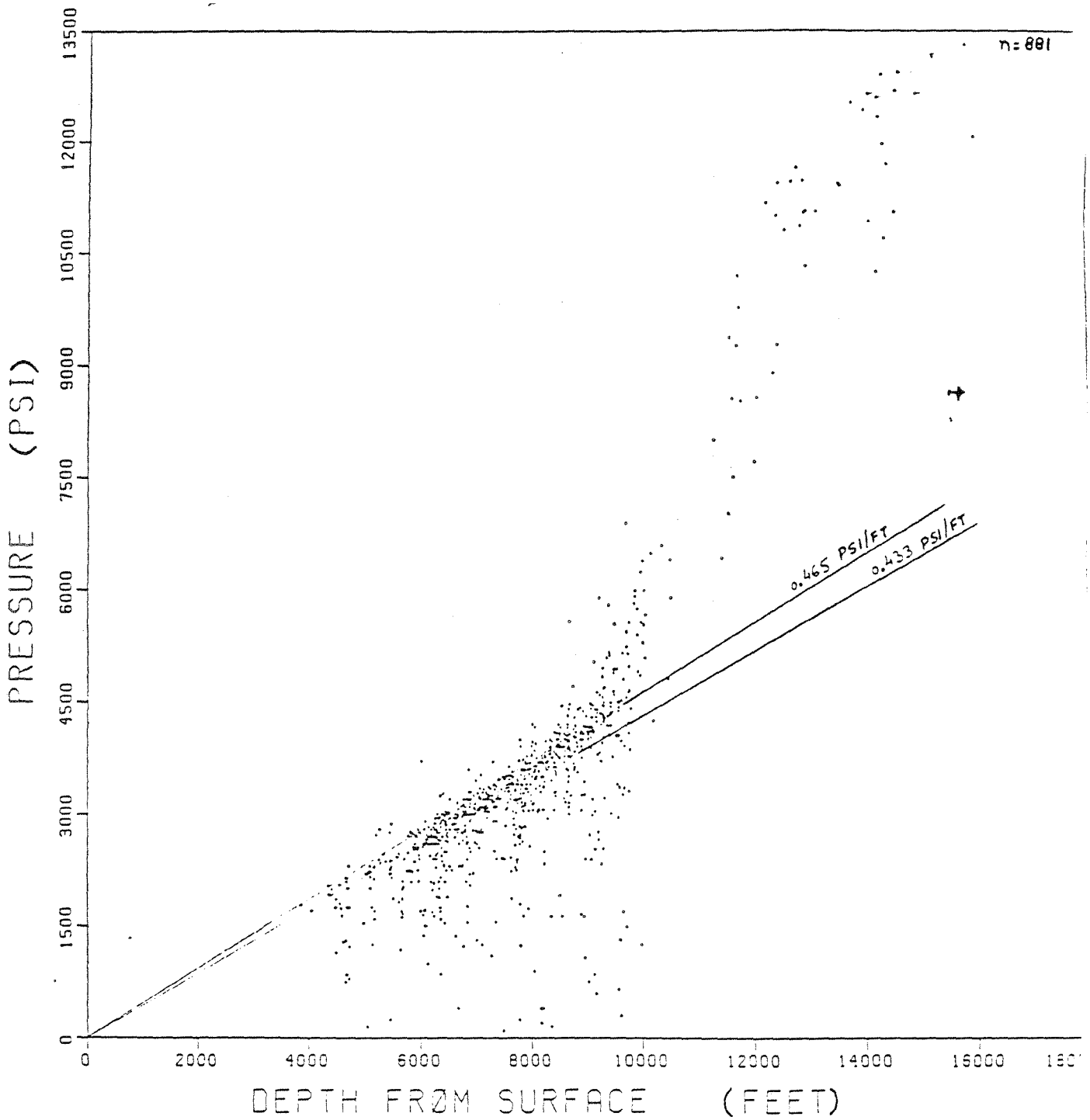

Figure 55. Pressure-depth diagram, Kenedy County data.

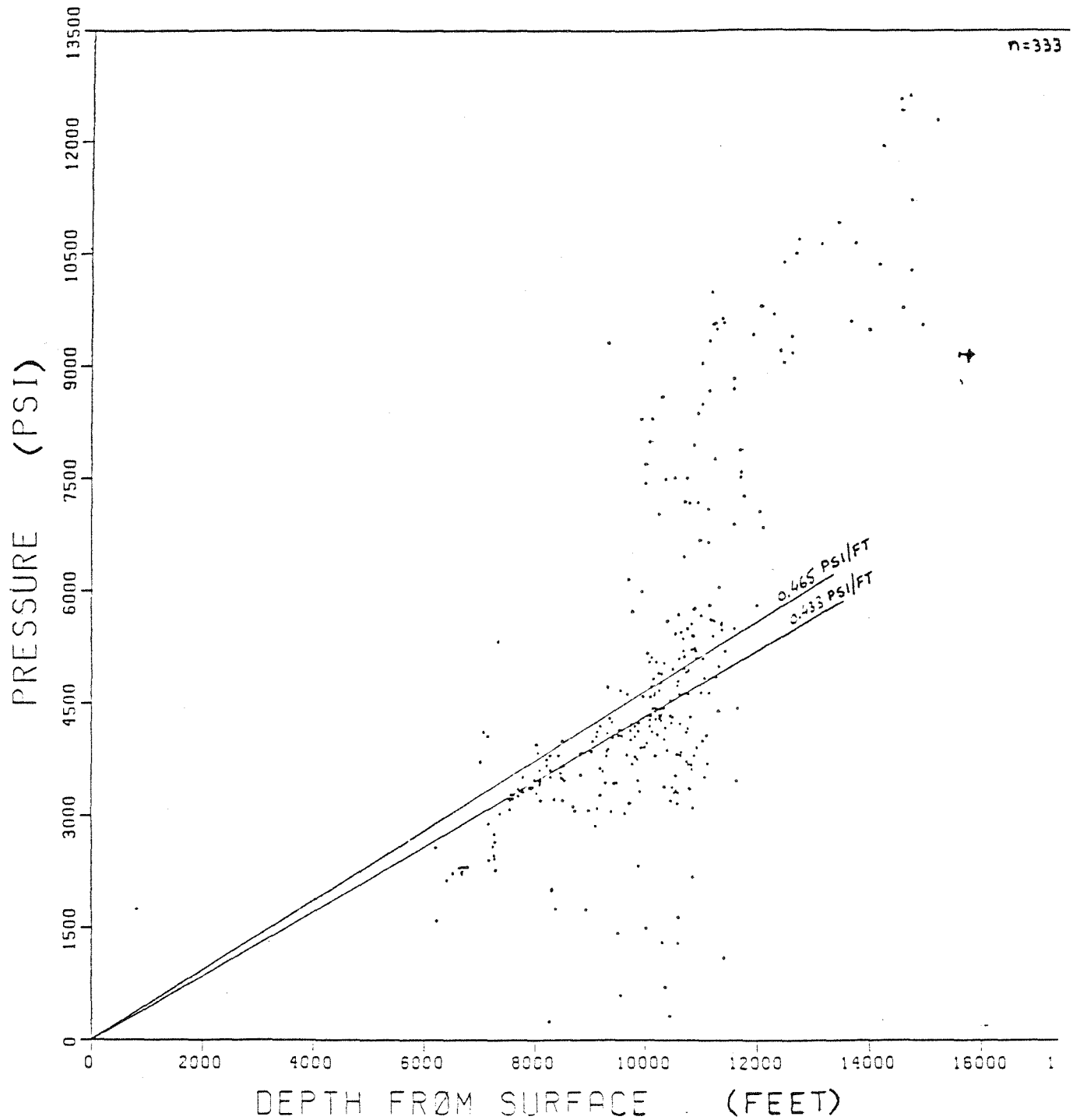

Figure 56. Pressure-depth diagram, Brazoria County data.

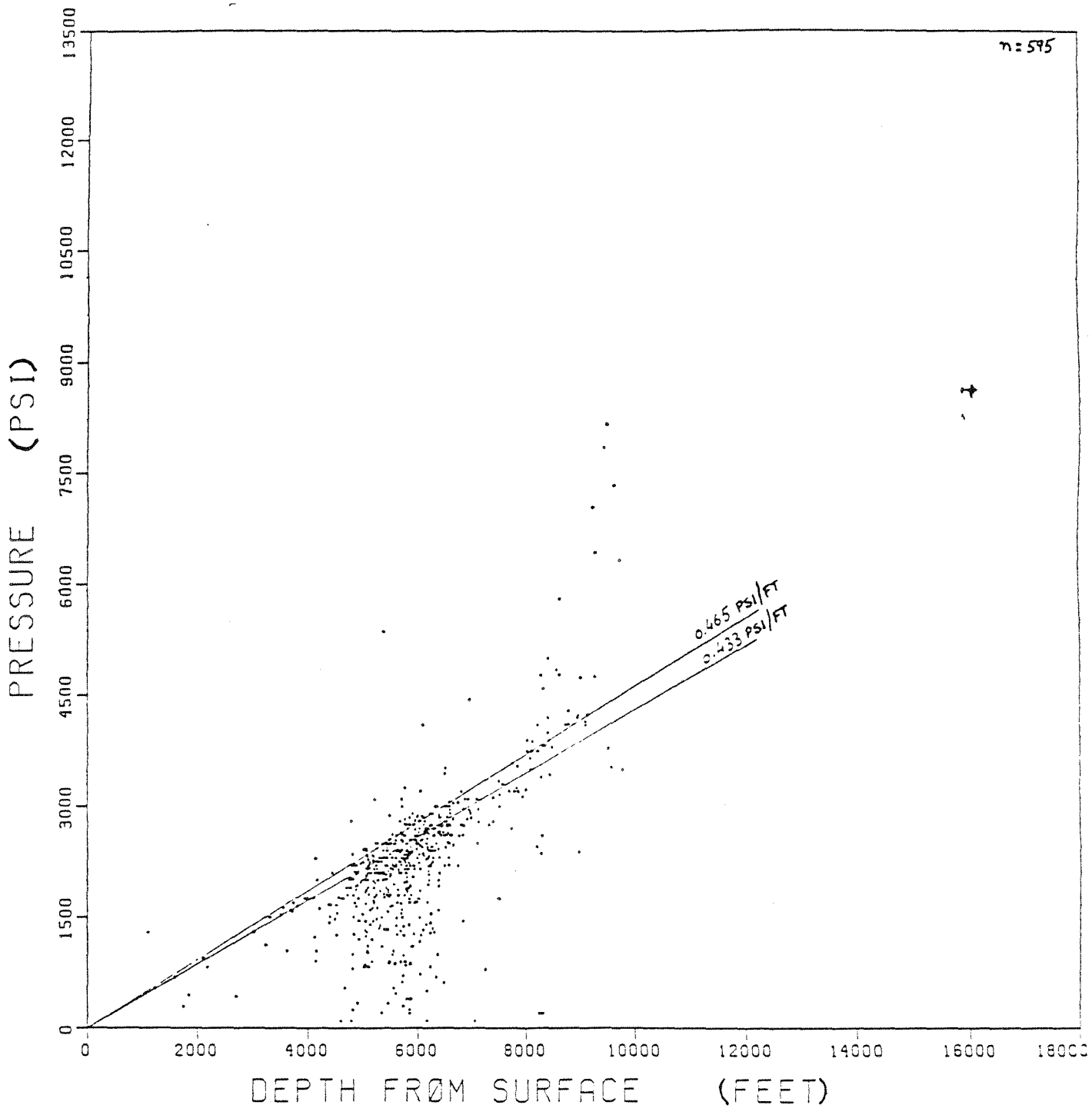

Figure 58. Pressure-depth diagram, Refugio County data.

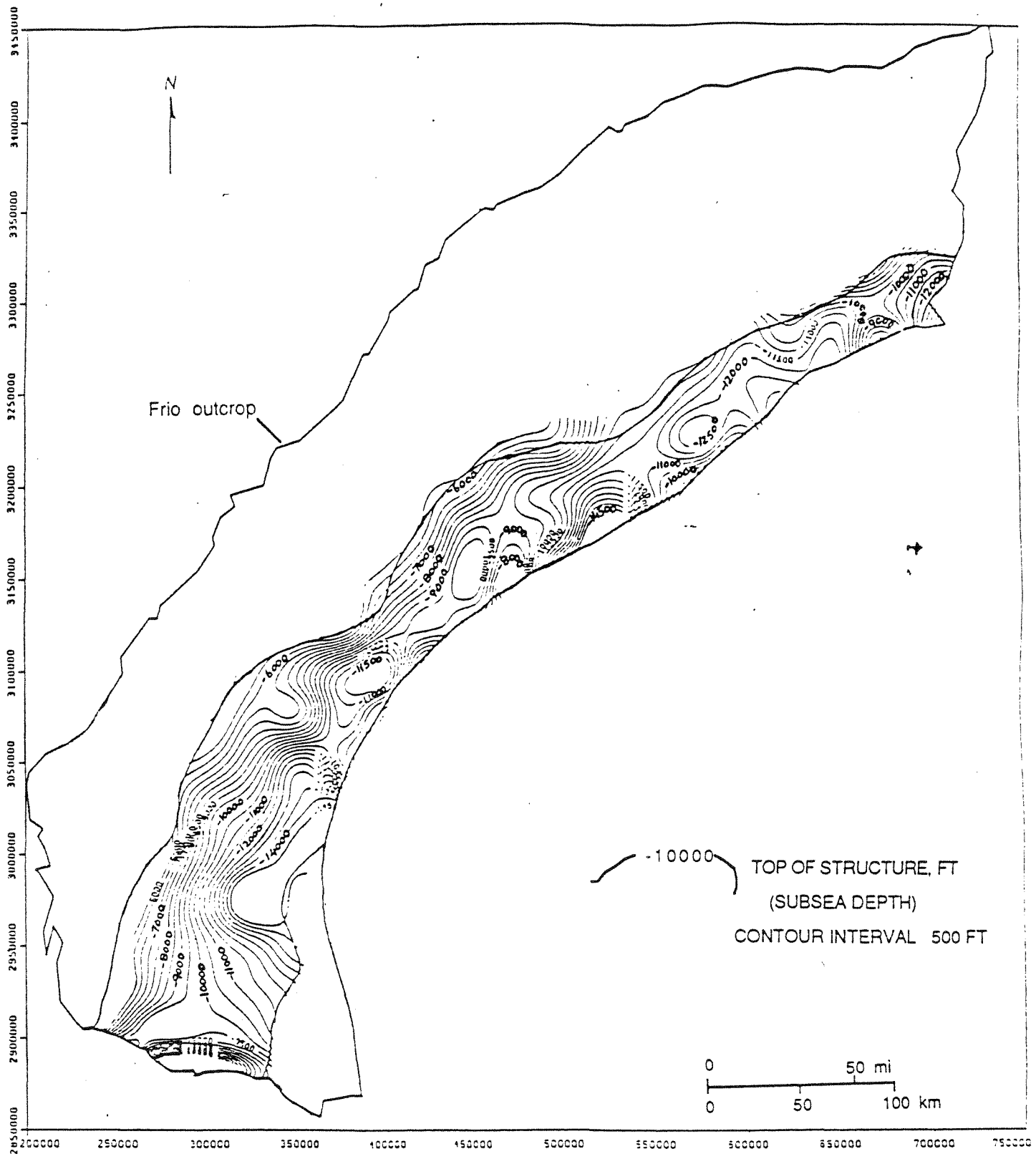

Figure 59. Top of geopressured section along the Texas Gulf Coast (mapped for shallowest occurrence of > 0.7 psi/ft fluid gradient).

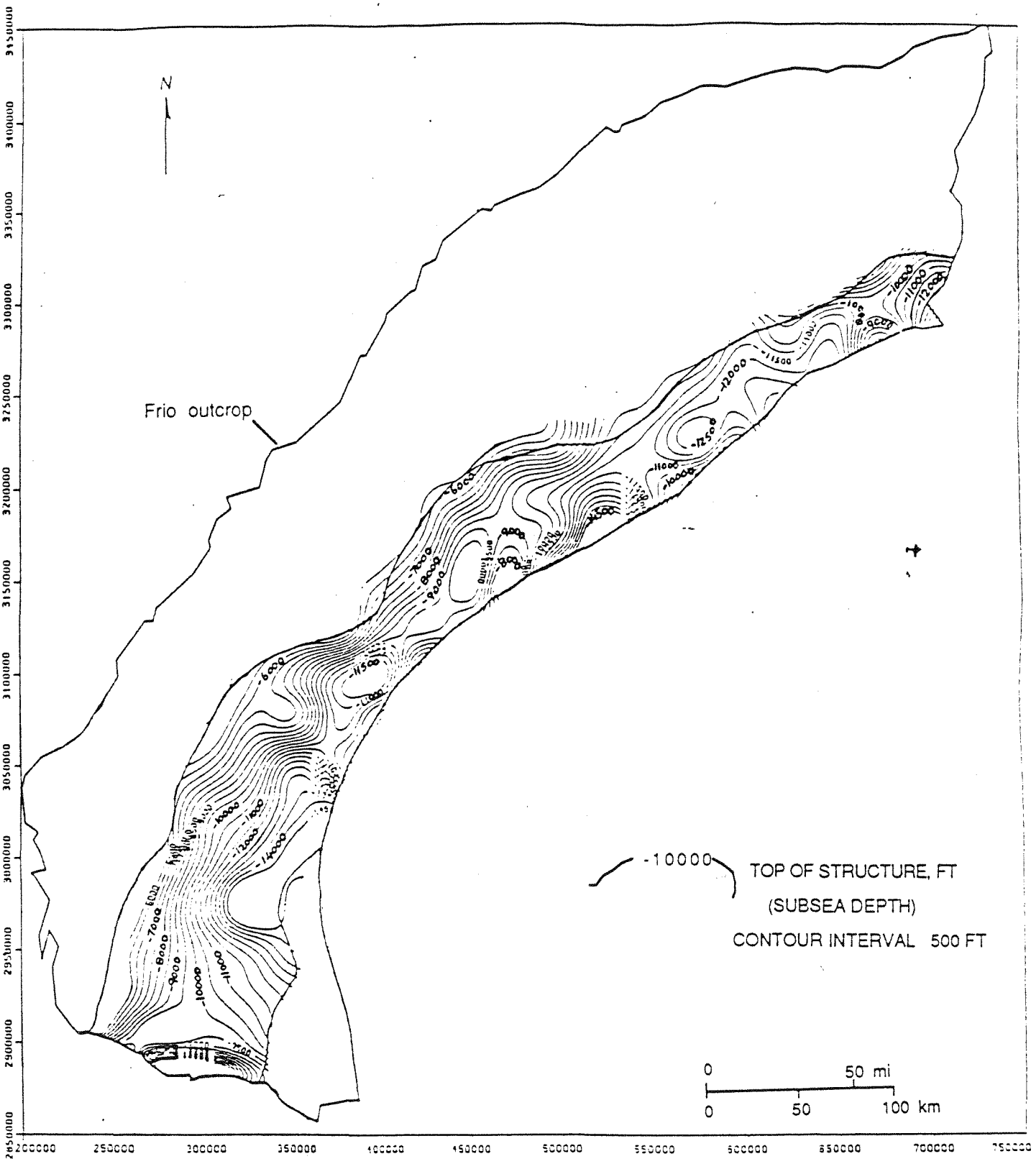

Figure 59. Top of geopressured section along the Texas Gulf Coast (mapped for shallowest occurrence of > 0.7 psi/ft fluid gradient).

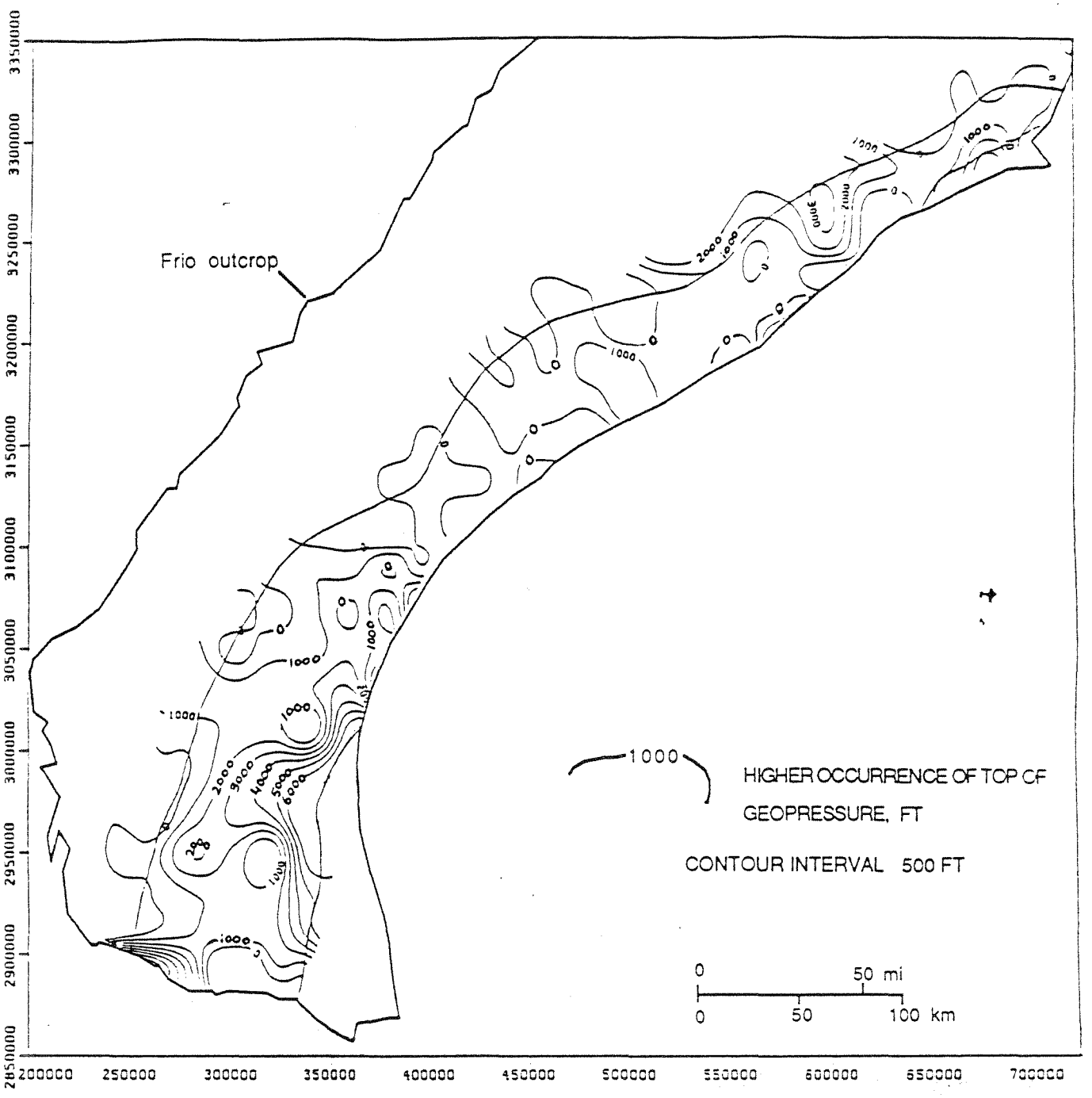

Figure 60. Difference between structure top of geopressure based on > 0.465 gradient and top of geopressure based on > 0.7 gradient (figs. 53 and 54).

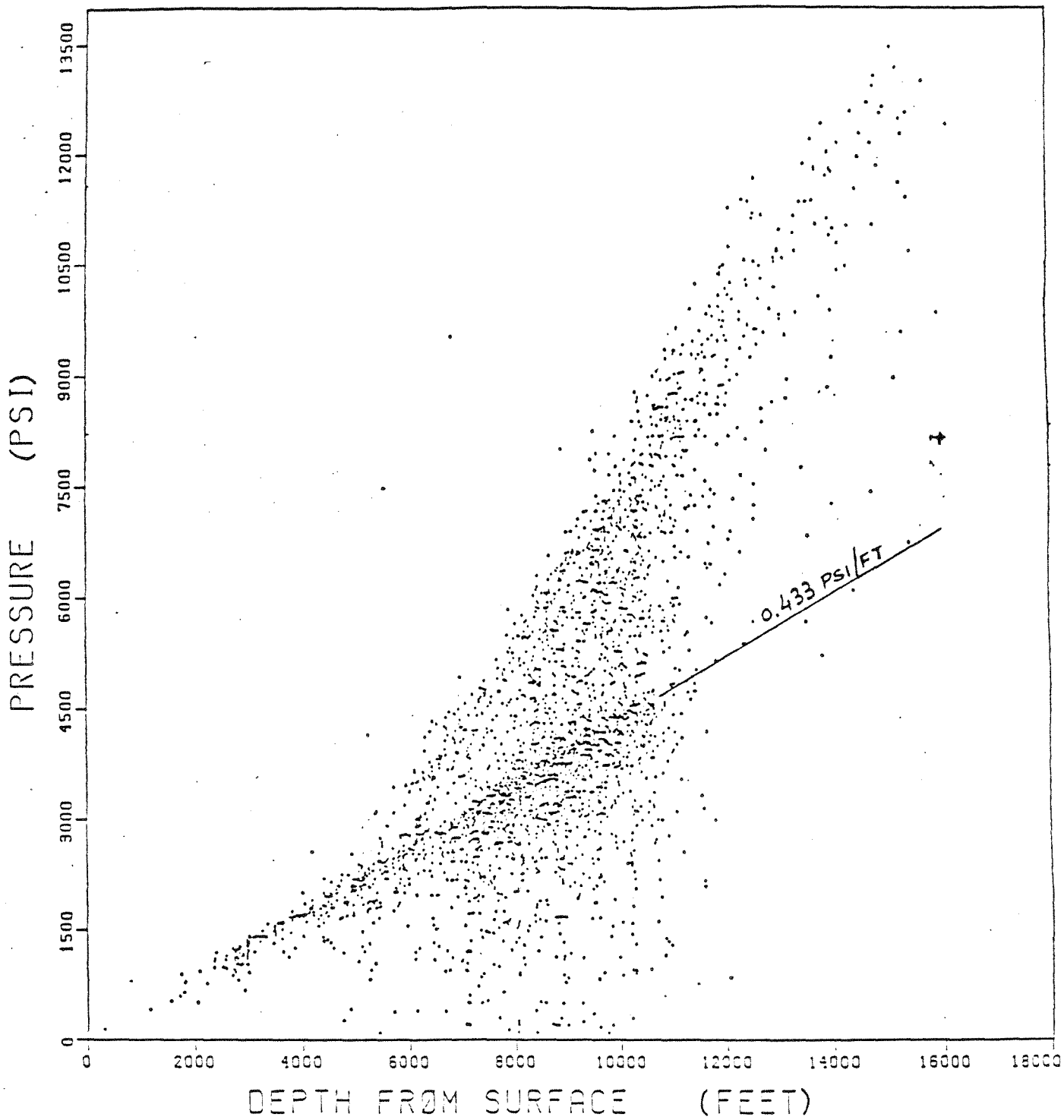

Figure 61. Pressure-depth diagram for middle Wilcox Formation, regions A-B-C data.

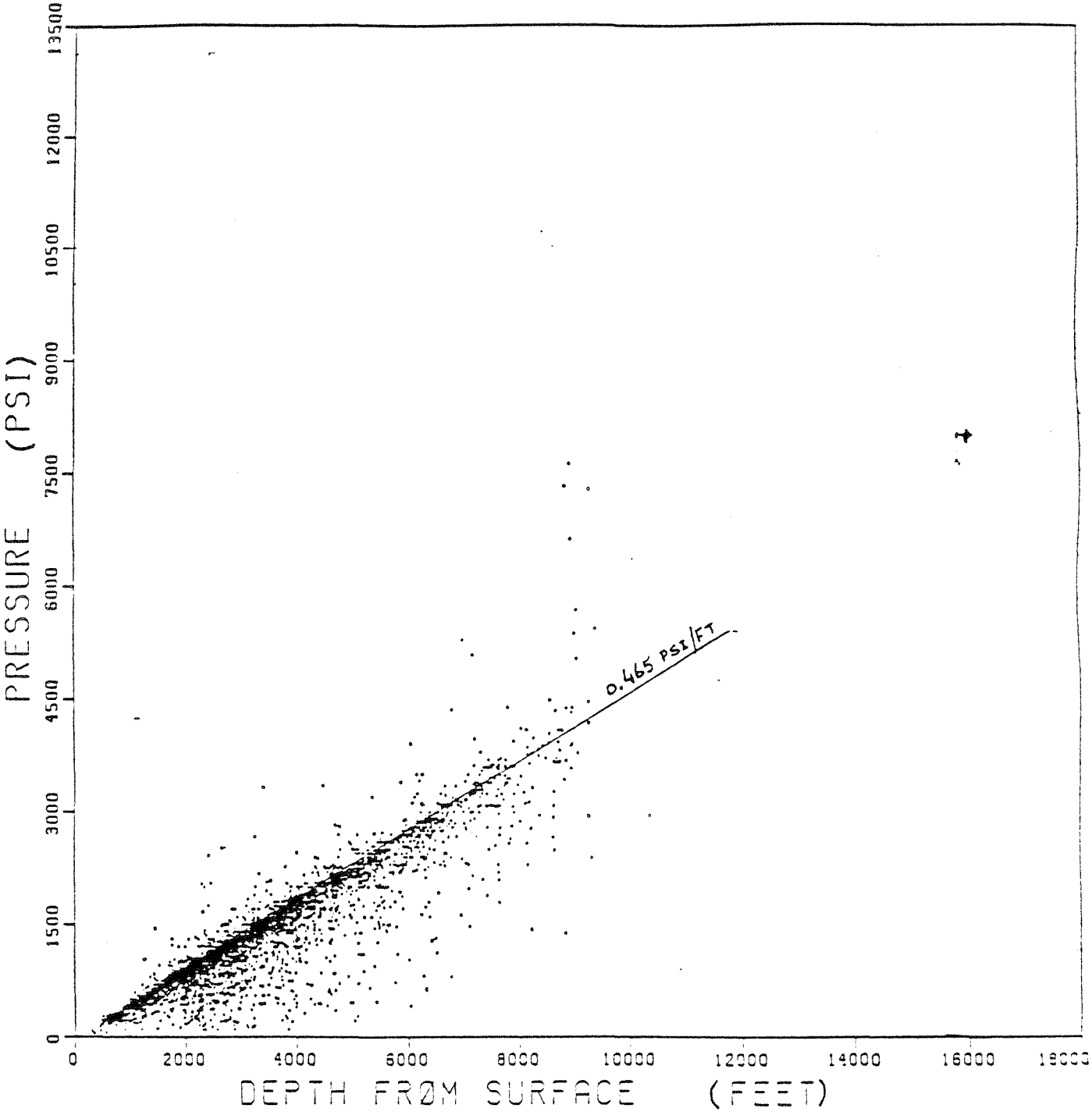

Figure 62. Pressure-depth diagram for undifferentiated Miocene Formation, regions A-B-C data.

7. WATER CHEMISTRY - INTRODUCTION

The chemical composition of saline Frio Formation waters provides additional information for understanding the process of deep-well injection of chemical wastes into deep saline formations in the Texas Gulf Coast, in three ways: (1) Chemical composition helps define the geochemical environment into which wastes are injected; (2) Fluid density is needed for the construction of potentiometric-surface maps based on DST pressure data; (3) Water chemistry, in conjunction with pressure data, helps define the regional hydrogeology of these saline formations.

7.1 Hydrochemical Environment

Kreitler and Richter (1986) previously characterized the geochemical environment of disposal horizons used in Gulf Coast saline formations as having varying salinities, predominantly NaCl in chemical composition, warm (<100°C), and possibly high in organic acids. The injection zone typically was a permeable argillaceous-arkosic, unconsolidated sandstone. To better characterize the geochemical conditions of injection zones, additional information was needed primarily on actual organic acid concentrations. The presence or absence of organic acids may indicate biologically mediated reactions (Carothers and Kharaka, 1978). The acids may also function as ligands for metal transport (Drez, 1988). The presence of organic acids generally has only been inferred from measurements of total alkalinity because the titration for total alkalinity measures bicarbonate, borate and sulfide as well as organic acids. Total alkalinity, not the concentrations of individual acids, is typically measured in routine oil-field brine analyses.

7.2 Construction of Potentiometric Surfaces

Construction of potentiometric surfaces in saline aquifers presents inherent problems because of the variability of water salinity within a formation and between formations (Lusczynski, 1961). To investigate ground-water flow in the horizontal direction, fresh-water equivalent head maps are often constructed. Head values are calculated from drill-stem-test pressure data as if the sampled waters were fresh. To investigate vertical flow between formations containing waters of differing salinities, potentiometric surfaces need to be adjusted to account for the varying densities (and salinities). For this second type of mapping the density of the waters is important. These maps are called environmental or point source head maps.

7.3 Hydrochemical Interpretation of the Hydrogeology of Saline Formations

The waters in the hydrostatic section of the Frio Formation may have been derived from three different origins: (1) continental meteoric waters that have penetrated deep beneath the fresh-water section, (2) original waters that were emplaced at the time of sediment deposition, and (3) waters that have migrated up from the overpressured section or are a mixture of these different water sources. If the waters are original formation waters, a stagnant hydrologic system is implied. If the waters originated as geopressured waters, upward migration of deeper waters into shallower horizons is implied. If the waters are meteoric in origin, deep penetration of contaminated water and a relatively active hydrodynamic system may be inferred. These three hypotheses for the origin of the waters in the Frio hydrostatic can be tested by evaluation of the water chemistry.

A. Deep penetration of meteoric waters. Four observations, based on previously collected geochemical data, suggest deep penetration of meteoric waters into the Frio Formation.

1. Many waters in the Gulf Coast saline formations, including the Frio Formation, have chlorinities less than sea water chlorinity (Kreitler and Richter, 1986).
2. The $\delta^{18}O$ values of waters from the hydrostatic section of the Wilcox Formation (stratigraphically beneath the Frio) are isotopically light and not in isotopic equilibrium for their depth and temperature of occurrence (Fisher, 1982). Waters from the hydrostatic section of the Frio might show a similar meteoric influence. A limited number of Frio waters showed enriched $\delta^{18}O$ values (Lundegard, 1985) and appeared to be in isotopic equilibrium; these samples, however, were collected from deeper in the geopressured section of the Frio. It was unknown whether the hydrostatic sections of the Frio may also contain isotopically light meteoric water.
3. Many oils from the hydrostatic section of the Frio Formation have high gravities (low API numbers) and high sulfur contents, suggesting biodegradation (Galloway and Hobday, 1983). Previous authors investigating biodegradation (for example, Bailey and others, 1973a) have suggested that meteoric waters have been the cause of biodegradation.
4. Kreitler and Richter (1986) observed an inverse correlation between total alkalinity and chlorinity. Deep formation waters often have high concentrations of aliphatic acids. Kerogen has been altered by thermal maturation to natural gas and organic acids. Shallow formation waters were expected to have low concentrations of

organic acids, because of biologic consumption of the short-chained, easily-degraded organics (Carothers and Kharaka, 1978). The observed inverse correlation between total alkalinity and chlorinity suggests a source of the organic acids other than thermal maturation. The low chlorinities suggest deep penetration of meteoric water, and the high alkalinities suggest biodegradation of hydrocarbons by these brackish waters and subsequent formation of organic acids as a resulting product.

These observations are tentative. The measurement of total alkalinity represents field titrated alkalinity and is not specific to organic acids. API gravity and sulfur content only imply degradation of oil. The presence of specific organic acids and degraded oils is confirmed by gas chromatograph analysis. The isotopic composition of waters in the Wilcox is known, but the isotopic composition of Frio waters in the hydrostatic section is not.

If there has been deep penetration of meteoric water in the Frio, one might expect low TDS waters, light oxygen and hydrogen isotopic values suggestive of meteoric recharge, and heavy oils indicating biodegradation and/or water washing. If these waters are meteoric in origin, is it also possible to date this process of penetration?

B. Original formation waters. If the waters in the Frio are the original waters trapped during sediment deposition, TDS concentrations should range from brackish to seawater, and concentration of select ions should be similar to that of seawater. Rock/water reactions may have altered the original seawater composition. Salt dome dissolution is considered to have an important control on the water chemistry in the geopressured section (Morton and Land, 1987). These waters may have isotopic compositions similar to that of seawater or have become isotopically enriched through reaction with the rock matrix or mixing with deeper upward migrating geopressured waters. Degraded oils would not be expected. The hydrocarbons have migrated to their present traps after sedimentation and burial (Galloway and others, 1982). If degradation has occurred, a mechanism is needed to explain either how bacteria can migrate to depths of at least 6,000 ft or how bacteria can survive from the time of initial sediment deposition to the time of oil migration, which may be millions of years later.

C. Upward migration of geopressured waters. The concept that waters that have migrated from deeper geopressured horizons up faults or along the flanks of salt domes into shallower hydrostatic horizons is based on four observations.

1. Many oil fields in the Gulf Coast occur at depths above the "oil window," the temperature/pressure regime where oil maturation occurs (Young and others, 1977), and may have temperature and salinity anomalies associated with them (Tyler and others, 1985).
2. Lead-zinc mineralization associated with salt dome caprocks must have resulted when metal-rich brines migrated from deeper in the sedimentary basin (Ulrich and others, 1984).
3. The low-TDS Na-acetate waters at the top of the geopressure sediments suggest thermal convection of low-density waters and that the high-Ca water in the Frio geopressured section may result from leakage of waters from deeper Mesozoic formations that are being metamorphosed (Morton and Land, 1987). They conclude that because of the large volumes of relatively insoluble cements that have been precipitated, large volumes of waters must have discharged through the geopressured section.
4. Sulfide alteration found in uranium deposits has sulfur isotope compositions that can only be attributed to fluid migration from Mesozoic rocks deep within the basin (Galloway, 1982; Morton and Land, 1987), and indicates that fluid migration has been into the fresh-water aquifers. This upward migration process is not limited to the saline section.

Thirty-two water samples collected from the Frio Formation were analyzed for pH, total alkalinity, and inorganic and organic composition of the dissolved species. Oils associated with the sampled waters were also collected. Gas chromatographic analyses of 11 samples were run to determine if the oils were biodegraded. These data along with the larger, but less complete data base of previously published and unpublished data were investigated to address the questions of geochemical environment, fluid density and variability, and hydrogeology.

8. WATER CHEMISTRY - METHODOLOGY

Chemical data used in this report are from Kreitler and Richter (1986). Approximately 850 Frio analyses are used, the majority of which contain only major cation and anion data from oil field operators and constitute a very good source of major ion data from the Texas Gulf Coast. These data are subdivided geographically into Northgulf, Northcentral, Southcentral and Southgulf (table 3a through d). A second data set (table 4), which contains approximately 150 analyses, includes major and minor ions and is based on minor element analyses from Kreitler and Richter (1986) and Morton and Land (1987). Thirty-two additional waters sampled by the Bureau of

Table 3a. Major ion chemistry from Frio Formation, Northgulf region. Ionic concentrations in mg/L. Data from Kreitler and Richter, 1986.

County	Latitude	Longitude	Ca	Mg	Na	K	Alkalinity	SO4	Cl	TDS	Depth (feet)
Newton	30.71	93.65	5800	2120	24500	0	220	8	42000	69018	2900
Newton	30.47	93.80	10000	3490	33900	0	186	4	59500	97507	3000- 3100
Fort Bend	29.47	95.25	5100	628	40307	0	193	8	73000	119236	3644
Fort Bend	29.47	95.25	3480	484	34856	0	169	3	61300	100292	3788
Fort Bend	29.47	95.25	3880	472	37145	0	181	6	65500	107184	4126
Fort Bend	29.55	95.05	2781	508	30980	0	311	1	54000	88581	3717
Fort Bend	29.47	95.57	2040	322	37937	0	195	1	63000	103495	5385
Fort Bend	29.47	95.57	2280	1160	32700	0	122	1	57784	94047	5400
Harris	29.75	95.10	2320	437	41415	0	61	0	69255	113375	6865-6875
Harris	25.97	95.05	2476	403	44214	0	111	98	73609	120924	6000-6700
Harris	29.75	95.10	2740	340	39200	0	115	5	70000	112400	4900-7200
Harris	29.75	95.10	1850	440	34500	0	150	11	60140	124900	6800-7650
Harris	29.72	95.09	2200	457	39400	0	0	0	70000	113400	6600-7535
Harris	29.72	95.09	2160	453	41200	0	0	0	70000	115400	6600-7535
Harris	29.75	95.10	5100	1150	76916	0	160	425	82639	166408	6340-6640
Harris	29.75	95.10	5700	1800	62982	0	127	23	70446	141192	6490-6550
Harris	29.75	95.10	6400	1400	55664	0	99	12	63548	127318	6590-6650
Harris	29.74	95.09	2400	480	43000	0	463	0	19018	704000	6800-7300
Harris	29.73	95.13	10	5	25000	0	1400	1600	65000	60140	6800-7650
Harris	29.72	95.09	2775	462	14700	0	148	150	0	66900	
Harris	29.67	95.33	4740	1007	27931	0	140	1	54400	88219	4495
Harris	29.67	95.33	2552	402	40600	0	170	1	67300	111025	4828
Harris	30.12	95.63	1540	122	14610	0	189	1	25500	41962	3695
Harris	29.62	95.27	1849	303	39120	0	116	1	64400	105789	4873
Harris	29.55	95.17	3050	397	35997	0	220	1	62000	101665	6048
Harris	29.62	95.02	2744	337	37720	0	122	1	64000	104924	5925
Harris	29.42	95.17	8350	710	44000	624	88	2	83600	139000	11398-11408
Harris	29.42	95.17	8580	670	42400	643	94	3	80900	133000	11472-11499
Galveston	29.30	95.13	2000	220	26500	400	333	3	42700	73300	11299
Galveston	29.30	95.13	380	70	16250	140	361	43	24000	42800	8609
Galveston	29.30	95.13	180	40	15750	110	525	42	22400	40000	8845
Galveston	29.30	95.13	130	30	16500	120	582	25	23800	42000	8796
Galveston	29.30	95.13	290	60	16500	110	397	39	16500	42100	8615
Galveston	29.30	95.13	2000	235	24000	300	317	1	40500	68600	11725
Galveston	29.30	95.14	140	30	14000	100	596	17	20400	36600	9278
Galveston	29.30	95.14	425	98	15165	0	1596	58	24181	41405	8675- 8680
Galveston	29.30	95.14	302	81	15124	0	1635	46	23151	40339	8755- 8770
Galveston	29.30	95.14	292	72	16467	0	1437	78	25234	43580	9158- 9163
Galveston	29.30	95.14	827	138	18043	0	655	39	29289	48991	10895-10905
Galveston	29.30	95.14	1600	185	20400	0	394	38	34625	57322	11422-11461
Galveston	29.30	95.14	302	81	15124	0	1635	46	23151	40339	8755- 8770
Galveston	29.30	95.14	292	72	16467	0	1437	78	25234	43580	9158- 9163
Galveston	29.30	95.14	827	138	18043	0	655	39	29289	48991	10895-10905

Table 3a (continued)

County	Latitude	Longitude	Ca	Mg	Na	K	Alkalinity	SO4	Cl	TDS	Depth (feet)
Galveston	29.30	95.14	1600	185	20400	0	394	38	34625	57322	11422-11461
Galveston	29.30	95.14	441	101	13843	0	1630	24	21459	37498	8822- 8832
Galveston	29.30	95.14	582	101	18306	0	1093	24	28934	49091	9374- 9386
Galveston	29.31	95.14	1104	168	23994	0	649	34	39102	65147	11056-11068
Galveston	29.31	95.14	4319	595	27820	0	369	1	52600	86685	12238-12248
Galveston	29.31	95.14	8980	625	42100	570	0	14	78500	129600	14650
Galveston	29.52	95.20	4260	660	49300	371	219	12	59500	98500	9767- 9784
Galveston	29.33	95.10	1490	151	29800	230	536	18	46300	79900	12270-12280
Galveston	29.33	95.10	783	95	22700	192	628	7	35200	58900	11250-11254
Galveston	29.33	95.10	606	88	24900	180	848	6	36700	62500	10800-
Galveston	29.33	95.07	480	98	15680	0	1122	0	24650	42085	9090- 9110
Galveston	29.50	95.05	4320	708	41030	0	793	1	72700	119339	8663- 8675
Galveston	29.33	95.10	880	183	15200	0	673	13	25180	42223	13014-13022
Galveston	29.33	95.10	660	134	18170	0	630	7	29260	49034	11150-11210
Galveston	29.47	95.10	2374	486	39996	0	453	40	67012	110361	9257
Galveston	29.47	95.10	1886	400	37432	0	450	25	61921	102114	9117
Galveston	29.45	94.95	512	235	20435	0	616	1	32750	54549	9078
Galveston	29.45	94.95	2852	496	27106	0	488	1	48100	79043	8031
Galveston	29.45	94.95	746	68	16542	0	561	1	26700	44618	8570
Galveston	29.45	94.95	2910	380	34170	0	458	1	58750	96669	8050
Galveston	29.45	94.95	2288	265	23783	0	561	1	41000	67898	8095
Galveston	29.45	94.95	1880	41	19056	0	885	25	32300	54187	8464
Galveston	29.33	95.10	418	81	17120	0	1089	103	26684	45495	9300
Galveston	29.33	95.10	629	163	23446	0	854	52	37233	62377	10360
Galveston	29.37	95.13	380	70	15250	140	414	31	23400	41300	8795
Galveston	29.37	95.13	400	75	16000	120	312	32	23800	42500	8828
Galveston	29.35	94.97	550	95	19000	180	334	31	26400	47600	8933
Galveston	29.35	94.97	470	85	17000	160	643	34	25200	44600	8933
Galveston	29.33	95.10	700	90	19500	190	787	11	31000	53100	11080
Galveston	29.33	95.10	1230	170	18250	190	506	8	29300	50400	12992
Chambers	29.63	94.90	1764	420	38472	265	244	373	63900	105789	5806- 5890
Chambers	29.63	94.90	2095	613	38878	226	195	186	63900	106498	5822- 5858
Chambers	29.63	94.90	1849	458	37482	262	231	230	63900	104776	5814- 5836
Chambers	29.63	94.90	2050	511	39672	240	207	360	65675	109142	5952- 5964
Chambers	29.67	94.50	4830	1010	41700	0	269	2	75700	123655	8300- 8335
Chambers	29.67	94.50	3420	1160	30100	0	162	0	56000	91072	8254- 8264
Chambers	29.67	94.50	4840	1330	47100	0	245	2	84900	138553	8236- 8246
Chambers	29.53	94.83	392	29	17991	0	898	20	28045	47728	9200
Chambers	29.80	94.40	2914	1770	33900	0	222	15	62150	100355	
Chambers	29.80	94.40	2320	732	37240	0	500	3	63480	104406	7610- 7612
Chambers	29.80	94.40	2240	561	37197	0	383	6	62770	103223	7820- 7826
Chambers	29.53	94.83	1020	197	16900	0	590	36	28200	46992	10098-10128
Chambers	29.53	94.83	1010	343	32900	0	485	0	53200	87982	9730- 9742

Table 3a (continued)

County	Latitude	Longitude	Ca	Mg	Na	K	Alkalinity	SO4	Cl	TDS	Depth (feet)
Chambers	29.53	94.83	1500	343	34600	0	554	0	56600	93652	10440-10450
Chambers	29.53	94.83	887	218	23700	0	546	0	38600	64000	10836-10846
Chambers	29.53	94.83	4870	9450	27200	0	179	0	78000	119819	8166- 8170
Chambers	29.54	94.84	7590	766	46300	0	185	0	87100	142203	9334- 9347
Chambers	29.77	94.38	4230	550	27900	0	0	0	52100	84800	10465-10469
Chambers	29.77	94.38	2190	953	27700	0	237	13	49400	80576	8396
Chambers	29.78	94.58	2608	312	42472	0	159	1	71000	116552	7127
Chambers	29.78	94.58	4310	517	31116	0	146	50	57000	93139	7126
Chambers	29.53	94.82	1286	220	37368	0	854	1	60100	99829	9767
Chambers	29.63	94.92	4350	450	34965	0	98	101	62800	102764	6095
Chambers	29.63	94.92	4130	347	28786	0	232	378	52300	86173	6096
Chambers	29.85	94.67	1725	483	25267	0	171	103	43261	71010	6643
Brazoria	29.22	95.15	15912	1000	36700	434	88	0	90800	144934	14894
Brazoria	29.22	95.15	19176	1137	40500	490	113	0	103500	164916	14622
Brazoria	29.22	95.15	61	9	5200	58	743	0	7000	13071	12362
Brazoria	29.40	95.28	1010	180	37900	292	600	12	59500	98500	10497-10574
Brazoria	29.27	95.30	2600	535	69700	218	30	16	52000	35000	12558-12568
Brazoria	29.37	95.25	330	60	22700	171	1280	21	34000	56600	10858-10864
Brazoria	29.32	95.20	380	70	16250	140	361	43	24000	42800	8610
Brazoria	29.32	95.20	280	60	15250	120	427	43	22500	40200	8615
Brazoria	29.32	95.20	180	40	15750	110	525	42	22400	40000	8845
Brazoria	29.32	95.20	290	60	16500	130	397	39	23200	42100	8615
Brazoria	29.32	95.20	130	30	16500	120	582	25	23800	42000	9780
Brazoria	29.32	95.20	2000	220	26500	400	333	3	42700	73300	11360
Brazoria	29.32	95.20	710	90	25000	280	269	11	36300	63700	10690
Brazoria	29.32	95.20	1700	200	22000	270	262	5	37500	63000	11164
Brazoria	29.32	95.20	130	25	13000	90	562	57	18100	33400	9255
Brazoria	29.32	95.20	160	35	14000	90	632	59	19600	35800	9285
Brazoria	29.32	95.20	610	95	23250	220	302	11	35200	60700	11286
Brazoria	29.32	95.20	2000	235	24000	300	317	1	40500	68600	11725
Brazoria	29.32	95.20	140	30	14000	100	596	17	20400	36600	9278
Brazoria	29.32	95.20	170	30	12500	100	484	59	19600	34300	9281
Galveston	29.37	95.13	380	70	15250	140	414	31	23400	41300	8795
Galveston	29.37	95.13	400	75	16000	120	312	32	23800	42500	8828
Brazoria	29.28	95.13	1800	170	20500	180	356	16	34500	58000	13650
Brazoria	29.28	95.13	1600	185	17750	240	400	6	29300	50200	12770
Brazoria	29.07	95.67	333	21	10750	0	1348	1	16450	28903	10115
Brazoria	29.07	95.67	98	21	10779	0	1815	60	15769	28542	9726
Brazoria	29.07	95.67	137	64	14155	0	1507	151	21276	37290	10137
Brazoria	29.07	95.67	24	17	7180	0	1808	256	9928	19213	10100
Brazoria	29.32	95.17	2244	360	29170	0	580	37	49951	82342	11407
Brazoria	29.27	95.33	638	112	16625	0	976	75	26500	44926	6617
Brazoria	29.27	95.33	1104	29	27400	0	921	1	43800	73255	5670

Table 3a (continued)

County	Latitude	Longitude	Ca	Mg	Na	K	Alkalinity	SO4	Cl	TDS	Depth (feet)
Brazoria	29.20	95.42	1688	68	17581	0	854	1	29800	49992	10582
Brazoria	29.50	95.25	1804	322	38852	0	183	1	64000	105162	6118
Brazoria	29.17	95.80	253	72	6890	0	665	1	10900	18781	6800
Brazoria	29.40	95.42	1808	338	36262	0	244	69	59927	98648	6497
Brazoria	29.40	95.42	2005	368	38899	0	104	37	64537	105950	6495
Brazoria	29.02	95.75	384	78	15467	0	781	16	24300	410260	10776
Brazoria	29.03	95.77	344	64	17520	0	878	14	27300	461200	10433
Brazoria	29.04	95.68	432	68	17046	0	695	72	26800	45113	10740 10766
Brazoria	29.04	95.69	184	31	12370	0	1720	69	18450	32849	10122 10140
Brazoria	29.06	95.68	90	18	9145	0	2180	68	13000	24512	10104 10122
Brazoria	29.06	95.69	144	39	14258	0	1270	32	21600	37343	10096 10142
Brazoria	29.06	95.73	120	44	9361	0	2310	50	13400	25285	10270 10280
Brazoria	29.06	96.59	1180	223	21822	0	140	4	36200	60000	4051
Brazoria	29.06	95.73	160	49	14480	0	1270	32	22000	37991	10350 10354
Brazoria	29.06	95.74	96	39	13152	0	1440	46	19700	34473	10165 10170
Brazoria	29.09	95.56	731	148	17553	0	850	578	27900	47760	12232 12244
Brazoria	29.09	95.56	1547	206	24338	0	468	730	40100	67389	11970 11992
Matagorda	28.97	95.49	450	80	4911	0	171	20	8510	14142	11302- 11329
Matagorda	28.97	95.49	847	188	13954	0	488	0	23290	38767	11302-11329
Matagorda	28.97	95.48	1660	259	20881	0	769	2	35460	59031	11306- 11348
Matagorda	29.01	96.13	3520	183	26300	0	241	0	47300	77613	3711-3719
Matagorda	28.97	95.92	4350	450	34965	0	98	101	62800	102764	8207
Matagorda	28.90	96.05	896	174	19780	0	1647	50	31636	54183	7926
Matagorda	28.97	96.03	244	59	16968	0	1198	51	26053	44573	8558
Matagorda	28.97	96.03	64	28	4616	0	1159	112	6560	12539	8938
Matagorda	28.97	96.03	52	51	6424	0	1824	66	9042	17459	9402
Matagorda	29.08	95.87	874	153	27000	306	230	0	45700	74263	9299
Matagorda	29.08	95.87	1583	289	34200	358	156	0	61000	97586	8984
Matagorda	29.08	95.87	1750	285	33700	431	338	0	60000	96504	8971
Matagorda	28.77	96.28	85	14	9100	81	629	0	12600	22509	10191
Matagorda	28.88	96.10	29	90	15431	0	1785	35	23000	40435	9800
Matagorda	28.95	95.17	25	4	5540	0	3510	670	6060	15813	10430-10458
Matagorda	28.78	96.30	83	12	9810	65	1790	0	13120	25390	10190-10268
Matagorda	28.78	96.30	100	9	5840	61	806	0	8470	15380	11655- 1171
Matagorda	29.07	95.90	1620	286	37400	310	230	15	61000	100000	8940- 8945
Matagorda	29.07	95.90	1660	277	36000	359	242	6	59100	98800	8996- 9000
Matagorda	29.07	95.90	1070	225	35900	260	257	7	56900	93700	8708- 8712
Matagorda	28.98	95.92	118	26	15040	110	1251	11	22480	39048	8893- 8899
Matagorda	28.95	96.17	1230	356	30900	0	171	6	50800	83540	8322- 8331
Matagorda	28.95	96.17	671	153	21500	0	469	18	34500	57341	8348- 8352
Matagorda	29.07	95.90	2006	648	27061	0	854	0	46718	78600	9195
Matagorda	29.07	95.90	1040	187	39146	0	511	45	62481	103600	9195
Matagorda	29.07	95.90	2890	401	35000	0	279	0	60200	98836	8897- 8902

Table 3a (continued)

County	Latitude	Longitude	Ca	Mg	Na	K	Alkalinity	SO4	Cl	TDS	Depth (feet)
Matagorda	29.07	95.90	2380	23	33000	0	263	360	54800	90938	8980- 8992
Matagorda	29.07	95.90	1710	349	40600	0	260	78	66600	109673	8920- 8928
Jefferson	30.01	94.41	2044	48	36568	0	244	0	59929	99585	7266- 7280
Jefferson	29.97	94.13	426	79	11903	0	537	62	19000	32007	7788
Jefferson	29.97	94.13	816	136	16290	0	287	1	26800	44330	7723
Jefferson	29.97	94.13	348	152	11869	0	659	80	18900	32008	7835
Jefferson	30.07	94.13	2756	606	35540	0	79	1	61400	100382	6778
Jefferson	30.07	94.13	1475	192	17670	0	43	1	30400	49781	6779
Jefferson	30.07	94.13	1568	238	20290	0	98	1	34700	56895	6778
Jefferson	30.02	94.40	2835	764	40100	0	27	11	69100	112837	6055
Jefferson	30.02	94.40	2970	611	38232	0	221	103	65794	107931	6038
Jefferson	29.80	94.28	4655	906	38383	0	908	96	69502	114450	8521
Jefferson	29.80	94.28	2658	211	30692	0	605	79	52268	86513	8825
Jefferson	29.60	94.42	480	100	22600	146	1130	14	33800	57200	10421-10434
Jefferson	28.00	97.25	190	31	10500	80	880	75	15500	27900	10906-10914
Jefferson	29.95	94.00	2248	272	28200	0	6751	250	45200	83131	10606-10616
Jefferson	29.95	94.00	2685	216	30080	0	158	134	48800	82258	10642-10650
Jefferson	29.92	94.00	2455	233	23860	0	660	48	41400	68790	11276-11286
Jefferson	29.92	94.00	1288	160	14496	0	530	19	25115	41878	10946-10956

Table 3b. Major ion chemistry from Frio Formation, Northcentral region. Ionic concentrations in mg/L. Data from Kreitler and Richter, 1986.

County	Latitude	Longitude	Ca	Mg	Na	K	Alkalinity	SO4	Cl	TDS	Depth (feet)
Wharton	29.15	96.05	2124	607	29890	0	390	0	51420	84621	5542-5546
Wharton	29.15	96.05	1470	638	32490	0	425	0	54340	89613	5543-5548
Wharton	29.17	96.08	2352	376	30583	0	817	1	52000	86129	5535
Wharton	29.08	96.37	870	109	19957	0	390	1	32400	53727	5814
Wharton	29.25	96.20	2660	220	23100	0	290	1	41000	67271	5500
Jackson	28.78	96.57	987	193	23200	212	245	0	41100	65937	6419
Jackson	28.78	96.57	956	187	24500	219	240	0	42400	68502	6412
Jackson	28.78	96.57	1023	178	23700	226	215	0	42400	67742	6258
Jackson	29.13	96.67	8260	730	33500	767	59	4	68100	114000	9246-9268
Jackson	29.02	96.50	652	123	23319	0	442	1	37250	61787	6633
Jackson	29.03	96.50	934	232	23290	0	488	15	38000	62959	5483
Jackson	28.92	96.42	1314	307	23616	0	305	1	39500	65043	5237
Jackson	28.88	96.50	1680	119	21598	0	183	1	38000	61581	5228
Jackson	28.83	96.50	900	170	25643	0	293	12	41500	68518	6398
Jackson	28.92	96.73	1832	93	21271	0	262	1	36200	59659	4602
Jackson	28.92	96.73	1052	68	18229	0	344	6	30000	49699	5451
Jackson	28.76	96.65	1150	192	22900	0	207	0	37800	63268	5731-5763
Jackson	28.76	96.65	1300	190	23300	0	182	0	38700	63700	5737-5753
Jackson	28.77	96.64	1200	210	21220	0	187	0	35420	58354	5592-5596
Jackson	28.77	96.64	1200	275	21590	0	189	6	36680	60000	5592-5602
Jackson	28.77	96.65	1200	319	9547	0	74	7	17731	28884	5590-5593
Jackson	28.77	96.65	1049	376	9602	0	48	5	17731	28821	5756-5757
Jackson	28.77	96.64	1096	271	21849	0	184	6	36314	59723	5583-5593
Jackson	28.77	96.64	1080	250	20780	0	209	6	35260	57669	5583-5593
Jackson	28.77	96.65	2890	464	13660	0	64	4	27830	45030	5593-5760
Jackson	28.84	96.53	1090	325	21780	0	255	0	36830	60333	5245-5279
Jackson	28.89	96.48	710	153	24334	0	415	123	38800	67500	6796-6798
Jackson	28.89	96.48	850	158	22425	0	329	41	36200	63500	5675-5678
Jackson	28.91	96.66	1100	203	22954	0	244	129	37600	53000	4715-4740
Jackson	28.95	96.61	1060	21	22236	0	201	4	36000	62500	4985-5005
Jackson	29.02	96.47	1400	235	16200	0	142	10	50500	66700	4833-4860
Victoria	28.63	96.87	1482	277	24112	144	208	0	40800	67234	4790-4810
Victoria	28.63	96.86	1120	170	22917	140	232	0	37850	62484	5558-5562
Victoria	28.58	96.95	1680	230	24900	0	249	20	41800	68918	4548-4553
Victoria	28.58	96.95	814	246	22400	0	755	43	36200	60467	4536-4556
Victoria	28.58	96.95	754	280	26300	0	293	0	42500	70141	4489-4492
Victoria	28.58	96.95	2260	327	22300	0	145	0	39200	64248	3500-3512
Victoria	28.62	96.89	1112	180	23125	0	390	0	31942	56749	5484-5494
Victoria	28.62	96.89	1280	170	22943	0	292	60	37942	62687	5478-5493
Victoria	28.62	96.87	1202	204	22955	0	330	0	37926	62617	5734-5738
Victoria	28.62	96.87	2035	266	23262	0	188	0	39411	65162	4204-4208
Victoria	28.62	96.88	1302	170	22391	0	2183	0	37220	61266	5589-5591

Table 3b (continued)

County	Latitude	Longitude	Ca	Mg	Na	K	Alkalinity	SO4	Cl	TDS	Depth (feet)
Victoria	28.63	96.87	132	19	8960	0	519	97	13730	23457	8322-8328
Victoria	28.63	96.87	1165	145	20895	0	293	5	34527	57030	7545-7548
Victoria	28.63	96.87	1425	168	19540	0	235	25	32980	54373	6940-6950
Victoria	28.63	96.87	1186	365	22752	0	209	20	38106	62638	4768-4773
Victoria	28.63	96.87	1150	333	22648	0	140	14	37833	62118	4768-4773
Victoria	28.63	96.87	1200	435	19280	0	245	8	32970	54138	4767-4772
Victoria	28.63	96.87	1530	395	21340	0	115	10	36690	60080	4768-4773
Victoria	28.63	96.87	1170	216	21600	0	462	0	35747	59195	5745-5747
Victoria	28.63	96.87	1300	206	22748	0	391	0	37750	62395	5745-5748
Victoria	28.63	96.87	2692	447	19858	0	125	0	36624	59746	3495-3505
Victoria	28.63	96.87	1305	390	21275	0	210	5	36120	59305	4760-4775
Victoria	28.63	96.87	1312	208	22720	0	354	0	37750	62344	5742-5744
Victoria	28.63	96.87	1288	206	21428	0	298	0	35758	58978	5742-5744
Victoria	28.63	96.87	1466	186	22403	0	214	0	37557	61826	6029-6041
Victoria	28.63	96.88	1456	194	22703	0	244	115	37942	62654	6139-6144
Victoria	28.63	96.87	1260	0	23316	0	439	5	37942	62962	5474-5486
Victoria	28.64	96.87	1305	206	21393	0	240	0	35768	58912	5743-5746
Victoria	28.68	96.82	1671	272	22801	0	237	0	38766	63510	4767-4774
Victoria	28.69	96.83	1705	275	22771	0	269	0	38770	63810	4754-4778
Victoria	28.69	97.13	770	160	16610	0	230	0	27300	45060	4821-4825
Victoria	28.73	97.08	1638	313	22294	0	219	5	38100	62569	3116-3126
Victoria	28.75	96.83	2324	329	25750	0	0	26	43890	72319	5874-5878
Victoria	28.75	96.83	1980	224	23880	0	103	11	40910	67108	5614-5619
Victoria	28.89	97.06	1338	188	13320	0	94	48	23360	38348	3515

Table 3c. Major ion chemistry from Frio Formation, Southcentral region. Ionic concentrations in mg/L. Data from Kreitler and Richter, 1986.

County	Latitude	Longitude	Ca	Mg	Na	K	Alkalinity	SO4	Cl	TDS	Depth (feet)
Jim Wells	27.87	98.00	133	15	4828	0	409	263	7300	12984	4449- 4480
Jim Wells	27.68	97.95	10643	698	23687	0	153	0	57400	92581	6133- 6141
Jim Wells	27.68	97.95	45	19	7713	0	1274	0	11150	20387	4061- 4094
Jim Wells	27.66	97.95	8168	234	25549	0	201	0	54499	88649	6196-6221
Goliad	28.56	97.37	740	122	12757	0	720	30	20900	35269	3513-3522
Goliad	28.56	97.37	860	134	12938	0	625	6	21500	36063	3456-3470
Goliad	28.56	97.37	40	5	2754	0	1490	220	3190	7795	3193-3199
Goliad	28.57	97.29	100	12	5367	0	1560	136	7480	14655	5592-5597
Goliad	28.57	97.29	96	18	5439	0	1600	120	7590	14863	5592-5597
Goliad	28.57	97.29	376	146	13969	0	720	24	22200	37435	5088-5093
Goliad	28.62	97.29	580	159	15225	0	537	82	24600	41183	4527-4532
Goliad	28.62	97.29	700	172	16143	0	395	15	26400	43825	4516-4521
Goliad	28.74	97.41	490	195	9205	0	220	0	15500	25610	3042-3047
Goliad	28.74	97.41	650	210	10586	0	317	0	17900	29663	3336-3350
Goliad	28.74	97.41	629	230	11333	0	323	0	19100	31615	3678-3692
Bee	28.38	97.45	210	290	23500	0	0	0	37500	61500	5032
Aransas	28.10	96.98	460	50	10500	112	490	7	17150	28400	11204-11250
Aransas	28.08	97.13	6320	482	30544	0	409	1	59720	98081	8352- 8362
Aransas	28.27	96.87	130	2	6700	47	1	5	24300	40500	9506- 9518
Aransas	27.78	97.45	315	17	8400	122	580	17	13050	22400	10904-10960
Aransas	27.78	97.45	330	29	8400	130	540	49	13400	22900	11697-11712
Aransas	28.23	96.83	30	5	7050	49	2040	86	8700	16600	9203- 9240
Calhoun	28.20	96.53	450	111	27200	171	574	24	41500	70100	9293- 9309
Calhoun	28.28	96.67	2100	170	22600	130	120	5	42050	59800	8882- 8892
Calhoun	28.28	96.67	740	105	17100	110	710	23	27800	49100	8780- 8790
Calhoun	28.28	96.67	185	31	11200	85	1300	45	17050	31000	8796- 8802
Calhoun	28.63	96.82	984	225	24154	0	311	1	39500	65175	5450
Calhoun	28.57	96.84	1320	163	22379	0	138	105	63847	39671	6750-8250
Calhoun	28.57	96.84	2000	100	80000	0	0	1000	99400	175700	6750-7500
Calhoun	28.56	96.87	2558	194	25404	0	113	0	44250	72519	5067-5072
Calhoun	28.56	96.87	3549	116	24889	0	120	0	45000	73683	7412-7419
Calhoun	28.57	96.52	80	60	4120	0	1705	135	5580	11680	8721-8727
Calhoun	28.57	96.53	30	8	3505	32	1438	62	4630	9705	8754-8804
Calhoun	28.58	96.73	59	39	6245	0	3739	245	7500	17827	8988-9002
Calhoun	28.58	96.73	62	39	5872	0	2392	330	7650	16345	8968-8970
Calhoun	28.58	96.73	55	52	5597	0	2778	230	7100	15812	8989-9002
Calhoun	28.58	96.73	22	19	5296	0	2814	150	6520	14821	8996-8999
Calhoun	28.58	96.73	22	19	5675	0	3092	170	6930	15908	9004-9011
Calhoun	28.59	96.73	172	73	5573	0	311	350	8680	15159	5640-5649
Calhoun	28.59	96.73	154	36	5054	0	476	500	7380	13600	5688-5697
Calhoun	28.59	96.73	1911	304	23804	0	115	102	40200	66436	5710-5720
Calhoun	28.61	96.86	2549	380	21669	0	135	0	39000	63733	5459-5466

Table 3c (continued)

County	Latitude	Longitude	Ca	Mg	Na	K	Alkalinity	SO4	Cl	TDS	Depth (feet)
Calhoun	28.61	96.86	1275	160	22380	0	207	23	37100	61145	5462-5470
Calhoun	28.61	96.86	2060	182	21045	0	397	0	36400	60084	5425
Calhoun	28.62	96.88	911	238	22930	0	173	6	37600	61858	5435-7536
Calhoun	28.62	96.88	913	177	23230	0	321	6	37800	62447	5435-7536
Calhoun	28.62	96.88	921	192	23581	0	321	6	38400	63421	5435-7536
Calhoun	28.62	96.87	962	167	24146	0	272	6	39300	64853	4769-5499
Calhoun	28.62	96.66	212	26	5743	0	1793	452	7940	16166	7945-7951
Calhoun	28.62	96.66	126	21	6304	0	1952	406	8580	17389	7896-7902
Calhoun	28.63	96.71	1041	140	15973	0	702	0	26500	44318	7932-7938
Calhoun	28.63	96.71	57	90	5707	0	2790	0	7550	16194	8390-8401
Calhoun	28.63	96.71	72	164	7396	0	3185	260	9975	21052	8613-8619
Calhoun	28.63	96.71	206	109	11353	0	1074	112	17500	30354	9421-9434
Calhoun	28.63	96.68	52	30	2307	0	2980	456	1670	7495	8924-8938
Calhoun	28.63	96.69	18	2	2259	0	2603	200	1620	6905	9036-9048
Calhoun	28.63	96.69	2728	963	8720	0	328	300	20700	33739	9224-9284
Calhoun	28.64	96.68	127	17	11707	0	1279	135	17500	30765	8858-8890
Calhoun	28.64	96.68	678	109	21312	0	514	24	34100	56737	8966=8971
Calhoun	28.67	96.41	26	8	4330	109	1871	128	5660	12132	7806-7810
Calhoun	28.67	96.41	280	55	4460	75	968	136	6935	12909	7806-7810
San Patricio	28.02	97.25	42	9	5650	33	800	66	7600	15900	10965-10983
San Patricio	28.02	97.25	45	8	7170	32	1720	64	9400	18600	10521-10535
San Patricio	27.90	97.37	2925	580	29282	0	148	1	51783	84719	5670
San Patricio	27.90	97.42	101	21	10000	62	915	40	15100	27500	10728
San Patricio	27.90	97.42	134	22	9000	59	939	46	13400	24600	10670
San Patricio	27.90	97.42	89	15	6500	68	1040	110	9270	17900	11528
San Patricio	27.90	97.42	101	18	7500	62	932	59	10700	20300	11050
San Patricio	27.90	97.42	54	9	5375	43	775	75	7400	14700	11480
San Patricio	27.90	97.42	47	9	6250	46	1213	67	8200	16600	11180
San Patricio	28.00	97.22	42	9	6500	51	858	54	8700	17500	10550
San Patricio	27.97	97.33	370	56	11750	44	575	26	18700	32400	12120
San Patricio	27.97	97.33	330	48	13250	72	200	42	21000	36300	11880
San Patricio	27.90	97.42	2500	455	29500	215	270	13	51700	85400	4900
San Patricio	27.90	97.42	3040	475	22750	77	97	67	42800	69800	3350
San Patricio	27.90	97.42	2500	590	28500	152	189	15	50600	83300	4600
San Patricio	27.90	97.42	2880	340	25250	125	113	50	45100	74600	5790
San Patricio	27.90	97.42	200	31	9250	70	278	22	14000	24800	10320
San Patricio	28.02	97.25	42	9	5650	33	800	66	7600	15900	10965-10983
San Patricio	28.02	97.25	45	8	7170	32	1720	64	9400	18600	10521-10535
San Patricio	27.98	97.30	484	29	31300	173	237	270	46100	77800	9656- 9695
San Patricio	27.98	97.30	24	12	8100	41	1220	9	10900	19900	9660- 9702
San Patricio	27.98	97.30	282	22	7550	73	687	15	12150	20700	10693-11134
San Patricio	27.98	97.30	398	46	12690	92	820	9	19000	32500	11074-13162

Table 3c (continued)

County	Latitude	Longitude	Ca	Mg	Na	K	Alkalinity	SO4	Cl	TDS	Depth (feet)
San Patricio	27.98	97.30	392	136	8924	89	1708	365	13500	25015	11962-11994
San Patricio	27.98	97.30	270	31	7500	0	970	60	11600	20465	12572-12582
San Patricio	27.99	97.30	330	48	13250	72	200	42	21000	36300	11880
San Patricio	27.99	97.30	370	56	11750	44	575	26	18700	32400	12001
San Patricio	27.87	97.30	156	23	10500	78	1120	52	15200	27400	10665-10745
San Patricio	27.87	97.30	48	8	7330	40	2760	37	8900	16900	9715- 9724
San Patricio	27.87	97.30	31	8	7860	55	1720	4	10200	19400	9480- 9490
San Patricio	27.87	97.30	64	37	4763	0	2013	260	6300	13485	12246-12263
San Patricio	27.87	97.30	60	37	9895	0	1574	45	14700	26360	10720-10735
San Patricio	27.87	97.30	88	24	7367	0	1488	109	10700	19805	11020-11080
San Patricio	27.87	97.30	3480	464	23541	0	506	10	43600	71625	9049- 9051
San Patricio	27.87	97.30	3760	293	29976	0	37	123	53800	88050	8848- 8857
San Patricio	27.87	97.30	3200	0	34592	0	0	1	64800	105595	8713- 8726
San Patricio	27.87	97.30	72	5	6010	0	1403	47	8600	16155	11444-11486
San Patricio	27.87	97.30	70	37	6366	0	1513	204	9100	17325	11520-11537
San Patricio	27.87	97.30	420	98	14469	0	586	56	23100	38790	10079-10306
San Patricio	27.87	97.30	120	32	8259	0	1427	73	12400	22430	10821-10844
San Patricio	27.87	97.30	100	18	5550	0	2111	104	7500	15390	11135-11220
San Patricio	27.87	97.30	101	21	10000	62	915	40	15100	27500	10667
San Patricio	27.87	97.30	134	22	9000	59	939	46	13400	24600	10667
San Patricio	27.87	97.30	89	15	6500	68	1104	110	9270	17900	11526
San Patricio	27.87	97.30	101	18	7500	62	932	59	10700	20300	11047
San Patricio	27.87	97.31	54	9	5375	43	775	75	7400	14700	11477
San Patricio	27.87	97.31	47	9	6250	46	1213	67	8200	16600	11175
San Patricio	27.99	97.30	159	4	5360	233	1678	1130	5380	14000	13365-13500
San Patricio	27.99	97.30	296	24	9340	198	737	172	14710	25480	13365-13500
San Patricio	25.97	97.23	27	9	7900	36	1750	58	10300	21000	10475-10490
San Patricio	28.03	97.38	2232	452	27010	0	123	1	46900	76718	4889- 4934
San Patricio	27.88	97.43	3170	370	29100	0	239	1	51400	84360	5008- 5016
San Patricio	27.88	97.44	1239	586	29790	0	197	6	49730	81550	5640- 5647
San Patricio	27.88	97.44	2360	393	29500	0	200	0	50600	83074	5612- 5655
San Patricio	27.88	97.44	1184	599	30294	0	191	6	50450	82727	5581- 5636
San Patricio	27.88	97.44	1156	500	30195	0	230	5	50041	82145	5603- 5624
San Patricio	27.88	97.44	3420	247	20800	0	434	60	38700	63728	6382- 6384
San Patricio	27.88	97.44	2870	281	25500	0	575	1	45100	74564	5942- 5944
San Patricio	27.88	97.44	1175	737	30742	0	129	6	51576	84379	6736- 6740
San Patricio	27.88	97.44	3184	475	29464	0	136	0	52380	85707	4987- 4992
San Patricio	27.88	97.44	1165	464	28544	0	448	6	47175	77803	5865- 5867
San Patricio	27.88	97.44	1175	562	26743	0	230	13	44822	73574	5939- 5942
San Patricio	27.88	97.44	2401	571	27405	0	274	0	48015	78741	5939- 5942
San Patricio	28.03	97.38	2232	485	27273	0	123	1	47400	77514	4366- 4371
San Patricio	28.03	97.38	2199	435	27276	0	123	0	47200	77233	4350- 4357

Table 3c (continued)

County	Latitude	Longitude	Ca	Mg	Na	K	Alkalinity	SO4	Cl	TDS	Depth (feet)
San Patricio	28.04	97.38	2202	381	26787	0	111	1	46300	75782	5595- 5745
San Patricio	27.90	97.27	760	68	2814	0	49	433	5500	9660	8060- 8080
San Patricio	27.90	97.27	1712	95	13931	0	354	287	24400	40779	8120- 8140
San Patricio	27.90	97.27	526	12	5550	0	183	300	9100	15645	7967- 7980
San Patricio	27.90	97.27	232	18	2751	0	37	280	4420	7792	8020- 8040
San Patricio	27.90	97.27	2404	58	7004	0	214	370	14850	24900	9120- 9140
San Patricio	27.90	97.27	8088	201	19918	0	146	0	45600	73953	9120- 9140
San Patricio	27.91	97.27	1190	122	17984	0	988	70	29600	49954	6736- 6746
San Patricio	27.92	97.27	608	302	24888	0	470	0	40100	66368	6017- 6022
San Patricio	27.98	97.27	1884	170	14645	0	231	80	26250	43260	8386- 8391
San Patricio	27.98	97.27	97	77	9392	0	2097	235	13400	25383	9978- 9984
San Patricio	27.88	97.43	2571	588	29918	0	265	7	52300	85649	5644- 5647
San Patricio	27.88	97.43	1732	387	28983	0	495	0	48650	80247	5652- 5674
San Patricio	27.88	97.44	2657	503	30084	0	365	7	52400	86016	5652- 5674
San Patricio	27.88	97.43	891	0	20872	0	0	198	33645	55737	5587- 5607
San Patricio	27.88	97.43	3060	359	29400	0	134	0	51800	84769	3310- 5655
San Patricio	27.88	97.43	2427	586	26566	0	221	0	46851	76726	4987- 4992
San Patricio	27.88	97.43	2767	729	30027	0	143	0	53253	73000	5627- 5630
San Patricio	27.88	97.44	2310	399	29800	0	138	0	51200	83865	5620- 5624
San Patricio	27.88	97.44	2870	464	32000	0	97	70	50700	86383	5608- 5664
San Patricio	27.88	97.44	1221	1562	29144	0	127	6	51576	83639	4996- 5002
San Patricio	27.88	97.43	2890	503	27500	0	199	0	48600	79993	4991- 4995
Refugio	28.53	97.10	2345	410	24402	0	110	1	42900	70168	4720
Refugio	28.53	97.10	2022	253	24812	0	122	1	42500	69710	4487
Refugio	28.53	97.10	1034	115	25900	0	256	1	42000	69306	5000
Refugio	28.53	97.10	1454	218	25217	0	211	1	42000	69101	5015
Refugio	28.42	97.17	626	195	27758	0	519	1	44000	73099	5459
Refugio	28.45	96.97	560	112	19500	177	753	3	31580	52731	7924- 7926
Refugio	28.53	97.04	1084	232	17173	0	122	0	29000	47611	4525- 4541
Refugio	28.53	97.05	2210	378	25510	0	244	0	44200	72542	5301- 5309
Refugio	28.49	97.00	2620	175	23284	0	256	0	40900	67235	5895- 5898
Refugio	28.37	97.17	1126	300	25473	0	673	0	41800	69372	5502- 5508
Refugio	28.37	97.17	1126	300	22266	0	417	0	37000	61109	5154- 5158
Refugio	28.38	97.18	626	195	27758	0	519	0	44000	73098	5459
Refugio	28.39	97.26	2020	212	21800	0	292	0	37700	62031	6204- 6212
Refugio	28.42	97.26	1980	174	22700	0	206	0	38900	64023	6177- 6192
Refugio	28.35	97.15	518	43	25217	0	335	0	42000	69133	5881
Refugio	28.35	97.15	1034	115	25900	0	256	0	42000	69305	5015
Refugio	28.29	97.22	2540	97	25775	0	121	5	44500	73038	5516- 5876
Refugio	28.27	97.23	2657	180	23293	0	138	19	41100	67387	5911- 5919
Refugio	28.27	97.23	2380	255	25679	0	174	3	44500	72991	4093- 5942
Refugio	28.28	97.23	1097	218	24206	0	555	31	39600	65707	5314- 5316

Table 3c (continued)

County	Latitude	Longitude	Ca	Mg	Na	K	Alkalinity	SO4	Cl	TDS	Depth (feet)
San Patricio	28.04	97.38	2202	381	26787	0	111	1	46300	75782	5595- 5745
San Patricio	27.90	97.27	760	68	2814	0	49	433	5500	9660	8060- 8080
San Patricio	27.90	97.27	1712	95	13931	0	354	287	24400	40779	8120- 8140
San Patricio	27.90	97.27	526	12	5550	0	183	300	9100	15645	7967- 7980
San Patricio	27.90	97.27	232	18	2751	0	37	280	4420	7792	8020- 8040
San Patricio	27.90	97.27	2404	58	7004	0	214	370	14850	24900	9120- 9140
San Patricio	27.90	97.27	8088	201	19918	0	146	0	45600	73953	9120- 9140
San Patricio	27.91	97.27	1190	122	17984	0	988	70	29600	49954	6736- 6746
San Patricio	27.92	97.27	608	302	24888	0	470	0	40100	66368	6017- 6022
San Patricio	27.98	97.27	1884	170	14645	0	231	80	26250	43260	8386- 8391
San Patricio	27.98	97.27	97	77	9392	0	2097	235	13400	25383	9978- 9984
San Patricio	27.88	97.43	2571	588	29918	0	265	7	52300	85649	5644- 5647
San Patricio	27.88	97.43	1732	387	28983	0	495	0	48650	80247	5652- 5674
San Patricio	27.88	97.44	2657	503	30084	0	365	7	52400	86016	5652- 5674
San Patricio	27.88	97.43	891	0	20872	0	0	198	33645	55737	5587- 5607
San Patricio	27.88	97.43	3060	359	29400	0	134	0	51800	84769	3310- 5655
San Patricio	27.88	97.43	2427	586	26566	0	221	0	46851	76726	4987- 4992
San Patricio	27.88	97.43	2767	729	30027	0	143	0	53253	73000	5627- 5630
San Patricio	27.88	97.44	2310	399	29800	0	138	0	51200	83865	5620- 5624
San Patricio	27.88	97.44	2870	464	32000	0	97	70	50700	86383	5608- 5664
San Patricio	27.88	97.44	1221	1562	29144	0	127	6	51576	83639	4996- 5002
San Patricio	27.88	97.43	2890	503	27500	0	199	0	48600	79993	4991- 4995
Refugio	28.53	97.10	2345	410	24402	0	110	1	42900	70168	4720
Refugio	28.53	97.10	2022	253	24812	0	122	1	42500	69710	4487
Refugio	28.53	97.10	1034	115	25900	0	256	1	42000	69306	5000
Refugio	28.53	97.10	1454	218	25217	0	211	1	42000	69101	5015
Refugio	28.42	97.17	626	195	27758	0	519	1	44000	73099	5459
Refugio	28.45	96.97	560	112	19500	177	753	3	31580	52731	7924- 7926
Refugio	28.53	97.04	1084	232	17173	0	122	0	29000	47611	4525- 4541
Refugio	28.53	97.05	2210	378	25510	0	244	0	44200	72542	5301- 5309
Refugio	28.49	97.00	2620	175	23284	0	256	0	40900	67235	5895- 5898
Refugio	28.37	97.17	1126	300	25473	0	673	0	41800	69372	5502- 5508
Refugio	28.37	97.17	1126	300	22266	0	417	0	37000	61109	5154- 5158
Refugio	28.38	97.18	626	195	27758	0	519	0	44000	73098	5459
Refugio	28.39	97.26	2020	212	21800	0	292	0	37700	62031	6204- 6212
Refugio	28.42	97.26	1980	174	22700	0	206	0	38900	64023	6177- 6192
Refugio	28.35	97.15	518	43	25217	0	335	0	42000	69133	5881
Refugio	28.35	97.15	1034	115	25900	0	256	0	42000	69305	5015
Refugio	28.29	97.22	2540	97	25775	0	121	5	44500	73038	5516- 5876
Refugio	28.27	97.23	2657	180	23293	0	138	19	41100	67387	5911- 5919
Refugio	28.27	97.23	2380	255	25679	0	174	3	44500	72991	4093- 5942
Refugio	28.28	97.23	1097	218	24206	0	555	31	39600	65707	5314- 5316

Table 3c (continued)

County	Latitude	Longitude	Ca	Mg	Na	K	Alkalinity	SO4	Cl	TDS	Depth (feet)
Refugio	28.29	97.23	189	24	9051	0	3529	97	12250	25140	8592- 8602
Refugio	28.29	97.23	143	24	8916	0	3554	110	11950	24702	8674- 8682
Refugio	28.27	97.24	2457	244	24632	0	151	6	43000	70490	5870- 5879
Refugio	28.27	97.24	2426	255	25474	0	117	3	44300	72575	5854- 5858
Refugio	28.27	97.24	2216	269	25608	0	247	3	44100	72443	5694- 5702
Refugio	28.27	97.24	2657	205	25306	0	120	6	44300	72594	5872- 5882
Refugio	28.24	97.26	491	47	12673	0	825	460	19750	34246	5446- 5550
Refugio	28.20	97.27	1183	141	18736	0	725	13	31000	51798	8122- 8148
Refugio	28.20	97.26	2171	467	26629	0	542	6	46000	75815	4556- 4560
Refugio	28.20	97.26	2500	480	25191	0	378	0	44500	73049	4494- 4583
Refugio	28.20	97.26	2409	508	26462	0	176	0	46500	76055	4570- 4581
Refugio	28.53	97.06	2345	410	24402	0	116	0	42900	70173	4720- 4738
Refugio	28.53	97.06	1737	360	19311	0	165	0	33800	55793	4716- 4732
Refugio	28.53	97.06	2436	505	23537	0	122	0	42000	68600	4825- 4830
Refugio	28.53	97.06	2244	460	23383	0	122	0	41300	67509	4995- 5018
Nueces	27.87	97.35	3700	375	26000	260	162	18	48200	80100	9000
Nueces	27.83	97.70	2148	91	19481	0	140	30	34050	55940	5974
Nueces	27.67	97.30	1026	241	25716	0	805	20	41700	69508	6680
Nueces	27.67	97.73	2090	493	23237	0	97	1	40892	66810	4700
Nueces	27.83	97.92	6	43	3808	0	1122	109	5274	10362	5586
Nueces	27.75	97.55	166	28	14400	76	1550	28	20600	37900	10460-10482
Nueces	27.75	97.55	181	30	13300	105	990	18	20000	34200	9340- 9346
Nueces	27.75	97.55	491	45	10600	264	570	46	16700	29900	10879-10898
Nueces	27.75	97.55	375	26	8860	375	400	5	14000	24500	12538-12586
Nueces	27.75	97.55	87	38	15200	211	1070	3	22000	38900	11658-11670
Nueces	27.78	97.25	21000	715	53600	485	114	8	125600	213000	10942-10993
Nueces	27.77	97.18	689	117	21988	0	846	75	34959	58674	8698- 8726
Nueces	27.77	97.18	498	125	20893	0	1292	21	32734	55563	9367- 9387
Nueces	27.77	97.18	2050	74	21036	0	317	12	36125	60183	10700
Nueces	27.77	97.18	532	105	20344	0	842	0	32117	53950	10200
Nueces	27.85	97.45	4200	120	21896	0	354	0	41180	67750	6800
Nueces	27.85	97.45	106	58	9075	0	1545	6	13453	24243	8831
Nueces	27.87	97.15	83	16	8000	4	740	25	11600	21200	10682
Nueces	27.87	97.15	3700	375	26000	260	162	18	48200	80100	9000
Nueces	27.87	97.15	1640	15	10500	95	115	47	18900	31800	8784
Nueces	27.78	97.25	36020	1664	42138	0	237	1	133680	214524	10942-10969
Nueces	27.78	97.25	29640	1791	53051	0	41	1	139700	226262	9983- 9996
Nueces	27.78	97.25	31190	1640	57732	0	123	1	149460	241606	12490-12496
Nueces	27.75	97.54	1331	2233	23640	0	340	9	45130	72700	7606- 7616
Nueces	27.75	97.54	4727	351	21220	0	352	6	41940	68600	8140- 8150
Nueces	27.75	97.53	207	0	8730	0	1360	44	13000	23411	9062- 9100
Nueces	27.76	97.53	7450	513	31700	0	92	0	63400	103200	6050- 6054

Table 3c (continued)

County	Latitude	Longitude	Ca	Mg	Na	K	Alkalinity	SO4	Cl	TDS	Depth (feet)
Nueces	27.76	97.53	5580	181	25400	0	350	0	49400	80908	7135- 7139
Nueces	27.82	97.20	684	80	17396	0	868	244	27666	47060	8980- 8986
Nueces	27.82	97.20	473	0	17295	0	618	136	26950	45554	8270- 8276
Nueces	27.80	97.16	826	289	23450	0	640	15	38100	63320	7957- 7976
Nueces	27.80	97.15	799	315	23590	0	615	44	38360	63730	7940- 7954
Nueces	27.80	97.16	1220	255	26000	0	814	28	42500	70848	7441- 7467
Nueces	27.80	97.16	907	178	22700	0	935	35	35000	61269	7819- 7836
Nueces	27.81	97.18	464	168	18756	0	1202	8	29522	50120	7946- 7995
Nueces	27.84	97.18	6496	896	33560	0	65	160	65696	106900	5600
Nueces	27.83	97.17	534	224	19172	0	1123	16	30492	51561	7972- 7986
Nueces	27.82	97.16	664	0	18200	0	0	0	27900	47537	8689- 8702
Nueces	27.82	97.15	154	61	10190	0	1175	590	15050	27220	8135
Nueces	27.80	97.15	534	321	20272	0	579	53	32657	54598	7912- 7934
Nueces	27.84	97.15	288	148	17200	0	1200	144	26700	45687	8712- 8714
Nueces	27.84	97.15	252	148	15100	0	1540	217	23100	40371	8432- 8450
Nueces	27.84	97.15	294	156	18800	0	1310	10	29200	49798	8332- 8339
Nueces	27.84	97.15	548	146	22300	0	1340	70	35000	59462	8047- 8055
Nueces	27.84	97.16	480	216	21700	0	1220	0	34200	57854	7970- 7980
Nueces	27.84	97.16	844	231	22300	0	966	98	36000	60491	8440- 8447
Nueces	27.84	97.15	287	88	19400	0	1220	0	30000	51012	8726- 8728
Nueces	27.73	97.19	872	488	24810	0	777	29	40740	67720	7312- 7332
Nueces	27.73	97.19	1260	300	25634	0	1176	25	42540	71058	7381- 7406
Nueces	27.68	97.31	1404	419	29947	0	0	567	49600	81945	6729- 6735
Nueces	27.66	97.29	296	71	9483	0	408	20	15100	25370	6640- 6655
Nueces	27.67	97.29	733	183	22000	0	641	0	35400	58950	6645- 6660
Nueces	27.66	97.29	1150	207	25590	0	763	1	41650	69360	6633- 6657
Nueces	27.67	97.30	2472	159	25340	0	781	23	43500	72280	6645- 6660
Nueces	27.80	97.63	2148	91	19480	0	140	30	34050	55940	5968- 5984
Nueces	27.75	97.54	1313	2308	24520	0	342	10	46660	75160	7888- 7898
Nueces	27.68	97.28	498	138	12620	0	756	276	20100	34380	6668- 6680
Nueces	27.68	97.28	1026	241	25710	0	805	1	41700	69480	6671- 6679
Nueces	27.68	97.28	1364	319	25620	0	756	0	42400	70460	6665- 6678
Nueces	27.68	97.27	6279	452	28600	0	42	1200	55700	92270	6601- 6605
Nueces	27.68	97.27	1427	181	25770	0	852	0	42350	70580	6617- 6628
Nueces	27.67	97.28	680	104	8202	0	616	267	13600	23470	6670- 6680
Nueces	27.65	97.28	1880	300	24400	0	610	27	41500	68720	6640- 6651
Nueces	27.68	97.26	1483	451	26580	0	813	9	44500	73840	6638- 6646
Nueces	27.75	97.53	211	14	8723	0	1352	48	13072	23467	8954- 8958
Nueces	27.82	97.15	835	143	14641	0	731	0	24153	40785	12410-12600
Nueces	27.66	97.14	1509	307	22850	0	833	145	38230	63920	7644- 7653
Kleberg	27.44	97.57	7678	196	25028	0	87	110	52700	85799	7234- 7235
Kleberg	27.44	97.57	7476	712	35961	0	87	6	70800	115000	5665- 5668

Table 3c (continued)

County	Latitude	Longitude	Ca	Mg	Na	K	Alkalinity	SO4	Cl	TDS	Depth (feet)
Kleberg	27.44	97.57	11241	307	18036	0	55	6	48650	78295	7215
Kleberg	27.44	97.57	10099	258	17530	0	49	10	45700	73646	7885
Kleberg	27.44	97.57	10789	355	19337	0	49	7	50000	80537	8290
Kleberg	27.44	97.57	8365	270	22856	0	49	115	50800	82455	7237- 7243
Kleberg	27.44	97.57	11436	73	17187	0	62	6	47000	75764	7890- 7893
Kleberg	27.47	97.58	7961	761	33800	0	25	11	68500	111100	5392- 5394
Kleberg	27.45	97.58	9092	73	20595	0	68	3	48100	77931	7565- 7568
Kleberg	27.45	97.59	9456	98	19610	0	62	3	47300	76529	7280- 7284
Kleberg	27.45	97.60	9335	49	21203	0	62	3	49400	80088	7526- 7529
Kleberg	27.45	97.58	7557	393	32638	0	43	15	64900	105500	6355- 6356
Kleberg	27.45	97.59	8082	245	24437	0	62	60	52700	85586	7113- 7117
Kleberg	27.44	97.59	8809	73	22103	0	105	7	49900	80997	7470- 7473
Kleberg	27.44	97.59	8283	614	30537	0	49	27	63500	103000	7080
Kleberg	27.44	97.59	8122	147	24725	0	93	76	52900	86063	7114- 7117
Kleberg	27.40	97.56	3686	10	11917	0	290	62	24750	40715	10069-10118

Table 3d. Major ion chemistry from Frio Formation, Southgulf region. Ionic concentrations in mg/L. Data from Kreitler and Richter, 1986.

County	Latitude	Longitude	Ca	Mg	Na	K	Alkalinity	SO4	Cl	TDS	Depth (feet)
Jim Wells	27.38	98.08	1016	220	11100	0	718	0	19200	32267	5930- 5933
Jim Wells	27.38	98.09	907	166	10790	0	724	0	18300	30910	6050- 6055
Jim Wells	27.37	98.13	615	617	10370	0	460	16	18600	30709	5536-5556
Jim Wells	27.37	98.11	542	129	8542	0	968	15	13930	24139	6117-6123
Jim Wells	27.37	98.12	1294	404	10620	0	187	31	19720	32259	5244-5288
Jim Wells	27.38	98.12	606	326	3004	0	296	5	6508	10820	6922-6942
Jim Wells	27.38	98.12	450	76	7194	0	149	7	12040	19920	6097-6137
Jim Wells	27.71	98.06	275	80	8105	0	194	74	13040	21769	5329-5343
Duval	27.64	98.30	90	182	4958	0	77	500	7840	13722	2984- 2996
Duval	27.64	98.30	112	6	4022	0	171	12	6290	10636	3768- 3791
Duval	27.64	98.30	359	90	6684	0	91	80	11050	18341	3450- 3454
Hidalgo	26.17	98.07	2128	36	5711	0	293	175	12375	20968	8125- 8265
Hidalgo	26.17	98.07	328	15	6081	0	315	327	9585	16649	7100
Hidalgo	26.17	98.07	512	58	10459	1	366	1812	15672	28904	6556- 6621
Hidalgo	26.17	98.07	733	36	7353	0	182	120	12544	21450	7780
Hidalgo	26.23	98.53	95	48	10321	0	84	83	16062	26693	2556
Hidalgo	26.23	98.53	173	44	6933	0	367	1	10912	18430	2775
Hidalgo	26.23	98.53	130	47	12048	0	809	4	18470	31508	3095
Hidalgo	26.27	98.42	1096	162	17028	0	182	10	28555	47033	4002
Hidalgo	26.27	98.42	1640	270	15251	0	157	3672	24297	45287	7505
Hidalgo	26.27	98.42	762	126	15548	0	194	1	25578	42209	4016
Hidalgo	26.27	98.42	925	96	11564	0	73	987	18963	32608	4666
Hidalgo	26.50	98.42	727	0	9045	0	0	1250	11234	24770	4785- 4792
Hidalgo	26.36	98.33	2801	168	12263	0	186	24	24319	39901	6490- 6498
Hidalgo	26.36	98.33	5497	207	23330	0	292	12	46137	75498	6490- 6498
Hidalgo	26.36	98.33	2290	170	12500	0	304	131	23100	38511	7920- 7935
Hidalgo	26.78	98.10	8018	172	20442	0	290	80	46000	75053	6627- 6637
Hidalgo	26.78	98.10	799	25	6667	0	0	1000	10300	19348	6766- 6776
Hidalgo	26.78	98.10	2387	148	13187	0	32	840	24000	40916	6827- 6836
Hidalgo	26.78	98.10	9181	387	29817	0	227	20	63300	102900	7231- 7238
Hidalgo	26.78	98.10	7706	161	28425	0	138	150	57600	94375	7350- 7365
Hidalgo	26.78	98.10	11088	387	35652	0	239	0	75700	123100	7795- 7809
Hidalgo	26.66	98.30	1070	0	7716	0	122	4000	10767	23700	2663- 2749
Brooks	26.83	98.40	2460	60	13502	0	66	32	25286	41406	4744
Brooks	26.97	98.25	3032	170	18941	0	610	12	34700	57465	4900
Brooks	26.82	98.39	2173	3	16507	0	1257	16	28600	48556	4970- 6551
Brooks	26.82	98.40	3200	90	14777	0	69	13	28700	46849	4710- 4719
Brooks	26.82	98.40	2599	7	11480	0	85	138	22200	36509	4462- 4508
Brooks	26.81	98.40	2914	148	14144	0	44	13	27400	44663	4718- 4728
Brooks	26.81	98.40	2800	151	13884	0	44	20	26800	43699	4487- 4494
Brooks	26.79	98.40	444	3	2476	0	165	4250	1300	8718	3368- 3400
Brooks	26.79	98.40	1946	33	15851	0	1025	26	27400	46281	6100- 6110
Brooks	26.79	98.40	595	0	4162	0	451	22	7200	12430	5661- 5669

Table 3d (continued)

County	Latitude	Longitude	Ca	Mg	Na	K	Alkalinity	SO4	Cl	TDS	Depth (feet)
Brooks	26.78	98.40	4567	214	25888	0	220	14	48550	79453	6721- 6729
Brooks	26.94	98.18	7688	1034	25924	0	262	32	56500	91440	6661- 6668
Brooks	26.94	98.17	6827	681	19788	0	104	120	44500	72020	5828- 5838
Brooks	26.94	98.17	7751	559	24852	0	232	18	53600	87012	6230- 6240
Brooks	26.93	98.17	4571	331	18294	0	470	124	36950	60740	6425- 6445
Brooks	26.85	98.08	9833	291	28801	0	160	1030	61900	102000	8205- 8219
Brooks	26.84	98.11	5678	1445	17042	0	231	50	40250	64846	6998- 7010
Brooks	26.84	98.11	912	73	9145	0	0	450	14600	25780	4411- 4429
Brooks	26.84	98.11	3853	36	16942	0	0	130	32400	53700	4674- 4688
Brooks	26.84	98.11	8619	273	24261	0	259	0	53350	86797	6167- 6174
Brooks	26.83	98.10	11466	516	28399	0	37	38	65600	106100	6903- 6914
Brooks	27.07	98.02	21284	242	26816	0	134	0	79800	128300	8222- 8229
Brooks	27.07	98.02	3881	121	12358	0	317	180	26000	42857	7191- 7198
Brooks	27.07	98.03	2619	299	10302	0	487	1000	20400	35107	6246- 6259
Brooks	27.07	98.03	5228	320	17900	0	407	10	37650	61545	7342- 7352
Brooks	27.07	98.03	4266	973	18377	0	418	180	38400	62614	8033- 8043
Brooks	27.07	98.03	2410	438	7961	0	531	180	17400	28920	7326- 7332
Brooks	27.07	98.03	7831	948	17847	0	232	110	44000	70968	6235- 6240
Brooks	27.06	98.03	121	268	2848	0	438	578	4695	8940	8085- 8087
Brooks	27.06	98.03	289	97	5959	0	590	1645	9160	17740	8575- 8582
Brooks	27.06	98.03	404	61	4744	0	420	480	7650	13759	8125- 8142
Brooks	27.02	98.12	30258	3190	50891	0	121	0	141500	226000	5836- 5854
Brooks	27.14	98.38	19600	1986	62633	0	61	4	137000	221300	4769- 4775
Brooks	27.00	98.28	4563	340	13750	0	639	20	30000	49312	6545- 6555
Brooks	27.00	98.28	3414	1520	14861	0	573	90	32800	53258	6552- 6578
Brooks	26.99	98.28	105	128	3962	0	328	80	6425	11028	6550- 6573
Brooks	26.98	98.28	4067	851	13930	0	342	10	31000	50200	6544- 6560
Brooks	26.83	98.38	2906	243	18242	0	1061	8	33400	55860	6141- 6144
Brooks	26.84	98.39	1946	289	21134	0	778	51	36400	60589	6169- 6176
Brooks	26.84	98.39	1875	122	15844	0	1165	80	27400	46486	5592- 5599
Brooks	26.84	98.39	1934	912	15415	0	1501	20	29000	48782	5783- 5791
Brooks	26.84	98.39	2460	821	22074	0	744	0	40400	66499	6167- 6173
Brooks	26.84	98.38	2480	547	16352	0	883	18	30700	50980	5626- 5632
Brooks	26.84	98.39	2000	1	16188	0	1366	22	27725	47301	5520- 5530
Brooks	26.84	98.39	1606	292	17968	0	903	14	30900	51683	6141- 6148
Brooks	26.84	98.39	2117	135	15560	0	1437	44	27300	46593	5570- 5577
Brooks	26.84	98.38	2053	71	16735	0	1708	130	27700	48397	5794- 5804
Brooks	26.83	98.39	1946	66	14882	0	1635	20	25650	44199	5582- 5593
Brooks	26.83	98.38	2594	1	18183	0	268	20	32500	53565	6108- 6125
Brooks	26.83	98.39	2811	328	17666	0	885	0	32700	54390	6231- 6241
Brooks	26.83	98.39	1861	109	17532	0	1122	40	30000	50664	6140- 6144
Brooks	26.83	98.40	2675	17	15191	0	122	100	28100	46205	4981- 4986
Brooks	26.83	98.41	4919	17	17175	0	55	8	35250	57424	4725- 4734

Table 3d (continued)

County	Latitude	Longitude	Ca	Mg	Na	K	Alkalinity	SO4	Cl	TDS	Depth (feet)
Brooks	26.83	98.40	676	1	9492	0	1427	26	15000	26621	5460- 5470
Brooks	26.83	98.40	2123	62	15157	0	171	60	27200	44773	5136- 5144
Brooks	26.82	98.39	2173	3	16061	0	1251	36	27900	47424	4970- 6551
Brooks	27.14	98.04	3373	255	7741	0	287	20	18500	30176	7502- 7524
Brooks	27.14	98.04	1673	121	16067	0	537	16	27800	46214	7584- 7591
Brooks	27.08	98.01	7904	696	18692	0	331	28	44600	72335	6789- 6794
Brooks	27.08	98.01	7904	127	19784	0	92	190	44400	72702	6280- 6292
Brooks	27.08	98.01	8052	190	20572	0	379	68	46300	75585	6615- 6652
Brooks	27.08	98.01	7825	443	20628	0	355	20	46800	76071	6809- 6818
Brooks	27.08	98.01	6876	443	20320	0	490	106	44400	72719	7110- 7120
Brooks	27.08	98.02	5434	411	16806	0	588	60	36400	59699	7374- 7389
Brooks	27.08	98.02	8200	570	20932	0	526	24	48200	78452	7774- 7751
Brooks	27.08	98.02	7212	506	19611	0	239	120	44200	71990	7792- 7801
Brooks	27.08	98.02	6547	963	16314	0	367	0	39400	63591	7118- 7123
Brooks	27.08	98.03	7114	1125	17218	0	318	100	42200	68099	6757- 6764
Brooks	27.07	98.02	11603	158	23746	0	183	0	57600	93290	7912- 7918
Brooks	27.07	98.02	9016	377	20471	0	159	12	48600	78635	6643- 6650
Brooks	27.07	98.02	5040	328	13463	0	165	120	30500	49616	6733- 6740
Brooks	27.07	98.02	5743	304	17644	0	317	40	38100	62148	7416- 7422
Starr	26.70	98.50	1656	73	13802	0	214	18	24244	40007	4140
Starr	26.77	98.47	2444	58	13819	0	116	53	25896	42386	4653
Starr	26.42	98.67	344	90	11921	0	842	1	18764	31962	2585
Starr	26.60	98.57	1268	50	7395	0	110	1400	12696	22919	3483
Starr	26.60	98.57	933	78	10707	0	78	445	17923	30164	4617
Starr	26.38	98.07	455	90	14583	0	288	37	23356	38809	3731
Starr	26.38	98.07	360	102	13714	0	433	112	21746	36467	3887
Starr	26.38	98.07	480	131	15606	0	444	78	24980	41719	3970
Starr	26.70	98.50	923	98	11008	0	1781	25	17839	31674	4932
Starr	26.60	98.57	801	96	14823	0	212	37	24400	40369	4395
Starr	26.60	98.57	192	46	6882	0	689	362	10418	18589	4377
Starr	26.38	98.12	190	55	8300	0	464	1	13023	22033	3775
Starr	26.70	98.57	690	87	10351	0	1060	91	16750	29029	4590
Starr	26.77	98.47	1096	88	12938	0	1647	1	21189	36959	5332
Starr	26.43	98.27	480	116	14085	0	350	1	22700	37732	1774
Starr	26.43	98.27	356	78	12189	0	562	1	19326	32512	1544
Starr	26.77	98.47	1786	76	13536	0	226	49	24084	39757	4350
Starr	26.77	98.47	4160	274	22074	0	368	1	41983	68860	5812
Starr	26.61	98.53	112	0	5710	0	1070	3080	6040	16078	4378- 4390
Starr	26.61	98.53	772	0	10045	0	395	1110	15700	28104	4582- 4588
Starr	26.60	98.54	7797	221	15717	0	376	0	38497	62668	6040- 6050
Starr	26.61	98.53	11701	266	15209	0	435	0	44697	72336	6465- 6469
Starr	26.61	98.53	1692	109	12534	0	565	44	22278	37222	5805- 5809
Starr	26.58	98.51	1996	78	15522	0	785	480	26883	45754	4676- 4685

Table 3d (continued)

County	Latitude	Longitude	Ca	Mg	Na	K	Alkalinity	SO4	Cl	TDS	Depth (feet)
Brooks	26.83	98.40	676	1	9492	0	1427	26	15000	26621	5460- 5470
Brooks	26.83	98.40	2123	62	15157	0	171	60	27200	44773	5136- 5144
Brooks	26.82	98.39	2173	3	16061	0	1251	36	27900	47424	4970- 6551
Brooks	27.14	98.04	3373	255	7741	0	287	20	18500	30176	7502- 7524
Brooks	27.14	98.04	1673	121	16067	0	537	16	27800	46214	7584- 7591
Brooks	27.08	98.01	7904	696	18692	0	331	28	44600	72335	6789- 6794
Brooks	27.08	98.01	7904	127	19784	0	92	190	44400	72702	6280- 6292
Brooks	27.08	98.01	8052	190	20572	0	379	68	46300	75585	6615- 6652
Brooks	27.08	98.01	7825	443	20628	0	355	20	46800	76071	6809- 6818
Brooks	27.08	98.01	6876	443	20320	0	490	106	44400	72719	7110- 7120
Brooks	27.08	98.02	5434	411	16806	0	588	60	36400	59699	7374- 7389
Brooks	27.08	98.02	8200	570	20932	0	526	24	48200	78452	7774- 7751
Brooks	27.08	98.02	7212	506	19611	0	239	120	44200	71990	7792- 7801
Brooks	27.08	98.02	6547	963	16314	0	367	0	39400	63591	7118- 7123
Brooks	27.08	98.03	7114	1125	17218	0	318	100	42200	68099	6757- 6764
Brooks	27.07	98.02	11603	158	23746	0	183	0	57600	93290	7912- 7918
Brooks	27.07	98.02	9016	377	20471	0	159	12	48600	78635	6643- 6650
Brooks	27.07	98.02	5040	328	13463	0	165	120	30500	49616	6733- 6740
Brooks	27.07	98.02	5743	304	17644	0	317	40	38100	62148	7416- 7422
Starr	26.70	98.50	1656	73	13802	0	214	18	24244	40007	4140
Starr	26.77	98.47	2444	58	13819	0	116	53	25896	42386	4653
Starr	26.42	98.67	344	90	11921	0	842	1	18764	31962	2585
Starr	26.60	98.57	1268	50	7395	0	110	1400	12696	22919	3483
Starr	26.60	98.57	933	78	10707	0	78	445	17923	30164	4617
Starr	26.38	98.07	455	90	14583	0	288	37	23356	38809	3731
Starr	26.38	98.07	360	102	13714	0	433	112	21746	36467	3887
Starr	26.38	98.07	480	131	15606	0	444	78	24980	41719	3970
Starr	26.70	98.50	923	98	11008	0	1781	25	17839	31674	4932
Starr	26.60	98.57	801	96	14823	0	212	37	24400	40369	4395
Starr	26.60	98.57	192	46	6882	0	689	362	10418	18589	4377
Starr	26.38	98.12	190	55	8300	0	464	1	13023	22033	3775
Starr	26.70	98.57	690	87	10351	0	1060	91	16750	29029	4590
Starr	26.77	98.47	1096	88	12938	0	1647	1	21189	36959	5332
Starr	26.43	98.27	480	116	14085	0	350	1	22700	37732	1774
Starr	26.43	98.27	356	78	12189	0	562	1	19326	32512	1544
Starr	26.77	98.47	1786	76	13536	0	226	49	24084	39757	4350
Starr	26.77	98.47	4160	274	22074	0	368	1	41983	68860	5812
Starr	26.61	98.53	112	0	5710	0	1070	3080	6040	16078	4378- 4390
Starr	26.61	98.53	772	0	10045	0	395	1110	15700	28104	4582- 4588
Starr	26.60	98.54	7797	221	15717	0	376	0	38497	62668	6040- 6050
Starr	26.61	98.53	11701	266	15209	0	435	0	44697	72336	6465- 6469
Starr	26.61	98.53	1692	109	12534	0	565	44	22278	37222	5805- 5809
Starr	26.58	98.51	1996	78	15522	0	785	480	26883	45754	4676- 4685

Table 3d (continued)

County	Latitude	Longitude	Ca	Mg	Na	K	Alkalinity	SO4	Cl	TDS	Depth (feet)
Starr	26.77	98.83	37	2	1175	0	150	376	1394	3262	1504- 1518
Starr	26.77	98.83	42	2	1212	0	110	360	1558	3365	1474- 1496
Starr	26.78	98.41	1986	28	10911	0	116	103	20250	33376	4749- 4752
Starr	26.78	98.42	1513	1	12842	0	641	48	22100	37144	5124- 5130
Starr	26.78	98.42	4432	230	25158	0	268	18	47200	77306	6506- 6516
Starr	26.77	98.39	509	12	2930	0	82	6750	420	10703	2114- 2152
Starr	26.77	98.39	589	20	4288	0	88	7840	1870	14695	2630- 2657
Starr	26.77	98.39	1177	6	6298	0	50	2430	10000	19961	3798- 3842
Starr	26.77	98.43	2594	33	13979	0	61	58	26200	42925	4747- 4759
Starr	26.69	98.37	2500	210	17336	0	656	64	31341	52108	5696- 5800
Starr	26.57	98.51	2359	280	18208	0	400	40	32810	54097	4770- 4773
Starr	26.58	98.51	2745	178	9936	0	442	17	20410	33728	4846- 4854
Starr	26.52	98.63	704	67	10140	0	128	30	17000	28069	3954- 3963
Starr	26.52	98.63	404	41	7973	0	268	930	12300	21916	3885- 3895
Starr	26.52	98.63	334	10	4142	0	311	3140	4500	12446	3646- 3655
Starr	26.52	98.63	658	34	10415	0	226	151	17100	28584	3898- 3907
Starr	26.52	98.63	300	61	6651	0	183	93	10800	18088	3892- 3912
Starr	26.43	98.76	526	64	12559	0	538	0	20176	33868	1432- 1437
Starr	26.43	98.77	500	64	11651	0	543	0	18724	31488	1417- 1425
Kleberg	27.43	98.03	738	35	8257	0	128	111	14000	23269	4695
Kleberg	27.43	98.03	1500	10	10634	0	384	54	19000	31582	5695
Kleberg	27.60	97.92	195	18	5800	0	1068	1	8750	15832	6669
Kleberg	27.60	97.92	8168	234	25551	0	201	1	54500	88655	6200
Kleberg	27.48	97.47	2400	24	13756	0	201	160	25300	41841	5233
Kleberg	27.50	98.02	754	17	11178	0	397	11	18400	30757	5754- 5757
Kleberg	27.50	98.03	1536	25	11175	0	253	268	19700	32957	4392- 4398
Kleberg	27.61	97.88	248	67	6028	0	1061	300	9100	16804	6654- 6663
Kleberg	27.60	97.88	126	7	6301	0	958	18	9400	16810	6645- 6655
Kleberg	27.60	97.88	164	7	6456	0	644	1	9900	17172	6633- 6655
Kleberg	27.60	97.88	195	18	5809	0	1068	0	8750	15840	6665- 6669
Kleberg	27.60	97.90	210	31	4282	0	647	262	6500	11932	6453- 6464
Kleberg	27.59	97.88	118	38	6457	0	943	50	9700	17306	6653- 6659
Kleberg	27.59	97.89	16	34	4313	0	1683	1110	4685	12094	6545- 6552
Kleberg	27.59	97.89	1567	250	5520	0	641	80	11600	19658	6614- 6624
Kleberg	27.59	97.95	445	194	5661	0	915	28	9550	16793	6393- 6399
Kleberg	27.58	97.95	284	61	5700	0	967	156	8800	15968	6368- 6374
Kleberg	27.55	98.06	79	45	6865	0	514	305	10300	18144	5958- 5967
Kleberg	27.53	98.01	436	15	9298	0	618	12	14800	25179	6097- 6100
Kleberg	27.53	98.01	139	16	8470	0	1666	173	11800	22264	6147- 6154
Kleberg	27.53	98.01	1386	7	10114	0	223	85	17900	29715	6209- 6213
Kleberg	27.51	98.03	1344	145	8573	0	85	400	15700	26247	4874- 4880
Kleberg	27.51	98.03	1265	230	8391	0	183	220	15600	25889	5121- 5127
Kleberg	27.51	98.03	165	79	9476	0	3346	0	13200	26266	6545- 6551

Table 3d (continued)

County	Latitude	Longitude	Ca	Mg	Na	K	Alkalinity	SO4	Cl	TDS	Depth (feet)
Kleberg	27.51	98.00	70	15	9774	0	1779	22	14200	25860	7140- 7146
Kleberg	27.50	98.00	152	22	9347	0	1372	15	13950	24858	6423- 6427
Kleberg	27.48	98.00	769	123	11906	0	677	8	19700	33183	6065- 6073
Kleberg	27.48	98.00	454	110	10703	0	907	28	17100	29302	6257- 6263
Kleberg	27.48	98.00	116	74	11102	0	1787	20	16500	29599	7043- 7055
Kleberg	27.51	98.00	103	20	10329	0	2034	0	15000	27486	7112- 7120
Kleberg	27.48	98.00	194	22	9938	0	1036	263	14950	26403	7311- 7322
Kleberg	27.50	98.00	703	25	11273	0	513	29	18400	30943	4872- 4877
Kleberg	27.50	98.03	544	31	10500	0	781	11	16800	28667	4402- 4408
Kleberg	27.50	98.03	1556	25	11100	0	266	286	19600	32833	4365- 4369
Kleberg	27.50	98.03	2442	31	12174	0	157	370	22850	38024	4434- 4442
Kleberg	27.50	98.03	1192	43	11159	0	297	125	19200	32016	4434- 4442
Kleberg	27.49	98.03	445	250	11059	0	1231	40	17800	30861	6129- 6135
Kleberg	27.49	98.01	213	49	4001	0	232	760	6000	11255	5116- 5126
Kleberg	27.49	98.01	803	145	7951	0	586	270	13600	23355	5463- 5473
Kleberg	27.49	98.01	285	158	9280	0	988	20	14700	25431	6171- 6179
Kleberg	27.49	98.01	122	44	10416	0	1587	0	15500	27669	6978- 6984
Kleberg	27.48	98.01	115	15	10288	0	1396	19	15300	27133	7104- 7109
Kleberg	27.48	98.01	93	21	10649	0	1459	19	15800	18041	7131- 7133
Kleberg	27.48	98.06	736	49	15129	0	420	7	24550	40891	6366- 6375
Kleberg	27.48	98.06	800	54	12543	0	407	1	20700	34505	6070- 6082
Kleberg	27.48	98.05	784	39	11055	0	445	14	18300	30637	6042- 6045
Kleberg	27.48	98.02	877	25	9364	0	482	1	15800	26594	5683- 5693
Kleberg	27.47	98.02	321	63	7163	0	759	495	11000	19801	6070- 6084
Kleberg	27.47	98.02	719	20	11238	0	383	9	18450	30819	6071- 6073
Kleberg	27.47	98.00	119	181	10339	0	2530	0	15500	28195	7117- 7137
Kleberg	27.47	98.02	150	101	10284	0	1421	12	15600	27568	6980- 6985
Kleberg	27.46	98.01	261	13	12079	0	1293	24	18375	32045	7099- 7113
Kleberg	27.46	98.02	439	75	9873	0	1041	40	15600	27068	6506- 6520
Kleberg	27.45	98.04	159	44	8864	0	1884	130	12900	23981	6962- 6969
Kleberg	27.44	98.02	759	39	10131	0	1012	30	16400	28443	6765- 6788
Kleberg	27.45	98.05	694	109	10347	0	691	24	17100	28965	5613- 5619
Kleberg	27.44	98.05	116	69	9312	0	1787	140	13600	25024	6762- 6768
Kleberg	27.44	98.05	100	59	10109	0	1932	38	14800	27038	6792- 6822
Kleberg	27.44	98.05	416	32	9323	0	721	3	14800	25295	6031- 6340
Kleberg	27.44	98.05	850	26	10176	0	411	3	17050	28516	6268- 6278
Kleberg	27.44	98.05	260	19	9934	0	1274	11	15100	26598	6268- 6278
Kleberg	27.45	98.06	747	29	10672	0	256	46	17700	29450	4876- 4890
Kleberg	27.45	98.06	402	28	9885	0	685	76	15600	26676	4000- 6699
Kleberg	27.45	98.06	695	44	9327	0	1607	32	14800	26505	4000- 6699
Kleberg	27.45	98.06	263	17	7542	0	803	63	11600	20325	4000- 6699
Kleberg	27.42	98.05	573	97	9418	0	1840	105	14650	26683	6143- 6150
Kleberg	27.42	98.05	158	18	6785	0	1801	40	9725	18527	7008- 7016

Table 3d (continued)

County	Latitude	Longitude	Ca	Mg	Na	K	Alkalinity	SO4	Cl	TDS	Depth (feet)
Kleberg	27.42	98.05	844	29	8764	0	110	63	15000	24810	4686- 4695
Kleberg	27.41	98.06	1404	177	9561	0	331	100	17500	29073	5258- 5268
Kleberg	27.41	98.06	474	177	8764	0	919	70	14300	24704	6140- 6147
Kleberg	27.41	98.06	115	193	9537	0	1800	40	14400	26058	7087- 7098
Kleberg	27.40	98.06	1526	34	9042	0	1372	101	16600	28675	5294- 5302
Kleberg	27.40	98.06	1590	10	10634	0	384	54	19000	31672	5692- 5699
Kleberg	27.40	98.05	334	48	6108	0	173	1	10060	16724	6902- 6921
Kleberg	27.57	97.93	140	44	9230	0	1734	52	13575	24775	6970- 6975
Kleberg	27.56	97.93	873	15	10579	0	371	7	17700	29545	6168- 6174
Kleberg	27.58	97.91	108	10	5844	0	1343	12	8450	15767	6631- 6638
Kleberg	27.57	97.90	1938	38	9924	0	411	39	18600	30950	6395- 6400
Kleberg	27.57	97.90	444	19	6626	0	425	3140	8500	19154	4000- 6699
Kleberg	27.57	97.90	707	14	6221	0	76	4400	7600	19018	6323- 6328
Kleberg	27.57	97.93	226	18	9884	0	1041	5	15100	26274	6323- 6526
Kleberg	27.57	97.91	614	24	8116	0	678	24	13725	22731	6175- 6183
Kleberg	27.56	97.92	198	15	9645	0	982	12	14700	25552	6985- 6988
Kleberg	27.54	97.99	154	35	9223	0	2254	0	13300	24966	6475- 6491
Kleberg	27.54	97.99	117	205	8578	0	2141	0	12800	23841	6949- 6957
Kleberg	27.53	97.99	1495	12	10134	0	173	42	18200	30056	5214- 5218
Kleberg	27.53	97.98	1394	11	7527	0	232	120	13900	23184	5222- 5229
Kleberg	27.53	97.98	103	12	6647	0	1676	260	9310	18008	6975- 6988
Kleberg	27.53	97.98	228	14	7846	0	1261	32	11800	21181	6335- 6343
Kleberg	27.53	97.98	103	14	5467	0	1826	0	14700	22110	7002- 7008
Kleberg	27.53	97.98	87	14	9543	0	1977	0	13775	25396	7024- 7031
Kleberg	27.53	97.98	323	29	7420	0	954	8	11550	20284	6291- 6298
Kleberg	27.53	97.98	77	5	9093	0	2456	77	12700	24408	4950- 4958
Kleberg	27.53	97.98	1	1	7741	0	1396	572	10200	19910	7131- 7141
Kleberg	27.53	98.00	82	25	9210	0	2237	43	13100	24697	6864- 6873
Kleberg	27.53	98.00	83	64	7754	0	2138	215	10900	21154	6951- 6957
Kleberg	27.53	98.00	65	3	7825	0	2272	40	10850	21055	7100- 7106
Kleberg	27.53	98.00	79	24	8437	0	2643	28	11675	22886	7209- 7216
Kleberg	27.53	97.99	1228	20	10093	0	346	21	17600	29308	6932- 6942
Kleberg	27.52	97.98	68	18	9532	0	2168	32	13600	25418	6932- 6942
Kleberg	27.51	97.99	291	17	9346	0	1080	16	14350	25100	6274- 6285
Kleberg	27.51	97.99	61	13	8973	0	1842	32	12900	23821	7151- 7155
Kleberg	27.51	97.99	156	16	9061	0	1557	3	13400	24193	6355- 6359
Kleberg	27.51	97.99	876	172	7514	0	459	700	12800	22580	5472- 5478
Kleberg	27.51	97.99	184	48	10607	0	1784	0	15800	28423	6467- 6473
Kleberg	27.51	97.99	754	121	8727	0	540	200	14700	25042	5808- 5817
Kleberg	27.51	97.99	1517	84	10576	0	641	120	18800	31738	5483- 5491
Kleberg	27.51	97.99	120	121	11509	0	1571	20	17400	30741	6936- 6948
Kleberg	27.51	97.99	104	109	10110	0	2010	50	14900	33155	4876- 4881
Kleberg	27.50	97.99	1788	43	11002	0	62	60	20200	33155	4876- 4881

Table 3d (continued)

County	Latitude	Longitude	Ca	Mg	Na	K	Alkalinity	SO4	Cl	TDS	Depth (feet)
Kleberg	27.50	97.99	1818	37	10919	0	74	60	20100	33008	5156- 5180
Kleberg	27.45	98.03	155	93	11032	0	1474	24	16700	29478	7020- 7029
Kleberg	27.45	98.03	399	172	9661	0	845	40	15600	26717	6476- 6486
Kleberg	27.48	97.79	2400	24	13756	0	201	160	25300	41841	5222- 5243
Kleberg	27.50	97.98	20	26	10994	0	555	597	16000	28192	7664- 7693
Kleberg	27.50	97.99	453	29	10444	0	816	47	16500	28289	5184
Kleberg	27.48	98.00	1629	172	10578	0	483	52	19400	32314	5143- 5151
Kenedy	26.79	97.96	1638	97	13430	0	362	8	23699	39229	8292-8304
Kenedy	26.88	97.84	9600	88	18880	0	353	320	45999	75239	8580-8588
Kenedy	26.89	97.85	8771	63	17570	0	107	752	42249	69509	6277-6291
Kenedy	26.90	97.17	5287	114	26119	0	233	3	49899	81659	17530-17580
Kenedy	26.96	97.76	6800	3	14060	0	25	128	33499	54659	8650-8663
Kenedy	27.24	97.73	7557	221	29169	0	0	62	58899	95909	5963-5967
Kenedy	27.25	97.72	8163	172	26369	0	111	175	55499	90489	6258-6260
Kenedy	27.26	97.74	9485	419	37498	0	176	0	60400	108000	7080- 7090
Kenedy	27.25	97.75	7554	1250	25819	0	61	370	56600	91654	6226- 6234
Kenedy	27.25	97.75	6859	1125	23226	0	147	300	51000	82657	6383- 6390
Kenedy	27.25	97.75	9534	1375	24509	0	245	32	58600	94295	6919- 6928
Kenedy	27.25	97.75	10078	1375	25442	0	270	20	61000	98185	7051- 7058
Kenedy	27.25	97.75	10621	1375	26867	0	233	0	64200	103300	7081- 7089
Kenedy	27.25	97.75	10433	625	20852	0	220	0	52400	84530	7704- 7712
Kenedy	27.25	97.75	3162	1000	6535	0	196	122	18400	29427	7777- 7785
Kenedy	27.00	97.87	16762	39	20284	0	0	48	60200	97510	8133- 8140
Kenedy	27.00	97.87	4365	542	12563	0	0	200	28400	46205	5982- 5991
Kenedy	27.00	97.87	4412	152	13875	0	0	460	29150	48186	6194- 6204
Kenedy	27.00	97.88	12648	602	16673	0	208	28	49800	79959	7333- 7343
Kenedy	27.00	97.88	6046	455	8815	0	300	800	24900	41316	8337- 8351
Kenedy	27.00	97.88	7577	485	7240	0	98	355	25550	41450	8176- 8188
Kenedy	27.38	97.55	8100	95	25600	150	84	25	53850	91200	7262- 7340
Kenedy	26.67	97.45	5939	241	38300	1066	173	22	61500	132573	15728-15775
Kenedy	26.67	97.45	15400	26	19750	143	59	5	56300	96300	8604- 8608
Kenedy	26.67	97.45	2440	8	1370	34	26	1	6530	10600	15728-15828
Kenedy	26.67	97.45	32240	220	39900	2900	47	12	129400	245600	12781-12870
Kenedy	26.67	97.45	34000	12	11300	200	70	2	76650	125200	10028-10040
Kenedy	26.67	97.45	35800	177	46000	3200	53	7	141000	252000	12781-12870
Kenedy	26.67	97.45	27500	46	14200	135	43	1	70000	111400	9304- 9316
Kenedy	26.67	97.45	22260	117	17870	140	48	2	65400	102600	9476- 9484
Kenedy	27.00	97.88	15800	70	13900	145	21	10	50150	81800	8801- 8836
Kenedy	27.00	97.88	14100	74	23400	148	120	10	59300	94600	7492- 7496
Kenedy	27.00	97.88	28700	98	33300	1870	127	2	105300	171000	12939-12946
Kenedy	27.27	97.73	6675	287	29000	142	51	5	57800	97700	7321- 7328
Kenedy	27.27	97.73	7670	112	25950	137	143	3	55900	95900	7439- 7443
Kenedy	27.27	97.73	5350	319	23350	225	135	100	47150	79100	13837-14667

Table 3d (continued)

County	Latitude	Longitude	Ca	Mg	Na	K	Alkalinity	SO4	Cl	TDS	Depth (feet)
Kenedy	27.27	97.73	25400	111	23850	1250	89	3	81400	146200	14302-14599
Kenedy	27.23	98.93	2045	65	19800	264	411	1	35000	57685	9364- 9370
Kenedy	27.00	97.88	9721	153	21500	1040	216	0	53300	85930	14304
Kenedy	27.00	97.88	12036	134	26200	1263	14	0	64600	104247	12687
Kenedy	27.15	97.73	23970	139	19300	1112	147	0	73200	117868	14304
Kenedy	27.00	97.88	2540	25	3800	219	227	0	10700	17511	12936
Kenedy	27.00	97.88	27438	138	27700	1773	271	0	95500	152820	12769

Table 4. Major and minor ion chemistry from Frio Formation. Ionic concentrations in mg/L. Data from Kreitler and Richter (1986), and Morton and Land (1987).

No.	County	Latitude	Longitude	Depth (ft)	TDS	Ca	Mg	Na	K	Alkalinity	SO4	Cl	Fe	SiO2	Sr	Ba	B	Br
1	Aransas	28.00	97.00	10932	25472	2234	120	6946	238	979	0	14955	0	478	35	0	1	1
2	Aransas	28.00	97.00	9509	17441	130	3	6700	48	1428	82	9050	0	149	10	0	0	0
3	Aransas	27.47	97.27	11697	22900	330	29	8400	130	540	49	13400	2.6	87	28	0	41	78
4	Aransas	28.14	96.50	9203	16600	30	5	7050	49	2040	86	8700	2	97	5	0	39	49
5	San Patricio	28.01	97.15	10965	15900	42	9	5650	33	800	66	7600	117	51	5	0	38	19
6	San Patricio	28.01	97.15	10521	18600	45	8	7170	32	1720	64	9400	36	82	4	0	51	34
7	San Patricio	27.54	97.25	10670	24600	134	22	9000	59	939	46	13400	8	80	9	3.8	54	34
8	San Patricio	27.54	97.25	11528	17900	89	15	6500	68	1040	110	9270	2	93	7	1.4	62	19
9	San Patricio	27.54	97.25	11050	20300	101	18	7500	62	932	59	10700	34	73	7	3.7	54	30
10	San Patricio	27.54	97.25	11480	14700	54	9	5375	43	775	75	7400	17	79	4	1.5	54	0
11	San Patricio	27.54	97.25	11180	16600	47	9	6250	46	1213	67	8200	5	86	4	1.4	55	21
12	San Patricio	28.00	97.13	10550	17500	42	9	6500	51	858	54	8700	0.1	85	5	1	58	24
13	San Patricio	27.58	97.20	12120	32400	370	56	11750	44	575	26	18700	6	92	28	11	41	29
14	San Patricio	27.58	97.20	11880	36300	330	48	13250	72	200	42	21000	2	132	23	13	35	45
15	San Patricio	27.54	97.25	4900	85400	2500	455	29500	215	270	13	51700	14	32	275	115	53	260
16	San Patricio	27.54	97.25	3350	69800	3040	475	22750	77	97	67	42800	17	18	155	61	35	200
17	San Patricio	27.54	97.25	4600	83300	2500	590	28500	152	189	15	50600	8	26	265	160	61	240
18	San Patricio	27.54	97.25	5790	74600	2880	340	25250	125	113	50	45100	9	35	275	140	55	210
19	San Patricio	27.54	97.25	10320	24800	200	31	9250	70	278	22	14000	70	34	25	12	24	37
20	San Patricio	28.01	97.15	10965	15900	42	9	5650	33	800	66	7600	117	51	5	0	38	19
21	San Patricio	28.01	97.15	10521	18600	45	8	7170	32	1720	64	9400	36	82	4	0	51	34
22	San Patricio	27.59	97.18	9656	77800	484	29	31300	173	237	270	46100	317	33	16	0	33	45
23	San Patricio	27.59	97.18	9660	19900	24	12	8100	41	1220	9	10900	0.8	53	10	0	37	45
24	San Patricio	27.59	97.18	10693	20700	282	22	7550	73	687	15	12150	1.6	134	22	0	40	40
25	San Patricio	27.59	97.18	11074	32500	398	46	12690	92	820	9	19000	3.4	124	34	0	48	54
26	San Patricio	27.52	97.18	10665	27400	156	23	10500	78	1120	52	15200	0.2	83	18	0	74	43
27	San Patricio	27.52	97.18	9715	16900	48	8	7330	40	2760	37	8900	0.4	111	5	0	56	40
28	San Patricio	27.52	97.18	9480	19400	31	8	7860	55	1720	4	10200	0.2	126	9	0	44	36
29	San Patricio	25.58	97.14	10475	21000	27	9	7900	36	1750	58	10300	1.9	88	5	0	41	36
30	San Patricio	27.52	97.18	10667	27500	101	21	10000	62	915	40	15100	32	70	11	0	49	38
31	San Patricio	27.50	97.00	10978	23875	158	26	9400	71	0	120	14100	0	122	11	0	1	0
32	San Patricio	27.50	97.00	10739	31203	207	34	11900	81	1143	38	17800	13	190	18	0	1	0
33	San Patricio	27.50	97.00	10535	17045	56	10	7230	45	0	4	9700	0	179	6	0	1	0
34	San Patricio	27.50	97.00	10906	26376	190	31	10500	80	0	75	15500	8	144	16	0	1	0
35	San Patricio	27.50	97.00	10653	35335	748	84	13300	156	0	47	21000	182	205	34	0	0	0
36	Nueces	27.50	97.30	11218	77481	7660	200	21600	270	0	1	47750	85	52	508	0	1	0
37	Nueces	27.50	97.30	9912	46618	6450	93	11400	124	0	1	28550	200	29	350	0	0	0
38	Nueces	27.50	97.30	8869	101815	9100	240	30200	300	0	5	61970	7	98	680	0	0	0
39	Nueces	27.50	97.30	10444	43770	298	48	17700	91	0	33	25600	0	128	31	0	0	0
40	Nueces	27.50	97.30	11119	44787	590	70	17140	177	0	10	26800	0	138	54	0	1	0
41	Nueces	27.50	97.30	32797	30181	2490	9	8830	845	407	0	17600	0	8	93	0	1	1

Table 4 (continued)

No.	County	Latitude	Longitude	Depth (ft)	TDS	Ca	Mg	Na	K	Alkalinity	SO4	Cl	Fe	SiO2	Sr	Ba	B	Br
42	Nueces	27.50	97.30	11329	24286	459	48	8850	328	800	1	13800	38	227	40	0	1	1
43	Nueces	27.50	97.30	32797	19311	430	395	6910	102	574	0	10900	0	114	46	0	1	1
44	Nueces	27.52	97.21	9000	80100	3700	375	26000	260	162	18	48200	14	55	440	92	33	267
45	Nueces	27.45	97.33	10460	37900	166	28	14400	76	1550	28	20600	4.8	114	20	0	44	127
46	Nueces	27.45	97.33	9340	34200	181	30	13300	105	990	18	20000	4.3	90	51	0	36	92
47	Nueces	27.45	97.33	10879	29900	491	45	10600	264	570	46	16700	2.6	108	46	0	47	63
48	Nueces	27.45	97.33	12538	24500	375	26	8860	375	400	5	14000	21.2	192	31	0	67	56
49	Nueces	27.45	97.33	11658	38900	87	38	15200	211	1070	3	22000	0.1	271	58	0	43	104
50	Nueces	27.47	97.15	10942	213000	21000	715	53600	485	114	8	125600	38	33	1300	0	34	580
51	Nueces	27.52	97.09	10682	21200	83	16	8000	4	740	25	11600	3	72	11	0	59	31
52	Nueces	27.52	97.09	8784	31800	1640	15	10500	95	115	47	18900	140	16	100	0	4	71
53	Nueces	27.47	97.15	10942	214524	36020	1664	42138	0	237	1	133680	220	17	0	548	0	0
54	Nueces	27.47	97.15	9983	226262	29640	1791	53051	0	41	1	139700	486	20	0	533	0	0
55	Nueces	27.47	97.15	12490	241606	31190	1640	57732	0	123	1	149460	280	78	0	103	0	0
56	Kenedy	27.23	97.33	7262	91200	8100	95	25600	150	84	25	53850	1.4	44	500	0	69	245
57	Kenedy	26.40	97.27	8604	96300	15400	26	19750	143	59	5	56300	2.8	54	800	0	64	225
58	Kenedy	26.40	97.27	15728	10600	2440	8	1370	34	26	1	6530	75	23	110	0	7	25
59	Kenedy	26.40	97.27	12781	245600	32240	220	39900	2900	47	12	129400	35	56	1670	0	100	800
60	Kenedy	26.40	97.27	10028	125200	34000	12	11300	200	70	2	76650	0.5	82	1180	0	36	353
61	Kenedy	26.40	97.27	12781	252000	35800	177	46000	3200	53	7	141000	81.5	88	1970	0	111	710
62	Kenedy	26.40	97.27	9304	111400	27500	46	14200	135	43	1	70000	8.5	73	1280	0	37	287
63	Kenedy	26.40	97.27	9476	102600	22260	117	17870	140	48	2	65400	24.6	144	1220	0	47	299
64	Kenedy	27.00	97.53	8801	81800	15800	70	13900	145	21	10	50150	50	41	740	0	34	220
65	Kenedy	27.00	97.53	7492	94600	14100	74	23400	148	120	10	59300	6.6	55	860	0	66	237
66	Kenedy	27.00	97.53	12939	171000	28700	98	33300	1870	127	2	105300	21.6	103	2120	0	122	567
67	Kenedy	27.16	97.44	7321	97700	6675	287	29000	142	51	5	57800	6.7	33	290	0	41	220
68	Kenedy	27.16	97.44	7439	95900	7670	112	25950	137	143	3	55900	0.6	56	643	0	76	239
69	Kenedy	27.16	97.44	13837	79100	5350	319	23350	225	135	100	47150	4.5	26	281	0	40	178
70	Kenedy	27.16	97.44	14302	146200	25400	111	23850	1250	89	3	81400	23.5	82	1100	0	78	215
71	Kenedy	27.00	97.50	6199	101749	3670	427	36300	217	85	350	60700	7	62	285	0.7	1	0
72	Kenedy	27.00	97.50	6098	94925	3140	360	32900	195	120	840	57370	20	68	214	0.7	1	0
73	Kenedy	27.00	97.50	6199	92522	2900	333	33050	184	65	260	55730	36	4	206	0.8	1	0
74	Kenedy	27.00	97.50	14248	91360	6510	178	27190	1160	0	22	56300	65	122	500	0	1	0
75	Jefferson	29.36	94.25	10421	57200	480	100	22600	146	1130	14	33800	0.1	58	70	0	65	67
76	Jefferson	28.00	97.15	10906	27900	190	31	10500	80	880	75	15500	8	90	15	0	96	42
77	Jefferson	29.48	94.10	6300	120067	3800	779	41800	0	80	15	73500	12	0	0	92	0	0
78	Jefferson	29.48	94.10	6900	121611	2930	1020	43000	0	89	1	74500	26	0	0	58	0	0
79	Jefferson	29.50	94.00	9489	42468	204	55	17250	99	0	460	24400	0	106	45	0	1	1
80	Chambers	29.38	94.54	5806	105789	1764	420	38472	265	244	373	63900	10.6	47	166	0	53	68
81	Chambers	29.38	94.54	5822	106498	2095	613	38878	226	195	186	63900	45.7	36	193	0	39	68
82	Chambers	29.38	94.54	5814	104776	1849	458	37482	262	237	230	63900	16.8	44	204	0	35	55

Table 4 (continued)

No.	County	Latitude	Longitude	Depth (ft)	TDS	Ca	Mg	Na	K	Alkalinity	SO4	Cl	Fe	SiO2	Sr	Ba	B	Br
83	Chambers	29.38	94.54	5952	109142	2050	511	39672	240	207	360	65675	9.3	34	245	0	49	68
84	Chambers	29.32	94.50	10098	46992	1020	197	16900	0	590	36	28200	272	0	0	15	0	0
85	Chambers	29.32	94.50	9730	87982	1010	343	32900	0	485	1	53200	6	0	0	40	0	0
86	Chambers	29.32	94.50	10440	93652	1500	343	34600	0	554	1	56600	20	0	0	53	0	0
87	Chambers	29.32	94.50	10836	64000	887	218	23700	0	546	1	38600	2	0	0	37	0	0
88	Chambers	29.32	94.50	8166	119819	4870	9450	27200	0	179	1	78000	11	0	0	115	0	0
89	Chambers	29.32	94.50	9334	142203	7590	766	46300	0	185	1	87100	30	0	0	224	0	0
90	Chambers	29.46	94.23	10465	84800	4230	550	27900	0	1	1	52100	185	0	0	6	0	0
91	Chambers	29.46	94.23	8396	80576	2190	953	27700	0	237	13	49400	12	0	0	83	0	0
92	Chambers	29.40	94.20	12149	122095	4280	465	43600	450	0	0	73300	0	117	415	0	0	1
93	Chambers	29.40	94.20	11598	78125	2485	430	27450	340	0	720	46700	0	101	230	0	0	1
94	Harris	29.45	95.06	6865	113375	2320	437	41415	0	61	1	69255	0	0	0	85	0	0
95	Harris	29.45	95.06	7650	124900	1850	440	34500	0	150	11	60140	13	29	130	43	25	0
96	Harris	29.43	95.07	7650	65000	10	5	25000	0	1400	1600	36800	3	0	0	0	0	0
97	Harris	29.25	95.10	11398	139000	8350	710	44000	624	88	2	83600	0.1	25	350	0	68	81
98	Harris	29.25	95.10	11472	133000	8580	670	42400	643	94	3	80900	0.1	22	380	0	64	80
99	Galveston	29.20	95.00	11401	137286	8350	710	44000	624	0	2	83600	0	40	350	0	1	1
100	Galveston	29.20	95.00	11483	133196	8580	670	42400	643	0	3	80900	0	35	380	0	1	1
101	Galveston	29.20	95.00	11277	55529	1190	153	20900	185	0	1	33100	5	71	143	0	0	0
102	Galveston	29.20	95.00	9774	138242	4260	660	49300	371	0	51	83600	0	14	381	0	1	1
103	Galveston	29.18	95.08	8615	42100	290	60	16500	110	397	39	23200	0.1	70	22	0	42	60
104	Galveston	29.20	95.06	12270	79900	1490	151	29800	230	536	18	46300	3.9	83	272	0	53	57
105	Galveston	29.20	95.06	11250	58900	783	95	22700	192	628	7	35200	0.1	114	145	0	39	43
106	Galveston	29.20	95.06	10800	62500	606	88	24900	180	848	6	36700	0.1	102	116	0	44	48
107	Galveston	29.30	95.03	8663	119339	4320	708	41030	0	793	1	72700	13	0	0	323	0	0
108	Galveston	29.20	95.06	13014	42223	880	183	15200	0	673	13	25180	0	0	0	94	0	0
109	Galveston	29.20	95.06	11150	49034	660	134	18170	0	630	7	29260	89	0	0	84	0	0
110	Galveston	29.22	95.08	8795	41300	380	70	15250	140	414	31	23400	1	62	21	14	45	55
111	Galveston	29.22	95.08	8828	42500	400	75	16000	120	312	32	23800	0.1	65	22	13	46	53
112	Galveston	29.21	94.58	8933	44600	470	85	17000	160	643	34	25200	0.1	64	35	16	41	25
113	Galveston	29.20	95.06	11080	53100	700	90	19500	190	787	11	31000	7	80	130	64	30	32
114	Galveston	29.20	95.06	12992	50400	1230	170	18250	190	506	8	29300	41	99	150	110	59	49
115	Brazoria	29.20	95.20	9715	81026	903	196	30600	216	0	11	49100	0	90	154	0	0	1
116	Brazoria	29.20	95.20	12402	92612	4621	535	29090	306	560	0	57500	999	110	657	0	1	1
117	Brazoria	29.24	95.17	10497	98500	1010	180	37900	292	600	12	59500	0.1	60	157	0	65	94
118	Brazoria	29.16	95.18	12558	235000	22600	1535	69700	1218	30	16	152000	0.1	60	0	0	0	342
119	Brazoria	29.22	95.15	10858	56600	330	60	22700	171	1280	21	34000	8	95	50	0	56	80
120	Brazoria	29.19	95.12	8610	42800	380	70	16250	140	361	43	24000	1	68	25	11	45	59
121	Brazoria	29.19	95.12	8615	40200	280	60	15250	120	427	43	22500	0.1	75	22	8.5	44	59
122	Brazoria	29.19	95.12	8845	40000	180	40	15750	110	525	42	22400	0.1	74	19	11	45	50
123	Brazoria	29.19	95.12	8615	42100	290	60	16500	130	397	39	23200	0.1	70	22	9	42	60

Table 4 (continued)

No.	County	Latitude	Longitude	Depth (ft)	TDS	Ca	Mg	Na	K	Alkalinity	SO4	Cl	Fe	SiO2	Sr	Ba	B	Br
124	Brazoria	29.19	95.12	9780	42000	130	30	16500	120	582	25	23800	0.1	84	22	12	40	38
125	Brazoria	29.19	95.12	11360	73300	2000	220	26500	400	333	3	42700	10	87	365	290	35	52
126	Brazoria	29.19	95.12	10690	63700	710	90	25000	280	269	11	36300	0.1	81	130	61	35	59
127	Brazoria	29.19	95.12	11164	63000	1700	200	22000	270	262	5	37500	15	63	360	240	27	43
128	Brazoria	29.19	95.12	9255	33400	130	25	13000	90	562	57	18100	0.1	84	12	7	48	46
129	Brazoria	29.19	95.12	9285	35800	160	35	14000	90	632	59	19600	8	95	13	6.8	47	37
130	Brazoria	29.19	95.12	11286	60700	610	95	23250	220	302	11	35200	8	87	150	6.6	33	49
131	Brazoria	29.19	95.12	11725	68600	2000	235	24000	300	317	1	40500	8	87	380	370	30	45
132	Brazoria	29.19	95.12	9278	36600	140	30	14000	100	596	17	20400	1	78	14	8	48	33
133	Brazoria	29.19	95.12	9281	34300	170	30	12500	100	484	59	19600	2	79	13	7.3	50	32
134	Brazoria	29.17	95.08	13650	58000	1800	170	20500	180	356	16	34500	22	110	170	59	91	32
135	Brazoria	29.17	95.08	12770	50200	1600	185	17750	240	400	6	29300	17	95	170	110	46	31
136	Matagorda	29.04	95.54	8940	100000	1620	286	37400	310	230	15	61000	0.1	47	213	0	48	80
137	Matagorda	29.04	95.54	8996	98800	1660	277	36000	359	242	6	59100	0.1	49	213	0	51	79
138	Matagorda	29.04	95.54	8708	93700	1070	225	35900	260	257	7	56900	0.1	52	182	0	50	66
139	Matagorda	28.59	95.55	8893	39048	118	26	15040	110	1251	11	22480	2.1	73	0	12	0	0
140	Matagorda	28.57	96.10	8322	83540	1230	356	30900	0	171	6	50800	21	0	0	71	0	0
141	Matagorda	28.57	96.10	8348	57341	671	153	21500	0	469	18	34500	10	0	0	30	0	0
142	Matagorda	29.04	95.54	9195	78600	2006	648	27061	0	854	1	46718	65	0	0	140	0	0
143	Matagorda	29.04	95.54	8897	98836	2890	401	35000	0	279	1	60200	14	0	0	61	0	0
144	Matagorda	29.04	95.54	8980	90938	2380	23	33000	0	263	360	54800	23	0	0	112	0	0
145	Matagorda	29.04	95.54	8920	109673	1710	349	40600	0	260	78	66600	35	0	0	79	0	0
146	Matagorda	29.00	95.50	8735	95418	1188	239	36200	270	515	6	57000	0	74	188	0	0	1
147	Matagorda	29.00	95.50	8961	104612	1770	296	38900	379	561	6	62700	0	82	217	0	0	1
148	Matagorda	29.00	95.50	10798	47256	4784	130	12590	144	286	22	29300	41	34	607	0	1	0
149	Matagorda	29.00	95.50	11690	14540	100	9	5840	61	0	60	8470	0	179	8	0	1	1
150	Matagorda	29.00	95.50	9397	30796	92	20	12097	80	0	7	18500	1	101	26	0	0	0
151	Matagorda	29.00	95.50	9378	10992	16	2	4822	30	0	22	6100	0	107	2	0	0	0
152	Jackson	29.08	96.40	9246	114000	8260	730	33500	767	59	4	68100	0.1	18	1080	0	56	107
153	Calhoun	28.12	96.32	7636	19200	34	16	7900	56	1710	44	10800	0.1	61	14	0	40	49
154	Calhoun	28.12	96.32	8840	57300	189	52	23000	139	1130	15	34100	0.1	61	55	0	49	110
155	Calhoun	28.12	96.32	9293	70100	450	111	27200	171	574	24	41500	0.1	58	162	0	51	131
156	Calhoun	28.17	96.40	8882	59800	2100	170	22600	130	120	5	42050	0.3	10	160	0	46	140
157	Calhoun	28.17	96.40	8780	49100	740	105	17100	110	710	23	27800	0.2	46	95	0	50	125
158	Calhoun	28.17	96.40	8796	31000	185	31	11200	85	1300	45	17050	0.1	66	19	0	46	105
159	Calhoun	28.34	96.50	6750	63847	1320	163	22379	0	138	105	39671	6	0	0	6	0	0
160	Calhoun	28.20	96.50	8384	44859	158	40	17300	90	1436	35	25800	0	89	37	0	1	1
161	Calhoun	28.20	96.50	9312	70527	450	111	27200	171	1090	5	41500	0	93	162	0	1	0
162	Calhoun	28.20	96.50	8918	61332	231	62	25000	132	0	7	35900	0	98	46	0	1	0
163	Calhoun	28.20	96.50	10532	18111	44	7	7400	63	0	47	10550	0	130	8	0	0	1
164	Calhoun	28.20	96.50	8836	29937	163	32	10710	90	1932	0	17010	999	114	18	0	1	1

Table 4 (continued)

No.	County	Latitude	Longitude	Depth (ft)	TDS	Ca	Mg	Na	K	Alkalinity	SO4	Cl	Fe	SiO2	Sr	Ba	B	Br
165	Kleberg	27.30	97.30	7298	87880	8100	95	25600	150	60	25	53850	1	70	500	0	1	0
166	Kleberg	27.30	97.30	8856	54135	1780	77	18990	131	0	7	33150	23	112	288	0	1	0
167	Kleberg	27.30	97.30	8498	61513	3490	61	20860	95	0	7	37000	85	37	335	0	1	0
168	Hidalgo	26.10	98.30	7997	55762	8720	38	12600	164	400	130	33710	114	18	563	0.6	0	0
169	Hidalgo	26.10	98.30	7997	54996	6800	34	12700	257	0	15	35190	220	29	491	1.8	0	0
170	Hidalgo	26.10	98.30	9522	7017	150	3	2630	45	0	59	4130	0	160	10	0	0	0
171	Hidalgo	26.10	98.30	9361	9017	430	7	2920	260	0	150	5250	4	117	19	0	0	0
172	Hidalgo	26.10	98.30	9414	7616	430	2	2530	46	0	20	4588	1	136	19	0	0	1
173	Hidalgo	26.10	98.30	6908	6693	380	14	2050	19	0	230	4000	120	8	7	0	0	0
174	Hidalgo	26.10	98.30	7908	13559	130	6	4940	33	0	1880	6570	5	110	5	0	0	0
175	Hidalgo	26.10	98.30	8741	9127	110	3	3510	31	0	750	4723	17	90	8	0	0	1
176	Hidalgo	26.10	98.30	9728	13343	910	6	4100	97	0	40	8190	11	168	46	0	0	1
177	Hidalgo	26.10	98.30	6839	14244	1110	12	4400	92	0	60	8570	35	192	60	0	0	1
178	Hidalgo	26.10	98.30	7997	69962	10200	72	14800	2290	0	10	42590	54	16	819	11.4	0	0

Economic Geology in August-September 1987 were analyzed for major and minor ions, isotopes, organic acids, and organic composition of oils (tables 5 through 7). Methods for selection, collection, and analysis are listed below.

8.1 Sample Selection

Thirty-two samples were collected from the Texas Gulf Coast oil and gas fields (tables 5 and 6). Several criteria were used in selecting sites, including API gravity of the oils, geographic location, and sample depth. Wells in the same zone as secondary recovery operations were avoided.

Heavy Oils--Because one of the effects of biodegradation and water washing of oils is to decrease its API gravity, wells that produce the heavier, relatively low API gravity oils were chosen. Most of the samples were taken from fields with oils that have API gravities of 25.0 or lower. Samples were also collected from fields with lighter oils in order to investigate waters associated with nondegraded oils.

Geographic Distribution--Samples were taken in the Texas Gulf Coast from Jim Wells County in the south to Jefferson County in the north (fig. 63). Sample locations were fairly evenly distributed throughout the Gulf Coast.

Depth--Samples were taken from depths of 3,000 ft to 10,000 ft. Owing to the lack of appropriate deep wells in the South Gulf Coast, more samples from shallow wells (3,000 to 6,000 ft) were collected there. There is a good representation for all depths between 3,000 and 10,000 ft.

8.2 Sample Collection

Samples were collected from the wellhead, separator, or "heater treater." In several instances operators added a chemical at the wellhead as a scale inhibitor. For this the feedline for the chemical was turned off and the well line was flushed for several minutes to avoid contamination of the field sample with the inhibitor. Samples were collected in a 5-gallon bucket, which was cleaned with distilled water and acetone and rinsed with the sample. After the brine and oil separated, the brine was filtered through glass wool to remove any oil and solids remaining in the sample and poured into a pressure filtration chamber, which was also cleaned and rinsed with distilled water and sample water. Samples were then filtered through a 0.45-μm filter using nitrogen gas to avoid atmospheric contamination. Samples taken for cation analysis were collected in 500-ml polyurethane bottles and acidified with 5 ml of 6N HCl. Samples taken for anion analysis were collected untreated in a 500-ml polyurethane bottle. Isotope samples were collected untreated in a 250-ml glass bottle. Organic acid samples were collected in a 500-ml glass bottle and treated with

Economic Geology in August-September 1987 were analyzed for major and minor ions, isotopes, organic acids, and organic composition of oils (tables 5 through 7). Methods for selection, collection, and analysis are listed below.

8.1 Sample Selection

Thirty-two samples were collected from the Texas Gulf Coast oil and gas fields (tables 5 and 6). Several criteria were used in selecting sites, including API gravity of the oils, geographic location, and sample depth. Wells in the same zone as secondary recovery operations were avoided.

Heavy Oils--Because one of the effects of biodegradation and water washing of oils is to decrease its API gravity, wells that produce the heavier, relatively low API gravity oils were chosen. Most of the samples were taken from fields with oils that have API gravities of 25.0 or lower. Samples were also collected from fields with lighter oils in order to investigate waters associated with nondegraded oils.

Geographic Distribution--Samples were taken in the Texas Gulf Coast from Jim Wells County in the south to Jefferson County in the north (fig. 63). Sample locations were fairly evenly distributed throughout the Gulf Coast.

Depth--Samples were taken from depths of 3,000 ft to 10,000 ft. Owing to the lack of appropriate deep wells in the South Gulf Coast, more samples from shallow wells (3,000 to 6,000 ft) were collected there. There is a good representation for all depths between 3,000 and 10,000 ft.

8.2 Sample Collection

Samples were collected from the wellhead, separator, or "heater treater." In several instances operators added a chemical at the wellhead as a scale inhibitor. For this the feedline for the chemical was turned off and the well line was flushed for several minutes to avoid contamination of the field sample with the inhibitor. Samples were collected in a 5-gallon bucket, which was cleaned with distilled water and acetone and rinsed with the sample. After the brine and oil separated, the brine was filtered through glass wool to remove any oil and solids remaining in the sample and poured into a pressure filtration chamber, which was also cleaned and rinsed with distilled water and sample water. Samples were then filtered through a 0.45-μm filter using nitrogen gas to avoid atmospheric contamination. Samples taken for cation analysis were collected in 500-ml polyurethane bottles and acidified with 5 ml of 6N HCl. Samples taken for anion analysis were collected untreated in a 500-ml polyurethane bottle. Isotope samples were collected untreated in a 250-ml glass bottle. Organic acid samples were collected in a 500-ml glass bottle and treated with

Table 5. All chemical analyses of Frio waters collected for this study. Ionic concentrations in mg/L.

Sample No.	Ca	Mg	Na	K	Alkalinity†	SO4	Cl	TDS	Depth (ft)	Si	Sr	Ba	Br	I	pH ††	del O18
1	934	183	24000	170	258	7	36600	62563	6023	15.7	230	75.1	79	18	7.15	4.75
2	1730	284	25100	234	319	<5	39300	67438	3499	8.7	196	81.4	168	17	7.52	4.01
3	184	360	12000	106	631	<5	17400	30824	4226	14.7	19.1	12.7	81	15	7.72	3.32
4	1700	287	25100	155	186	<5	40300	68257	5545	14.3	233	89.2	173	19	7.50	4.11
5	769	2980	24800	176	515	<5	38200	67731	3606	16.5	104	87.2	70	13	7.12	-0.25
6	5280	173	26400	162	423	7	47600	80861	6652	17.2	405	159	219	23	7.07	3.92
7	67	27	10900	114	845	7	15800	27848	3930	18.0	13.9	4.3	39	20	7.76	1.06
8	2130	173	23300	150	309	14	38500	64887	5000	15.5	106	36.6	143	24	6.65	1.33
9	863	118	18000	195	274	<5	28000	47683	4768	15.9	52.5	23.7	125	16	6.70	4.09
10	2230	267	26600	187	237	<5	43700	73830	4537	12.3	284	109	185	19	6.60	3.47
11	2430	327	28000	167	165	<5	46600	78295	4388	10.7	268	104	203	20	6.79	3.36
12	281	51	8710	147	468	<5	13100	22864	3040	29.8	9.8	2.9	47	17	6.77	0.42
13	131	24	8670	94	695	<5	12500	22213	3942	15.4	8.7	6.5	50	18	7.32	3.11
14	818	168	18400	195	264	<5	29000	49012	4640	15.2	70.4	27.4	36	18	6.48	4.22
15	243	17	10400	71	948	<5	15100	26893	5000	19.1	16.6	12.4	44	22	7.01	2.97
16	8970	346	32600	144	124	15	64000	106914	6304	15.2	397	72.1	230	16	6.77	2.00
17	9460	463	34700	153	58	22	68900	114411	5700	13.3	369	30.2	247	17	6.68	1.01
18	1450	249	25600	157	412	<5	40200	68373	4682	14.7	117	73.9	80	19	6.46	3.63
19	2160	480	27500	159	225	<5	45000	75859	5096	11.5	137	84	80	22	6.44	2.44
20	2660	658	40600	262	93	<5	67700	112401	6571	10.0	225	83.7	89	20	6.26	6.40
23	393	97	18900	149	1696	120	27500	49027	9646	27.7	54.7	4.6	66	19	7.19	5.47
24	2687	368	28133	207	1226	19	46800	79848	8760	17.7	274	36.4	78	21	6.69	4.72
25	2890	520	43300	229	193	<5	71400	118802	7752	11.7	120	43.6	76	19	6.00	1.88
26	2290	448	38100	188	355	11	63000	104621	8310	15.9	103	36.5	66	19	5.93	1.01
27	2630	623	37100	230	212	<5	61500	102643	6721	12.2	176	79	63	18	5.70	2.05
28	2170	538	38500	211	185	6	63200	105173	4574	11.2	179	87.5	72	19	6.31	2.46
29	12	2	3730	23	2448	<5	4300	10598	7666	23.7	2.2	1.5	23	33	8.24	4.63
31	992	150	28900	356	1253	9	44000	76095	9950	30.2	219	112	58	25	6.72	3.58
32	1190	261	35700	250	460	15	56600	94834	9074	23.1	187	81.1	64	18	6.31	3.08
33	1660	490	38400	278	322	<5	61300	102738	5902	13.4	143	56	57	19	6.12	2.72
34	1860	451	38400	288	245	11	61300	102975	6244	14.1	252	66	82	17	6.13	4.19
35	1760	369	34500	217	804	17	55400	93399	8382	18.3	163	39.1	115	14	6.21	3.99

Table 5 (continued)

Sample No.	del D	API Gravity †††	Total Alkalinity	Acetate	Propionate	Butyrate	HCO3-	Tot. Org. Acids	Titrated Org. Alk.	Temp (°C)††††
1	-14.9	26.0	258	0	0	0	258	0	na	69
2	-14.4	23.0	319	0	0	0	319	0	na	49
3	-14.0	24.0	631	0	0	0	631	0	131	54
4	-13.3	28.0	186	0	0	0	186	0	na	66
5	-5.6	29.1	515	0	0	0	515	0	na	50
6	-10.6	23.8	423	300	32	3	88	335	399	75
7	-14.7	26.0	845	6.5	0	0	839	6.5	44	52
8	-15.0	25.0	198	104	38	3.5	53	145.5	199	62
9	-13.2	25.0	274	4.7	0	0	269	4.7	na	59
10	-12.4	24.0	237	0	0	0	237	0	na	58
11	-10.7	23.0	165	0	0	0	165	0	na	56
12	-15.5	22.8	468	0	0	0	468	0	na	44
13	-14.9	24.0	695	0	0	0	695	0	60	52
14	-14.0	20.5	264	0	0	0	264	0	na	59
15	-11.8	22.0	948	440	135	15	358	590	678	62
16	-10.6	23.0	124	47	9	0	68	56	283	72
17	-15.5	23.0	58	0	0	0	58	0	na	67
18	-15.1	25.0	412	0	0	0	412	0	na	59
19	-15.2	23.0	225	0	0	0	225	0	68	62
20	-13.0	29.5	93	0	0	0	93	0	na	74
23	-12.2	30.0	1696	814	95	10	777	919	1000	104
24	-10.7	33.5	1226	697	71	8	450	776	887	99
25	-19.6	26.3	193	40	3.5	0	150	43.5	146	88
26	-24.0	29.1	355	136	22	3	194	161	217	94
27	-18.0	29.0	212	0	0	0	212	0	na	77
28	-16.3	28.0	185	0	0	0	185	0	na	58
29	-12.3	32.4	2448	1270	207	23.5	948	1500.5	1476	87
31	-15.3	28.0	1253	728	113	18	394	859	857	107
32	-15.5	28.0	460	190	40	5	225	235	na	101
33	-16.4	28.0	322	0	0	0	322	0	na	68
34	-17.4	31.3	245	0	0	0	245	0	na	71
35	-12.6	30.4	804	326	2	4	472	332	538	95

Alkalinity† field alkalinity titration

pH †† field pH

API Gravity ††† API gravity from Railroad Commission of Texas, Oil and Gas Division proration schedules

Temp (°C)†††† temperatures estimated from geothermal gradient

Table 6. Water samples with location and operator information of Frio waters collected for this study. Ionic concentrations in mg/L.

Sample No.	1	2	3	4	5
Field	Placedo	Lonnie Glasscock	Tynan,E	Placedo, E	Tesoro
County	Victoria	Victoria	Bee	Victoria	Duval
Operator	Global Natural Resources	Three Mile Joint Venture	TXO Production Corp.	Westland Oil Development Inc.	A. H. Garcia
Lease/Well No.	Henderson & Pickering No. 14	M.S. Welder No. G-5	Ramirez No. B-2	Vendenberge & Hill No. 10	Parr No. 2A
Depth (feet)	6019'-6023'	3499'-3503'	4222'-4226'	5545'	3606'
TDS	62570	67443	30829	68262	67736
Ca	934	1730	184	1700	769
Mg	183	284	360	287	2980
Na	24000	25100	12000	25100	24800
K	170	234	106	155	176
Alkalinity	258	319	631	186	515
SO4	7	<5	<5	<5	<5
Cl	36600	39300	17400	40300	38200
Sl	15.7	8.7	14.7	14.3	16.5
Sr	230	196	19.1	233	104
Ba	75.1	81.4	12.7	89.2	87.2
Br	79	168	81	173	70
I	18	17	15	19	13
∂ O18	4.75	4.01	3.32	4.11	-0.25
∂ D	-14.9	-14.4	-14	-13.3	-5.6
pH	7.15	7.52	7.72	7.5	7.12
Acetate	trace	trace	trace	trace	trace
Propionate	0	0	0	0	0
Butyrate	0	0	0	0	0
Tot. Org. Acids	0	0	0	0	0
Titrated Org. Alkalinity	na	na	131	na	na

Table 6 (continued)

Sample No.	6	7	8	9	10
Field	Triple -A-	Magnolia City, W	Minnie Bock	Pridham Lake, W	Lake Pasture
County	San Patricio	Jim Wells	Nueces	Victoria	Refugio
Operator	Robinson Interests, Inc.	Verado Energy, Inc.	Sanchez-O'Brien Oil & Gas Corp.	Mandarin Oil & Gas	T-C Oil Co.
Lease/Well No.	A. E. Nelson No. 4	Perez No. 1	Wright Trust No. 1	Calhoun Farms No. 2	O'Connor No. 79
Depth (feet)	6652'	3930'	5000'	4768'	4537'
TDS	80868	27855	64901	47688	73835
Ca	5280	67	2130	863	2230
Mg	173	27	173	118	267
Na	26400	10900	23300	18000	26600
K	162	114	150	195	187
Alkalinity	423	845	309	274	237
SO4	7	7	14	<5	<5
Cl	47600	15800	38500	28000	43700
Si	17.2	18	15.5	15.9	12.3
Sr	405	13.9	106	52.5	284
Ba	159	4.3	36.6	23.7	109
Br	219	39	143	125	185
I	23	20	24	16	19
∂ O18	3.92	1.06	1.33	4.09	3.47
∂ D	-10.6	-14.7	-15	-13.2	-12.4
pH	7.07	7.76	6.65	6.7	6.6
Acetate	300	6.5	104	4.7	trace
Propionate	32	0	38	0	0
Butyrate	3	0	3.5	0	0
Tot. Org. Acids	335	6.5	145.5	4.7	0
Titrated Org. Alkalinity	399	44	199	na	na

Table 6 (continued)

Sample No.	11	12	13	14	15	16
Field	Tom O'Connor	Silva, SW	Silva, SW	Blanconia, N	Richard King	Luby
County	Refugio	Bee	Bee	Bee	Nueces	Nueces
Operator	Hewit & Dougherty	Good Day Energy	KTX Management	Legacy Exploration	Kamlok, Inc.	Kamlok, Inc.
Lease/Well No.	M. F. Lampert No. 95	Riggle-Wendtland No. 3	Paul Treptow No. 2	Roberts No. 1	Richard King No. C-9	McCann No. 38
Depth (feet)	4388'	3040'	3942'	4640'	5000'	6304'
TDS	78300	22869	22218	49017	26898	106929
Ca	2430	281	131	818	243	8970
Mg	327	51	24	168	17	346
Na	28000	8710	8670	18400	10400	32600
K	167	147	94	195	71	144
Alkalinity	165	468	695	264	948	124
SO4	<5	<5	<5	<5	<5	15
Cl	46600	13100	12500	29000	15100	64000
Si	10.7	29.8	15.4	15.2	19.1	15.2
Sr	268	9.8	8.7	70.4	16.6	397
Ba	104	2.9	6.5	27.4	12.4	72.1
Br	203	47	50	36	44	230
I	20	17	18	18	22	16
∂ O18	3.36	0.42	3.11	4.22	2.97	2
∂ D	-10.7	-15.5	-14.9	-14	-11.8	-10.6
pH	6.79	6.77	7.32	6.48	7.01	6.77
Acetate	trace	trace	trace	trace	440	47
Propionate	0	0	0	0	135	9
Butyrate	0	0	0	0	15	0
Tot. Org. Acids	0	0	0	0	590	56
Titrated Org. Alkalinity	na	na	60	na	678	283

Table 6 (continued)

Sample No.	31	32	33	34	35
Field	Sugar Valley, S	Sugar Valley, N	Clear Lake	Webster	Fishers Reef
County	Brazoria	Brazoria	Harris	Harris	Chambers
Operator	Exxon	Exxon	Exxon	Exxon	Exxon
Lease/Well No.	Truitt & Grevaer No. 8	John F. Grant No. 11-J	Exxon West Fee "C" No. 85	West Production Co. A/C No. 29	FR Tract No. 2
Depth (feet)	9950'	9074'	5902'	6244'	8382'
TDS	76104	94849	102743	102986	93416
Ca	992	1190	1660	1860	1760
Mg	150	261	490	451	369
Na	28900	35700	38400	38400	34500
K	356	250	278	288	217
Alkalinity	1253	460	322	245	804
SO4	9	15	<5	11	17
Cl	44000	56600	61300	61300	55400
Si	30.2	23.1	13.4	14.1	18.3
Sr	219	187	143	252	163
Ba	112	81.1	56	66	39.1
Br	58	64	57	82	115
I	25	18	19	17	14
∂ O18	3.58	3.08	2.72	4.19	3.99
∂ D	-15.3	-15.5	-16.4	-17.4	-12.6
pH	6.72	6.31	6.12	6.13	6.21
Acetate	728	190	trace	trace	326
Propionate	113	40	0	0	2
Butyrate	18	5	0	0	4
Tot. Org. Acids	859	235	0	0	332
Titrated Org. Alkalinity	857	na	na	na	538

Table 7. Oxygen and hydrogen isotopic data for Frio and Wilcox Formations. "EPA data" are samples collected for this study. "Frio data" from L.S. Land. Wilcox data from Fisher (1982). Ionic concentrations in mg/L.

EPA Data				Frio Data			Wilcox Data		
Sample No.	∂O18	∂D	Depth (feet)	∂O18	∂D	Depth (feet)	∂O18	∂D	Depth (feet)
1	4.75	-14.9	6023	5.22	-17.0	9312	1.20	-21.0	8453
2	4.01	-14.4	3499	4.91	-9.5	8843	-2.50	1.4	9345
3	3.32	-14.0	4226	4.65	-8.1	8613	-5.40	-20.8	10198
4	4.11	-13.3	5545	4.65	-8.1	9778	-0.30	-15.0	7984
5	-0.25	-5.6	3606	5.70	-17.0	11359	2.10	-11.0	6471
6	3.92	-10.6	6652	4.93	-18.8	10690	2.10	-15.0	9505
7	1.06	-14.7	3930	5.64	-18.0	11723	2.20	-10.0	6068
8	1.33	-15.0	5000	4.00	-10.4	8794	2.10	-13.0	6849
9	4.09	-13.2	4768	5.92	-14.1	10683	5.40	-2.4	10407
10	3.47	-12.4	4537	7.57	-14.3	10726	4.20	-4.0	10463
11	3.36	-10.7	4388	6.74	-11.7	11526	4.60	-11.9	10995
12	0.42	-15.5	3040	7.56	-15.0	10548	0.80	6.6	7000
13	3.11	-14.9	3942	5.96	-13.7	12116	-4.70	-42.0	8597
14	4.22	-14.0	4640	4.45	-16.1	11880	3.60	-10.0	11897
15	2.97	-11.8	5000				-3.20	-35.0	10630
16	2.00	-10.6	6304				-3.70	-15.5	10000
17	1.01	-15.5	5700				-3.10	-15.7	6029
18	3.63	-15.1	4682				-4.10	-13.1	5258
19	2.44	-15.2	5096				-4.40	-7.1	4595
20	2.50	-13.0	6571				-3.10	-13.4	5858
23	5.47	-12.2	9646				-4.40	-17.2	4854
24	4.72	-10.7	8760				-5.40	-20.0	7167
25	1.88	-19.6	7752				1.90	3.3	7554
26	1.01	-24.0	8310				2.00	-4.3	7564
27	2.05	-18.0	6721				2.70	2.6	7606
28	2.46	-16.3	4574				2.70	-5.7	8174
29	4.63	-12.3	7666				1.20	-11.0	9154
31	3.58	-15.3	9950				0.20	-5.6	7797
32	3.08	-15.5	9074				-4.20	-17.4	7921
33	2.72	-16.4	5902				-3.90	-15.0	5081
34	4.19	-17.4	6244				-2.10	-16.0	4920
35	3.99	-12.6	8382				-3.90	-7.0	5960
							3.00	3.0	7560
							-0.70	1.0	9056
							-0.90	3.0	7150
							2.10	2.0	8239
							3.20	-12.0	8177
							1.30	-2.0	7311
							2.30	-7.0	9197
							2.80	-6.0	8125

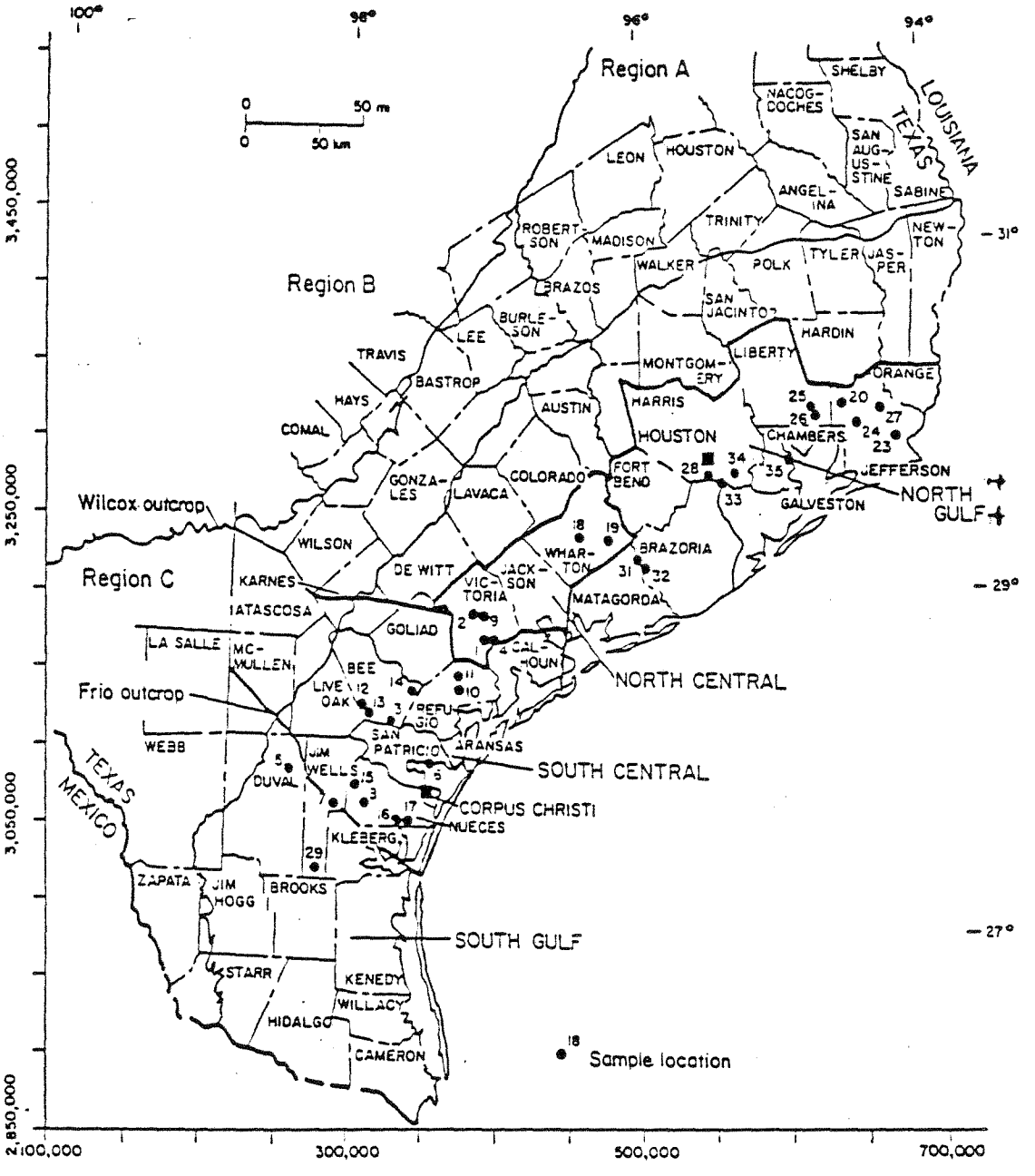

Figure 63. Location of wells sampled for this study.

a few drops of $HgCl_2$. A sample diluted with deionized water in a proportion of 1:10 was collected in a 1-L polyurethane bottle. An untreated, unfiltered sample was also taken. For each brine collected, an oil sample was gathered in a 125-ml glass bottle. All sample bottles were tightly capped and sealed with Parafilm.

Alkalinity titrations were done in the field. Dilute HCl was titrated into 50 ml of unfiltered sample in 1- to 2 ml-additions to a pH of 2.5. Sample collection followed Bureau of Economic Geology Specific Work Instruction (BEG SWI) 3.1.a, Quality Assurance document.

8.3 Sample Analysis

All samples were analyzed and archived at the Bureau of Economic Geology's Mineral Studies Laboratory. Samples were analyzed for major cations and anions, oxygen and hydrogen isotopes, and organic acids. Eleven samples were analyzed by ARCO Service Laboratory for evidence of degradation.

Inorganic Chemistry

Chloride: A small aliquot of the untreated, filtered sample (0.1-1 ml) was diluted with deionized water to approximately 100 ml and adjusted to a pH of 7 to 9. One ml of K_2CrO_4 indicator solution was added, and the solution was titrated with a silver nitrate solution to a light orange endpoint, which was then used to calculate the chloride concentration. Sample analysis followed BEG SWI 1.1.

Bromide: A 1-ml aliquot of untreated, filtered sample was diluted to 25 ml with deionized water. The solution was then reacted with $Ca(ClO)_2$ to oxidize the bromide to bromate (BrO_3^-) at a pH of 7.2. The excess hypochlorite (ClO^-) was then eliminated, and the bromate was reacted with iodide to produce iodine, which was then measured spectrophotometrically in solution. Sample analysis followed BEG SWI 1.2.

Sulfate: An appropriate aliquot of sample (<10 ml) was acidified with HCl and stabilized (for the $BaSO_4$ suspension) with gum arabic solution. $BaCl_2$ was then added and was mixed to dissolve all crystals. After at least 8 minutes the turbidity was measured at 420 nm using the secondary light path on the spectrophotometer. This result was compared to curves prepared with standard sulfate solutions. Sample analysis followed BEG SWI 1.3.

Ammonia: A small portion of each sample was extracted with cyclo-hexane, to eliminate any organic nitrogen present, and then steam distilled. The remaining distillate was then titrated with standardized hydrochloric acid to determine NH3-N concentrations (Mineral Studies Laboratory Procedure No. 001).

a few drops of $HgCl_2$. A sample diluted with deionized water in a proportion of 1:10 was collected in a 1-L polyurethane bottle. An untreated, unfiltered sample was also taken. For each brine collected, an oil sample was gathered in a 125-ml glass bottle. All sample bottles were tightly capped and sealed with Parafilm.

Alkalinity titrations were done in the field. Dilute HCl was titrated into 50 ml of unfiltered sample in 1- to 2 ml-additions to a pH of 2.5. Sample collection followed Bureau of Economic Geology Specific Work Instruction (BEG SWI) 3.1.a, Quality Assurance document.

8.3 Sample Analysis

All samples were analyzed and archived at the Bureau of Economic Geology's Mineral Studies Laboratory. Samples were analyzed for major cations and anions, oxygen and hydrogen isotopes, and organic acids. Eleven samples were analyzed by ARCO Service Laboratory for evidence of degradation.

Inorganic Chemistry

Chloride: A small aliquot of the untreated, filtered sample (0.1-1 ml) was diluted with deionized water to approximately 100 ml and adjusted to a pH of 7 to 9. One ml of K_2CrO_4 indicator solution was added, and the solution was titrated with a silver nitrate solution to a light orange endpoint, which was then used to calculate the chloride concentration. Sample analysis followed BEG SWI 1.1.

Bromide: A 1-ml aliquot of untreated, filtered sample was diluted to 25 ml with deionized water. The solution was then reacted with $Ca(ClO)_2$ to oxidize the bromide to bromate (BrO_3^-) at a pH of 7.2. The excess hypochlorite (ClO^-) was then eliminated, and the bromate was reacted with iodide to produce iodine, which was then measured spectrophotometrically in solution. Sample analysis followed BEG SWI 1.2.

Sulfate: An appropriate aliquot of sample (<10 ml) was acidified with HCl and stabilized (for the $BaSO_4$ suspension) with gum arabic solution. $BaCl_2$ was then added and was mixed to dissolve all crystals. After at least 8 minutes the turbidity was measured at 420 nm using the secondary light path on the spectrophotometer. This result was compared to curves prepared with standard sulfate solutions. Sample analysis followed BEG SWI 1.3.

Ammonia: A small portion of each sample was extracted with cyclo-hexane, to eliminate any organic nitrogen present, and then steam distilled. The remaining distillate was then titrated with standardized hydrochloric acid to determine NH3-N concentrations (Mineral Studies Laboratory Procedure No. 001).

Iodide: A ~2-ml aliquot of untreated, filtered sample was diluted to 10 ml. The sample was mixed with bromine water and then with sodium formate to destroy excess bromine. KI was then added to form iodine, which was then measured spectrophotometrically. Sample analysis followed BEG SWI 1.4.

Major and Minor Cations: Major and minor cations were analyzed using an inductively coupled plasma-optical emission spectrometer (ICP-OES). For K, Mg, Na, Sr, Ba, Si, and Ca the sample was diluted to approximately 1000 mg/L Na and acidified with 6N HCl and diluted further with double deionized water. This was then heated, cooled, and then analyzed on the ICP-OES, using seawater as a reference sample. For minor elements 10 ml of the sample was acidified with 5 ml of 6N HCl and heated and cooled as above. The solution was analyzed with the ICP-OES, with special attention given to elements with concentrations near the detection limits of the system. Sample analysis followed BEG SWI 1.5 and 1.6.

Isotopic Analyses

Oxygen: An aliquot of water (2 ml) was acidified with concentrated phosphoric acid and degassed three times under vacuum. Carbon dioxide was added to the water (18 ml and ~60 torr) and allowed to equilibrate with the water for 80 to 130 hours. The equilibrated carbon dioxide was transferred back to the vacuum line and purified. The purified gas was then analyzed with a VG SIRA 12 mass spectrometer to determine the relative abundances of the oxygen isotopes.

Hydrogen: An aliquot of water (5 μl) was reduced in a sealed tube under vacuum pressure over hot zinc (430°C) for 24 hours. The evolved hydrogen gas was analyzed directly with a VG SIRA 12 mass spectrometer to determine the relative abundance of hydrogen isotopes.

Organic Acids

Organic acid concentrations were determined using a Hewlett-Packard Gas Chromatograph equipped with a Flame Ionization Detector (FID) and a 0.32 mm ID x 6 m long fused silica capillary column coated with 0.1 μm Superox. The column was run isothermally at 110°C. The flow rate was 7 ml/min, and the carrier gas was helium. Before gas chromatograph analysis the samples were acidified to a pH of 1-2 with concentrated phosphoric acid in order to convert organic salts into organic acids. The sample was then injected in sample sizes of 2.5 μm. A standard solution of acetic, propionic, and i- and n- butyric acids in ~100,000 ppm NaCl was used to calibrate the FID response. To check the accuracy of the gas chromatograph analyses, 14 samples were analyzed for total aliphatic acids by the titration (fig. 64)

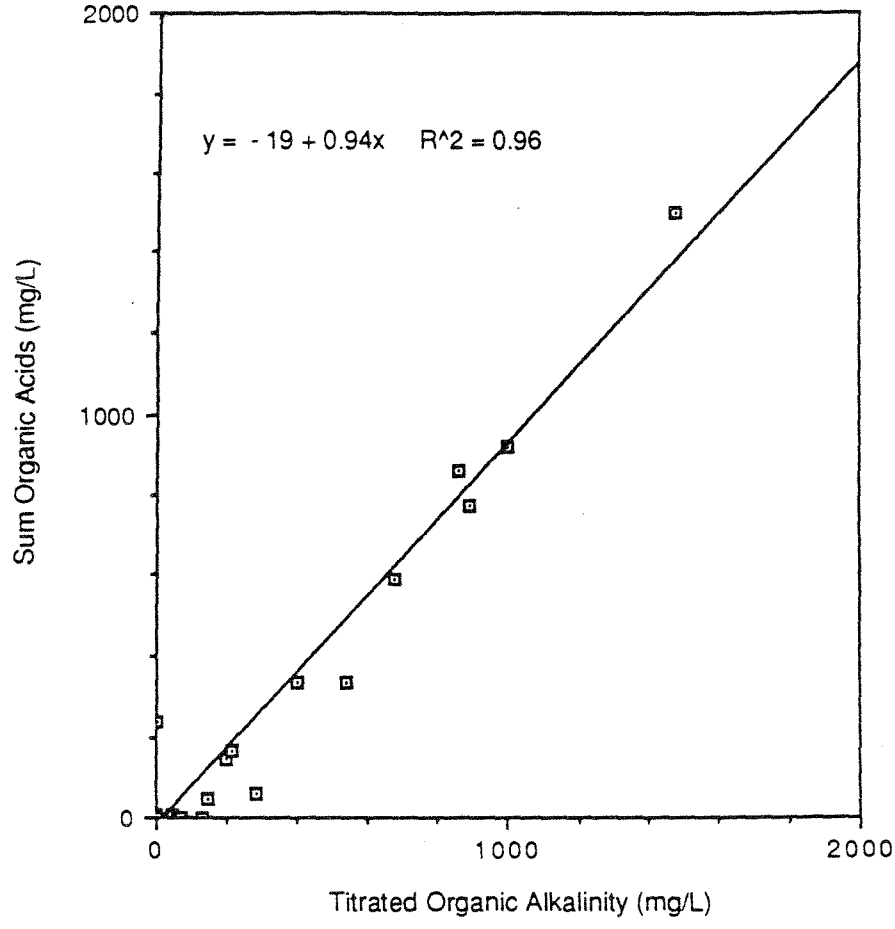

Figure 64. Titration of organic alkalinity versus sum of acetate, propionate, and butyrate. Note that titration concentrations are consistently higher than the summation of organic acids. This suggests the presence of other organic acids in the waters.

as defined in the manual of Standard Methods for the Examination of Water and Wastewater (1975). There is a linear trend of total aliphatic acids from titration versus the sum of the aliphatic acids from gas chromatograph analysis (fig. 65 and table 3), but concentrations from titration results generally are greater than the sum of the acids from the gas chromatograph analysis. This may indicate the presence of other short-chained aliphatic acids that were not analyzed.

Total Organic Alkalinity: Total organic alkalinity titrations were done on approximately half of the samples. The titration procedure followed was from Standard Methods for the Examination of Water and Wastewater (1975). The sample was acidified with six drops of concentrated HCl, and thymol blue was added. Then 5 ml of the sample was drawn through a column of silicic acid by vacuum, which was immediately followed by 65 ml of a chloroform-butanol mix. A phenolphthalein indicator was added, and the sample was then titrated to the phenolphthalein endpoint with .02N NaOH in absolute methanol.

Gas chromatographic analyses of oil: Eleven samples were analyzed by Research and Technical Services, ARCO Oil and Gas Co., to determine whether the oils exhibited biodegradation. Oils were analyzed with a Hewlett-Packard 558 gas chromotograph fitted with a 25-mm, cross-linked 5% phenolmethyl styrene column. Column temperature was initiated at -60°C, then 20°/min up to 40°C, then 5.5°C per minute up to 240° then 6°/min up to 300°C and held for 23 minutes (M. Robinson-Lewis, personal communication, 1988). Two blind samples were included in the set sent for analysis to test the reproducibility of their analysis. The duplicates are identical to original samples sent (fig. 65).

8.4 Quality Assurance

For all analyses except the organic acids analysis, strict quality assurance methods were adhered to. For inorganic analyses, 10 percent of the samples were analyzed several times to ensure the reproducibility of results. For oxygen and hydrogen isotopes, multiple analyses were also performed on several samples to ensure accuracy of the results. Because the organic acid analysis was new, no standard quality assurance methods exist. Multiple analyses were performed on one sample, and reasonable reproducibility was found.

9. WATER CHEMISTRY - RESULTS

The inorganic and organic chemical and isotopic composition, depth, and location of the 32 water samples collected for this study are shown in tables 5 and 6 and

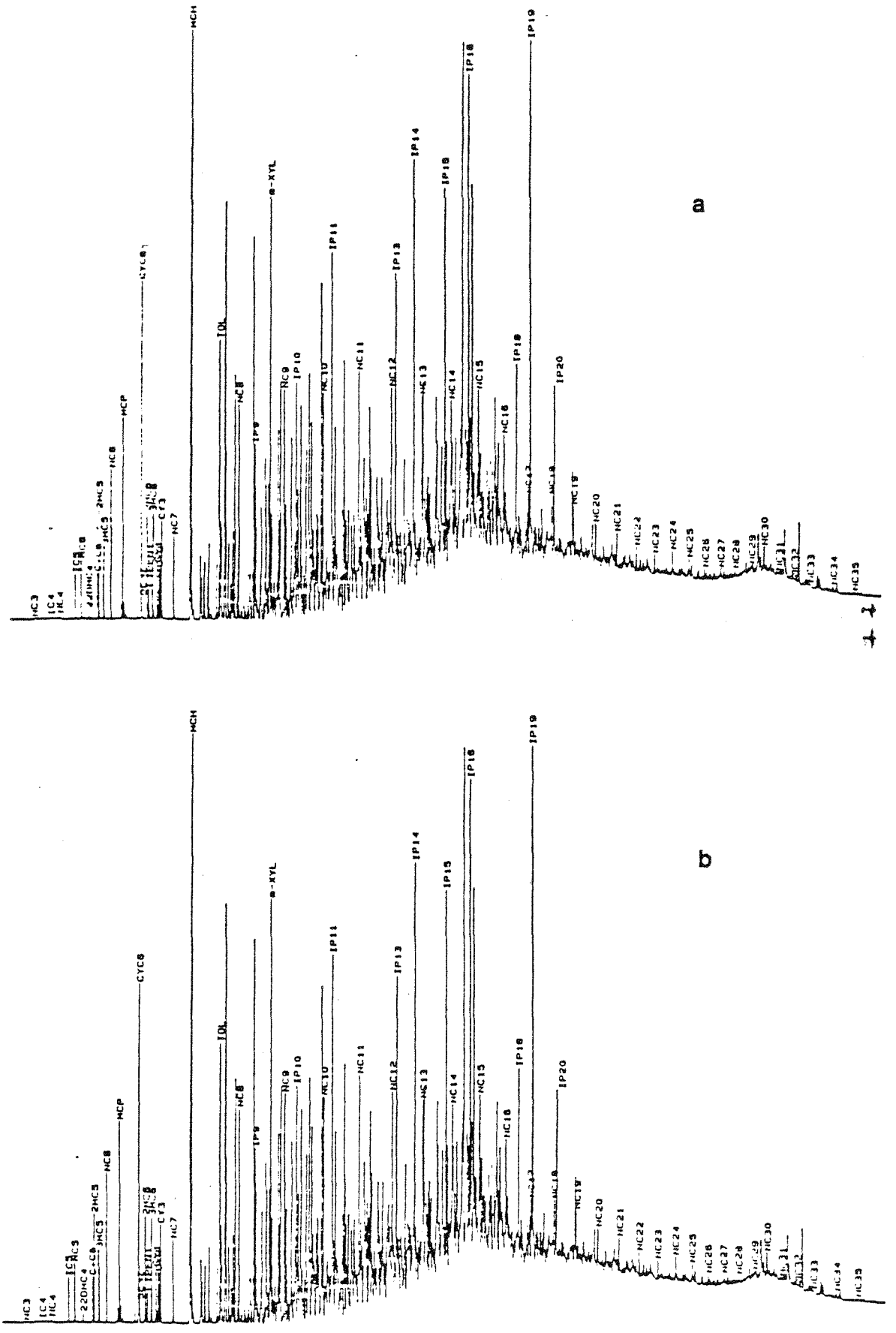

Figure 65. a, b, c, and d. Comparison of gas chromatograph traces for samples ARCO-1989 (TBEG-1) to ARCO-2000, and ARCO-1997 (TBEG-29) to ARCO-2001. ARCO-2000 and ARCO-2001 were unidentified duplicate samples sent to ARCO Service labs to provide a check on their quality. Good replication was found.

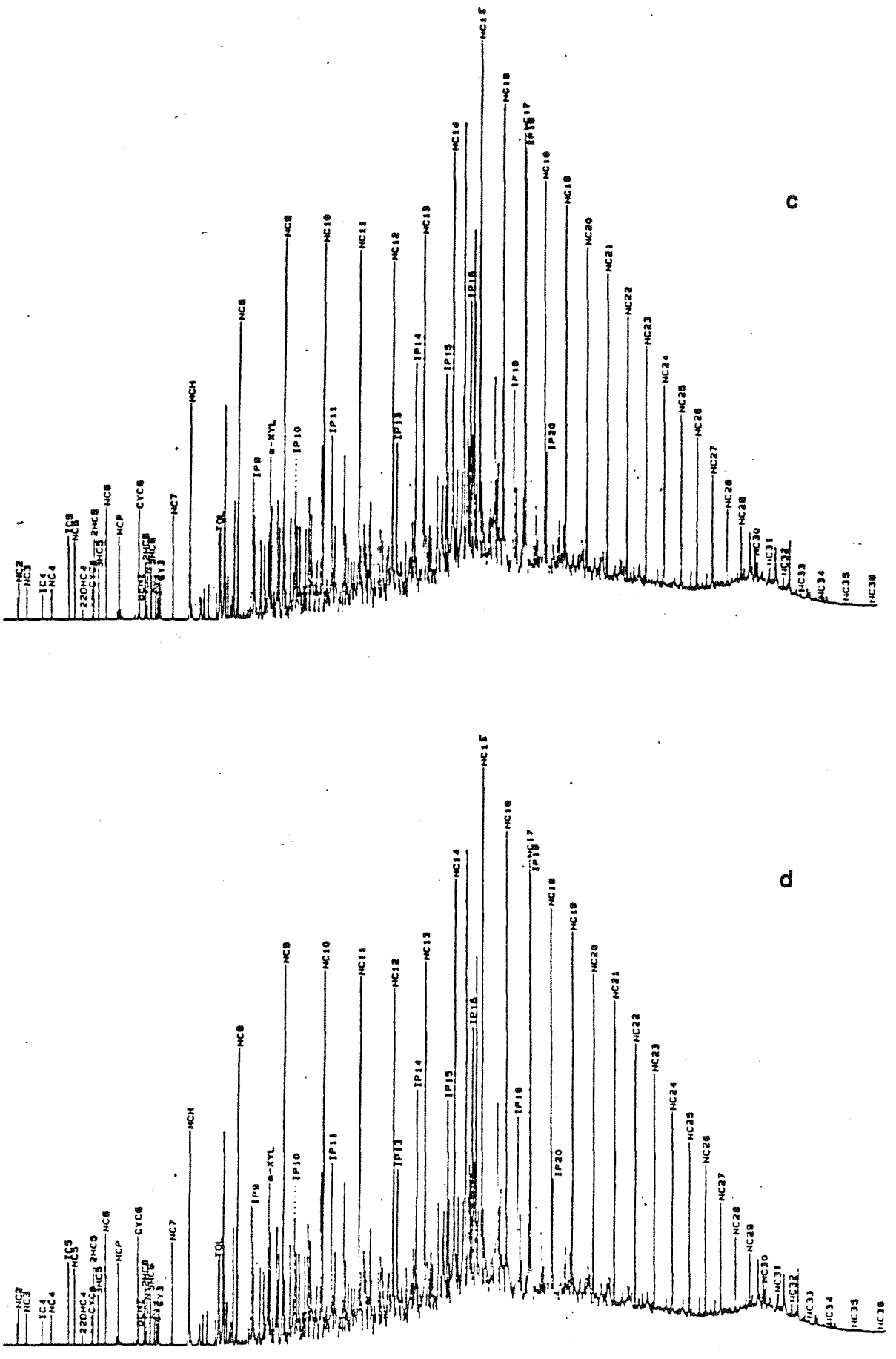

Figure 65 (continued)

figure 63. For trilinear diagrams and maps, these data are based on the Frio chemistry data base previously collected by Kreitler and Richter (1986) (table 3a through d). Scatter diagrams include information from samples collected specifically for this study, or from both this study and the Frio data from Kreitler and Richter (1986). The data set used in the following figures is specified in the captions. In the presentation of the stable isotope data (table 7), the data collected from this study is integrated with Fisher (1982), and unpublished data from Lynton S. Land (Department of Geological Sciences, The University of Texas at Austin). Data from Kreitler and Richter (1986) are presented geographically as the total data set, by county or general region of the Texas Gulf Coast (table 3a through d). It was found that reasonable subregions for our study were Northgulf, Northcentral, Southcentral, and Southgulf. Northgulf region includes Brazoria, Chambers, Fort Bend, Galveston, Harris, Jefferson, Matagorda, and Newton Counties. Northcentral region includes Jackson, Victoria, and Wharton Counties. Southcentral region includes Aransas, Bee, Calhoun, Goliad, parts of Jim Wells, parts of Kleberg, Nueces, Refugio, and San Patricio Counties. Southgulf region includes Brooks, Duval, Hidalgo, parts of Jim Wells, Kenedy, parts of Kleberg, and Starr Counties.

9.1 Trilinear Diagrams

Trilinear diagrams for the Frio show a gradual shift from Na-Cl water in the north and north-central region to Na-Ca-Cl water in the south-central region and Na-Ca-Cl-SO_4 in the south (fig. 66a through d). These trends are similar to those observed by Morton and Land (1987) deeper in the Frio section. Their data show higher Ca concentrations in the south but lower SO_4 values in this southern area.

9.2 Major Anion Distributions (Cl, SO_4)

Chloride

Chloride concentrations in the Frio range from less than 5000 mg/L to approximately 100,000 mg/L. Chloride concentrations typically represent more than 90% of the anions (fig. 66a through d) and therefore are generally correlative with salinity (TDS). The highest Cl concentrations for all depths are generally found in the northern Gulf region, the region that encompasses the Houston Embayment and its salt domes (fig. 67a through d). Kreitler and Richter (1986) and Morton and Land (1987) suggest that these high Cl values are related to salt dome dissolution. A smaller salt basin is present in South Texas, but chloride concentrations in this region are variable with depth, as indicated on the Cl versus depth plot for each county (appendix). Previous authors have suggested that salinity decreases with depth and

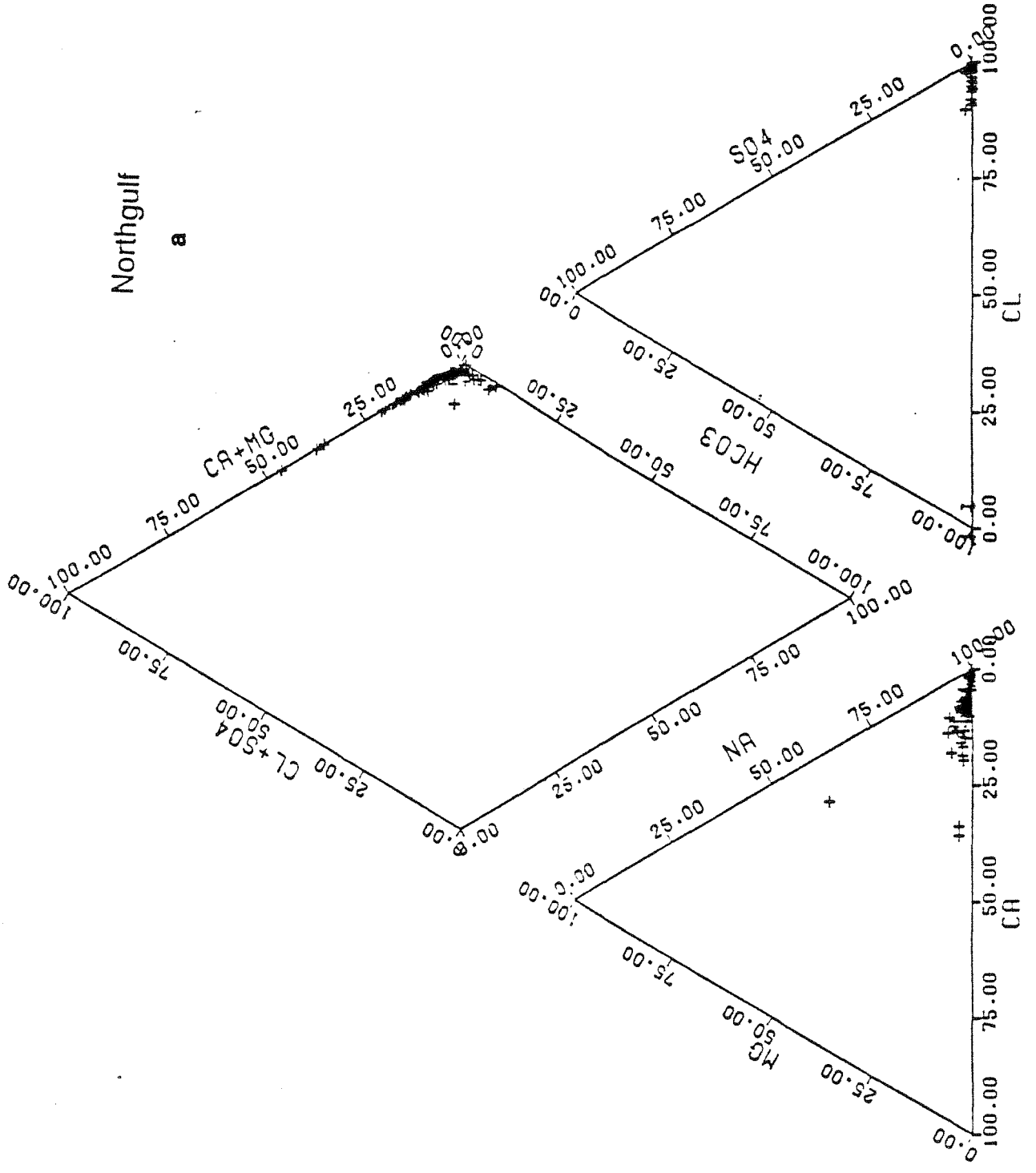

Figure 66. a, b, c, d. Trilinear diagrams for Northgulf, Northcentral, Southcentral, and Southgulf regions of the Frio Formation. Chemical compositions based on Table 1a, b, c, and d.

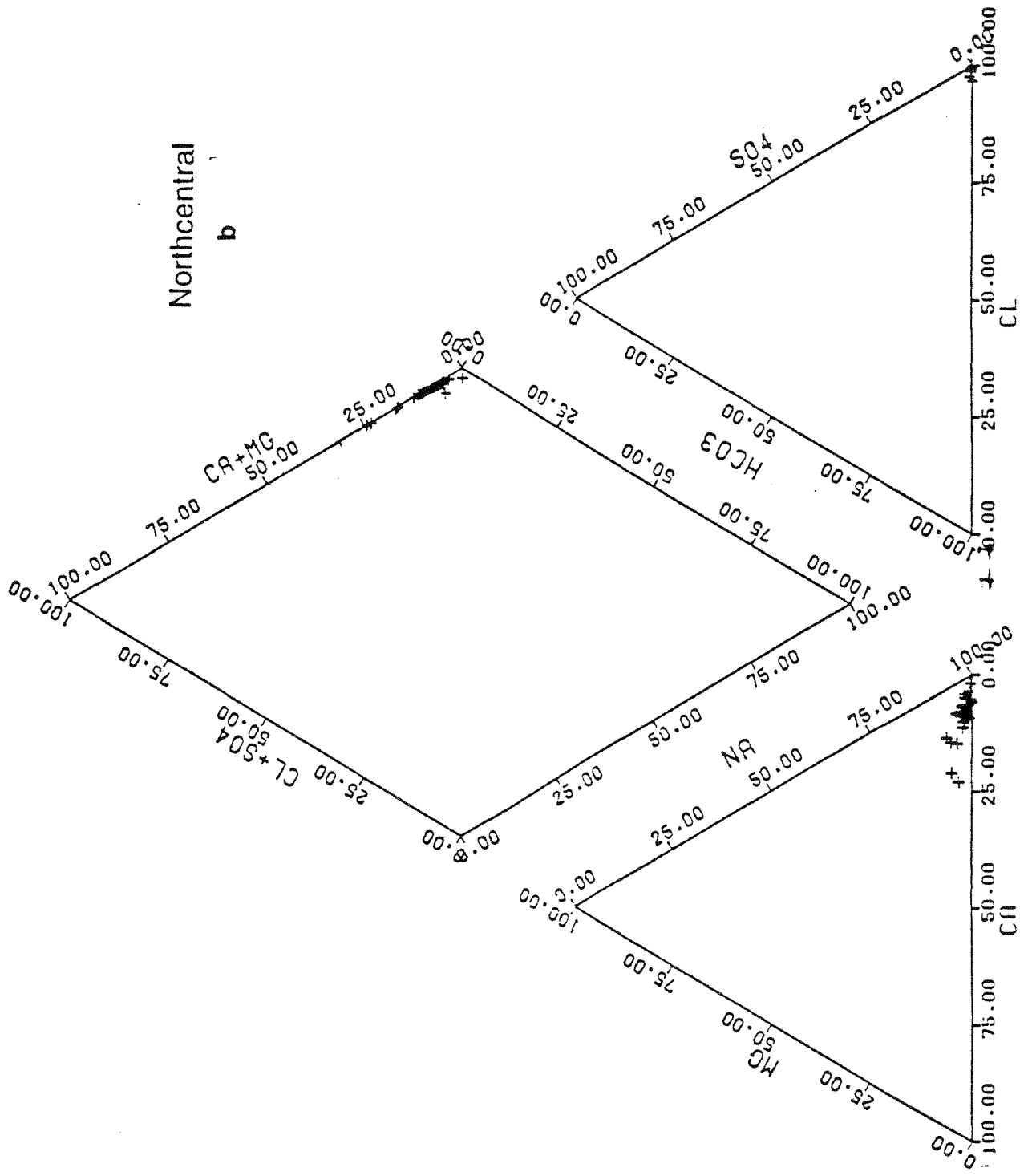

Figure 66 (continued)

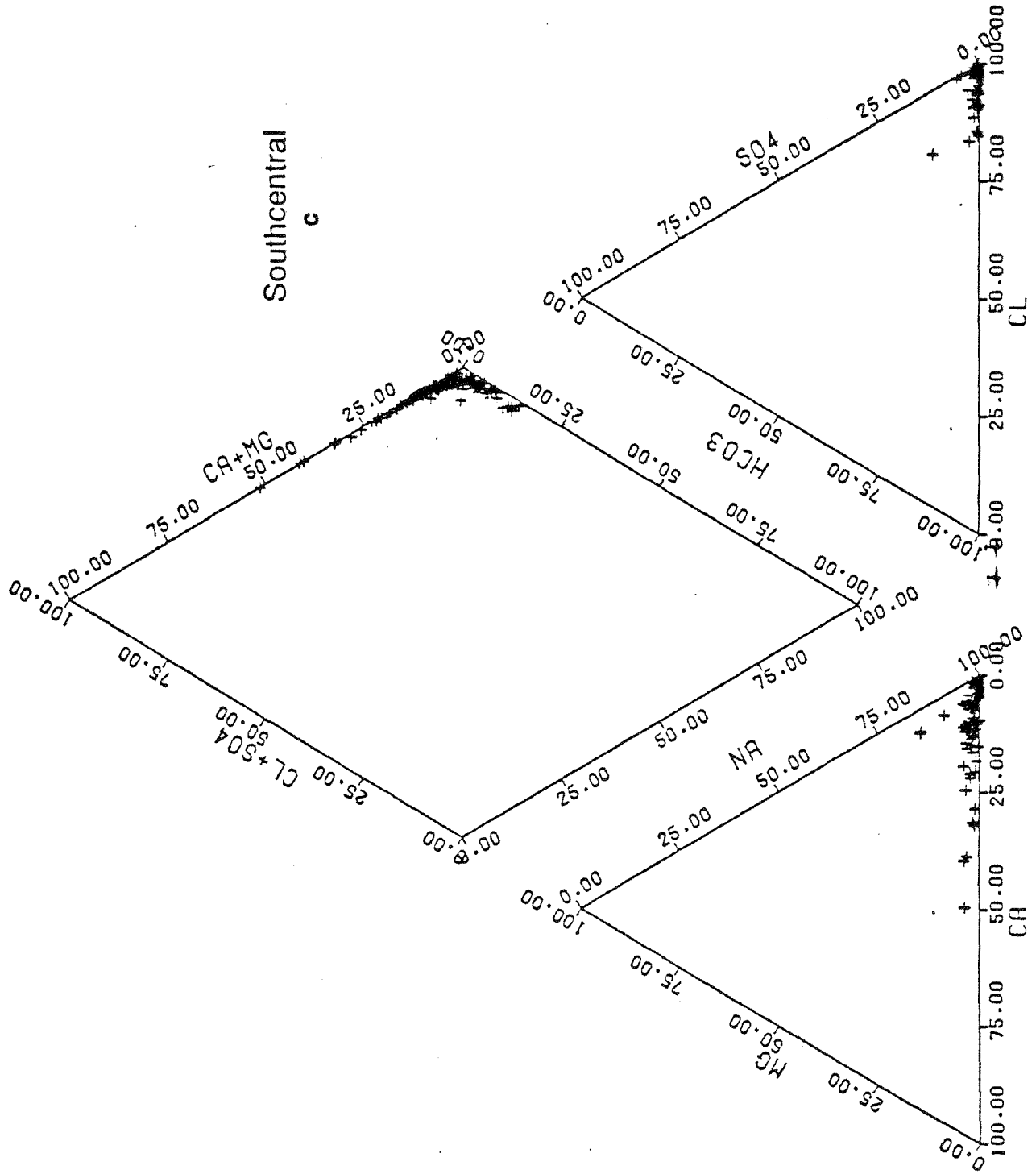

Figure 66 (continued)

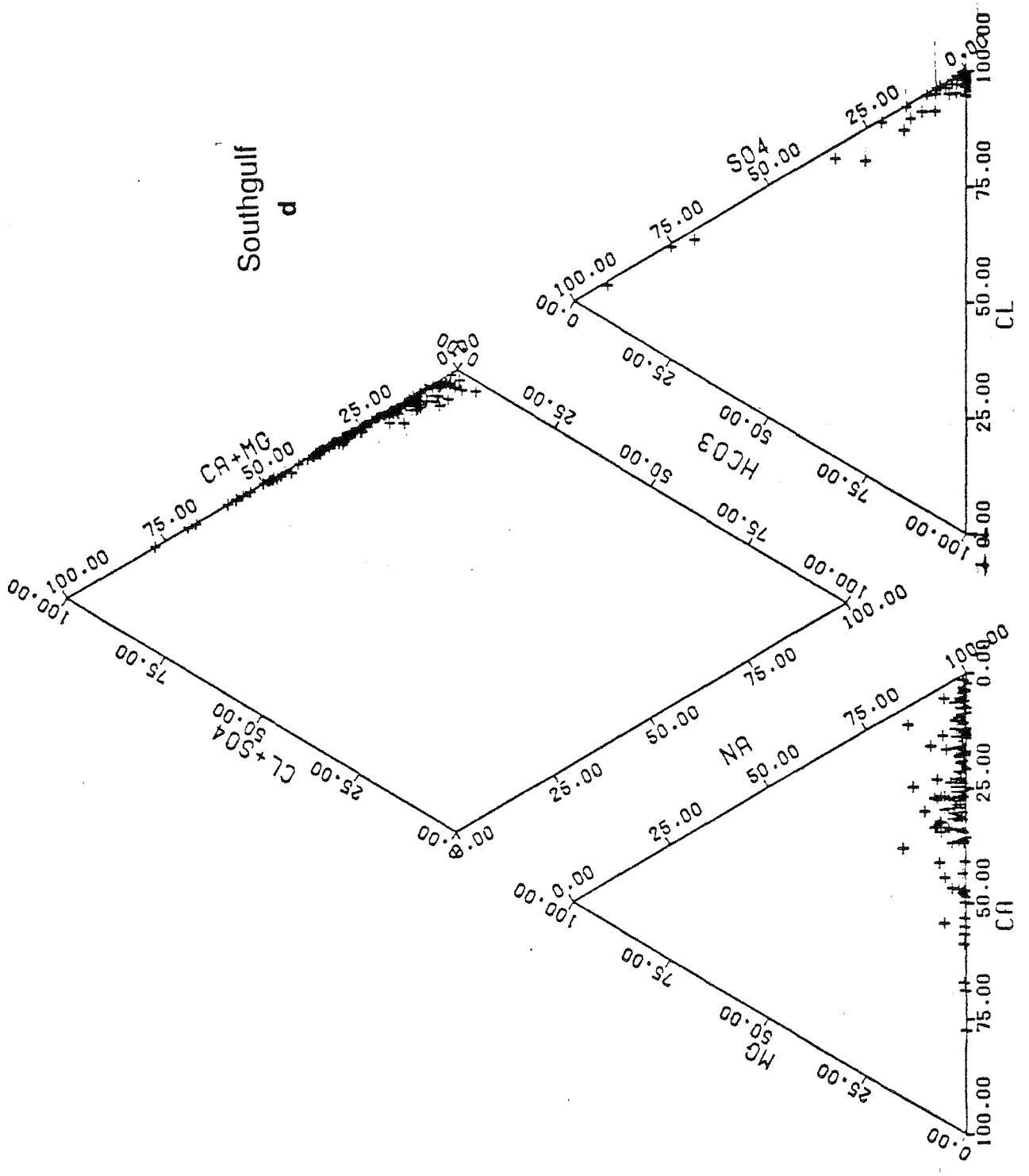

Figure 66 (continued)

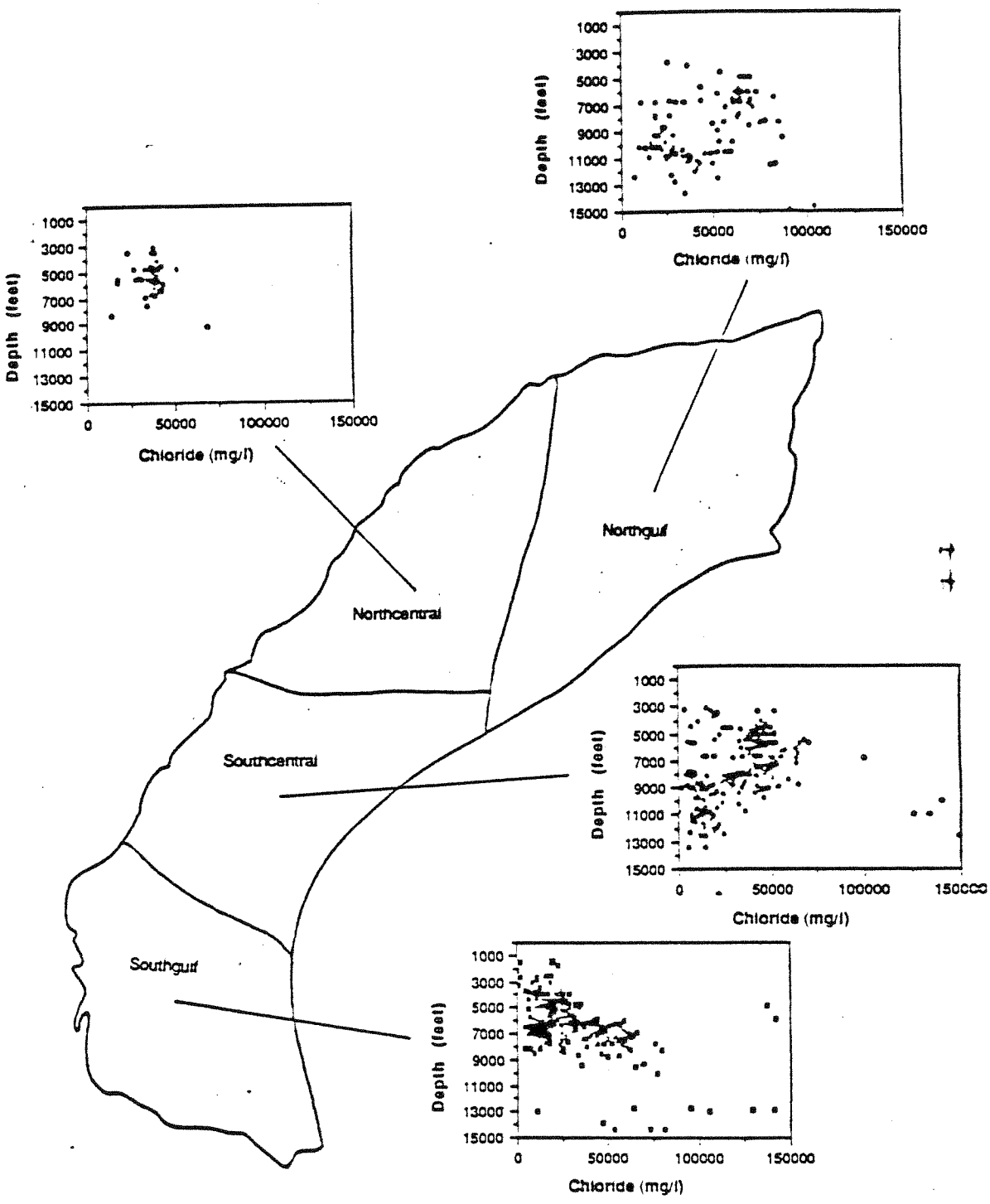

Figure 67. Chloride distribution for the Frio Formation for various depths from Northgulf, Northcentral, Southcentral and Southgulf regions. Chemical compositions based on Table 1a ,b ,c, and d. Units in mg/l.

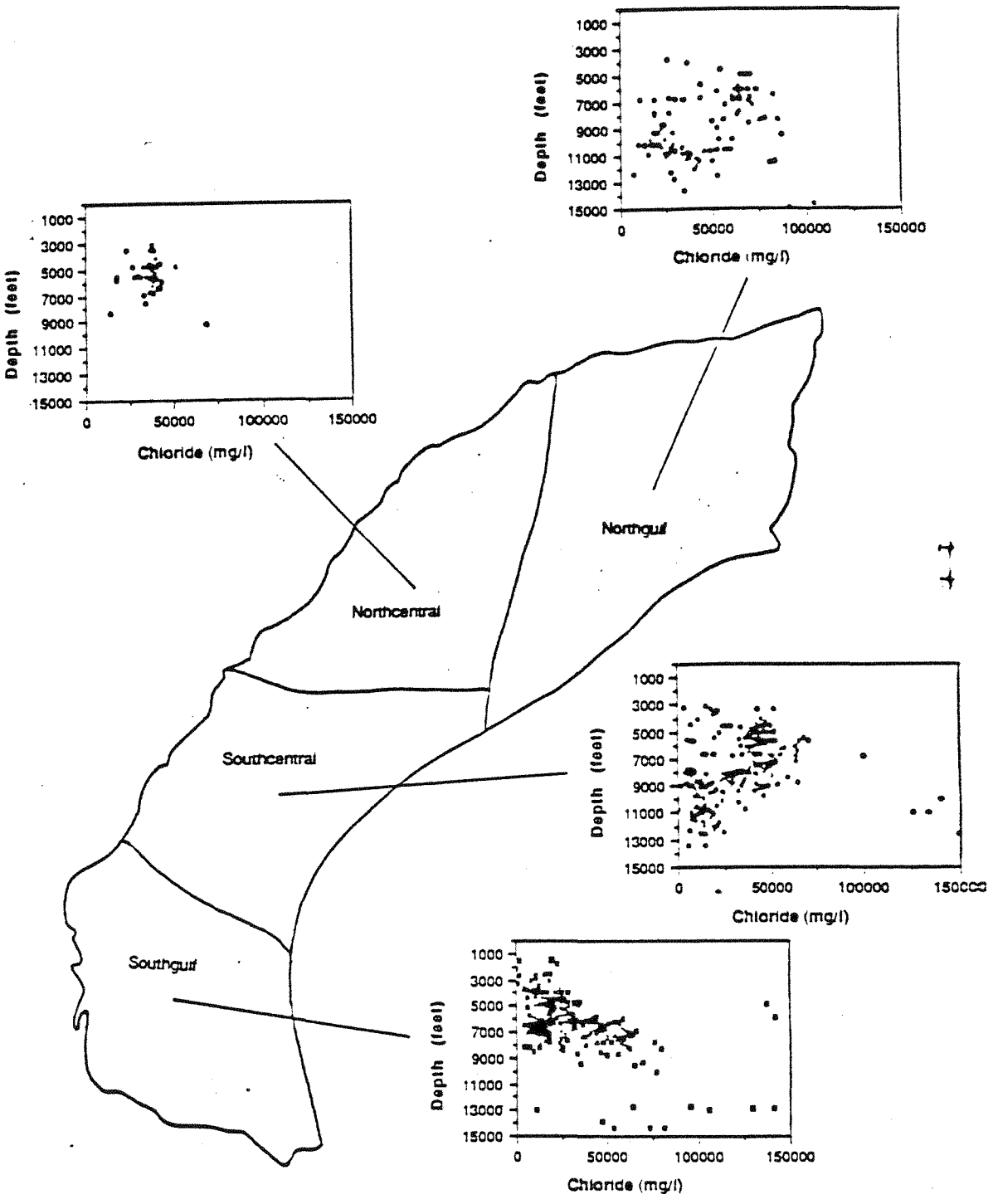

Figure 67. Chloride distribution for the Frio Formation for various depths from Northgulf, Northcentral, Southcentral and Southgulf regions. Chemical compositions based on Table 1a ,b ,c, and d. Units in mg/l.

may be related to the transition from hydrostatic to geopressured conditions. This trend of decreasing salinities is observed in San Patricio and Nueces Counties (fig. 68a, b).

Our pressure/depth plot from the previous description on hydrostatic section of the Frio Formation (fig. 11) also indicates variable salinities. Two hydrostatic lines are evident: one line with a slope of 0.433, which indicates low total dissolved solids, and a second line or zone with a slope of 0.465, which indicates brines of 80,000 mg/L or greater salinities. These two different distributions of data suggest waters with different salinities. We were unable to integrate our pressure data base with chemical composition to the pressure data base to confirm the different salinities for the different hydrostatic lines. It is interesting to note that the hydrostatic line for the middle Wilcox Formation (fig. 57), which generally contains lower TDS values than the Frio, has only the 0.433 hydrostatic line; the 0.465 line is absent.

Sulfate

Sulfate concentrations generally are low in Frio Formation waters (fig. 69a through e). Only in Southgulf are higher values evident. Low sulfate concentrations probably result from a reducing environment in the organic-rich Frio Formation.

9.3 Major Cation Distributions (Na, Ca)

Sodium concentrations increase linearly with chloride for most of the samples except for the Southgulf region (fig. 70a through e). Calcium concentrations versus chloride form a dogleg for Southgulf, Southcentral, and Northgulf (fig. 71a through e). Land and Prezbindowski (1983), Fisher and Kreitler (1987), and Kreitler and Seni (1984) have suggested that the increase in calcium results from cation exchange reactions where Na from a NaCl brine is replaced by Ca from either clays or calcic feldspars. This reaction may be the cause of high calcium in the Southgulf region. Morton and Land (1987) observed similar calcium-rich brines in the geopressured section of this South Texas region and suggest that these calcium-rich brines are deeper brines that have migrated to shallower depths.

9.4 Minor Elements (Br), and Cl/Br and Na/Cl Ratios

A plot of bromide versus chloride (fig. 72) shows two different populations of data, a population where bromide increases linearly with chloride (this will be referred to as Na-Cl, high-Br water type, and a population where bromide concentration remains constant with increasing chloride (this will be referred to as Na-Cl, low-Br water type; all discussion of these two water types is based on this differentiation in

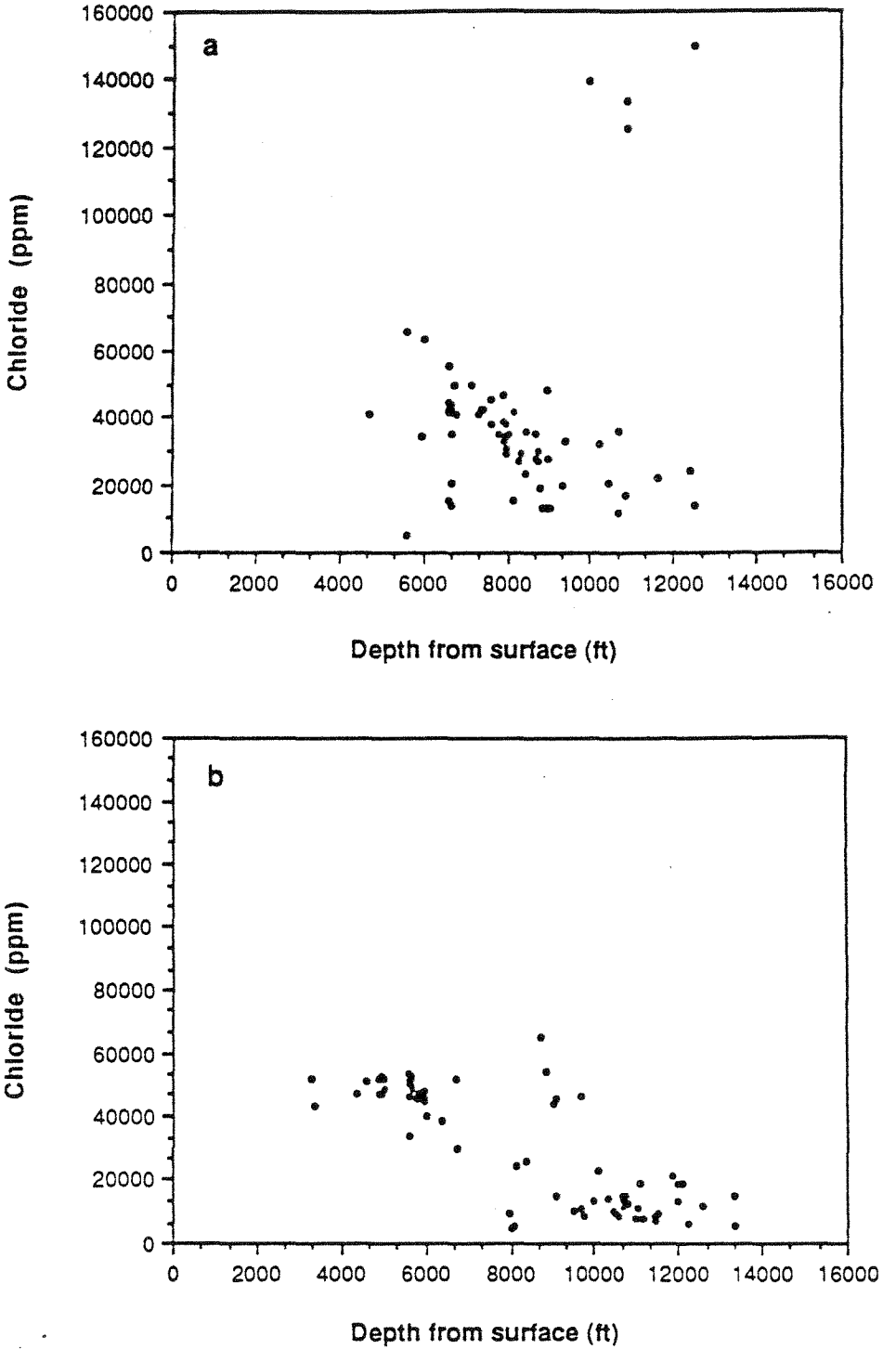

Figure 68. (a) Cl versus depth for Nueces County, (b) Cl versus depth for San Patricio County. Data from Kreitler and Richter (1986).

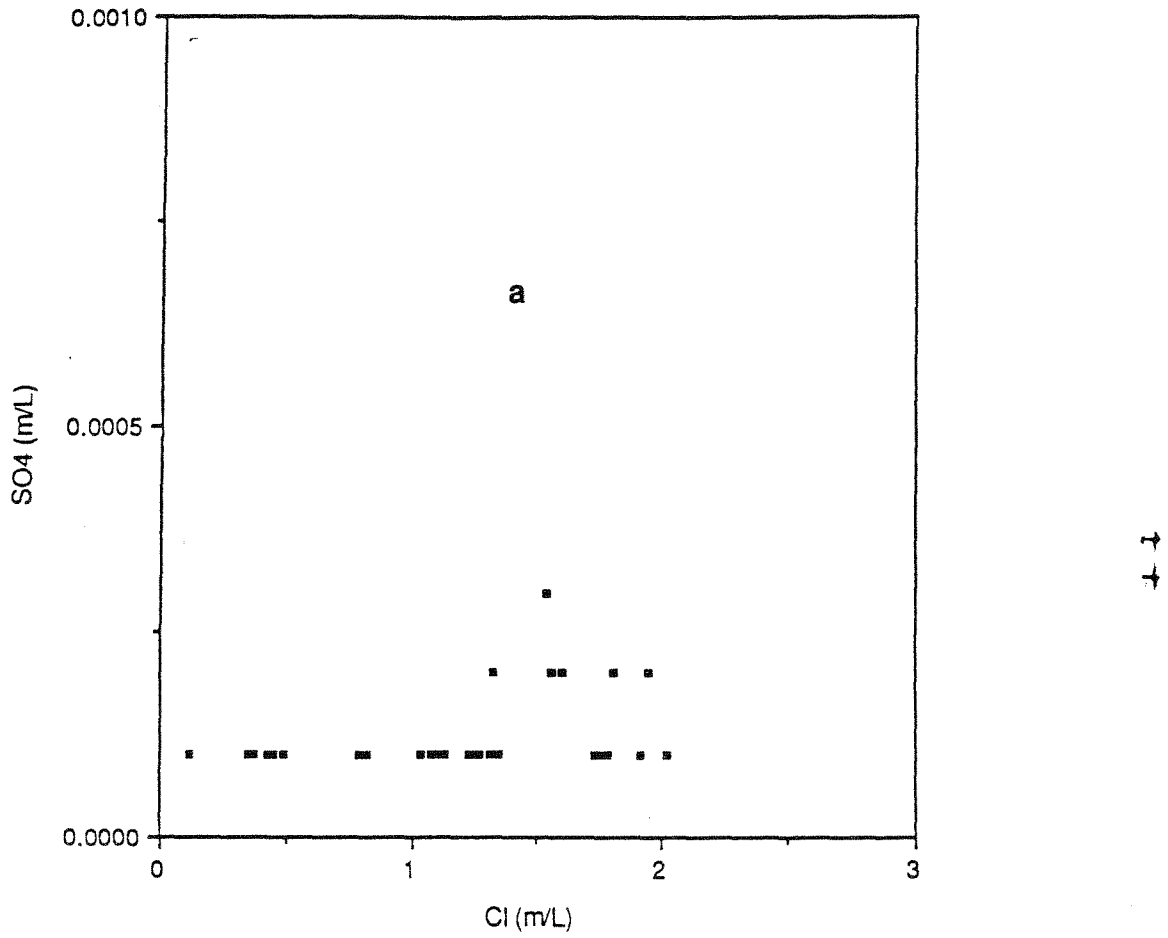

Figure 69. (a) Sulfate concentrations versus chloride in the Frio Formation collected for this study (Table 3). Sulfate concentrations versus chloride for the Frio Formation for Northgulf (b), Northcentral (c), Southcentral (d), and Southgulf (e). Chemical compositions based on Table 2.

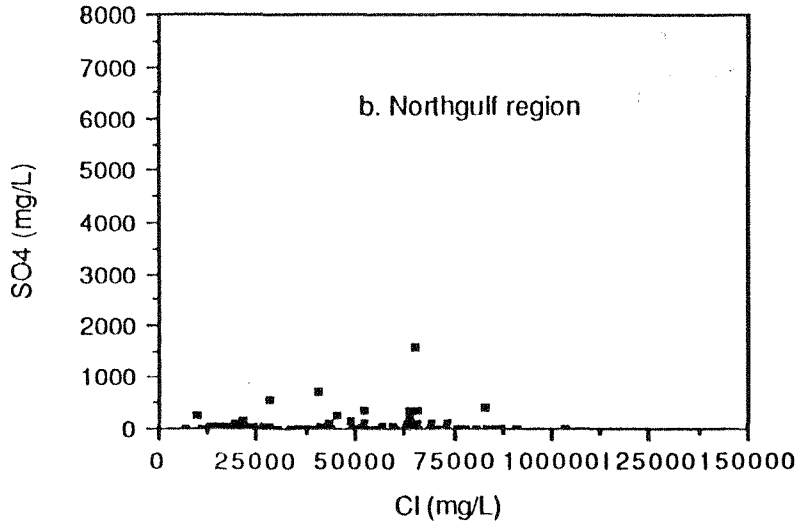

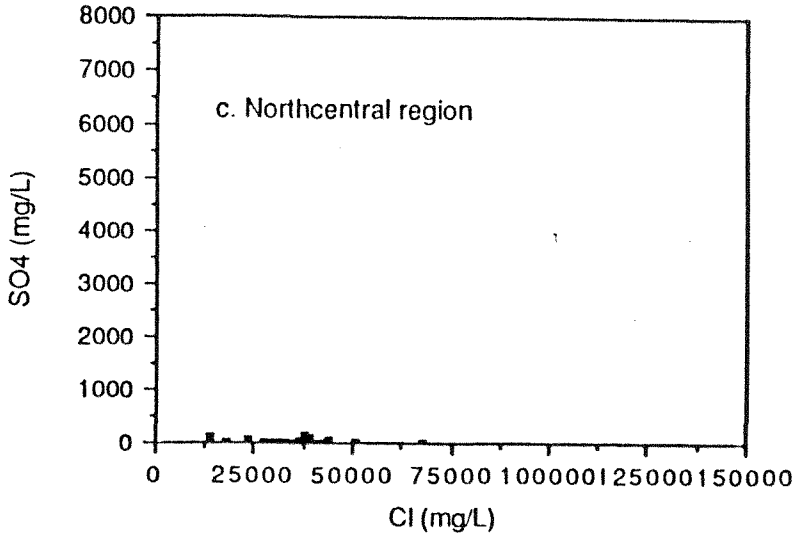

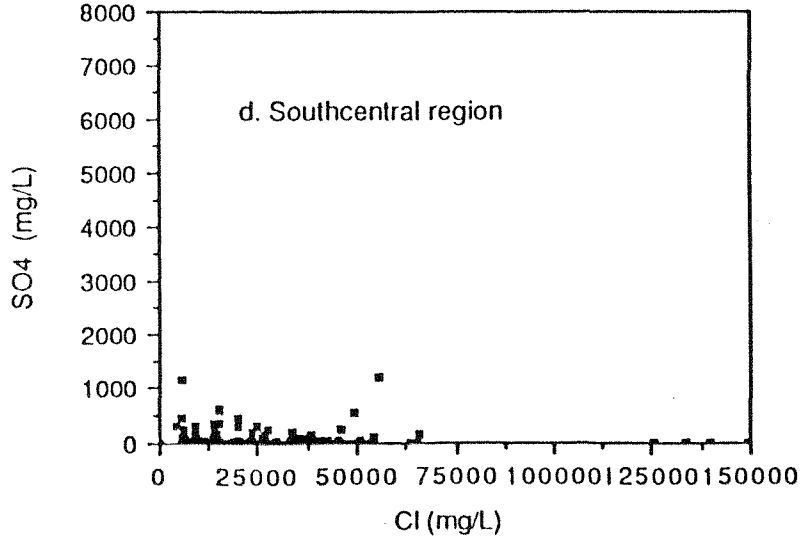

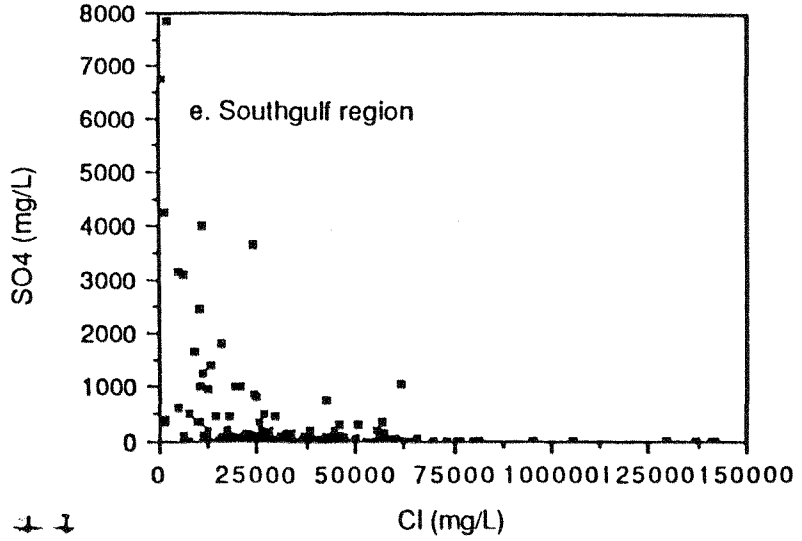

Figure 69 (continued)

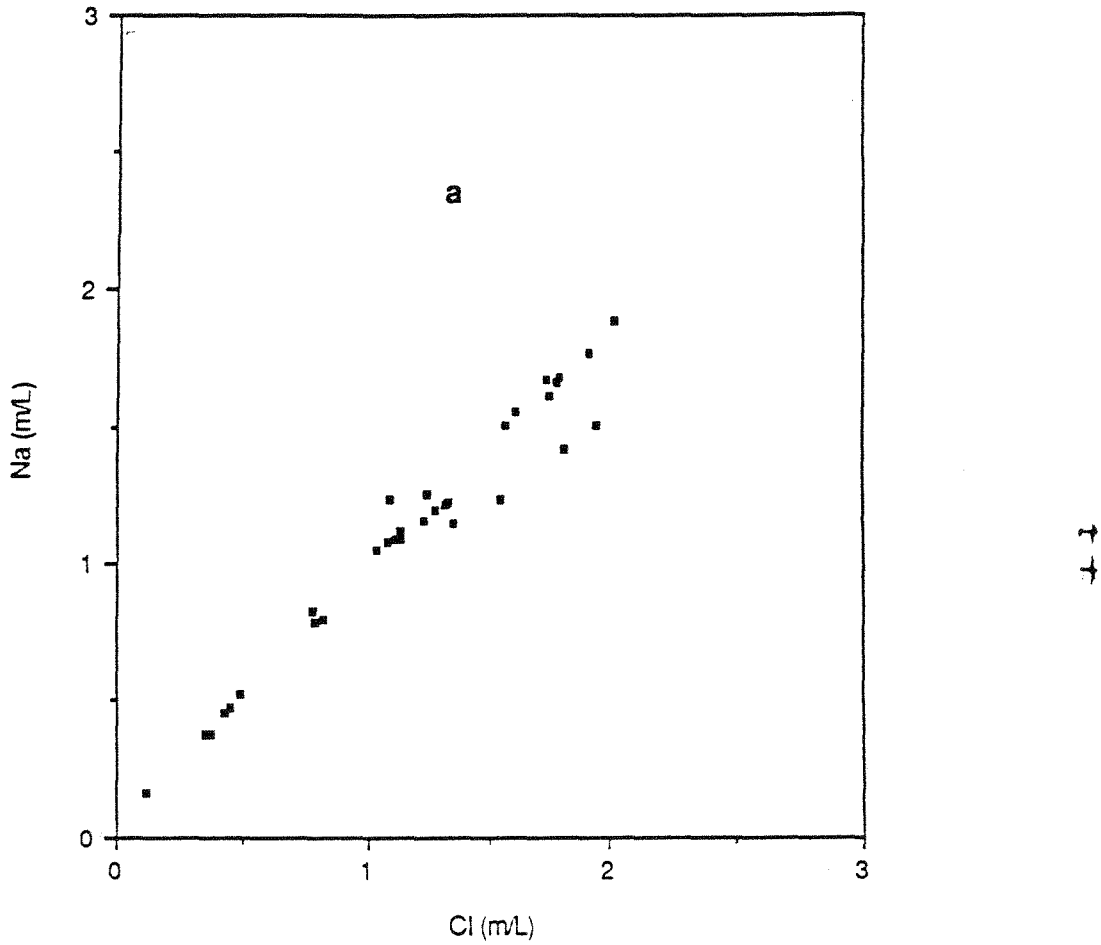

Figure 70. (a) Sodium concentration in the Frio Formation from data collected for this study (Table 3). Sodium concentrations versus chloride for the Frio Formation for Northgulf (b), Northcentral (c), Southcentral (d), and Southgulf (e). Chemical compositions based on Table 1a, b, c, and d.

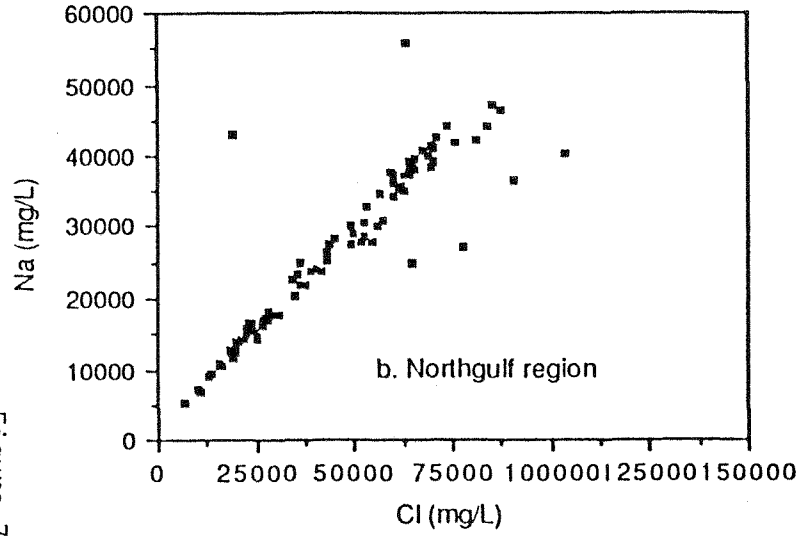

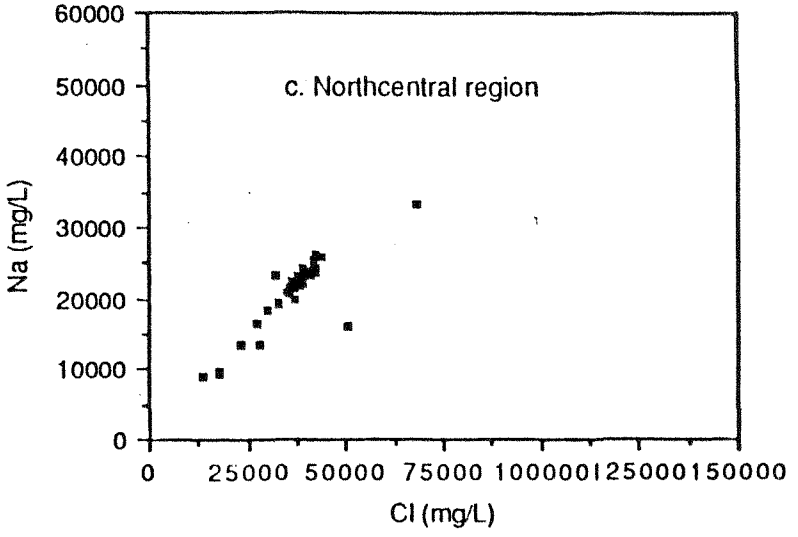

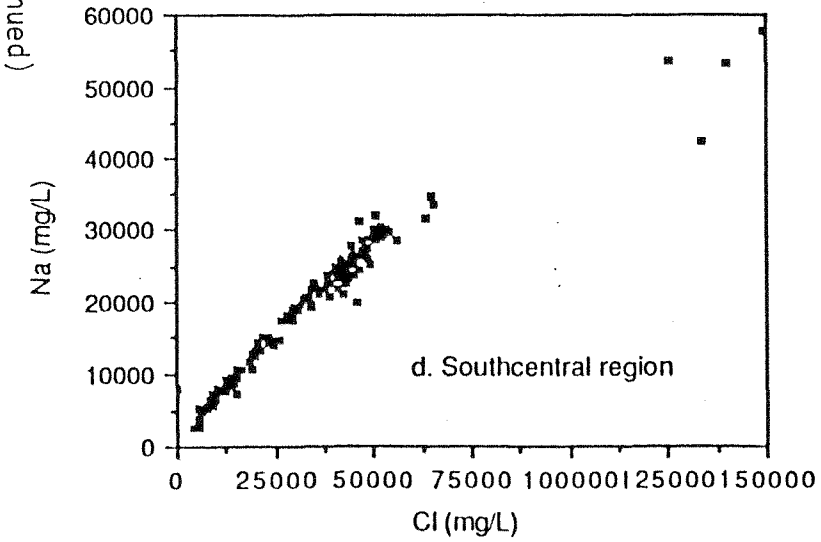

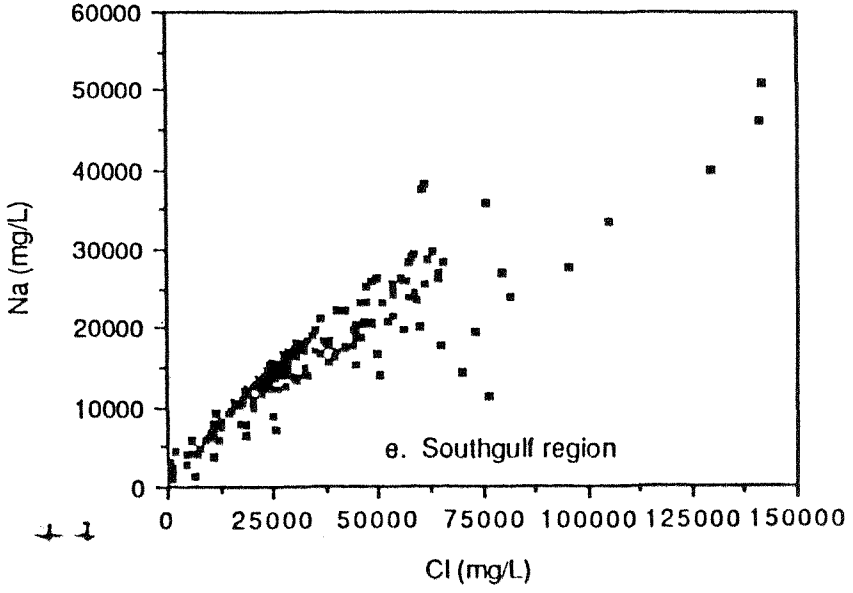

Figure 70 (continued)

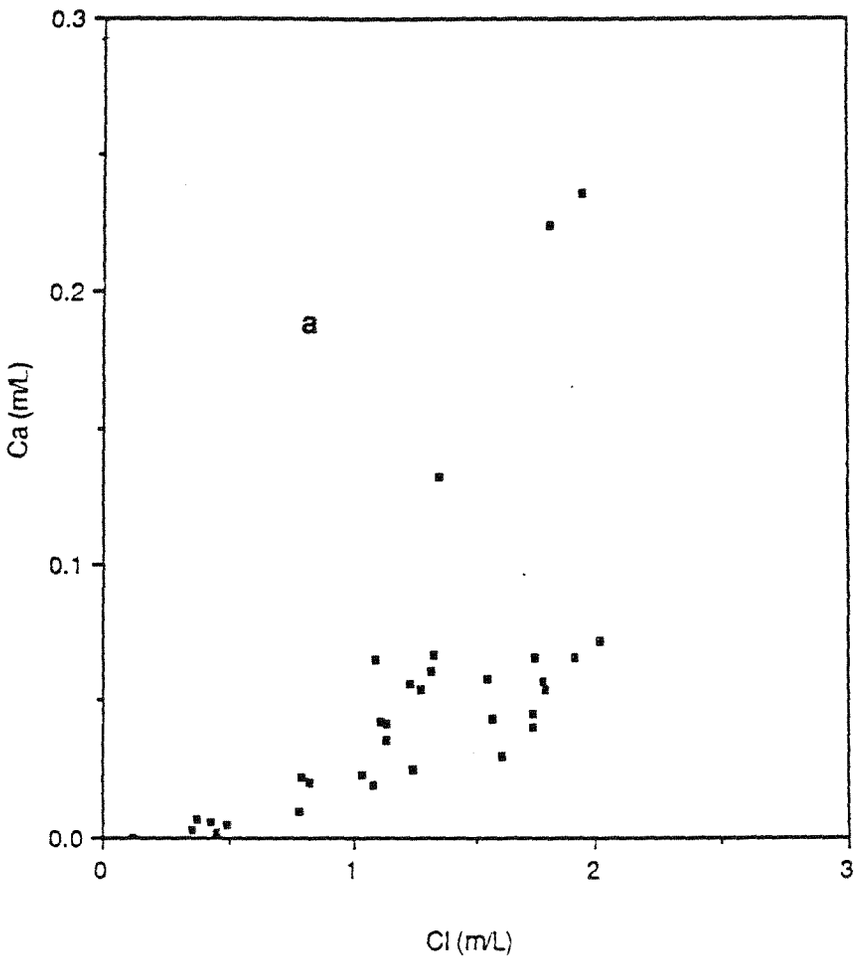

Figure 71. (a) Calcium concentrations versus chloride in the Frio Formation from data collected for this study (Table 3). Calcium concentrations versus chloride for the Frio Formation for Northgulf (b), Northcentral (c), Southcentral (d), and Southgulf (e). Chemical composition based on Table 1a, b, c, and d.

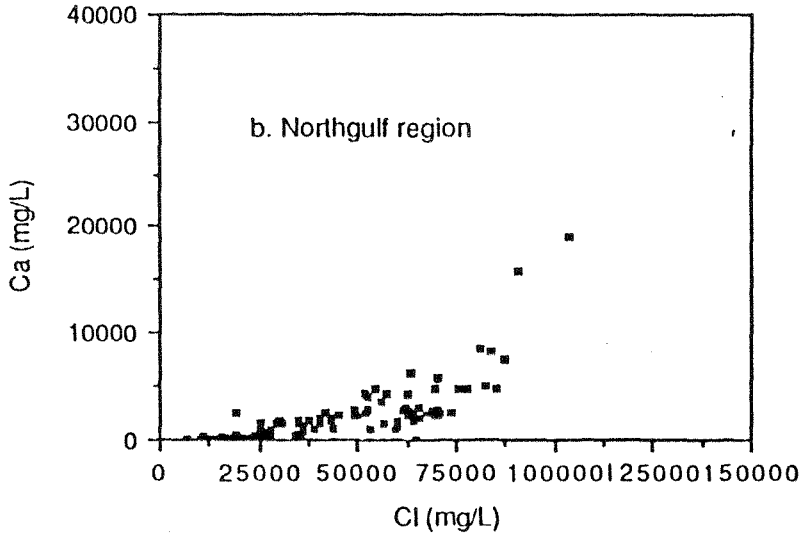

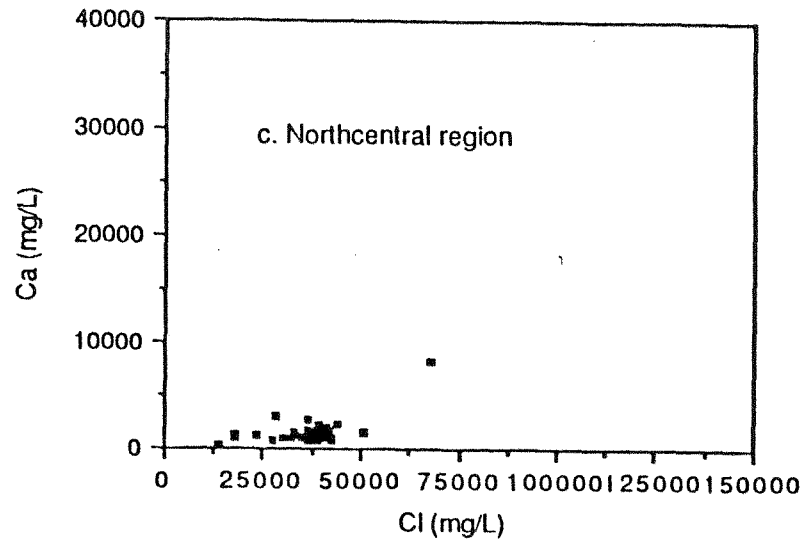

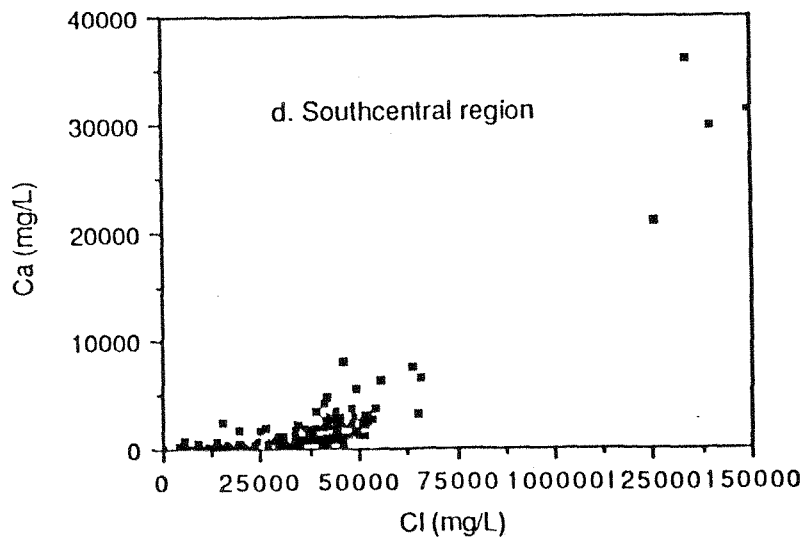

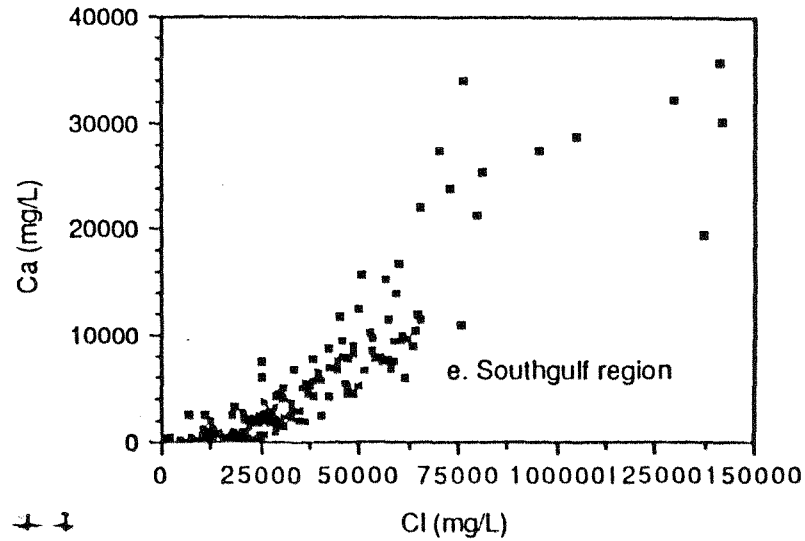

Figure 71 (continued)

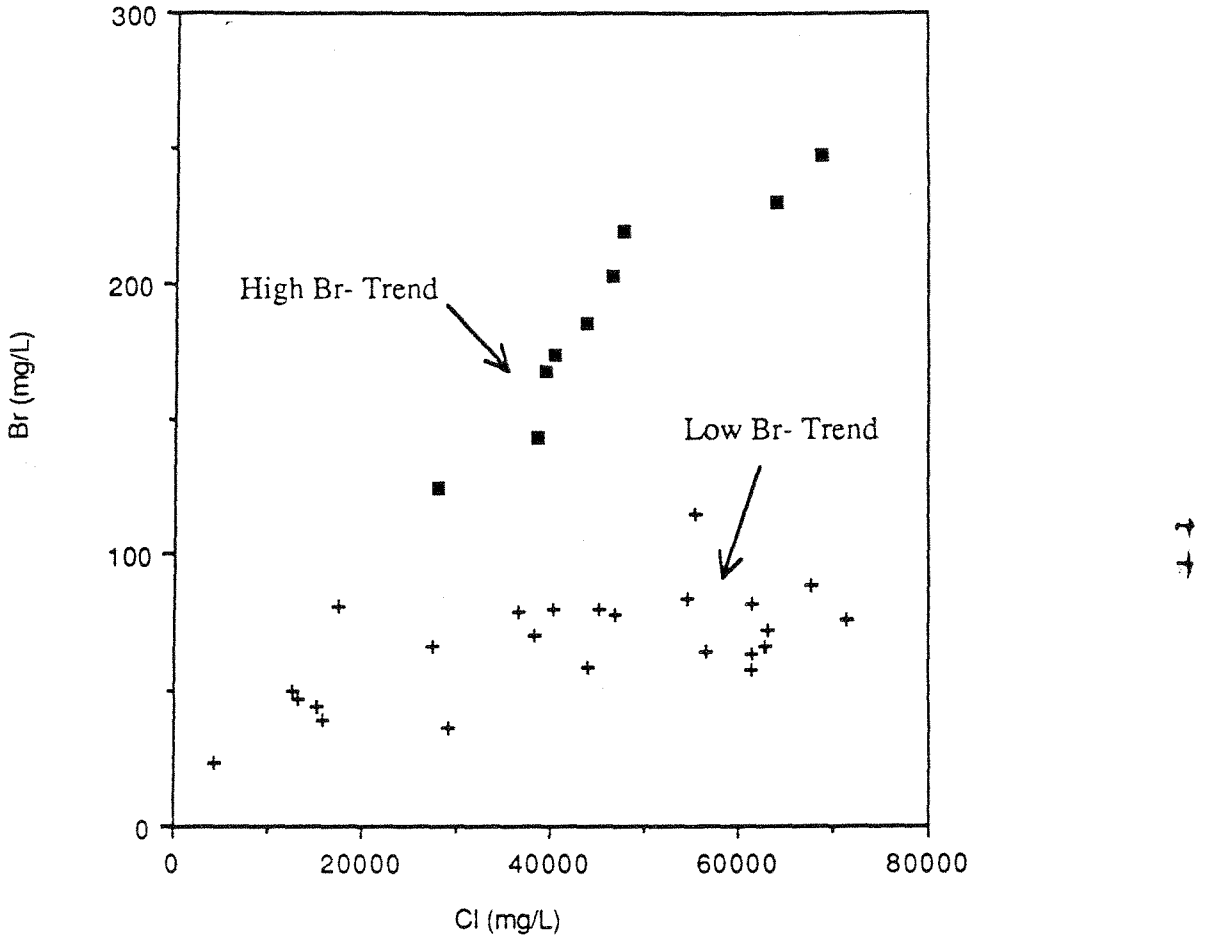

Figure 72. Plot of bromide versus chloride from data collected for this study (Table 3). Note two different populations of data.

fig. 72). With the addition of Southgulf region data, the linear relationship of the high-Br trend is extended to much higher Br concentrations (fig. 73). Figure 74, a plot of Cl/Br versus Cl, shows a similar separation of the two populations. Bromide and Cl/Br ratios have been used as an effective tool for determining the source of chloride in a brine. High Cl/Br ratios indicate that halite dissolution is the source of chloride (Whittemore and others, 1981; Richter and Kreitler, 1986). Low Cl/Br ratios are typical of the average basinal brine (Richter and Kreitler, 1986), seawater, and residual brines from bittern salt precipitation (Carpenter, 1978). The ratio of Na/Cl is another effective tool for determining the source of Cl in a brine. Seawater has a molar Na/Cl ratio of 0.77, whereas brines resulting from halite dissolution approximate 1.0. Low-salinity meteoric waters typically have an Na/Cl ratio > 1.0, because of possible generation of sodium bicarbonate waters that is independent of chloride. Figure 75, a plot of Na/Cl versus Cl again shows two different populations. The low-Br waters trend from approximately 1.1 to 0.95, whereas the high-Br waters trend from 1.0 to 0.75. The Cl/Br and the Na/Cl ratios for the low-Br data both suggest halite dissolution as the source of NaCl in these waters. The geographic location of these samples in the salt basin further confirms halite dissolution (fig. 76 a and b). These two populations are geographically distributed such that the low-Br values are predominantly in the Houston Embayment salt dome region. The high-Br waters occur predominantly in the middle to south coastal region. The source of the high Br cannot be as easily determined. A high-Br water is mixing with a low-Br, low-salinity water. A plot of Br versus Ca (fig. 77) shows that the high Br also correlates with the high Ca previously discussed and may result from mixing. High Br also correlates with high Sr concentrations and follows a slope of 9:10 (a molar ratio of approximately 1:1) (fig. 78). Deeper formation waters in the Gulf of Mexico basin are high in Ca, Sr, and Br (Morton and Land, 1987). These waters may be leaking into shallower sections, resulting in the observed chemistry changes. Figure 79 shows the increase in Br with depth for the samples from the high-Br population. Plotting Na/Cl versus Cl/Br (fig. 80) again separates the two trends. Both populations (low Br and high Br) appear to originate from the same source, a water with a Na/Cl ratio of 1.0 or higher and a Cl/Br ratio of about 200. These ratios suggest a continental ground water, or possibly brackish water in a deltaic setting like the original water, and not a marine water as has been previously suggested. If this initial water is an original depositional (connate) water, then the hypothesis of a more continental-deltaic water like the original water may be reasonable for the Frio, which is composed predominantly of fluvial and deltaic, not marine, facies.

fig. 72). With the addition of Southgulf region data, the linear relationship of the high-Br trend is extended to much higher Br concentrations (fig. 73). Figure 74, a plot of Cl/Br versus Cl, shows a similar separation of the two populations. Bromide and Cl/Br ratios have been used as an effective tool for determining the source of chloride in a brine. High Cl/Br ratios indicate that halite dissolution is the source of chloride (Whittemore and others, 1981; Richter and Kreitler, 1986). Low Cl/Br ratios are typical of the average basinal brine (Richter and Kreitler, 1986), seawater, and residual brines from bittern salt precipitation (Carpenter, 1978). The ratio of Na/Cl is another effective tool for determining the source of Cl in a brine. Seawater has a molar Na/Cl ratio of 0.77, whereas brines resulting from halite dissolution approximate 1.0. Low-salinity meteoric waters typically have an Na/Cl ratio > 1.0, because of possible generation of sodium bicarbonate waters that is independent of chloride. Figure 75, a plot of Na/Cl versus Cl again shows two different populations. The low-Br waters trend from approximately 1.1 to 0.95, whereas the high-Br waters trend from 1.0 to 0.75. The Cl/Br and the Na/Cl ratios for the low-Br data both suggest halite dissolution as the source of NaCl in these waters. The geographic location of these samples in the salt basin further confirms halite dissolution (fig. 76 a and b). These two populations are geographically distributed such that the low-Br values are predominantly in the Houston Embayment salt dome region. The high-Br waters occur predominantly in the middle to south coastal region. The source of the high Br cannot be as easily determined. A high-Br water is mixing with a low-Br, low-salinity water. A plot of Br versus Ca (fig. 77) shows that the high Br also correlates with the high Ca previously discussed and may result from mixing. High Br also correlates with high Sr concentrations and follows a slope of 9:10 (a molar ratio of approximately 1:1) (fig. 78). Deeper formation waters in the Gulf of Mexico basin are high in Ca, Sr, and Br (Morton and Land, 1987). These waters may be leaking into shallower sections, resulting in the observed chemistry changes. Figure 79 shows the increase in Br with depth for the samples from the high-Br population. Plotting Na/Cl versus Cl/Br (fig. 80) again separates the two trends. Both populations (low Br and high Br) appear to originate from the same source, a water with a Na/Cl ratio of 1.0 or higher and a Cl/Br ratio of about 200. These ratios suggest a continental ground water, or possibly brackish water in a deltaic setting like the original water, and not a marine water as has been previously suggested. If this initial water is an original depositional (connate) water, then the hypothesis of a more continental-deltaic water like the original water may be reasonable for the Frio, which is composed predominantly of fluvial and deltaic, not marine, facies.

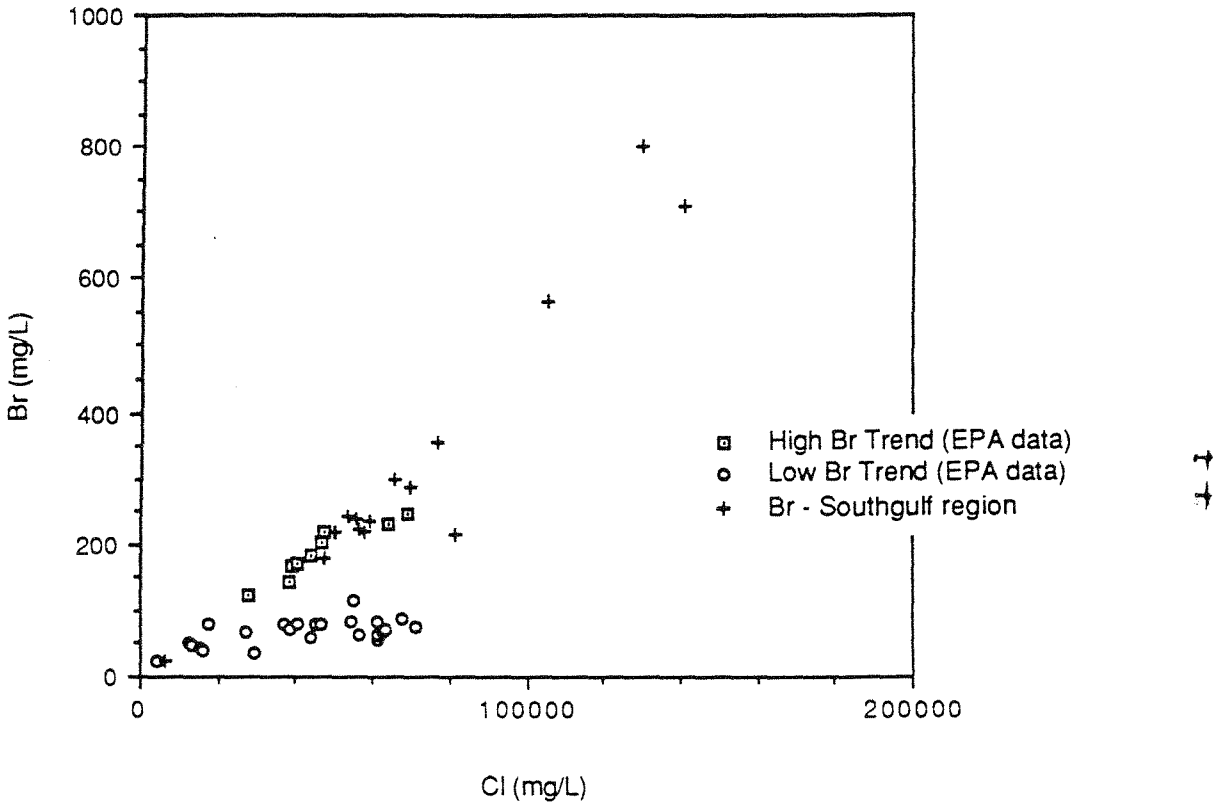

Figure 73. Br versus Cl for high Br trend and low Br trend based on EPA data (Table 3) and Southgulf region data (Table 2). Note linear increase of Br with Cl to very high Br concentrations.

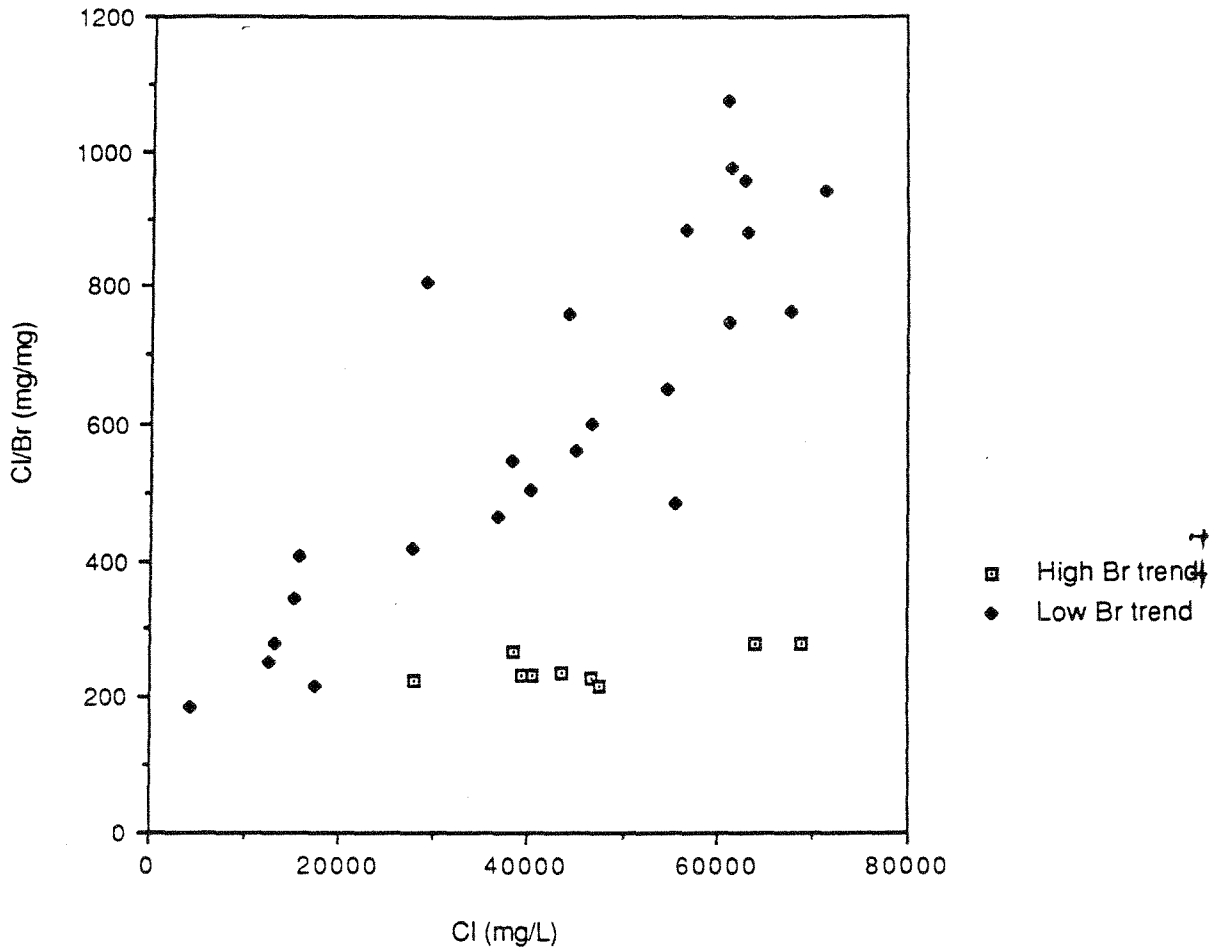

Figure 74. Plot of Cl/Br versus chloride, Frio Formation, from data collected for this study (Table 3).

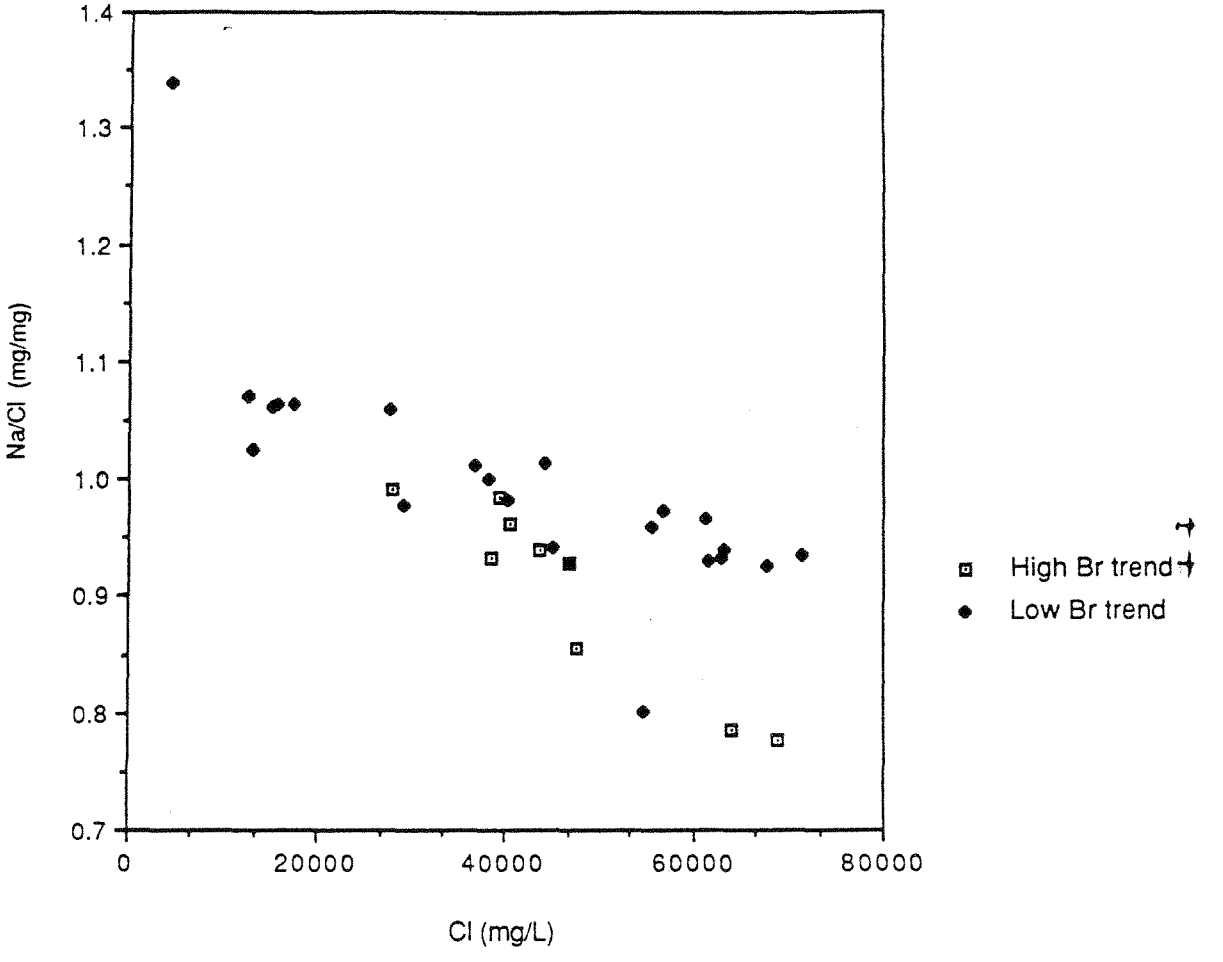

Figure 75. Na/Cl versus chloride, Frio Formation, from data collected for this study (Table 3).

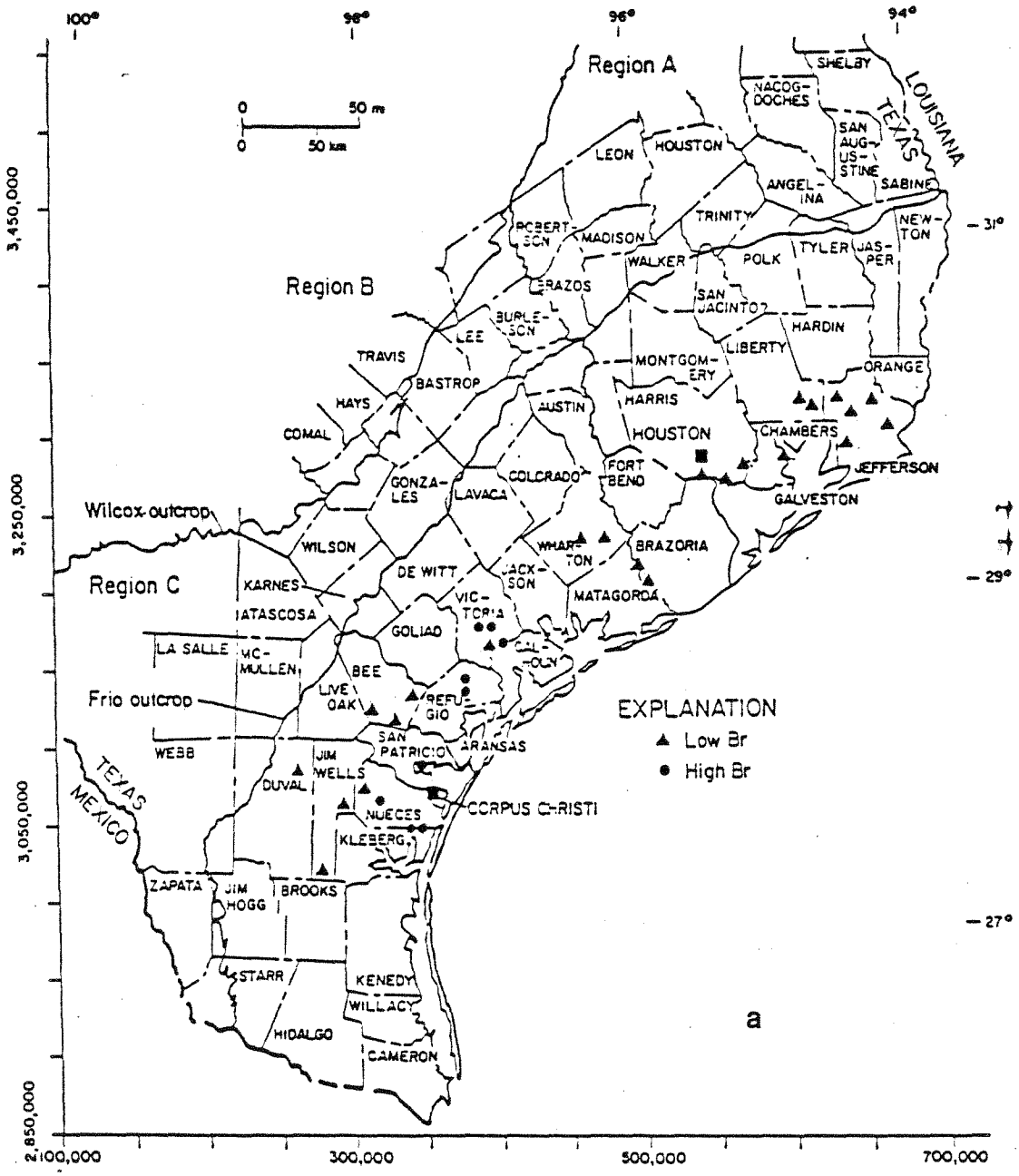

Figure 76. (a) Geographic distribution of the two different populations of data, Na-Cl, low-Br waters and Na-Cl, high Br waters, and (b) salt dome locations. Note the low-Br waters are predominantly in the Houston Emabayment salt dome region. The low-Br waters in Duval, Jim Wells and Nueces Counties are near two salt domes in Duval County. Data from this study (Table 3).

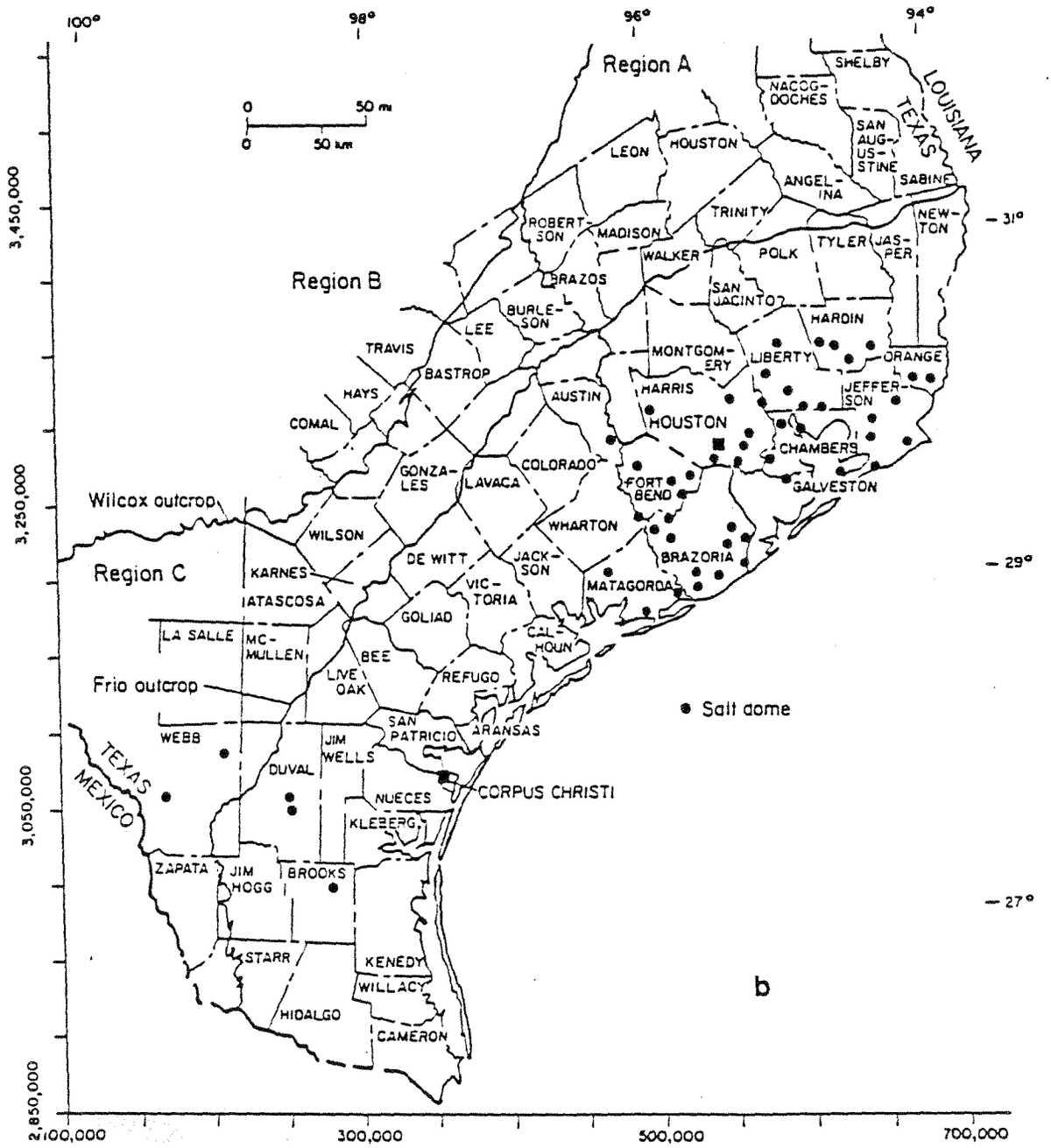

Figure 76 (continued)

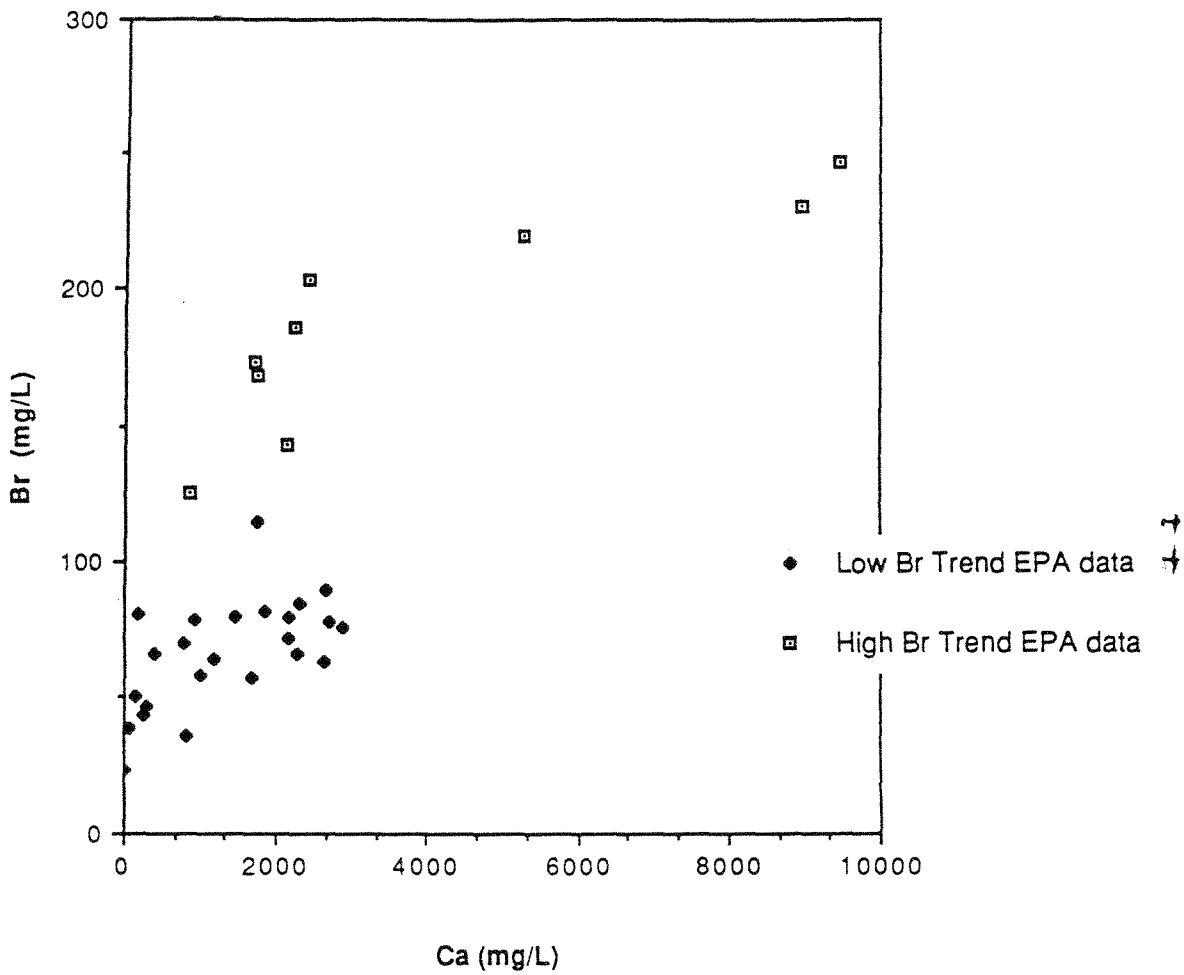

Figure 77. Plot of Br versus Ca or Frio Formation. Data from this study (Table3).

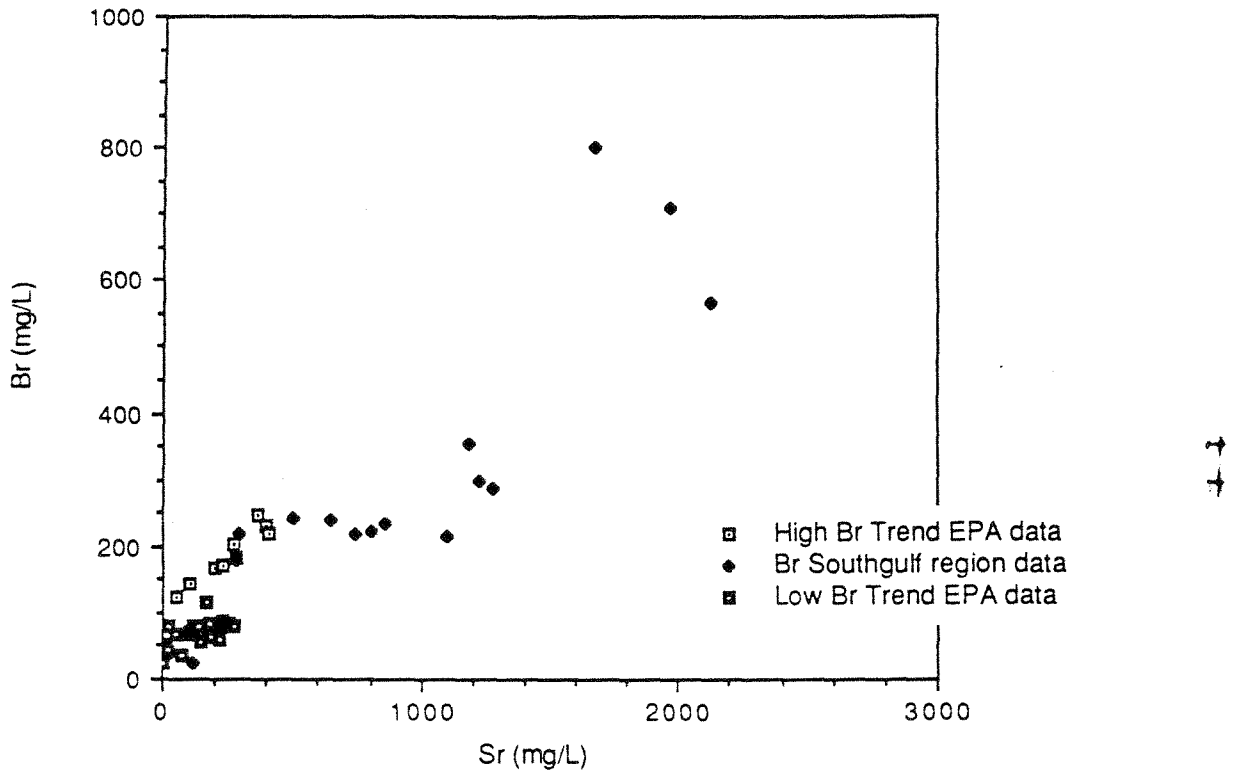

Figure 78. Plot of Br versus Sr. Data from this study (Table 3) and Southgulf region (Table 2).

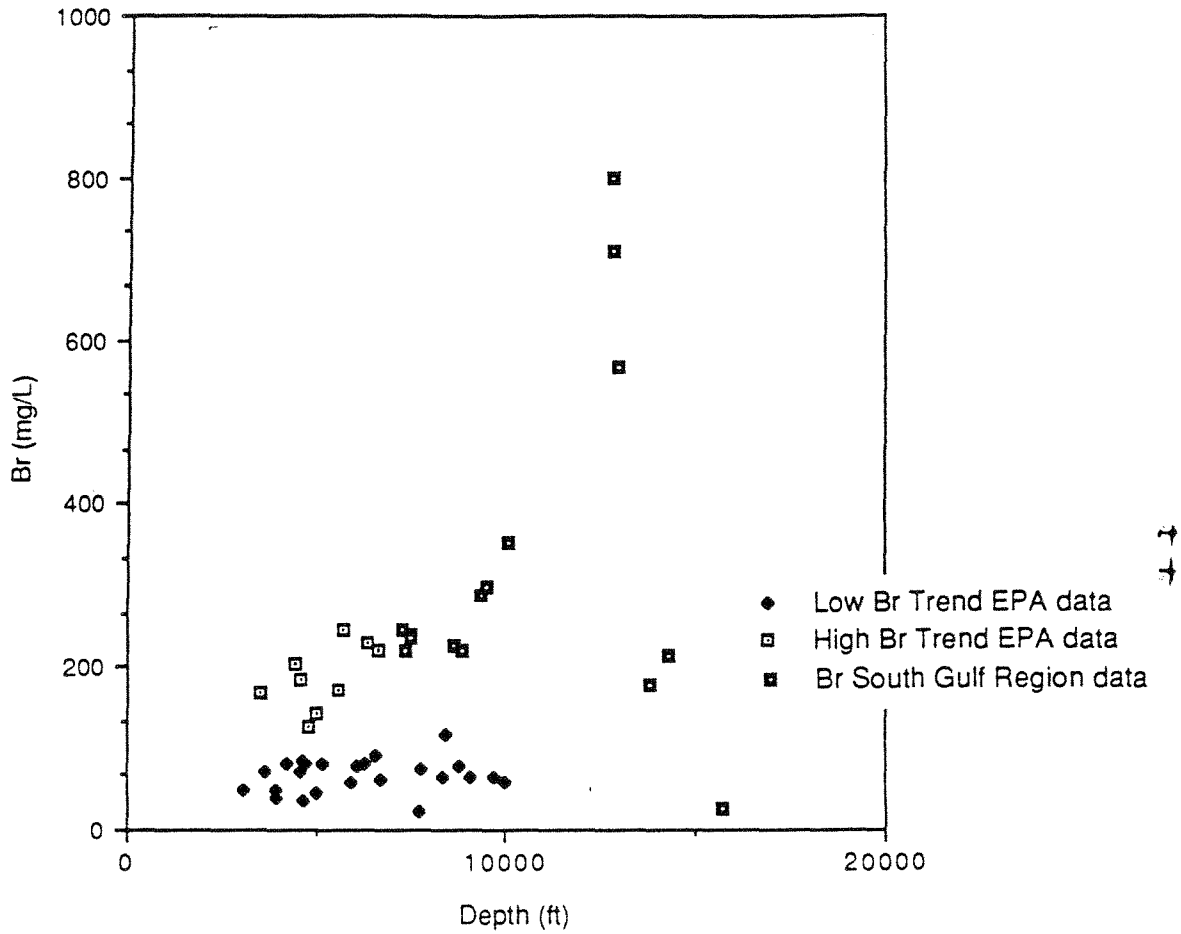

Figure 79. Plot of Br versus depth. Data from this study (Table 3) and Southgulf region (Table 2).

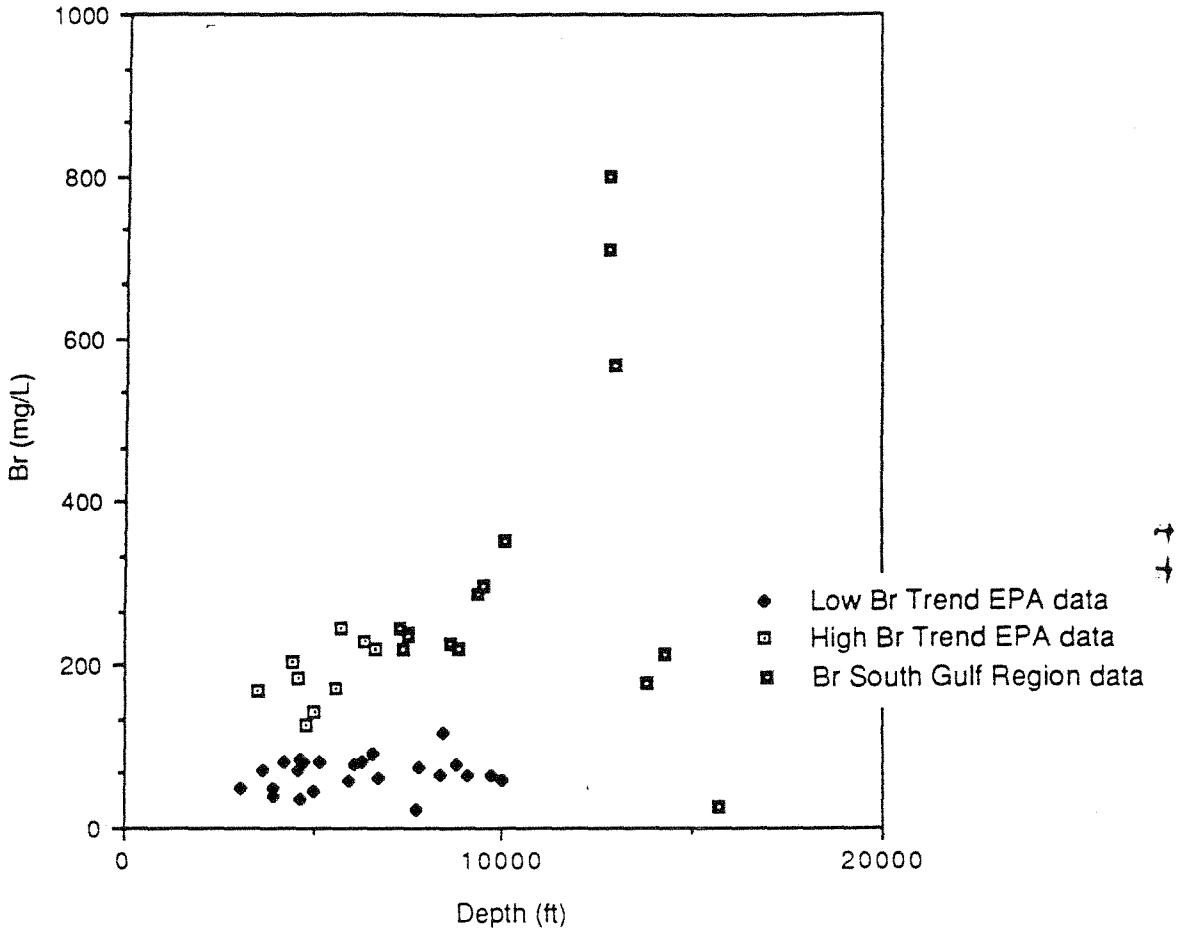

Figure 79. Plot of Br versus depth. Data from this study (Table 3) and Southgulf region (Table 2).

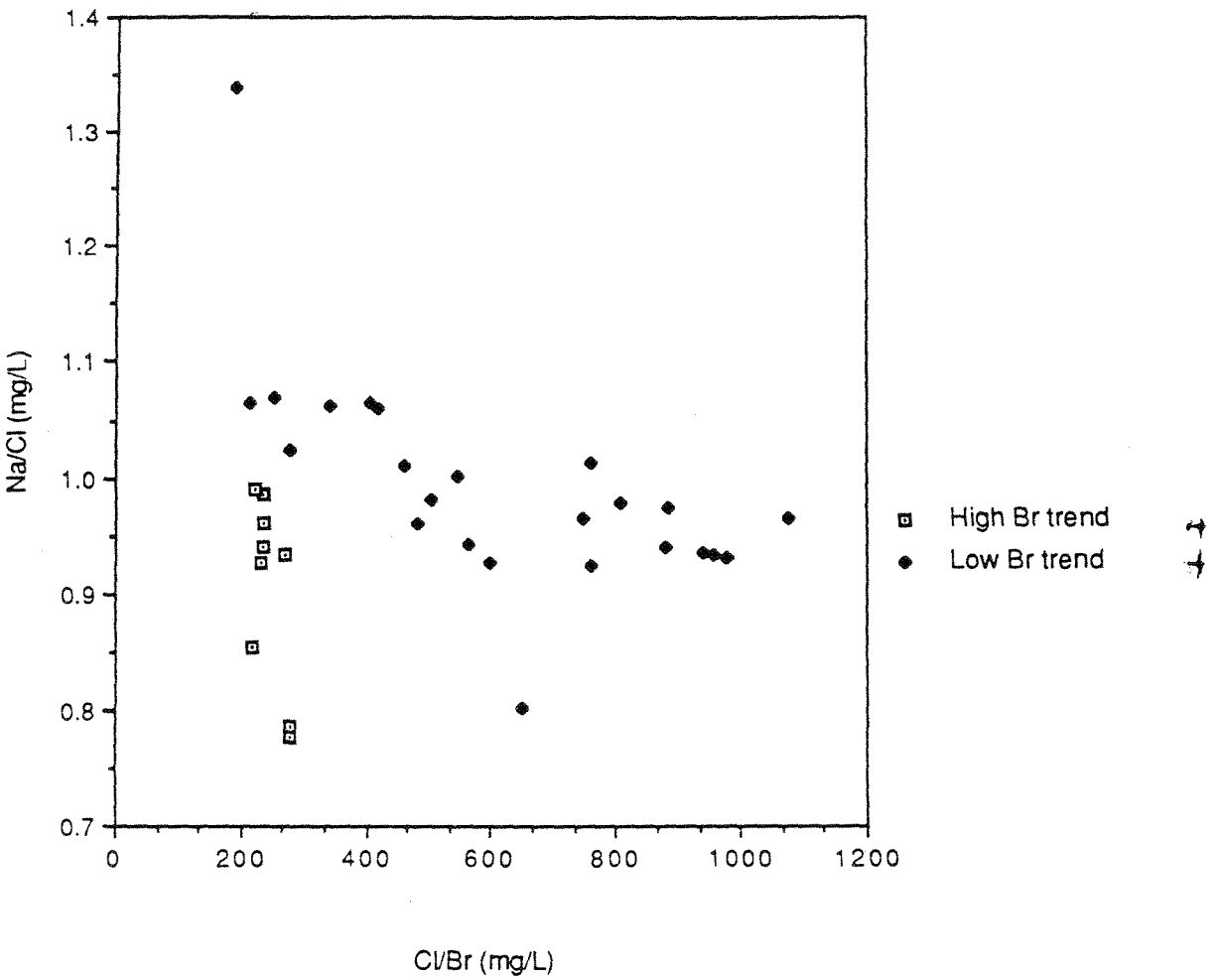

Figure 80. Plot of Na/Cl versus Cl/Br, Frio Fromation. Data from this study (Table 3).

9.5 Alkalinity

Total field-titrated alkalinity is a qualitative estimate of the organic acids in deep formation waters (Carothers and Kharaka, 1980; Fisher, 1987; Morton and Land, 1987). A plot of total alkalinity versus organic alkalinity (fig. 81) shows two trends for the Frio: (1) organic acid concentration that increases linearly with total alkalinity, and (2) total alkalinity for samples with some total alkalinity but little or no organic acids. Trend 1 shows a linear relationship with approximately 50% of the total alkalinity attributable to organic acids. The data from Lundegard (1985) also follow this 1:1 molar slope (fig. 82). Most of the organic alkalinity is acetate with minor amounts of propionate and butyrate (fig. 83). The 1:1 molar ratio between organic alkalinity and inorganic alkalinity suggests that the inorganic alkalinity is integrally related to the organic acids. Carothers and Kharaka (1980) suggested that decarboxylation of acetate produces bicarbonate and methane. Light $\delta^{13}C$ of the bicarbonate of oil-field brines further substantiated the decarboxylation reaction. This 1:1 ratio of organic acids to bicarbonate suggests that this reaction is in equilibrium.

Trend 2 data indicate trace to zero concentrations of organic acids for total alkalinity concentrations less than 800 mg/L. Carothers and Kharaka (1980) suggested that organic acid concentrations should be very low if not absent because of biodegradation of the acids in formations where temperatures were below 80°C. Data from this study suggest that the upper temperature for degradation is approximately 70°C (fig. 84), slightly lower than Carothers and Kharaka's estimate. As the organic acids degraded to CO_2, they increased the total inorganic alkalinity by a similar amount. The high inorganic alkalinity of 900 ppm suggests that the organic acids up to 450 ppm may have been originally present but have been degraded. The degradation of 450 ppm organic acids suggests a healthy appetite for the bacteria as well as a significant CO_2 source (up to ~8 mmoles) for other diagenetic reactions. The complete loss of organic acids also indicates that more degradation could have occurred if there had been greater concentrations of the available organic acids. This biodegradation reaction of organic acids has important implications to deep-well injection of chemical wastes. It suggests that organic waste could be degraded biologically by naturally occurring bacteria within the formations with temperatures below 70°C.

Redox Environment

Low sulfate concentrations and occurrence of organic acids and oil indicate a general reducing environment. Eh measurements were not made.

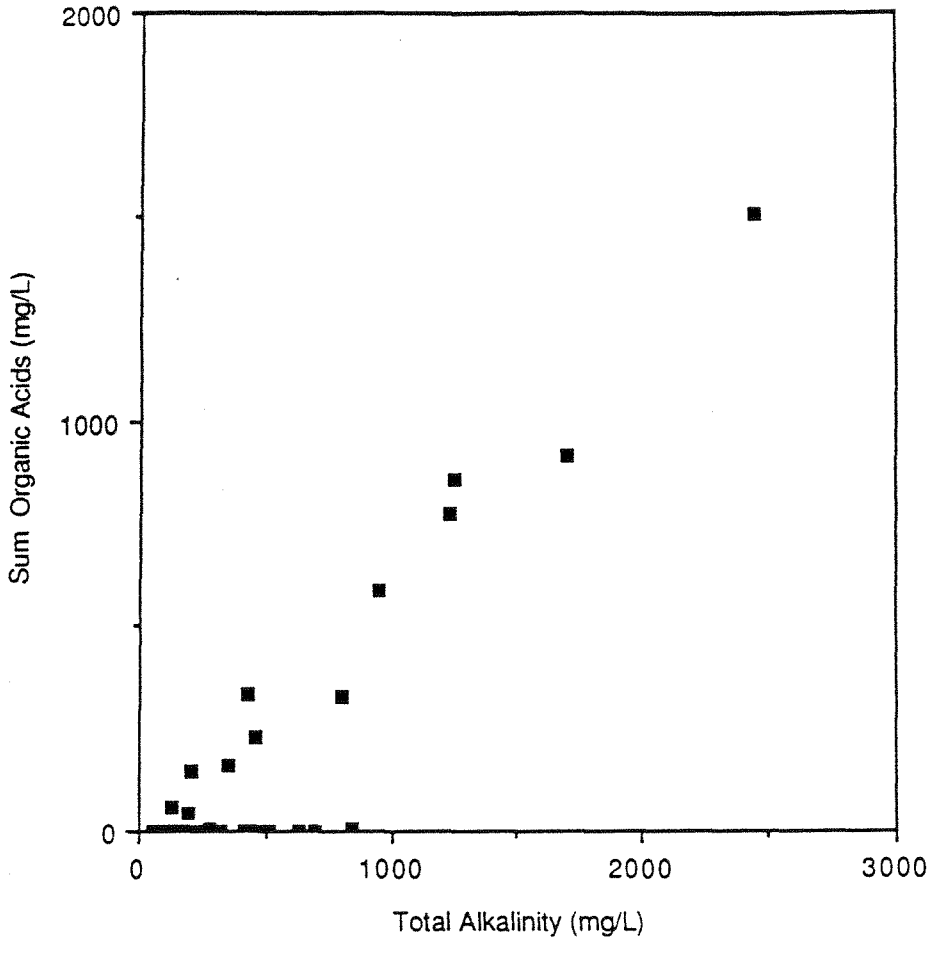

Figure 81. Plot of total field alkalinity versus sum of organic acids. Note the two different populations of data. Data from this study (Table 3).

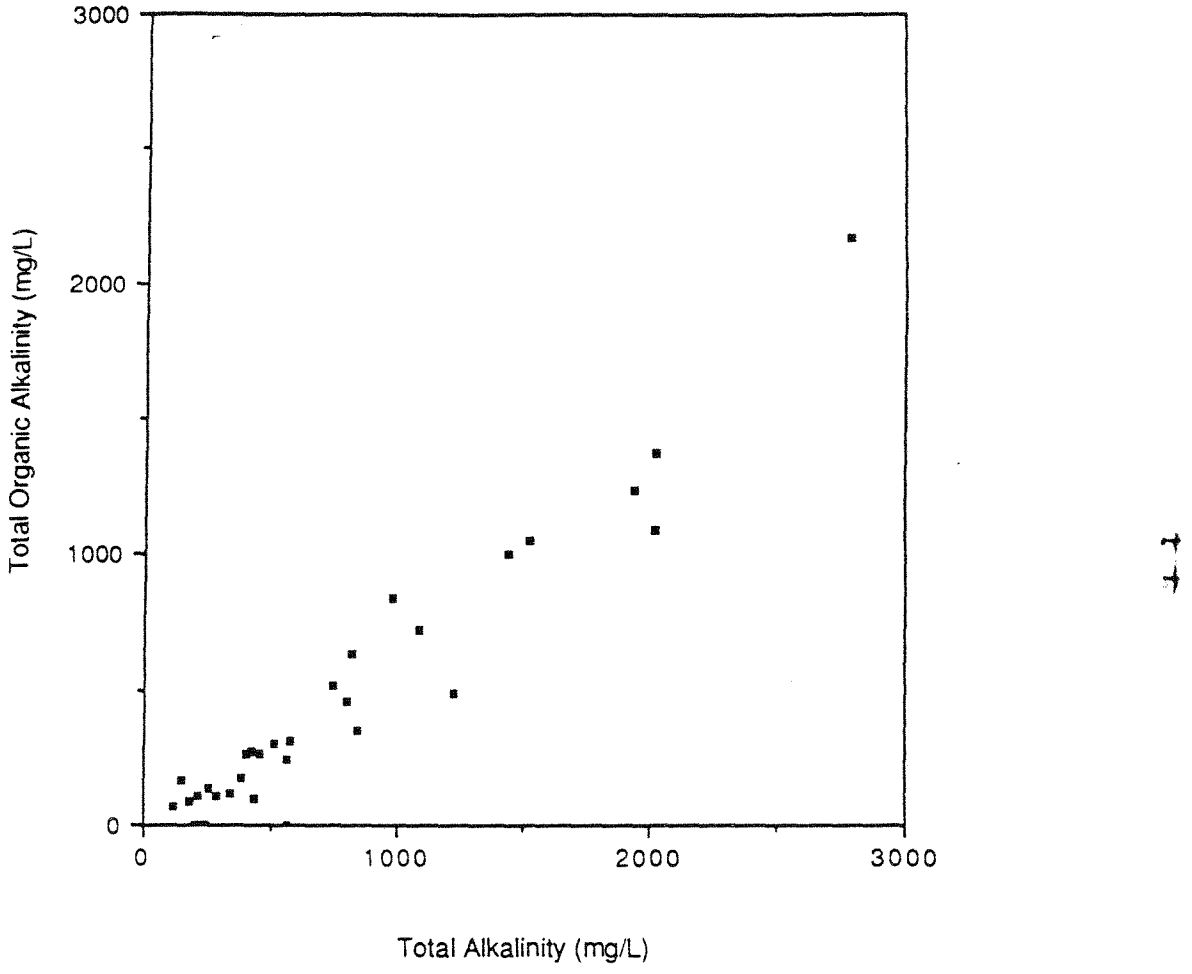

Figure 82. Plot of total field alkalinity versus sum of organic alkalinity from Lundegard (1985). Note how Lundegard's data follow the same trend as observed in Figure 17.

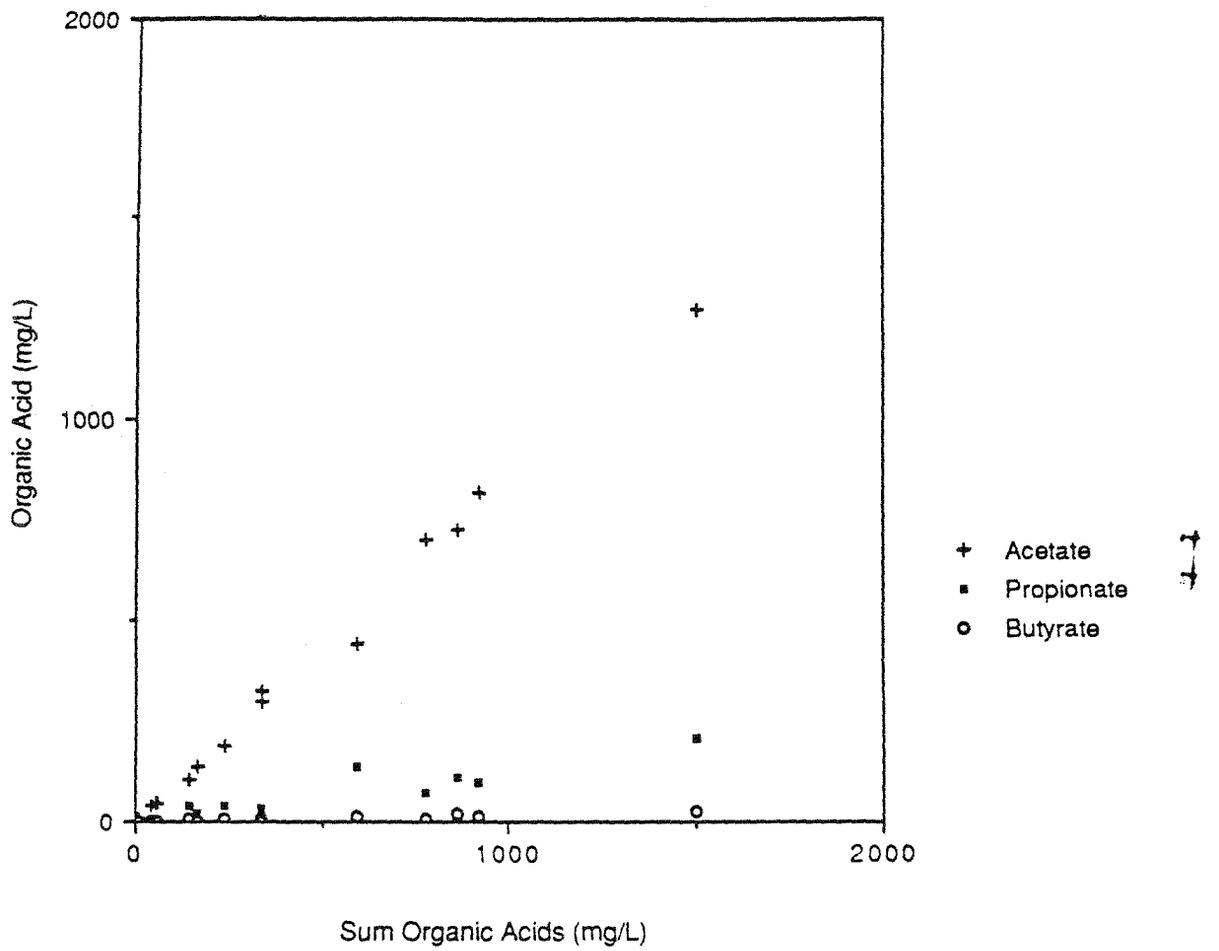

Figure 83. Plot of total alkalinity versus the individual organic acids, acetate, propionate and butyrate. The organic acids are composed predominantly of acetate.

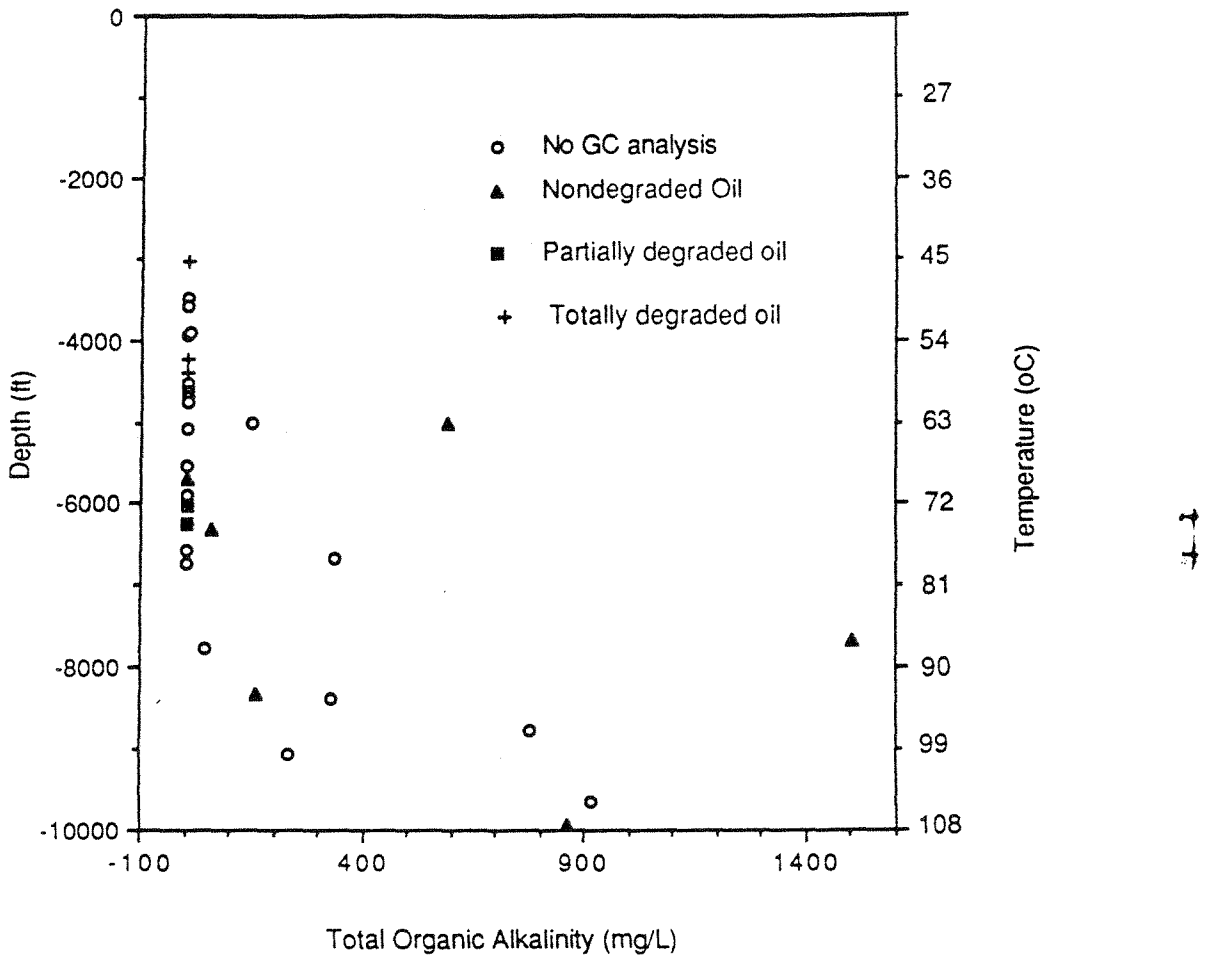

Figure 84. Total organic acids versus depth. All samples with degraded and partially degraded oils contain no organic acids.

9.6 Gas Chromatographic Analysis of Oil

The high concentrations of inorganic alkalinity and zero to trace organic acids could also represent deep penetration of meteoric waters and not the product of biodegradation. Kreitler and Wuerch (1981) observed HCO_3 concentrations as high as 1,000 mg/L in the fresh-water section of the Wilcox Formation in East Texas. A second approach to further test this hypothesis of biodegradation reaction is gas chromatograph analysis of whole oils associated with these waters. Eleven whole oils were analyzed by gas chromatograph to determine whether there was evidence of biodegradation. Nearly all organic compounds in crude oil are susceptible to biodegradation. The normal paraffins degrade before the isoprenoids or napthalenes. The paraffins between C5-C10 are the most susceptible (Bailey and others, 1973b). Milner and others (1977) suggest that C12 and C13 are the most susceptible. Another test for degradation is the ratio of NC17 to IP19. Degraded oils will show the loss of the NC17 peak in comparison to the IP19 peak (Zvi Sofer, personal communication, 1988). Samples 15, 16, 17, 26, 29, and 31 (figs. 85 through 90) do not appear to be degraded. They contain high concentrations of the normal paraffins (NC) and the isoprenoids (IP), which appear to dominate the composition of these oils. Samples 3, 11, and 12 exhibit significant biodegradation (figs. 91 through 93) with the loss of nearly all organic compounds. Samples 1 and 34 (figs. 94 and 95) appear to exhibit less degradation, not because of the loss of the heavy paraffins (greater than NC15) but because of the loss of the light paraffins (C5-C13). These interpretations of biodegradation are qualitative, because of the variables that control the basic distributions of the organics in crude oil. The composition of the unaltered oils is affected by source, maturation processes, and migration, all of which may alter the concentrations of the different organic compounds. Water washing may also alter the oil (LaFargue and Barker, 1988). Ground water flowing through an oil field may dissolve some of the more soluble compounds and chemically change the unaltered oil. Water washing may also occur concomitantly with biodegradation, because the flowing ground water may be carrying the bacteria for biodegradation. Precise identification of biodegradation is difficult because of these factors. Even though these interpretations should be considered preliminary, there has been a significant change in gas chromatograph pattern of samples 1, 3, 11, 12, and 34 (figs. 91 through 95) in comparison to the gas chromatograph traces for the unaltered oils, and therefore are considered to be biodegraded.

There is also a correlation between the biodegraded oil and the concentration of short-chained organic acids (fig. 84). None of the water samples with strongly or

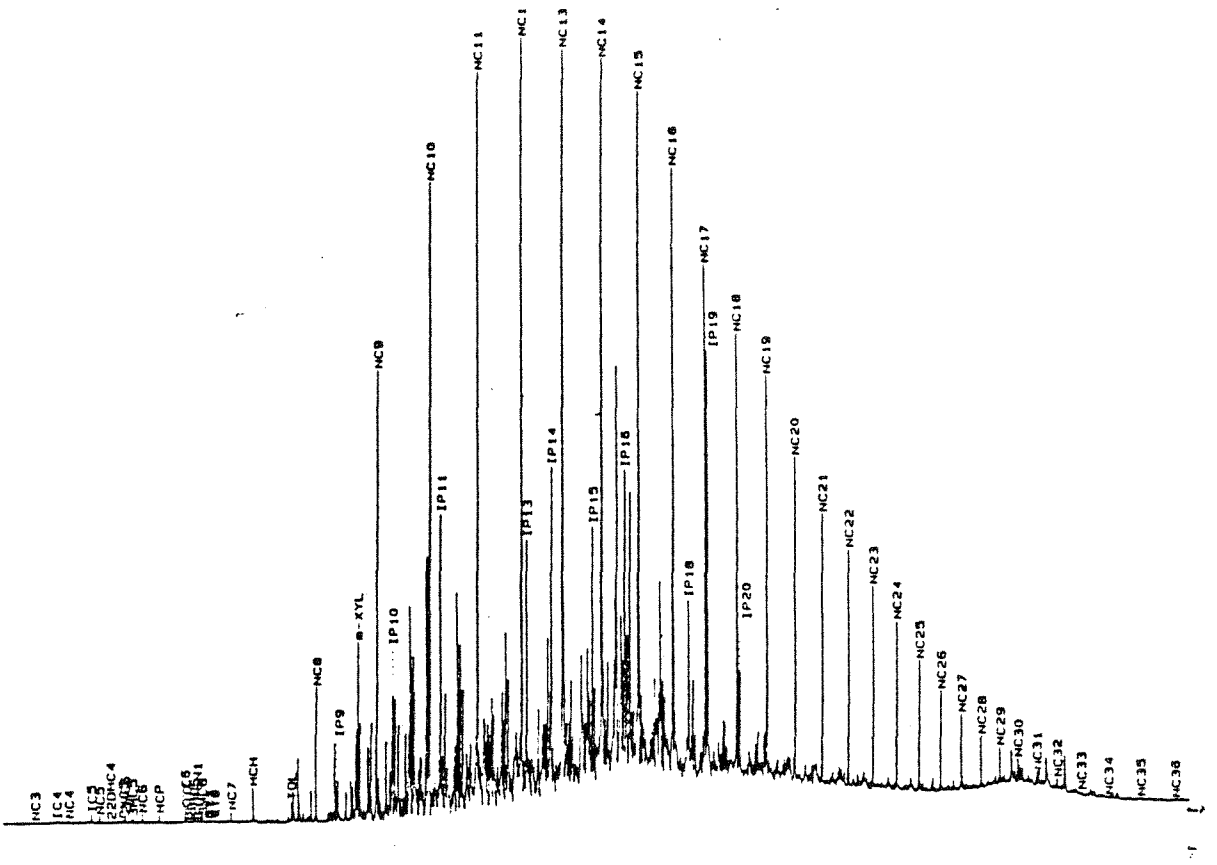

Figure 85. Gas chromatograph trace of whole oil sample TBEG-15. Sample does not appear to be degraded. Sample depth is 5,000 ft.

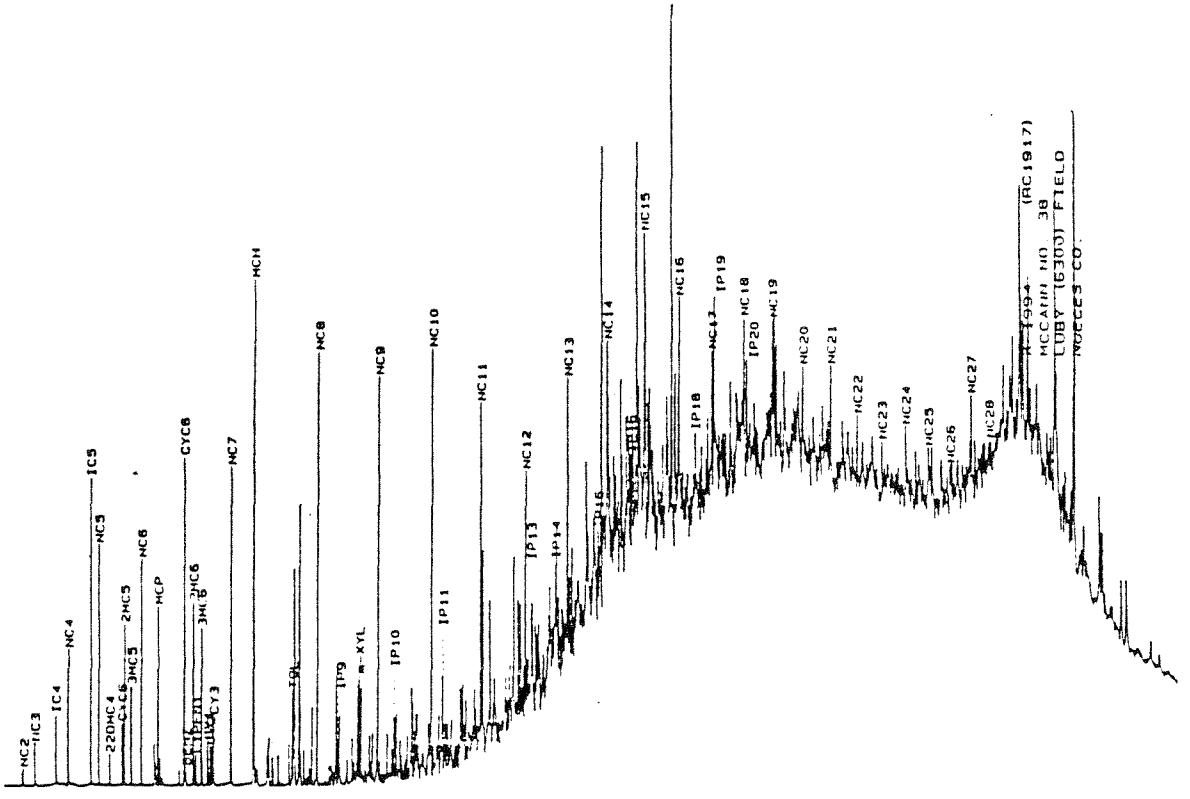

Figure 86. Gas chromatograph trace of whole oil sample TBEG-16. Sample does not appear to be degraded. Sample depth is 6,304 ft.

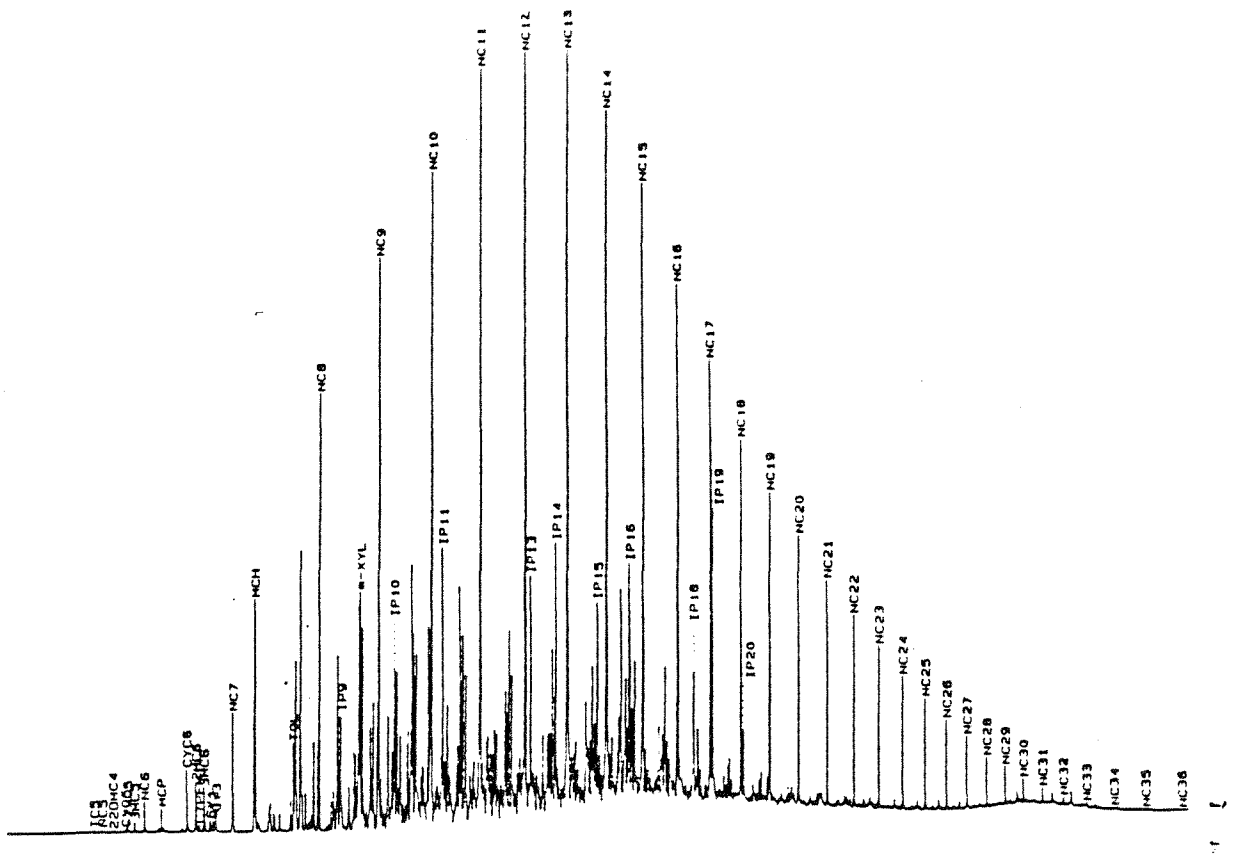

Figure 87. Gas chromatograph trace of whole oil sample TBEG-17. Sample does not appear to be degraded. Sample depth is 5,700 ft.

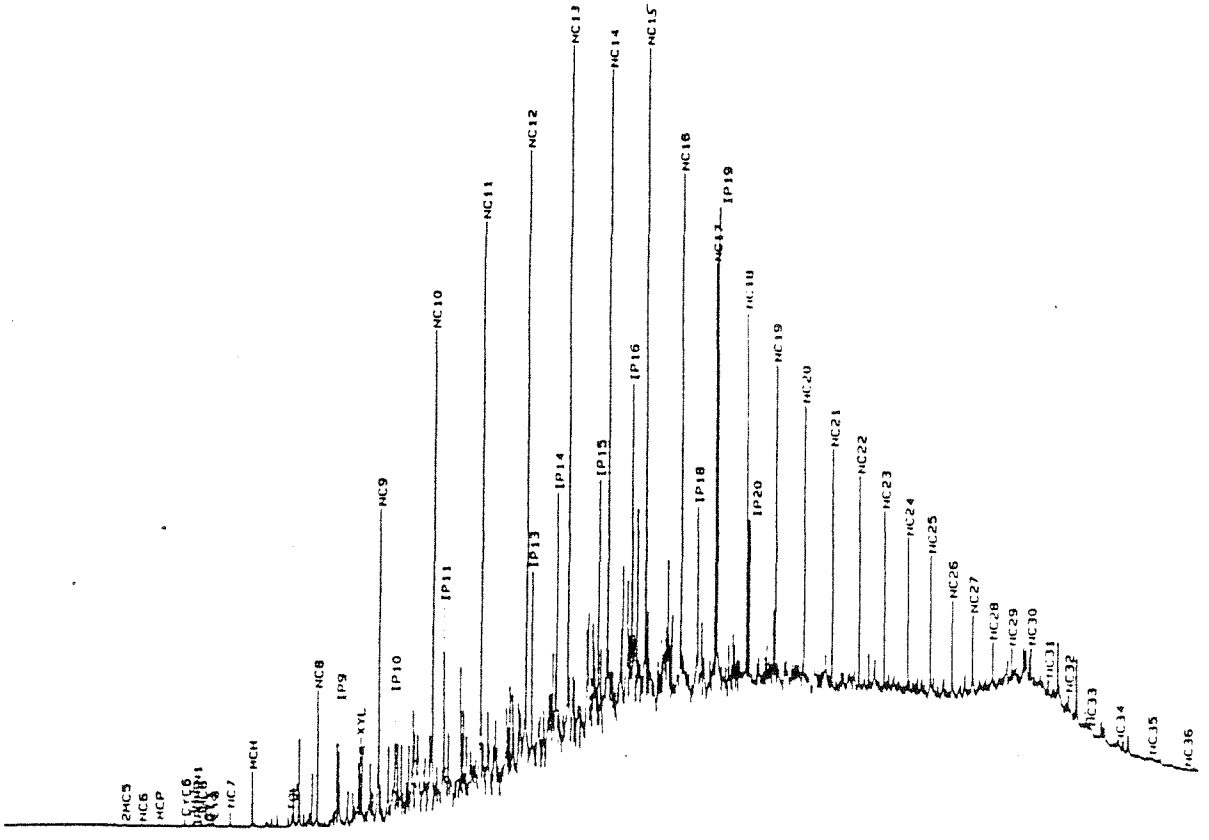

Figure 88. Gas chromatograph trace of whole oil sample TBEG-26. Sample does not appear to be degraded. Sample depth is 8,310 ft.

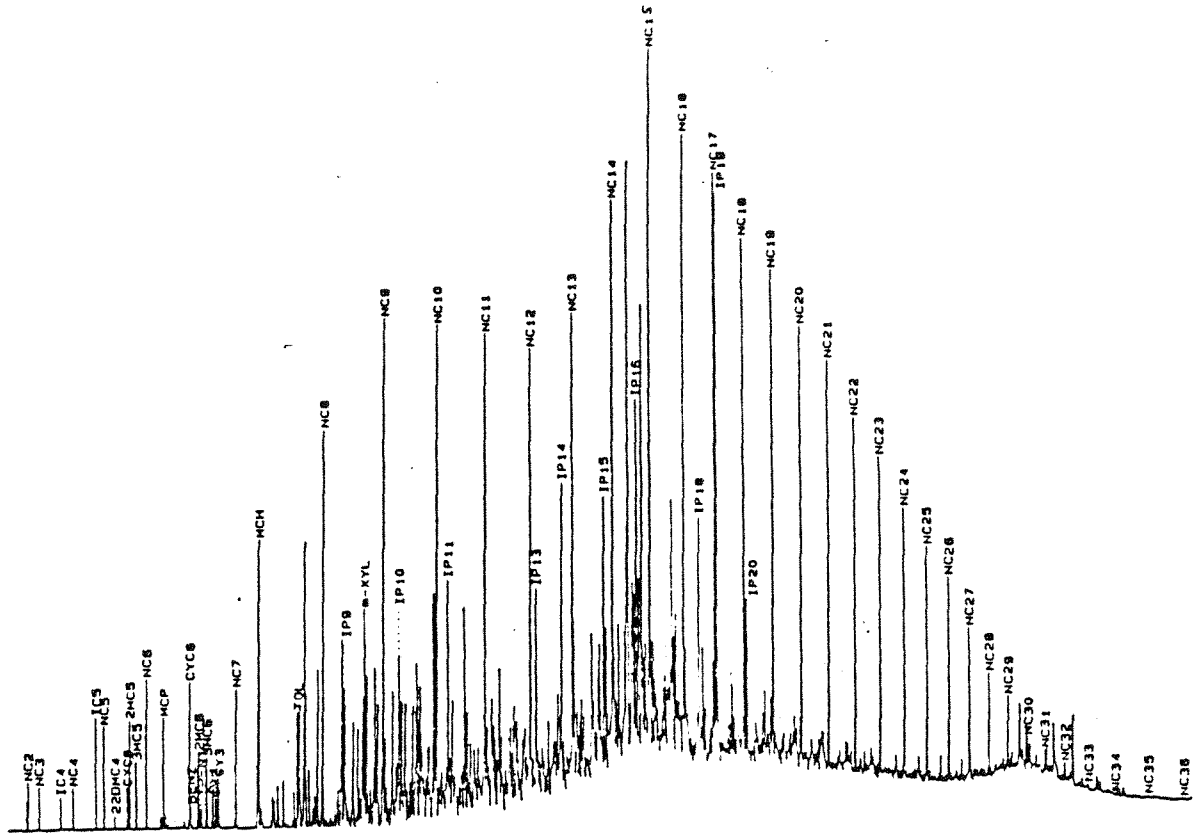

Figure 89. Gas chromatograph trace of whole oil sample TBEG-29. Sample does not appear to be degraded. Sample depth is 7,666 ft.

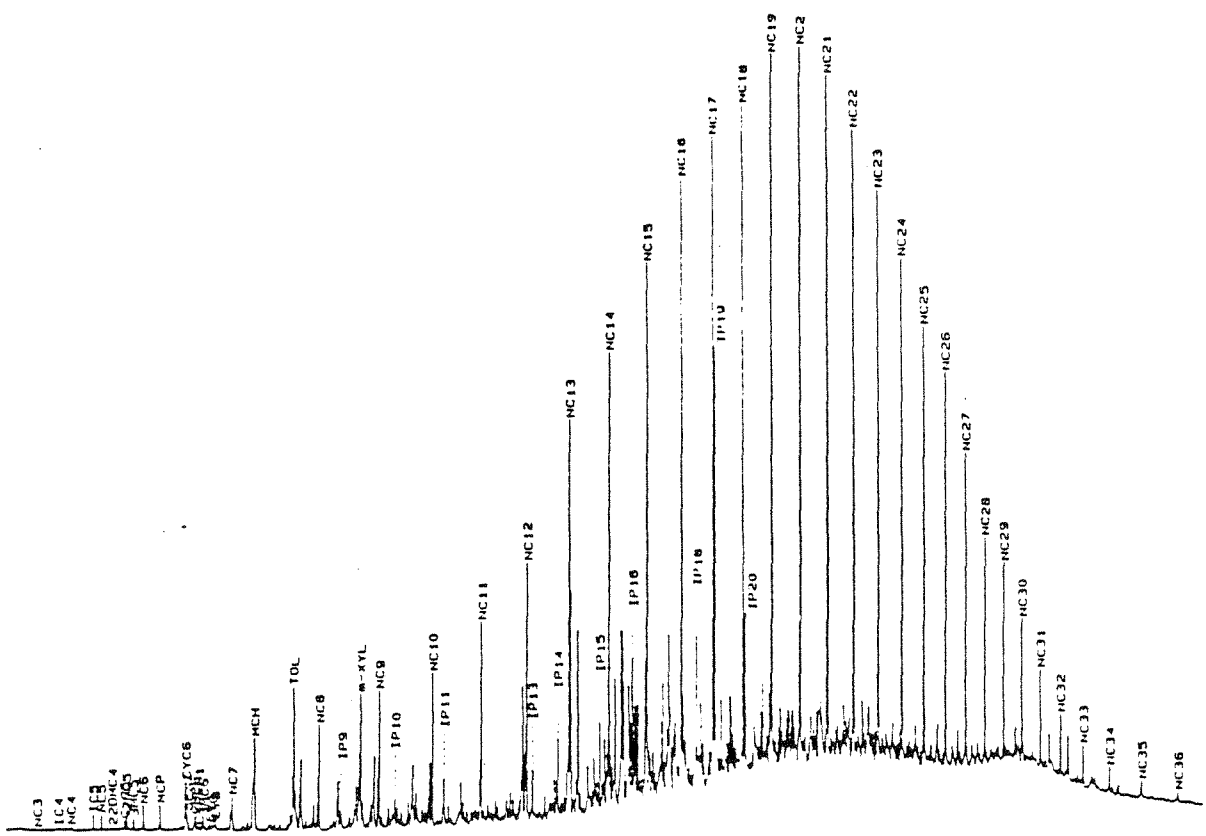

Figure 90. Gas chromatograph trace of whole oil sample TBEG-31. Sample does not appear to be degraded. Sample depth is 9,950 ft.

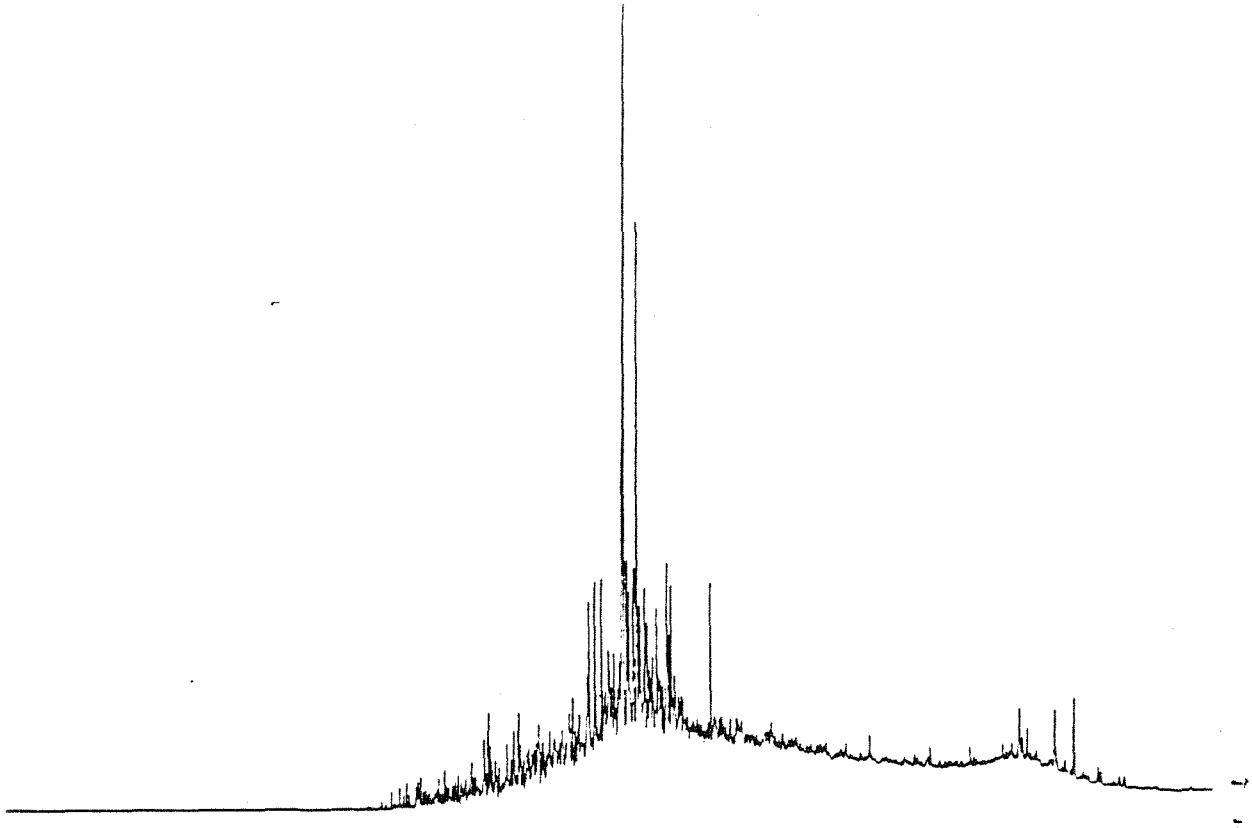

Figure 91. Gas chromatograph trace of whole oil sample TBEG-3. Sample appears to be significantly degraded. Sample depth is 4,222-4,226 ft.

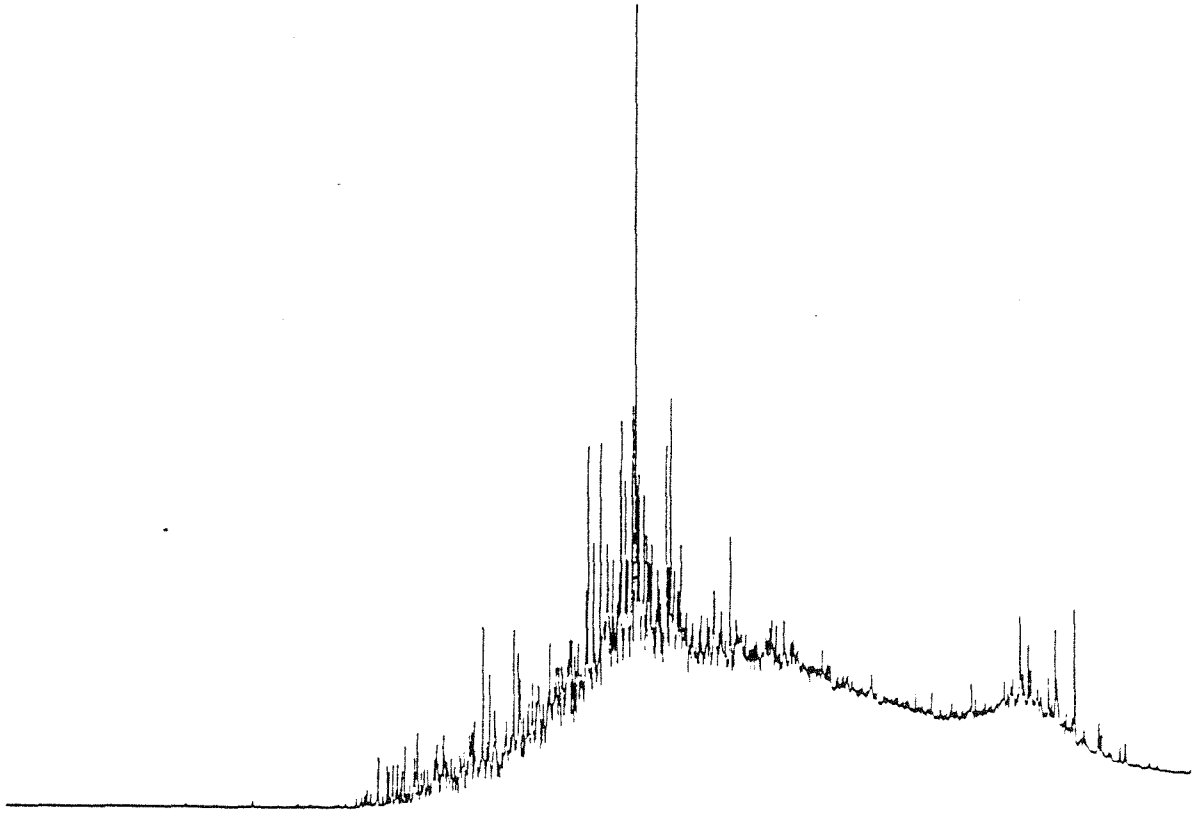

Figure 92. Gas chromatograph trace of whole oil sample TBEG-11. Sample appears to be significantly degraded. Sample depth is 4,388 ft.

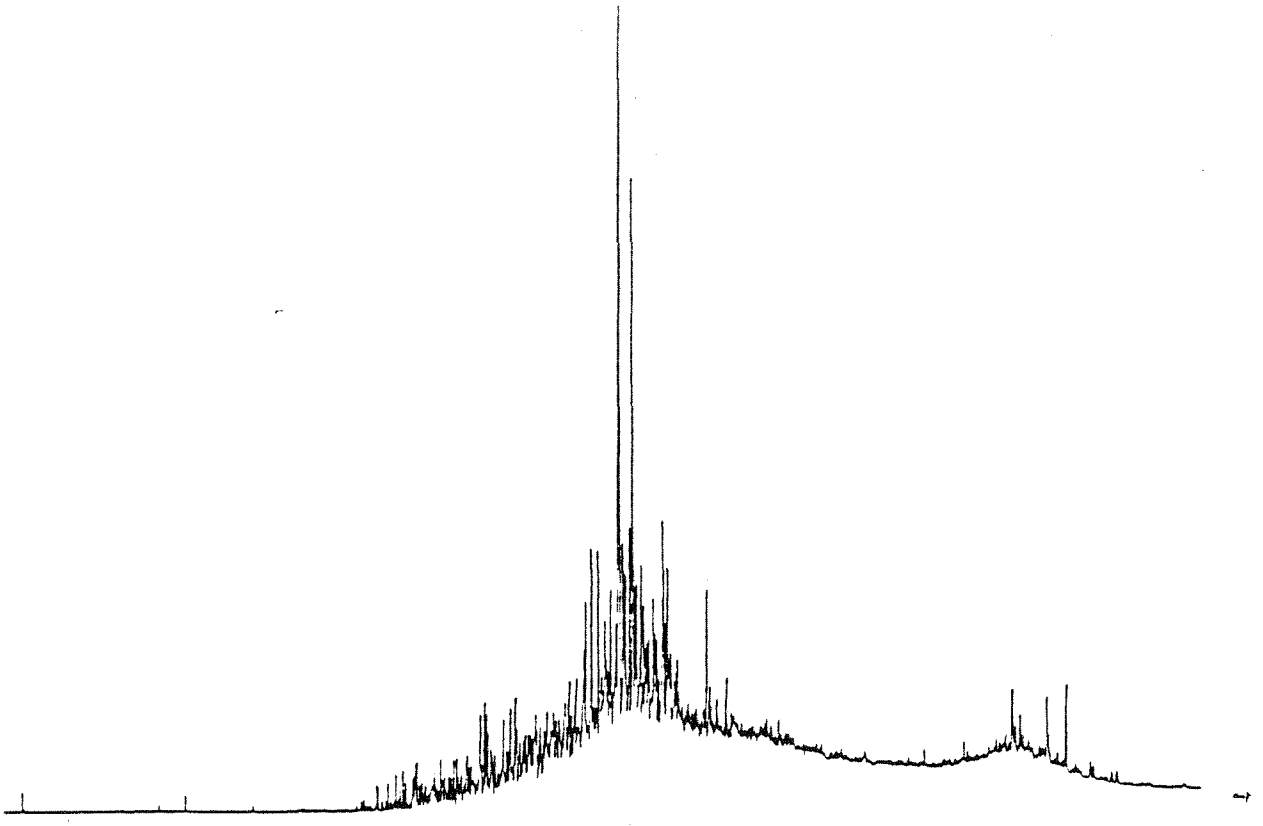

Figure 93. Gas chromatograph trace of whole oil sample TBEG-12. Sample appears to be significantly degraded. Sample depth is 3,040 ft.

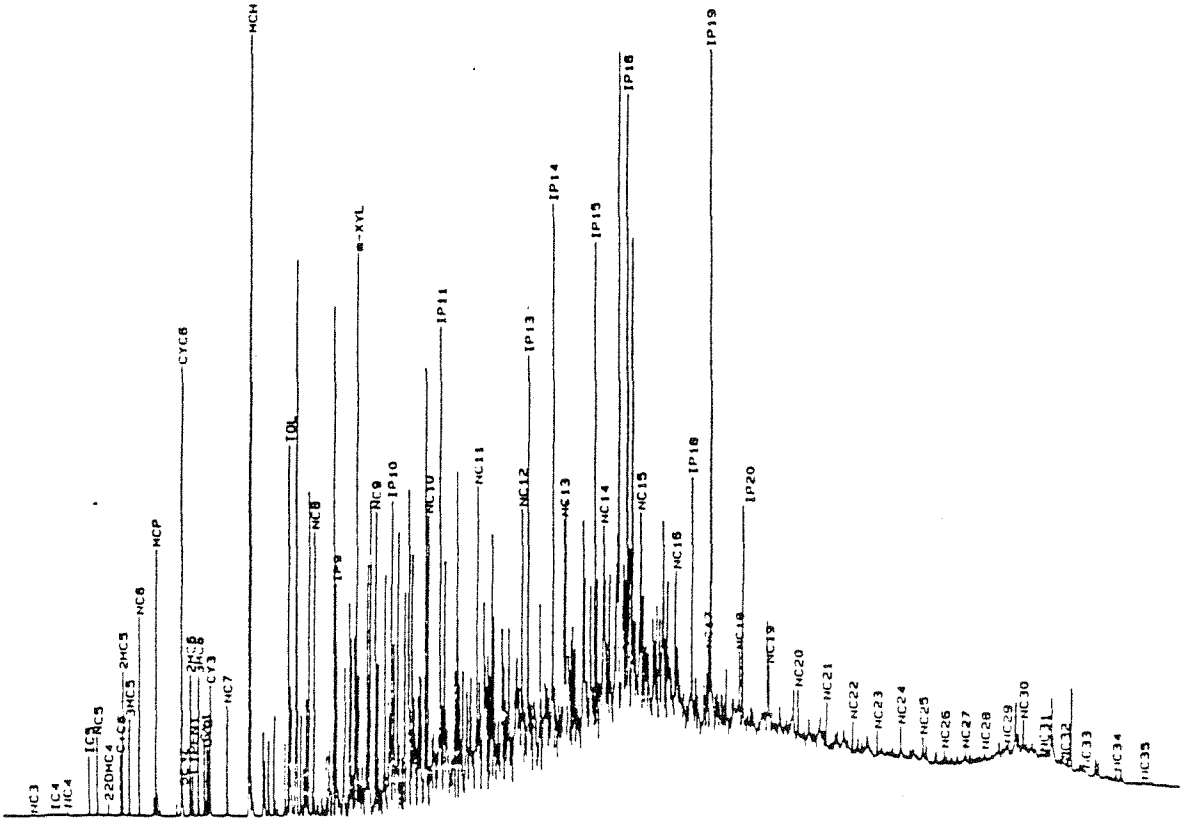

Figure 94. Gas chromatograph trace of whole oil sample TBEG-1. Sample appears to be degraded but less than samples TBEG-3, 11, or 12. Sample depth is 6,019-6,023 ft.

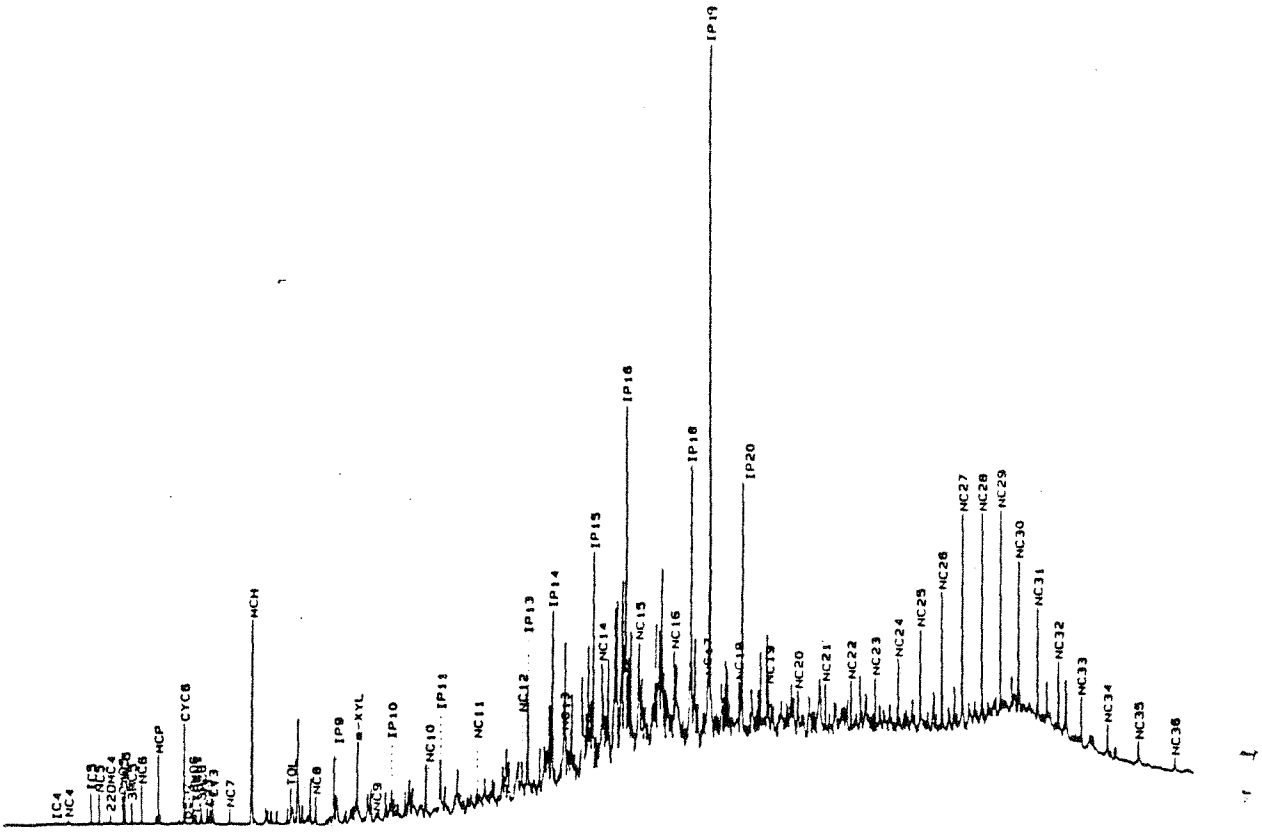

Figure 95. Gas chromatograph trace of whole oil sample TBEG-34. Sample appears to be degraded but less degraded than samples TBEG-3, 11, or 12. Sample depth is 6,244 ft.

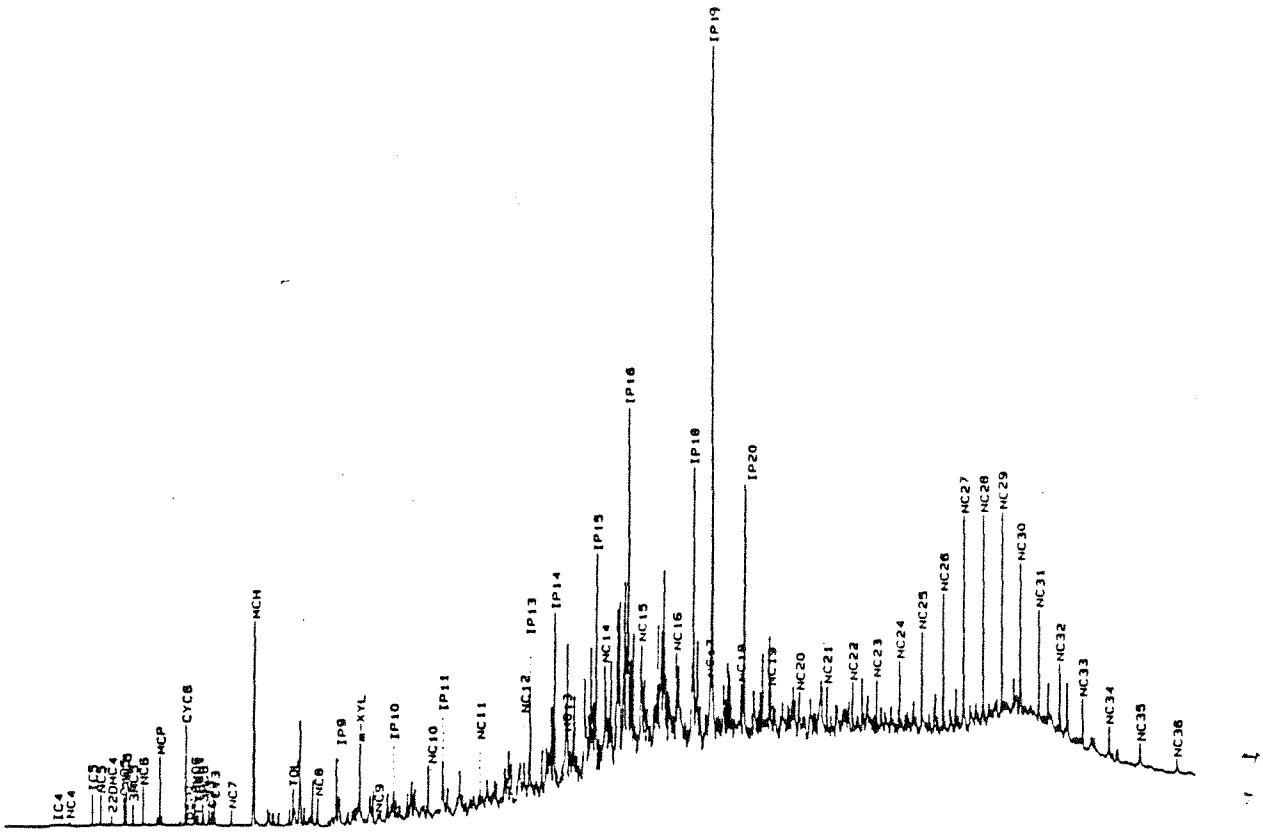

Figure 95. Gas chromatograph trace of whole oil sample TBEG-34. Sample appears to be degraded but less degraded than samples TBEG-3, 11, or 12. Sample depth is 6,244 ft.

partially degraded oils (1, 3, 11, 12, and 34) (figs. 91, 92, 93 and 94, respectively) had measurable organic acids. Conversely, five of the six nondegraded oils had appreciable organic acid concentrations. (Sample 17, a nondegraded oil, contained no organic acids.)

The API gravities of the totally degraded oils were 24 or less. Nondegraded oils ranged from 23 to 31, and the partially degraded oil ranged from 26 to 31. The API number of an oil does not appear to be a reliable indicator of biodegradation.

Presence of degraded oil and absence of short-chained organic acids appear to be good geochemical indicators of biologic activity at depths shallower than 7,000 ft and temperatures lower than 70-80°C. The good correlation between zero to trace concentrations of organic acids and degraded oil indicates that the organic acids had probably been there originally and had been subsequently degraded. An alternate hypothesis, that the organic acids were never present and that the field alkalinity represents high bicarbonate in meteoric water, is considered to be incorrect. Another important question is whether biodegradation is still occurring or whether it represents a geologically dead process. The occurrence of both degraded oil and zero organic acid concentrations suggests that the degradation process occurred after oil migration. This assumes that the occurrence of oil and organic acids followed two separate geochemical pathways. The coincidence of two degradation products indicates that the reactions occurred in situ. The potential for biodegradation may still be present. Oil degradation also indicates that these subsurface organisms are capable of consuming organic compounds far more complex than simple organic acids such as acetate. If the degradation of organic compounds is occurring biotically (rather than abiotically) then the degradation reactions may be occurring almost instantaneously in the context of geologic time. Bailey and others (1973) showed experimentally that biotically-driven degradation of hydrocarbons occurred within weeks. These hypotheses have significant implications to the possibility of biologic degradation of chemical wastes disposed of by deep-well injection.

9.7 Estimated In-Situ pH

The pH of deep basinal brines has always been considered unreliable because of CO_2 degassing as the sample depressurizes when it comes up the well bore or comes in contact with the atmosphere. The loss of CO_2 shifts the pH to more basic values. Neutral to basic pH values were measured for all samples indicating degassing (fig. 96). This degassing, however, does not cause a significant loss of inorganic alkalinity in the samples. The previous discussion on organic acids

demonstrated that 50% of the field titrated total alkalinity represents the in situ concentration of inorganic alkalinity. The consistency of the slope of total alkalinity versus sum of the organic acids (figs. 81 and 82) indicates that the samples are not losing significant quantities of inorganic alkalinity by CO_2 degassing either as the water flows from the well or where water is stored in separator tanks. An in situ pH in the range of 5-6 can also be estimated from the alkalinity titration data. A plot of pH versus inorganic alkalinity (fig. 96) shows a general trend of increasing pH with increasing concentrations of inorganic alkalinity. This degassing permits an estimate of in situ pH. This linear trend of higher pH for higher alkalinities results because the higher alkalinities have higher initial CO_2 pressures and therefore undergo greater degassing when these waters come in contact with the lower partial pressure of CO_2 in the atmosphere. The greater the degassing, the greater the shift toward more basic pH. Assuming that subsurface Frio conditions are acidic, then the inorganic CO_2 species will be in the carbonic acid form, and HCO_3 concentrations (total inorganic alkalinity) should be very low. The pH of zero bicarbonate value should approximate the in situ value (fig. 96). An in situ pH of 5-6 is estimated. (This approximation does not account for pH shifts and changes in carbonate equalization associated with the higher temperatures of in situ conditions at depth.)

9.8 Oxygen and Hydrogen Isotopes

Oxygen and hydrogen isotopes for 32 samples collected for this study plus 14 analyses provided by L. S. Land (personal communication, 1987) are shown in figures 97 through 99 and table 5. Most surface water, ground water, and precipitation worldwide have hydrogen and oxygen isotope compositions that plot approximately on a single line, referred to as the global meteoric water line (fig. 97) (Craig, 1961). Sedimentary basin waters typically trend away from that line toward heavier oxygen and hydrogen isotope values because of isotopic reactions between the water and sediments (Clayton and others, 1966). If deep-basinal brines have isotopic compositions similar to the isotopic composition of shallow, low-TDS ground waters, then there is a hydrologic connection between the shallow and the deep system, and the lack of isotopic enrichment suggests that this recharge process is relatively recent (in the context of geologic time). A plot of $\delta^{18}O$ versus $\delta^{2}H$ for Frio waters (fig. 97) shows a general trend of isotopic enrichment for $\delta^{18}O$ away from the meteoric water line. The trend appears to be controlled by isotopic fractionation of the water with the sediments. The amount of fractionation of the oxygen increases with increasing temperature. A plot of $\delta^{18}O$ versus depth (fig. 98) shows an enrichment of $\delta^{18}O$ with depth (and therefore temperature). An increase in $\delta^{18}O$ is expected for

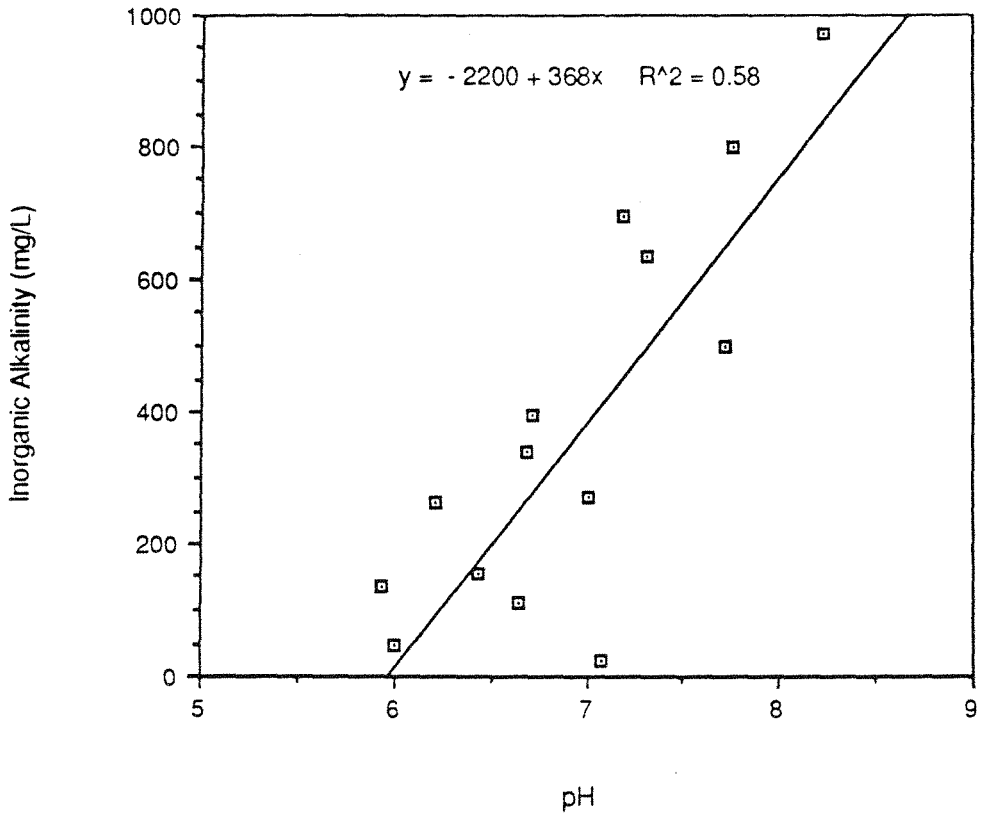

Figure 96. Inorganic alkalinity (total field alkalinity minus total titrated organic acids) versus pH. Note the rise in pH with higher alkalinities.

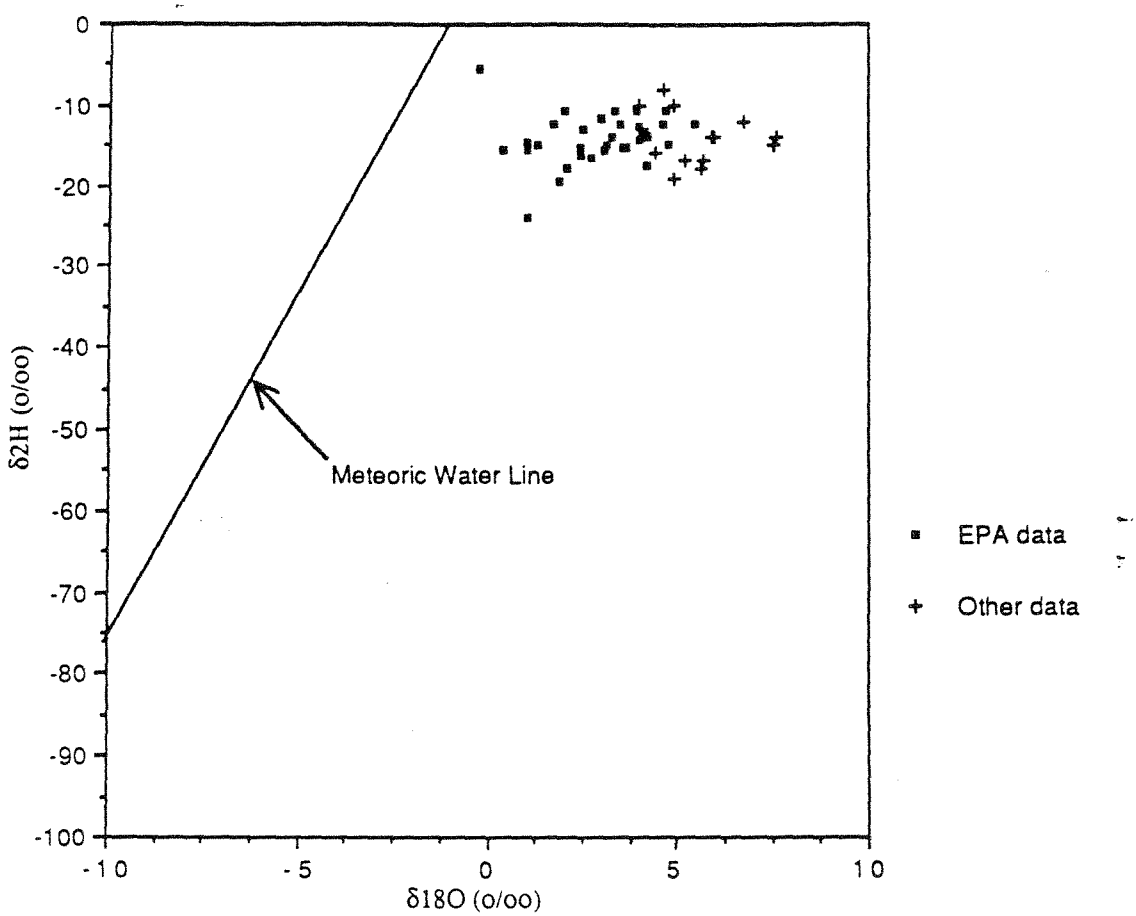

Figure 97. Hydrogen versus oxygen isotopic composition of waters from the Frio Formation. Data from this study (Table 5). Global meteoric water line from Craig (1961).

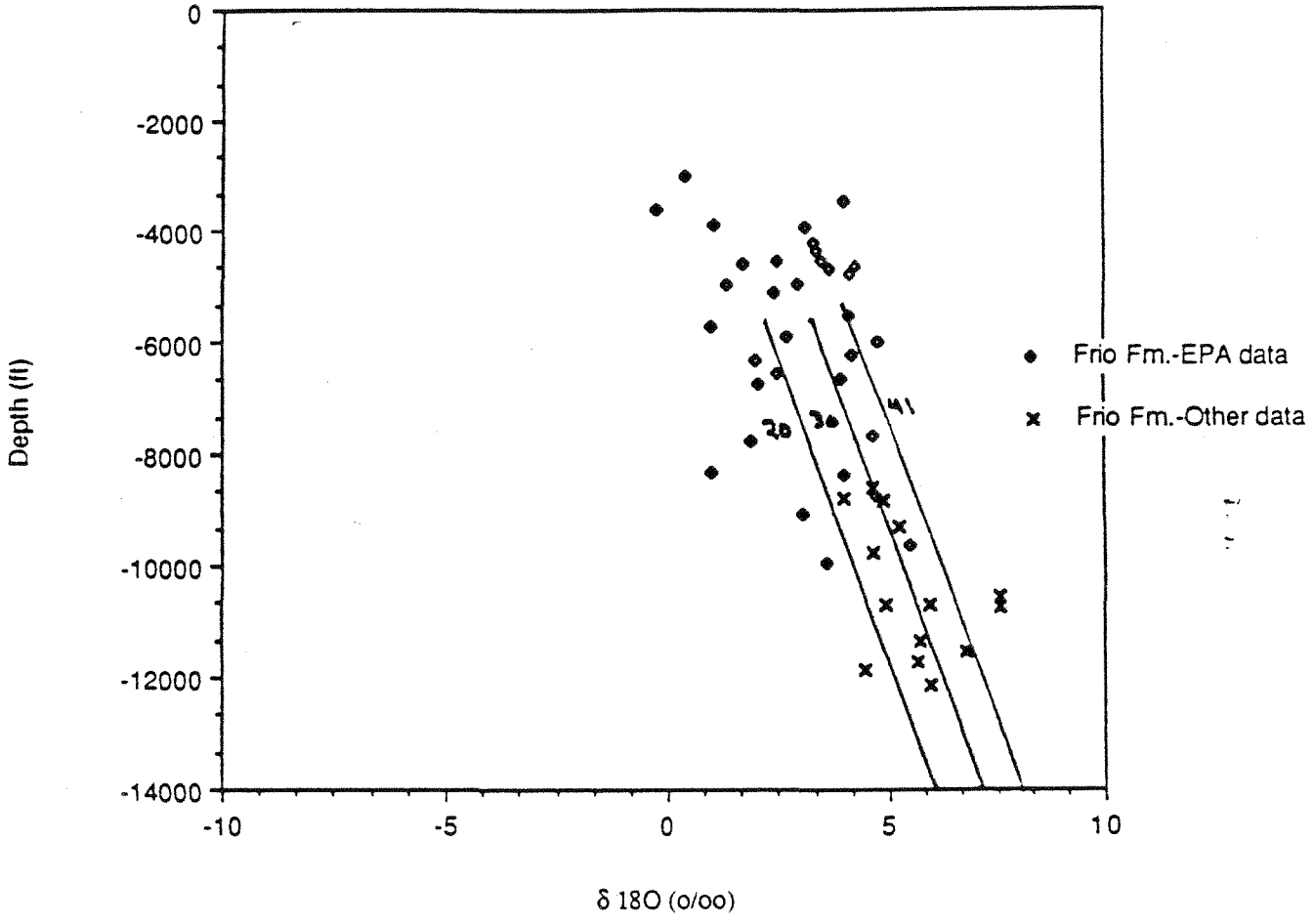

Figure 98. $\delta^{18}O$ versus depth. Data show a general enrichment of $\delta^{18}O$ with increasing depth (temperature). Data follows the isotope equilibration lines between water and illite (Epstein and Savin, 1973) for different geothermal gradients. Data from this study (Table 5).

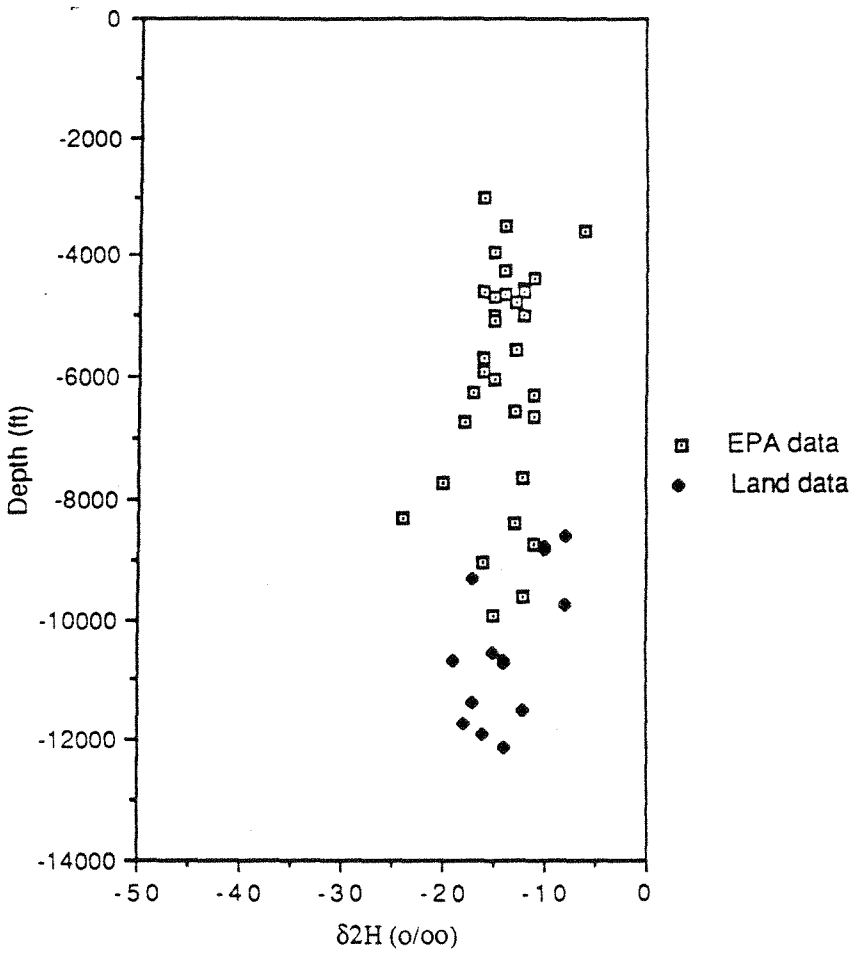

Figure 99. δ^2H versus depth for waters in the Frio Formation. Note consistency of isotopic composition with depth. Data from this study (Table 5).

Gulf Coast formation waters with increased temperature if the waters have equilibrated with the clays in the formation (Fisher, 1982). Whether these waters are in isotopic equilibrium can be estimated by plotting the isotope equilibration line between illite and water (Epstein and Savin, 1973) for different geothermal gradients (fig. 98). The equation used is:

$$10^3 \ln\alpha = 2.43 \times 10^{-6} T^{-2} - 4.82$$

If the water data plot close to these equilibrium curves, the waters are considered to have equilibrated with the clay in the formation. Most of the Frio data appear to be approaching these equilibrium lines.

The hydrogen isotope composition appears relatively constant versus depth, with δ^2H values ranging from -10 to -20°/oo. This consistency of isotopic values with depth strongly suggests isotopic equilibrium of the hydrogen in the water with hydrogen in clays. The clay with which the waters are equilibrating probably is montmorillonite, the dominant clay in the Gulf of Mexico basin. O'Neil and Kharaka (1976) in laboratory experiments identified rapid hydrogen isotope exchange between water and clays in temperatures as low as 100°C. They also argued that the process should occur in nature at lower temperatures. This exchange appears to be occurring in our Frio samples. Fisher (1982) constructed an equilibrium curve from Yeh (1980) for expected hydrogen isotopic compositions of waters equilibrated with illite. This curve predicts that the isotopic composition of the waters should progressively decrease with depth (fig. 99). This relationship is not observed for the Frio water data.

9.9 Age Determination

Determining the age of these Frio waters is important for understanding the hydrogeology of the saline Frio Formation as well as its implications for residence time of wastes injected into the Frio. There are, however, no appropriate radioisotopes for determining the absolute age of old saline waters such as in the Frio Formation. Absolute ages of ground waters can be estimated from radioactive isotopes such as ^3H (tritium), ^{14}C, ^{36}Cl, and ^{129}I, which have half-lives of 12.3 years, 5,730 years, 300,000 years, and 16 million years, respectively (Fritz and Fontes, 1980; Fabryka-Martin and others, 1985; Bentley and others, 1986). Of these, ^{14}C, ^{36}Cl, or ^{129}I are the most appropriate for dating old ground waters. All dating techniques relying on radioactive decay, however, have limitations, whether they be restricted by the short half-life of the radioisotope (for example, ^3H) or the complexities created by multiple sources or competing chemical reactions. For example, ^{36}Cl cannot be used for dating deep-basin brines. The radioactive isotope, ^{36}Cl, which results from cosmogenic fallout (Bentley and others, 1986), is overwhelmed by other chloride

Gulf Coast formation waters with increased temperature if the waters have equilibrated with the clays in the formation (Fisher, 1982). Whether these waters are in isotopic equilibrium can be estimated by plotting the isotope equilibration line between illite and water (Epstein and Savin, 1973) for different geothermal gradients (fig. 98). The equation used is:

$$10^3 \ln\alpha = 2.43 \times 10^{-6} T^{-2} - 4.82$$

If the water data plot close to these equilibrium curves, the waters are considered to have equilibrated with the clay in the formation. Most of the Frio data appear to be approaching these equilibrium lines.

The hydrogen isotope composition appears relatively constant versus depth, with δ^2H values ranging from -10 to -20°/oo. This consistency of isotopic values with depth strongly suggests isotopic equilibrium of the hydrogen in the water with hydrogen in clays. The clay with which the waters are equilibrating probably is montmorillonite, the dominant clay in the Gulf of Mexico basin. O'Neil and Kharaka (1976) in laboratory experiments identified rapid hydrogen isotope exchange between water and clays in temperatures as low as 100°C. They also argued that the process should occur in nature at lower temperatures. This exchange appears to be occurring in our Frio samples. Fisher (1982) constructed an equilibrium curve from Yeh (1980) for expected hydrogen isotopic compositions of waters equilibrated with illite. This curve predicts that the isotopic composition of the waters should progressively decrease with depth (fig. 99). This relationship is not observed for the Frio water data.

9.9 Age Determination

Determining the age of these Frio waters is important for understanding the hydrogeology of the saline Frio Formation as well as its implications for residence time of wastes injected into the Frio. There are, however, no appropriate radioisotopes for determining the absolute age of old saline waters such as in the Frio Formation. Absolute ages of ground waters can be estimated from radioactive isotopes such as ^3H (tritium), ^{14}C, ^{36}Cl, and ^{129}I, which have half-lives of 12.3 years, 5,730 years, 300,000 years, and 16 million years, respectively (Fritz and Fontes, 1980; Fabryka-Martin and others, 1985; Bentley and others, 1986). Of these, ^{14}C, ^{36}Cl, or ^{129}I are the most appropriate for dating old ground waters. All dating techniques relying on radioactive decay, however, have limitations, whether they be restricted by the short half-life of the radioisotope (for example, ^3H) or the complexities created by multiple sources or competing chemical reactions. For example, ^{36}Cl cannot be used for dating deep-basin brines. The radioactive isotope, ^{36}Cl, which results from cosmogenic fallout (Bentley and others, 1986), is overwhelmed by other chloride

sources (for example, salt dome dissolution, connate brines, etc.), which, because of their old age, no longer contain original cosmogenic ^{36}Cl. In addition, there is subsurface generation of ^{36}Cl by neutron flux from the decay of radioactive minerals (Feige and others, 1968; Kuhn, 1984). Next, ^{129}I, another long-lived radioisotope with a half-life of 16 million years may be appropriate for dating old waters but has problems similar to those of ^{36}Cl; iodide is leached from the basinal formations and ^{129}I is produced in the subsurface by neutron flux (Fabryka-Martin and others, 1985). Even though these radiometric dating techniques have serious problems, they may provide general ages or, more importantly, approximate minimum ages. The presence of high ^{36}Cl or ^{14}C activities indicates a relatively young water, whereas the absence of these species may indicate an older water.

Carbon-14 (^{14}C), the best method for dating waters less than 20,000 to 40,000 years old, was considered for the Frio, but was not analyzed for two reasons. Based on the following reasoning, Frio waters are considered to be older than can be dated with ^{14}C. Previous work by Pearson and White (1967) showed that the deep, downdip, fresh waters in the Gulf Coast Carrizo-Wilcox aquifer had reached the lower limit of ^{14}C activity. Fisher (1982) sampled waters farther downdip in the Wilcox than those sampled by Pearson and White (1967) (fig. 100) and found depleted $\delta^{18}O$ values that are significantly lighter than the isotope equilibration curves for clay-mineral reactions. These light values indicate a meteoric component of geologically recent recharge. In contrast, the Frio waters are significantly heavier and appear to be equilibrated. Because the Frio waters have equilibrated and the Wilcox waters have not, they are assumed to be older than the Wilcox waters which, in turn, were collected downdip from the Carrizo-Wilcox water sampled by Pearson and White (1967). On the basis of this line of reasoning, the Frio waters are considered to be older than 20,000 to 40,000 years, that is, older than can be easily dated by ^{14}C. In general, ^{14}C analyses are routinely done by liquid scintillation or proportional counting techniques, which limits the maximum age of the water sample to approximately 40,000 years.

Accelerator mass spectrometry has extended the possible maximum age such that older waters can be analyzed. Application of more sensitive methods of analysis is precluded, however, by the second problem, the source of the dissolved carbon in deep saline formations. Dating of ground waters depends upon our adding a naturally occurring radioisotope in the recharge zone, knowing the decay rate, and measuring the radioisotope activity at the point of sampling. With this information, we can estimate how long the radioisotope has been within the aquifer. In saline aquifers, ^{14}C has problems similar to those of ^{36}Cl and ^{129}I in that there are subsurface sources for

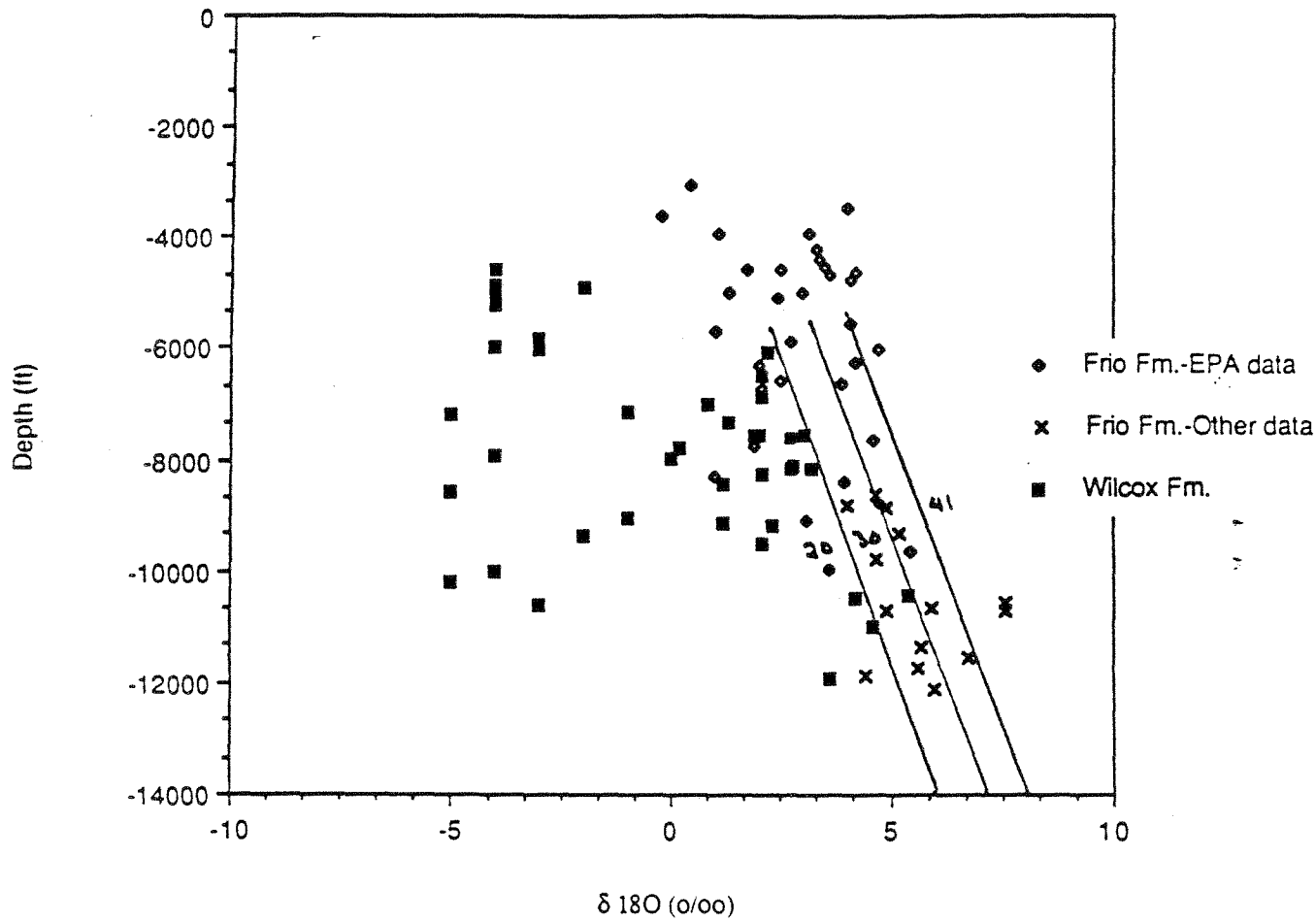

Figure 100. Comparison of ^{18}O composition of Wilcox waters (Fisher, 1982) to Frio waters collected for this study (Table 5). Wilcox waters are much lighter and do not appear to be in isotopic equilibrium with sediments.

carbon as there are for chlorine and iodine. As discussed previously, the source of dissolved carbon (as either an organic acid or bicarbonate/CO_2) in saline Gulf Coast formation waters probably is from the maturation of organic material. The dissolved carbon therefore is derived from Oligocene-aged Frio sediments and not from the recharge at the outcrop. Saline formation waters are not expected to be datable with ^{14}C because of their pre-^{14}C age and in situ source of carbon.

10. WATER CHEMISTRY - DISCUSSION

10.1 Hydrochemical Environment

The hydrochemistry of Frio formation water within a depth range of 4,000-7,000 ft, the range used for deep-well injection, typically is slightly acidic (pH 5-6), very saline to briny (Cl generally ranges from 20,000 to greater than 60,000 ppm), reducing (presence of NH_4), warm (less than 80°C), and potentially biologically active (zero to trace organic acid concentrations and degraded oil). Each of the above geochemical conditions may have an impact on the long-term fate of injected chemical wastes.

The varying salinity of natural brines may affect the flow of wastes away from an injection well. Salinity determines whether injected wastes would float on top because of lower density, sink to the bottom because of higher density, or flow from the well as a plug flow because of similar densities (Miller and others, 1985). The potential for wastes floating on top because of a density contrast probably is much greater in other sedimentary basins used for injection where brines have typical chlorinities of greater than 100,000 ppm (such as the Illinois basin). Figure 68a and b and the appendix provide salinity information on a county scale, which enabled us to estimate density of formation waters.

The estimated pH range of 5-6 is controlled by rock-water chemical reactions. The pH of the chemical wastes, regardless of whether they are acidic or basic, should ultimately reach this slightly acidic range. Scrivner and others (1985) suggested that hydrolysis reactions are important for waste degradation (for example, decomposition of cyanide). The speed of reaction (the kinetics) for hydrolysis, however, strongly favors either high or low pH, and not the neutral values of the natural conditions. Hydrolysis reactions of wastes need to be completed before acid or basic liquids are neutralized by the sedimentary formation.

Increased temperatures may increase reaction rates, but to significantly benefit, higher temperatures (probably above 100°C) are needed (O'Neil and Kharaka, 1976;

Lundegard, 1985; Boles and others, 1988). The lower temperatures in the shallow hydrostatic section may be optimal because of the possibility of biologically mediated waste degradation reactions. In the Texas Gulf Coast the predominant injected waste types are organics. If these wastes will degrade biotically, reaction rates may be significantly faster than for abiotic reactions such as hydrolysis. Under natural conditions, acetate and complex organic admixtures, such as crude oil, appear to be biologically consumed as deep as 7,000 ft and at temperatures as high as 70°C.

The presence of bacteria or other microorganisms was not investigated during this study. Bacteria have been identified as deep as 1,300 ft at Savannah River, Georgia (Wobber, 1986). If bacteria are present, they could be anaerobic (reducing environment) and may utilize methane. Methane occurs pervasively through the subsurface of the Gulf Coast (Lundegard, 1985). Previous investigators of hydrocarbon biodegradation have assumed that shallower oxidizing conditions were necessary and that aerobic bacteria were the dominant bacterial type (Bailey and others, 1973a). Neither the type of bacterial population in the subsurface (up to 70°C) nor whether they now exist is known. The presence of degraded oil may only indicate previous reactions. If bacteria are present, they may or may not be capable of degrading organic wastes. Even if they are not, this geochemical environment may be suitable for anaerobic bacteria, which can degrade organic wastes. This possibility needs to be investigated.

10.2 Hydrochemical Interpretation of Hydrogeologic Environment

The chemical and isotopic compositions of the sampled brines indicate two types of water in the shallower hydrostatic section (in comparison to the deeper geopressured horizons sampled by Morton and Land [1987]): an Na-Cl, low-Br water type (A), and an Na-Cl, high-Br water type (B). The chemical composition of Type A is controlled by halite dissolution. These waters occur in the Houston Embayment region and have high Na-Cl concentration as deep as 10,000 ft. The Na-Cl, high-Br waters typically are in the San Marcos Arch (central region) and South Texas region. These waters exhibit an increase of Br with depth, suggesting leakage of high-Br, high-Sr, and high-Ca waters from deeper in the section. Chemically both water types A and B appear to have originated from the same water type because both appear to be in isotopic equilibrium with oxygen and hydrogen. Both water types contain degraded oils and zero to trace concentrations of organic acids.

Based on these hydrochemical characteristics, what can we say about the hydrogeology of the Frio saline aquifer? Three scenarios were suggested in the introduction to hydrochemistry:

1. A meteoric origin for Frio waters
2. Original depositional (connate) waters
3. Waters leaking up from the deeper geopressured sections.

1. Meteoric origin: Active recharge of continental waters is not occurring in the Frio. All waters sampled appear in isotopic equilibrium with the rock matrix (figs. 98 and 99). This is in contrast with the underlying Wilcox, which contains isotopically nonequilibrated waters (fig. 99). Total dissolved solutes are also much higher than in the Wilcox (Kreitler and Richter, 1986). The inverse correlation of salinity and total alkalinity observed by Kreitler and Richter (1986) does not appear to correlate with shallow depths but to the deep section at the top of geopressure in South Texas (Land and Morton, 1987). The original water (before salt dome dissolution or deeper brine leakage) in the Frio had a Na/Cl ratio slightly greater than 1.0, which could suggest a post-depositional circulating water or a connate water that had a continental rather than a marine origin. The occurrence of biodegraded oils and lack of organic acids to depths of 7,000 ft imply biodegradation. Previous authors investigating biodegradation, however, believe that circulating meteoric waters are needed for transport of bacteria to the oils. Bacteria here, however, are found as deep as 1,300 ft in fresh-water aquifers. The other chemical data argue against an active circulation system.

2. and 3. Original depositional water and leakage: The Frio waters may predominantly represent original depositional waters that have subsequently dissolved salt domes or been mixed with a high-Br Na-Cl brine: the presence of Br-rich brines in the shallow hydrostatic sections offers geochemical evidence of fluid leakage from the undercompacted, geopressured section. It is surprising that high-Br concentrations occur only in Central and South Texas and not in the Houston Embayment region. In this region salt dome dissolution is the dominant reaction, but the increase in NaCl still should not mask this leakage. If there is leakage, Br concentrations should still rise. The Br concentrations in the salt dome region, however, remain constant regardless of NaCl concentrations. Vertical migration appears to occur in Central and South Texas but not in the Houston Embayment. This appears contradictory because of the extensive growth faults and salt domes in the Houston Embayment, which should provide excellent pathways for fluid migration. Lead-zinc mineralization along salt dome flanks in this region has been used for evidence of upward fluid migration. This paradox needs further explanation.

The evidence of salt dome dissolution and leakage in the hydrostatic section of the Frio indicates that hydrologic conditions are not stagnant. For salt dome dissolution to occur, advection or diffusion must be occurring. Fluid leakage from depth also implies fluid movement. This fluid movement may be geologic in time-scale and not critical for short timespans such as the time period needed for isolation of chemical wastes.

11. SUMMARY AND CONCLUSIONS

1. A very large pressure data base is available from which potentiometric maps and pressure depth plots can be constructed. More than 17,000 pressure measurements are available for the Frio Formation in Texas. Potentiometric maps can be made on a regional to site-specific scale. The regional scale is too large for evaluating individual injection facilities. Site-specific potentiometric surfaces are probably too small to identify the impact of oil production on an injection operation. County-scale maps appear appropriate. These data can be used to provide boundary conditions as well as confirm numerical models of injection.

2. Although some previous researchers have discredited the value of DST data, the pressure data from DSTs and other bottom-hole pressure measurements appear to be reliable. Good tests have been obtained from Gulf Coast Tertiary formations because of good porosity and permeability, which permit rapid pressure equilibrium within the tool. The pressure data have been invaluable for constructing potentiometric maps and, to some extent, for calculating permeability values. Other researchers attempting to describe regional or site-specific hydrology in the Texas Gulf Coast are strongly encouraged to use the pressure files, not only for research in hazardous waste disposal but also for studies related to oil and gas recovery.

3. Construction of potentiometric maps required development of arbitrary zones of investigations. Formations such as the Frio are thick and contain more than one hydrologic regime. A single integrated potentiometric surface is therefore not representative of the potential distribution at any specific depth within the Frio. For analysis of specific injection zones, a balance is needed between analyzing a thin injection zone and trying to develop a reasonable size data base. A similar problem occurs with the temporal distribution of pressure analysis; data have been collected for 50 years. It is important to use limited time intervals for construction of

potentiometric maps. Maintaining a balance between site-specific and time-specific data versus the use of large data bases to better understand a hydrologic system requires a subjective interpretation of the data and therefore a subjective interpretation of the maps. In that context, it must be remembered that these maps represent interpretations.

4. Because of the large amount of pressure data available, development of a computerized data base as well as computerized mapping proved to be the most efficient use of time and staff.

5. The Frio Formation was chosen because of the large volumes of wastes injected into the formation and because of the extensive geochemical, geologic, and pressure data bases available for interpretations. It was an excellent formation to use as a test case. Similar approaches can be developed for the other formations used for injection.

6. The geohydrologic environment of the Texas Gulf Coast saline formations is a complex interaction of the region's geology and hydrology. Pressure-depth plots indicate the presence of different pressure regimes that influence the fluid flow directions in and between the various hydrologic units. Formation fluid pressures are a good indicator of the hydrologic regime within a given formation. Thus, pressure gradients may be used as hydrologic markers for delineating different flow regimes. These pressure regimes can be classified as: shallow fresh- to moderately saline water hydropressured (<4,000 ft), intermediate depth (4,000 to 8,000 ft) brine hydrostatic, and deep overpressured. The pressure-depth profiles show that the transition to overpressured sediments is encountered at a depth shallower (around 6,500 ft) than what has been proposed by earlier researchers during drilling and geophysical logging measurements. Using the pressure gradient of 0.465 psi/ft as a marker, a new base of hydrostatic and top of geopressured section were delineated (figs. 52 and 53). As outlined in figure 53, there are areas where overpressured sediments are interspersed within the hydrostatic section.

7. Pressure/depth and potentiometric surface analyses indicate extensive depressurization in the 4,000- to 8,000-ft-depth range. This presumably results from the production of 20 billion barrels of oil and gas equivalent as well as large volumes of brine produced with the oil. If this depressurization results from oil and brine production, then the oil fields potentially become the ultimate sinks and pathways to

the biosphere for chemical wastes. Based on the available permeability data and flow gradients calculated from potentiometric surfaces, average horizontal linear flow velocity in the Frio Formation ranges from 0.01 to 105 ft/year. This reflects the flow potential toward a moderately depressurized oil field. For a better estimate of flow potential between an injection zone and an oil field, additional pressure distribution data in the injection sites are required. This process may be enhanced by the typical high permeability (greater than 1 darcy) of Gulf Coast sands. Conversely, flow may be impeded by geologic barriers such as growth faults. The use of pressure data in conjunction with structure and geology is the most appropriate technique for a complete hydrogeologic characterization. Detailed geologic investigations were not conducted for this study. They are needed, however, for a complete characterization of an injection site. Oil field depressurization may be a transient process. When the fields are depleted and production stops, reservoir pressures should return to higher values. The time or percentage of recovery, however, is unknown. It is important to bear in mind that the current study is based mainly on formation pressures from the oil- and gas-producing areas and is thus biased toward describing the complexity of those systems.

Because of this depressurization, a potentiometric surface cannot be constructed to determine natural gradients or natural points of discharge. Present hydrologic conditions do not mimic natural conditions. Conversely, hydrochemical tracers (such as high-Br waters) and mineralogical indicators (such as lead-zinc mineralization along salt dome flanks) do not represent current hydrologic conditions but represent preproduction, natural flow patterns.

9. Upward migration of water in hydrostatic section is currently limited by depressurization, density differences between shallow fresh water aquifers and the deeper saline aquifers and the interlayered low-permeability shales. The densities of the injected wastes and formation waters should be used in comparing the potential for vertical migration. Environmental heads maps rather than fresh-water head equivalent maps provide a more accurate picture of vertical flow potential. Using environmental head maps further decreases the potential for upward migration of brine into shallower fresh waters. Potentiometric surfaces that are above land surface using fresh water head equivalent may correct to a below-land-surface elevation when density is taken into consideration. However, density measurements rarely are included with pressure data for a well. Regional interpretation of salinity, and therefore density, can be estimated with the county salinity depth profiles shown in the appendix.

10. Hydrochemical data from the Frio suggest that a slow-moving, sluggish hydrologic environment existed under natural conditions. The Frio is not being actively recharged in geologic time by continental meteoric waters, as the Wilcox appears to be. Frio waters are considered to be older than can be dated by ^{14}C methods. Brines from the deeper geopressured section may be leaking into the hydrostatic section of the central and southern Frio. Vertical leakage does not appear to be occurring in the northern region. In this northern region the chemical composition of the brines is strongly influenced by salt dome dissolution. This leakage presumably extends only to the shallow saline hydrostatic section and not into the fresh ground water. The Gulf of Mexico sedimentary basin typically has been referred to as a compacting basin (Galloway and Hobday, 1983). This term "compacting" has been misapplied because it implies that waters from both the hydrostatic and geopressured section are migrating up faults or up structural dip to the outcrop. The only part in the Gulf of Mexico sedimentary basin out of compaction equilibrium (and therefore capable of fluid flow because of compaction) is the geopressured section. As the geopressured section compacts, fluids migrate to the brine hydrostatic section either by porous media flow or along faults. The only pathways through which compactional waters can reach land surface or the fresh-water section and bypass the brine hydrostatic section is up structural discontinuities such as faults and flanks of salt domes. Waters from the brine hydrostatic section are not expected to be currently flowing into the fresh-water sections because these brines appear from geochemical data to be relatively stagnant and from hydrologic data to be either depressurized or at hydrostatic pressures (i.e., no potential for upward migration) as well as being denser than the shallower fresh waters.

11. The presence of degraded hydrocarbons and the absence of organic acids suggest that bacteria may be degrading organic compounds as deep as 7,000 ft. Most injection zones should be in this potentially biologically active zone. If biodegradation of oils has occurred, it probably took place at rates significantly faster than abiotic reactions such as hydrolysis. Though these bacteria may not be capable of degrading other organic compounds, such as injected wastes, their presence does suggest that these shallow saline zones are in suitable biologic environments that might support the bacteria capable of degrading wastes. Hydrocarbon degradation may have occurred only in the past and may not be ongoing. The presence of bacteria in these zones needs to be documented.

12. FUTURE RESEARCH DIRECTIONS

This study has raised some important issues that need to be addressed to ensure safe disposal of hazardous chemical wastes. These issues are also relevant to the oil and gas industry.

12.1 Better Understanding of Depressurization

A more detailed study of the extent and effects of underpressuring is needed to determine the ultimate fate of the injected chemical wastes. The severe pressure depletion has altered the hydrologic equilibrium in the subsurface. Depressurization has enhanced the potential for migration of injected fluids toward oil fields. In a depleted field, high-permeability sediments may accentuate flow velocities. Other issues linked to depressurization are: land subsidence in oil fields, possible activation of faults, and efficiency of primary and secondary hydrocarbon recovery operations. For example, is it possible to reenter an old depleted oil field and conduct enhanced recovery operations, or does the extreme depressurization alter the fluid dynamics to such an extent that such operations become infeasible?

During mapping of potentiometric surfaces it was observed that not all the cones of depression circled by negative contours centered on oil and gas fields. Thus, in addition to hydrocarbon production, there may be other factors contributing to depressurization. Severe depressurization may also lead to stress alteration in the rocks. These factors require further investigation.

The Wilcox and Miocene formations do not seem to be as severely affected by depressurization as the Frio. This may be due to less hydrocarbon production from these formations. Determinations of the areal extent of depressurization and of the rates of pressure equilibration and pressure recovery due to fluid injection require integration of transient pressure data with static pressure information. The limitation of working with static pressures alone is that localized and temporal effects may become significant. Efforts need to be directed toward acquisition of transient pressure data from oil and gas fields for assessment of the effects of depressurization. The effects of extensive reinjection of brine also need to be investigated in the context of pressure equilibration.

12.2 Research in Overpressure Formation Mechanisms

The top of geopressured sediments, as observed from the pressure-depth profiles and potentiometric surfaces, is shallower than was previously recognized. Similarities between the character of the pressure-depth profiles in the Frio, Wilcox, and Miocene

indicate similar processes controlling the formation of overpressuring in all these sediments.

At this point the following questions still need to be answered:

1. Why does overpressuring start at approximately 6,000 ft in depth?
2. Why does the maximum gradient lie close to 0.9 psi/ft line (fig. 101)? Is this related to a formation fracture gradient? How does it correlate to the lithostatic gradient of 1.0 psi/ft?
3. What light can overpressuring shed on the processes of sediment compaction?
4. What path do the sediments traverse during burial? Do they follow the 0.465 trend line and then move into the overpressured zone, or first into the overpressured zone and then along a curved overpressured trend?
5. What role does the extensive faulting of Gulf Coast sediments play in the formation of overpressures? Do the faults impede compaction and diagenesis, or do they act as conduits for migration of overpressured brines to the shallower regions?
6. How does the process of equilibration of overpressures take place? Is the shallow occurrence of overpressuring a result of continued compaction, or is it due to the release of deep pressured brines that have not yet equilibrated to the lithostatic load?

The understanding of overpressuring phenomenon is also linked to the exploitation of energy resources and involves the synthesis of hydrologic data with geologic and geochemical information.

12.3 Potential for Biodegradation

The possibility of biodegradation as an important mechanism for waste degradation needs to be investigated. Organic wastes represent the largest type of waste injected in the Gulf Coast saline formations. If biodegradation is occurring or could occur, then reaction rates may be significantly faster than if degradation is dependent on abiotic reactions.

Investigating the potential for biodegradation may be a multistage program. Initially subsurface brines in this potentially biologically active zone should be tested for the presence of bacteria and other indicators of biologic activity. Secondly, an injection well needs to be tested to determine whether there are bacterial populations associated with the injection process. Bacterial populations for both studies need to be sampled so that types and population densities can be determined. Thirdly, laboratory experiments need to be designed to evaluate this potential for deep subsurface biodegradation, its potential for degrading organic wastes, and possible enhancement of the process.

indicate similar processes controlling the formation of overpressuring in all these sediments.

At this point the following questions still need to be answered:

1. Why does overpressuring start at approximately 6,000 ft in depth?
2. Why does the maximum gradient lie close to 0.9 psi/ft line (fig. 101)? Is this related to a formation fracture gradient? How does it correlate to the lithostatic gradient of 1.0 psi/ft?
3. What light can overpressuring shed on the processes of sediment compaction?
4. What path do the sediments traverse during burial? Do they follow the 0.465 trend line and then move into the overpressured zone, or first into the overpressured zone and then along a curved overpressured trend?
5. What role does the extensive faulting of Gulf Coast sediments play in the formation of overpressures? Do the faults impede compaction and diagenesis, or do they act as conduits for migration of overpressured brines to the shallower regions?
6. How does the process of equilibration of overpressures take place? Is the shallow occurrence of overpressuring a result of continued compaction, or is it due to the release of deep pressured brines that have not yet equilibrated to the lithostatic load?

The understanding of overpressuring phenomenon is also linked to the exploitation of energy resources and involves the synthesis of hydrologic data with geologic and geochemical information.

12.3 Potential for Biodegradation

The possibility of biodegradation as an important mechanism for waste degradation needs to be investigated. Organic wastes represent the largest type of waste injected in the Gulf Coast saline formations. If biodegradation is occurring or could occur, then reaction rates may be significantly faster than if degradation is dependent on abiotic reactions.

Investigating the potential for biodegradation may be a multistage program. Initially subsurface brines in this potentially biologically active zone should be tested for the presence of bacteria and other indicators of biologic activity. Secondly, an injection well needs to be tested to determine whether there are bacterial populations associated with the injection process. Bacterial populations for both studies need to be sampled so that types and population densities can be determined. Thirdly, laboratory experiments need to be designed to evaluate this potential for deep subsurface biodegradation, its potential for degrading organic wastes, and possible enhancement of the process.

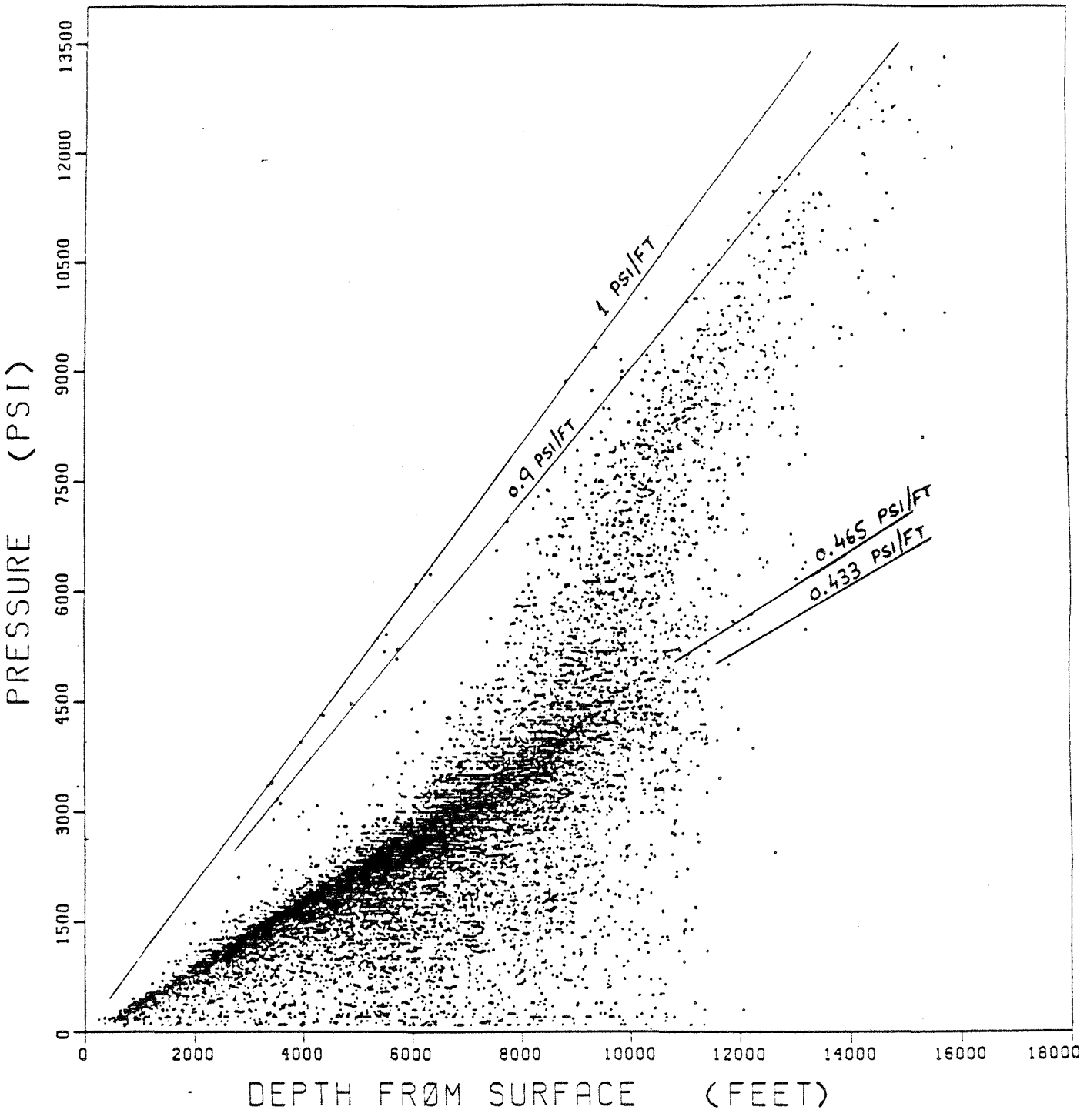

Figure 101. Pressure-depth diagram for Frio regions A-B-C data with overburden pressure line 1 psi/ft, and possible fracture gradient 0.9 psi/ft.

The presence of biodegradation within the Wilcox Formation should also be investigated. Low-TDS ground water appears to extend significantly deeper in the Wilcox than in the Frio. The effects of biodegradation, therefore, may also extend significantly deeper.

12.4 Thermal Regimes

A complete characterization of the Gulf Coast Tertiary formations is viable only when the thermal component of fluid properties is also integrated with the hydrologic description. A significant amount of temperature data was retrieved from the PI data base and was plotted as the temperature-depth profile of the Frio in region C (fig. 102). An in-depth screening and evaluation of these data is needed because it may provide new insight into the thermal gradients and their influence on the mechanism of overpressure formation. The thermal environment may play a critical role in the chemical degradation of injected wastes.

12.5 Geohydrologic Computer Modeling

The synthesis of geologic, hydrologic, geochemical, and geothermal information facilitates compilation of models that can provide practical answers to questions of chemical waste injection, confinement, migration, and degradation within the Gulf Coast injection zones. These answers need to be corroborated by the development of analytical processes and mathematical computer models. Efforts are underway at the Bureau of Economic Geology, Austin, to develop analytical capabilities and to test certain geochemical simulators that can be incorporated in the modeling process. A program is in place to compile a comprehensive data base of formation fluid and injected fluid chemistry. Subsequently, research will continue in parameter estimation to describe the chemical degradation reactions. These need to be integrated with laboratory and field studies.

12.6 Other Gulf Coast Formations Used for Injection

The hydrology of other Texas Gulf Coast formations used for deep-well injection of chemical wastes should be investigated with the approaches developed in this report. Data are available, as is evident in the pressure-depth profiles of the Wilcox and undifferentiated Miocene strata (figs. 57 and 58).

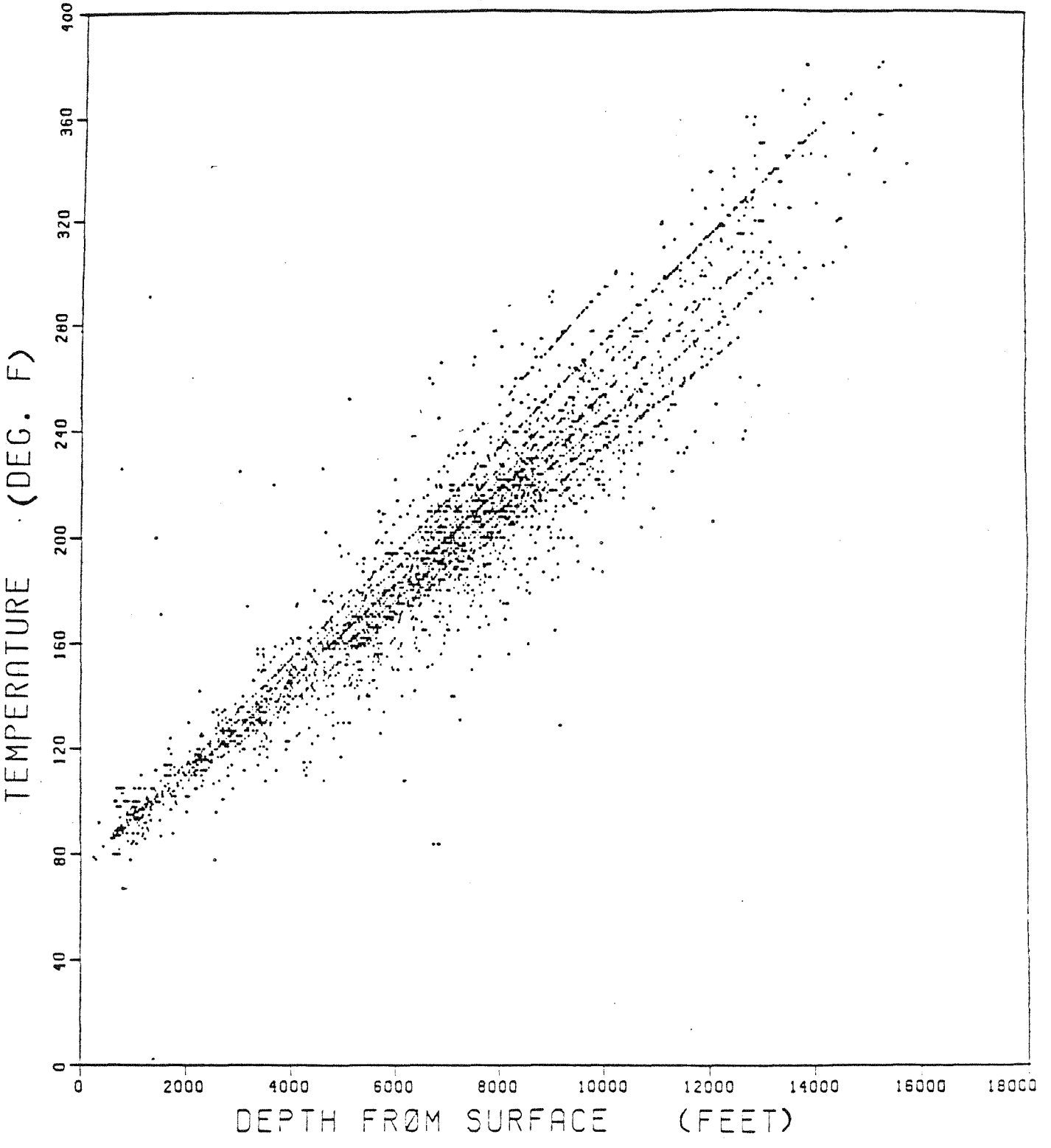

Figure 102. Temperature-depth profile for Frio Formation, region C. Data reliability has not been confirmed.

13 ACKNOWLEDGMENTS

Funding for this research was provided by the U.S. Environmental Protection Agency under Cooperative Agreement ID No. CR812786-01-0. The support provided by Jerry Thornhill, Project Officer, U.S. Environmental Protection Agency (Robert S. Kerr Environmental Research Laboratory, Ada, Oklahoma), was greatly appreciated. Numerous oil field operators willingly provided access to oil wells for water chemistry sampling. Zvi Sofer of the Mineral Studies Laboratory, Bureau of Economic Geology, performed the isotopic and organic carbon analyses. Steve Tweedy of the Bureau's Mineral Studies Laboratory provided the chemical analyses. Merill Robinson-Lewis of ARCO Services Laboratory conducted the gas chromatographic analyses. Regina Capuano provide valuable comments during the final writing of this report. Maria Saenz drafted the illustrations, under the direction of Richard L. Dillon.

14. REFERENCES

Bachman, A. L., 1979, Subsurface Disposal of Geopressured Fluids: Potential Geologic and Operational Problems with Recommendations for Disposal System Testing, in Dorfman, M. H., and Fisher, W. L., Proceedings, 4th U.S. Gulf Coast Geopressured-Geothermal Energy Conference; Research and Development: The University of Texas at Austin, Center for Energy Studies, v. 2, p. 972-999.

Bailey, N. J. L., Krouse, H. R., Evans, C. R., and Rogers, M. A., 1973a, Alteration of Crude Oil by Waters and Bacteria - Evidence from Geochemical and Isotope Studies: American Association of Petroleum Geologists Bulletin, v. 57(7), p. 1276-1290.

Bailey, N. J. L., Jobson, A. M., and Rogers, M. A., 1973b, Bacterial Degradation of Crude Oil: Comparison of Field and Experimental Data: Chemical Geology, v. 11, p. 203-221.

Baker, E. T., Jr., 1979, Stratigraphic and Hydrogeologic Framework of Part of the Coastal Plain of Texas: Texas Department of Water Resources, Austin, Texas, Report no. 236.

Bebout, D. G., Loucks, R. G., and Gregory, A. R., 1978, Frio Sandstone Reservoirs in the Deep Subsurface along the Texas Gulf Coast: The University of Texas at Austin, Bureau of Economic Geology Report of Investigations No. 91, 92 p.

Bentley, H. W., Phillips, F. M., and Davis, S. N., 1986, ^{36}Cl in the Terrestrial Environment, in Handbook of Environmental Isotope Chemistry (Fritz, P., and Fontes, J. C., eds.), v. 2, p. 427-480.

Boles, J. S., Crerar, D. A., Grissom, G., and Key, T. C., 1988, Aqueous Thermal Degradation of Gallic Acid: Geochimica et Cosmochimica Acta, v. 52, p. 341-344.

Bond, D. C., 1972, Hydrodynamics in Deep Aquifers of the Illinois Basin: Illinois State Geological Survey, Circular 470, p. 51.

Bradley, J. S., 1975, Abnormal Formation Pressure: American Association of Petroleum Geologists Bulletin, v. 59, no. 6, p. 957-973.

Carothers, W. W., and Kharaka, Y. K., 1978, Aliphatic Acid Anions in Oil-field Waters--Implications for Origin of Natural Gas: American Association of Petroleum Geologists Bulletin, v. 62, no. 12, p. 2441-2453.

_____ 1980, Stable Carbon Isotopes of HCO_3 in Oil-Field Waters - Implications for the Origin of CO_2: Geochimica et Cosmochimica Acta, v. 44, p. 323-332.

Carpenter, A. B., 1978, Origins and Chemical Evolution of Brines in Sedimentary Basins: Oklahoma Geological Survey Circular 79, p. 60-77.

Carpenter, R., 1987, The Road to Recovery: Texas Engineering Experimental Station Windows, v. 6, no. 3, p. 3-5.

Clayton, R. N., Friedman, I., Graf, D. L., Mayeda, T. K., Meents, M. F., and Shrimp, N. F., 1966, The Origin of Saline Formation Waters - 1. Isotopic Composition: Journal of Geophysical Research, v. 77(16), p. 3869-3882.

Craig, H., 1961, Isotopic Variations in Meteoric Waters: Science, v. 133, p. 1702-1703.

Dickey, P. A., Shriram, C. R., and Paine, W. R., 1968, Abnormal Pressures in Deep Wells of Southwestern Louisiana: Science, v. 160, no. 3828, p. 609-615.

Dodge, M. M., and Posey, J. S., 1981, Structural Cross Sections, Tertiary Formations, Texas Gulf Coast: The University of Texas at Austin, Bureau of Economic Geology Cross Sections, 6-p. text, 23 cross sections.

Drez, P. E., 1988, Rock-Water Interaction between Injected Waste and Host Formations and Mineralogy during Deep Well Injection (abs.): EOS, v. 69, no. 16, p. 350.

DuBar, J. R., 1982, unpublished, Structure Map, Top of Undifferentiated Miocene Formation: The University of Texas at Austin, Bureau of Economic Geology Open-File Report.

Earlougher, R. C., 1977, Advances in Well Test Analysis: Society of Petroleum Engineers of American Institute of Mining and Metallurgical Engineers, Monograph Volume 5, p. 93-94.

Epstein, E. V., and Savin, S. M., 1973, Oxygen Isotope Geothermometry of the Burial Metamorphic Rocks of the Precambrian Belt Supergroup, Glacier National Park, Montana: Geological Society of America Bulletin, v. 84, p. 2549-2560.

Fabryka-Martin, J., Bentley, H., Elmore, D., and Airey, P. L., 1985, Natural Iodine-129 as an Environmental Tracer: Geochimica et Cosmochimica Acta, v. 49, p. 337-347.

Federal Register, August 27, 1987: Environmental Protection Agency, Proposed Rule, Part III, v. 52, no. 166.

Feige, Y., Oltman, B. G., and Kastner, J. M., 1968, Production of Neutrons in Soils due to Natural Radioactivity: Journal of Geophysical Research, v. 37, p. 3135-3142.

Fisher, J. B., 1987, Distribution and Occurrence of Aliphatic Acid Anions in Deep Subsurface Waters: Geochimica et Cosmochimica Acta, v. 51, p. 2459-2468.

Fisher, R. S., 1982, Diagenetic History of Eocene Wilcox Sandstones and Associated Formation Waters, South-Central Texas: The University of Texas at Austin, Ph.D. dissertation, 185 p.

Fisher, R. S., and Kreitler, C. W., 1987, Origin and Evolution of Deep-Basin Brines, Palo Duro Basin, Texas: The University of Texas at Austin, Bureau of Economic Geology Report of Investigations No. 166, 33 p.

Frank, J. C., 1986, Injection Zone Pressure Profile at E. I. Du Pont de Nemours and Company, Victoria Site, Texas, in Proceedings of the International Symposium on Subsurface Injection of Liquid Wastes, New Orleans, p. 509-519.

Fritz, P., and Fontes, J. C., 1980, Handbook of Environmental Isotope Geochemistry: Elsevier, Amsterdam, 545 p.

Galloway, W. E., 1982, Epigenetic Zonation and Fluid Flow History of Uranium-bearing Fluvial Aquifer Systems, South Texas Uranium Province: The University of Texas at Austin, Bureau of Economic Geology Report of Investigations No. 119, 31 p.

Galloway, W. E., Hobday, D. K., and Magara, K., 1982, Frio Formation of the Texas Gulf Coast Basin--depositional systems, structural framework, and hydrocarbon origin, migration, distribution, and exploration potential: The University of Texas at Austin, Bureau of Economic Geology Report of Investigations No. 122, 78 p.

Galloway, W. E., and Hobday, D. K., 1983, Terrigenous Clastic Depositional Systems: Applications to Petroleum, Coal, and Uranium Exploration: Springer-Verlag, New York, 423 p.

Hanor, J. S., and Bailey, J. E., 1983, Use of Hydraulic Head and Hydraulic Gradient to Characterize Geopressured Sediments and the Direction of Fluid Migration in the Louisiana Gulf Coast: Gulf Coast Association of Geological Societies Transactions, v. 33, p. 115-122.

Hantush, M. S., and Jacob, C. E., 1954, Plain Potential Flow of Groundwater with Linear Leakage: EOS Transactions of the American Geophysical Union, v. 35, p. 917-936.

Hubbert, M. K., 1957, Darcy's Law and the Field Equations of the Flow of Underground Fluids: Bulletin of the International Association of Scientific Hydrology, no. 5, p. 24-59.

Jessen, F. W., and Rolshausen, F. W., 1944, Waters from the Frio Formation, Texas Gulf Coast: American Institute of Mining and Metallurgical Engineers Transactions, v. 7, no. 3, p. 1-16.

Jones, P. H., 1968, Hydrology of Neogene Deposits in the Northern Gulf of Mexico: U.S. Geological Survey Open-File Report, 132 p.

Jones, P. H., 1975, Geothermal and Hydrocarbon Regimes, Northern Gulf of Mexico Basin, in Dorfman, M. H., and Deller, R. W., eds., Proceedings, First Geopressured Geothermal Energy Conference, Center for Energy Studies, The University of Texas at Austin, p. 42-44.

Knape, B. K., 1984, Underground Injection Operations in Texas - a classification and assessment of underground injection activities: Texas Department of Water Resources Report 291, 207 p.

Kreitler, C. W., 1979, Ground-Water Hydrology of Depositional Systems, in Galloway, W. E., and others, Depositional and Ground-Water Flow Systems in the Exploration for Uranium: A Research Colloquium: The University of Texas at Austin, Bureau of Economic Geology, p. 118-176.

Kreitler, C. W., 1986, Hydrogeology of Sedimentary Basins as it Relates to Deep-Well Injection of Chemical Wastes: preprint of paper presented at the International Symposium on Subsurface Injection of Liquid Wastes, New Orleans, March 3-5, 27 p.

Kreitler, C. W., and Richter, B. C., 1986, Hydrochemical Characterization of Saline Aquifers of the Texas Gulf Coast Used for the Disposal of Industrial Waste: The University of Texas at Austin, Bureau of Economic Geology, contract report to the U.S. Environmental Protection Agency, Contract No. R-812785-01-0, 164 p.

Kreitler, C. W., and Seni, S. J., 1983, Origin and Evolution of Na-Cl to Na-Ca-Cl Brines, East Texas Basin (abs.): Geological Society of America, v. 15(6), p. 618-619.

Kreitler, C. W., and Wuerch, H. V., 1981, Water Chemistry, Oakwood Salt Dome: in Kreitler, C. W., and others, Geology and Geohydrology of the East Texas Basin, A Report on the Progress of Nuclear Waste Isolation Feasibility Studies: The University of Texas at Austin, Bureau of Economic Geology Geological Circular 81-7, p. 156-161.

Kuhn, M. W., 1984, Subsurface Neutron Production and Its Impact on ^{36}Cl Ground Water Dating: The University of Arizona, Master's thesis, 45 p.

LaFargue, E., and Barker, C., 1988, Effect of Water Washing on Crude Oil Compositions: American Association of Petroleum Geologists Bulletin, v. 72, no. 3, p. 263-276.

Land, L. S., and Prezbindowski, D. R., 1981, The Origin and Evolution of Saline Formation Water, Lower Cretaceous Carbonates, South-Central Texas, U.S.A.: Journal of Hydrology, v. 54, p. 51-74.

_____ 1985, Chemical Constraints and Origins of Four Groups of Gulf Coast Reservoir Fluids: American Association of Petroleum Geologists Bulletin, v. 69, no. 1, p. 119-129.

Lewis, C. T., and Rose, S. C., 1970, A Theory Relating High Temperatures to Overpressures: Journal of Petroleum Technology, v. 22, p. 11-16.

Lundegard, P. D., 1985, Carbon Dioxide and Organic Acids: Origin and Role in Burial Diagenesis (Texas Gulf Coast Tertiary Formations): The University of Texas at Austin, Ph.D. dissertation, 145 p.

Lusczynski, N. J., 1961, Head and Flow of Ground Water of Variable Density: Journal of Geophysical Research, v. 66, no. 12, p. 4247-4256.

Magara, Kinji, 1976, Water Expulsion from Clastic Sediments during Compaction - Directions and Volumes: American Association of Petroleum Geologists Bulletin, v. 60, no. 4, p. 543-553.

Miller, C., Fisher, T. A., II, Clark, J. E., Hales, C. H., Porter, W. M., and Tilton, J. N., 1986, Flow and Containment of Injected Waste, in Proceedings, International Symposium: Subsurface Injection of Liquid Wastes, New Orleans, March 3-5, p. 520-559.

Milner, C. W. D., Rogers, M. A., and Evans, C. R., 1977, Petroleum Transformations in Reservoirs: Journal of Geochemical Exploration, v. 7, p. 101-153.

Morton, R. O., and Land, L. S., 1987, Regional Variations in Formation Water Chemistry, Frio Formation (Oligocene), Texas Gulf Coast: American Association of Petroleum Geologists Bulletin, v. 71(2), p. 191-206.

O'Neil, J. R., and Kharaka, Y. K., 1976, Hydrogen and Oxygen Isotope Exchange between Clay Minerals and Water: Geochimica et Cosmochimica Acta, v. 40, p. 241-246.

Pearson, F. J., and White, D. E., 1967, Carbon 14 Ages and Flow Rates of Water in Carrizo Sand, Atascosa County, Texas: Water Resources Research, v. 3, 251 p.

Pearson, F. J., Jr., Fisher, D. W., and Plummer, L. N., 1978, Correction of Ground-Water Chemistry and Carbon Isotopic Composition for Effects of CO_2 Outgassing: Geochimica et Cosmochimica Acta, v. 42, p. 1799-1807.

Powers, M. C., 1967, Fluid Release Mechanisms in Compacting Marine Mudrocks and their Importance in Oil Exploration: American Association of Petroleum Geologists Bulletin, v. 51, no. 7, p. 1240-1254.

Railroad Commission of Texas, 1978, A Survey of Secondary and Enhanced Recovery Operations in Texas to 1976: Railroad Commission of Texas, Oil and Gas Division Bulletin 76, 487 p.

Richter, B. C., and Kreitler, C. W., 1986, Geochemistry of Salt-Spring and Shallow Subsurface Brines in the Rolling Plains of Texas and Southwestern Oklahoma: The University of Texas at Austin, Bureau of Economic Geology Report of Investigations No. 155, 47 p.

Scrivner, N. C., Bennett, K. E., Pease, R. A., Kopatsis, A., Sanders, S. J., Clark, D. M., and Rafal, M., 1986, Chemical Fate of Injected Waste, in Proceedings, International Symposium on Subsurface Injection of Liquid Wastes: New Orleans, p. 560-609.

Standard Methods for the Examination of Water and Wastewater, 1975, 14th ed., American Public Health Association - American Waterworks Association - Water Pollution Control Federation, p. 527-529.

Texas Water Commission, Austin, Texas, 1987, Annual Injection Data Book.

Toth, J., 1978, Gravity-Induced Cross-Formational Flow of Formation Fluids, Red Earth Region, Alberta, Canada - Analysis, Patterns, and Evolution: Water Resources Research, v. 14, no. 5, p. 805-843.

Tyler, N., Light, M. P. R., and Ewing, T. E., 1985, Saline Fluid Flow and Hydrocarbon Migration and Maturation as Related to Geopressure, Frio Formation, Brazoria County, Texas, in Dorfman, M. H., and Morton, R. A., eds., Proceedings, Sixth Geopressured Geothermal Energy Conference, Center for Energy Studies, The University of Texas at Austin, p. 83-92.

Ulrich, M. R., Kyle, J. R., and Price, P. E., 1984, Metallic Sulfide Deposits of the Winnfield Salt Dome, Louisiana: Evidence for Episodic Introduction of Metalliferous Brines During Cap Rock Formation: Gulf Coast Association of Geological Societies Transactions, v. 34, p. 435-442.

Whittemore, D. O., Basel, C. L., Galle, O. K., and Waugh, T. C., 1981, Geochemical Identification of Saltwater Sources in the Smoky Hill River Valley, McPherson, Saline, and Dickinson Counties, Kansas: Kansas Geological Survey Open-File Report 81-6, 78 p.

Wobber, F. L., 1986, Proceedings, Microbiology of Subsurface Environments: Second Investigators' Meeting - Savannah River Exploratory Probe, September 23, 1986, 24 p.

Wood, L. A., Gabrysch, R. K., and Marvin, R., 1963, Reconnaissance Investigation of the Ground-Water Resources of the Gulf Coast Region, Texas: Texas Water Commission Bulletin 6305, 114 p.

Yeh, H. W., 1980, D/H Ratios and Late-Stage Dehydration of Shales during Burial: Geochimica et Cosmochimica Acta, v. 42, p. 140-143.

Young, A., Monaghan, P. H., and Schweisberger, R. T., 1977, Calculation of Ages of Hydrocarbons in Oils: Physical Chemistry Applied or Petroleum Geochemistry, Part I: American Association of Petroleum Geologists Bulletin, v. 61, p. 573-600.

Appendix. Chloride versus depth for Gulf Coast counties.

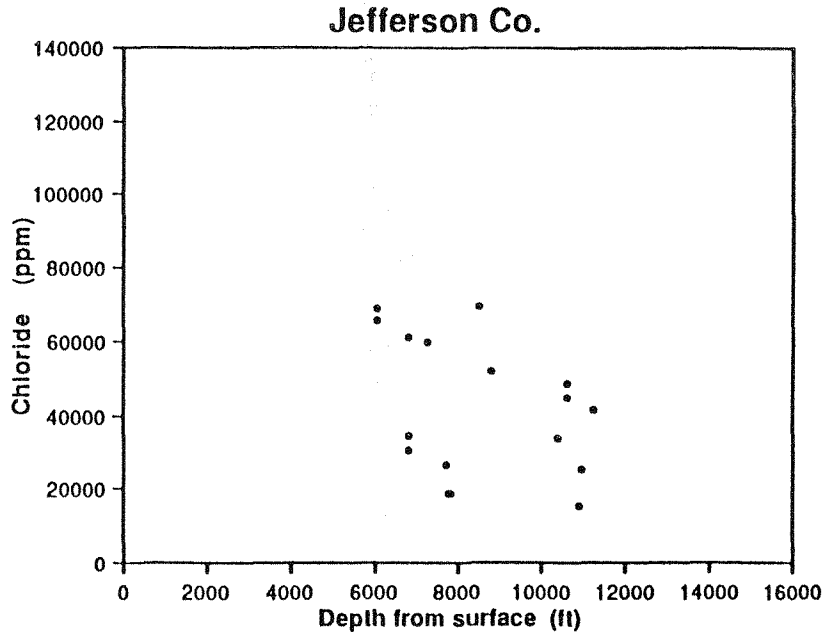

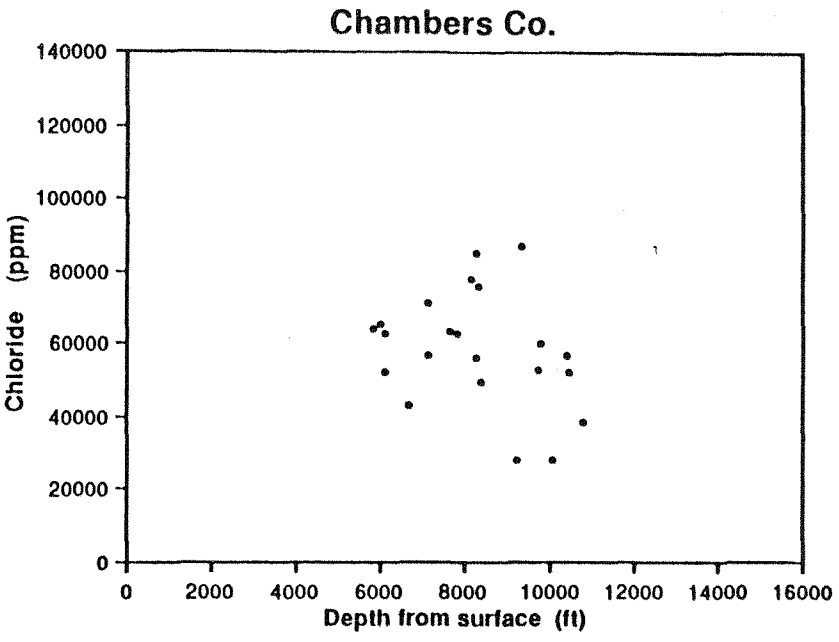

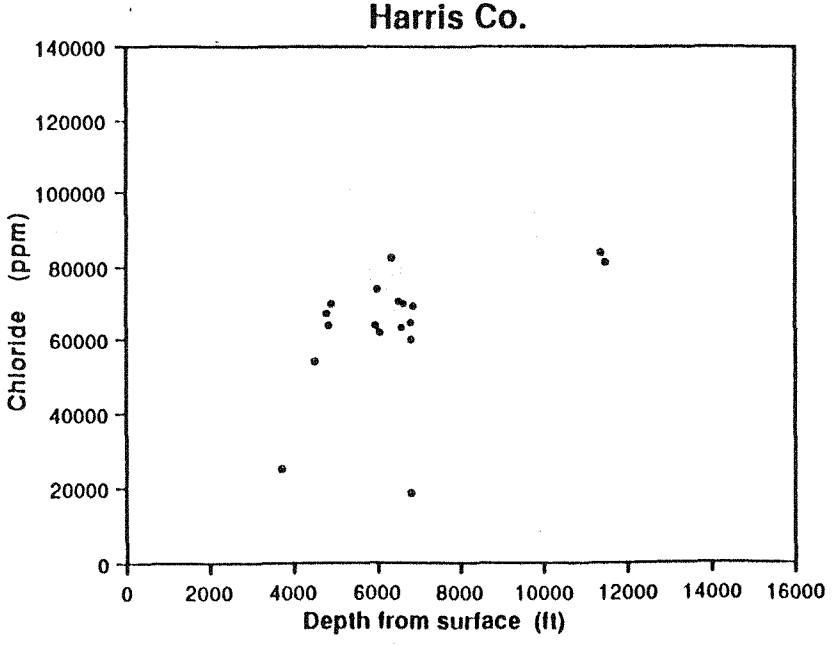

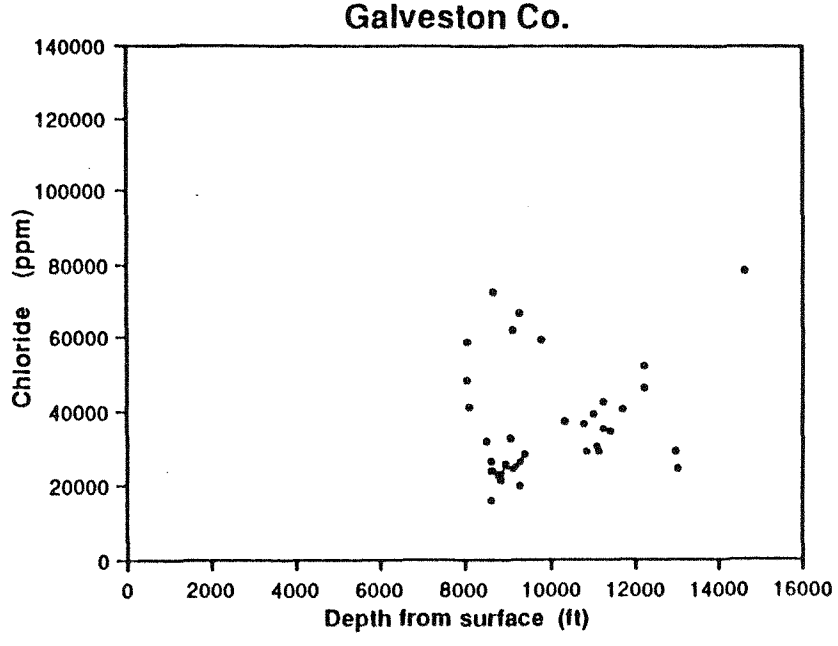

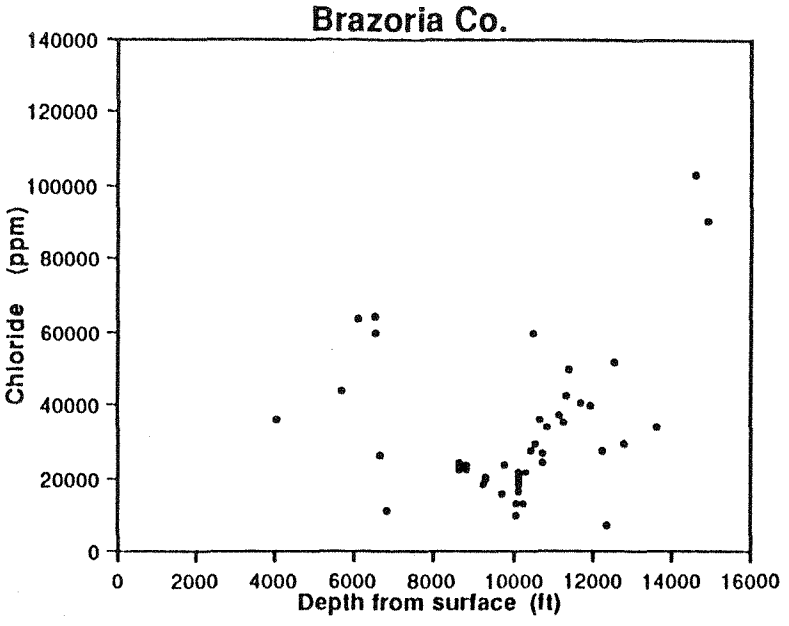
Brazoria Co.
Chloride (ppm)
140000
120000
100000
80000
60000
40000
20000
0
0 2000 4000 6000 8000 10000 12000 14000 16000
Depth from surface (ft)

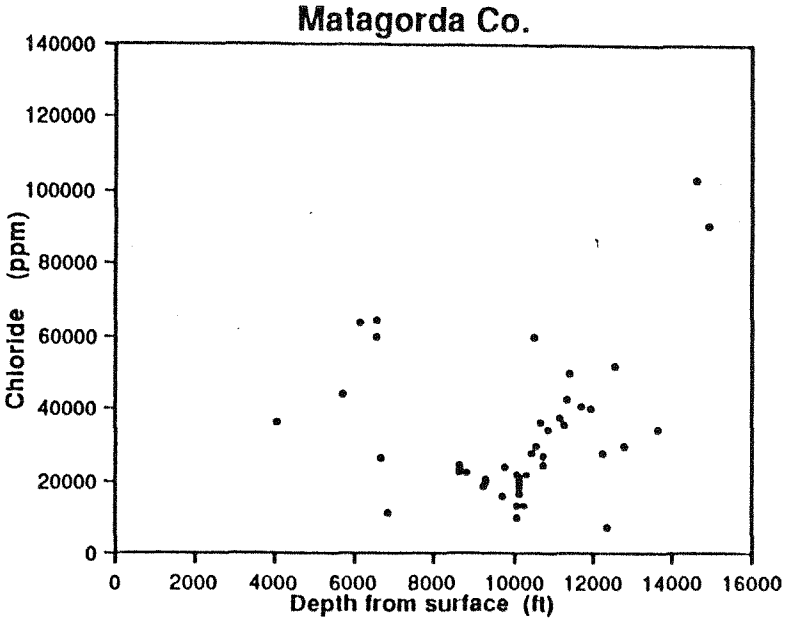
Matagorda Co.
Chloride (ppm)
140000
120000
100000
80000
60000
40000
20000
0
0 2000 4000 6000 8000 10000 12000 14000 16000
Depth from surface (ft)

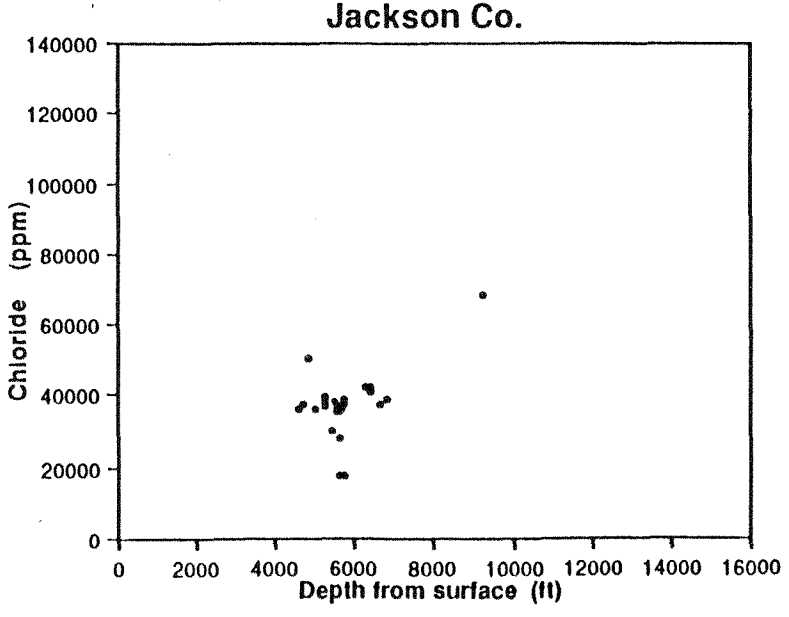
Jackson Co.
Chloride (ppm)
140000
120000
100000
80000
60000
40000
20000
0
0 2000 4000 6000 8000 10000 12000 14000 16000
Depth from surface (ft)

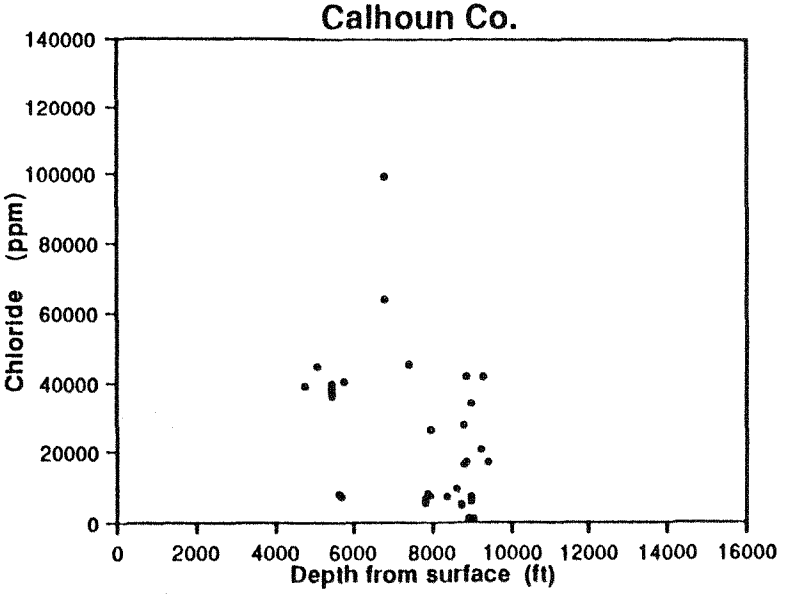
Calhoun Co.
Chloride (ppm)
140000
120000
100000
80000
60000
40000
20000
0
0 2000 4000 6000 8000 10000 12000 14000 16000
Depth from surface (ft)

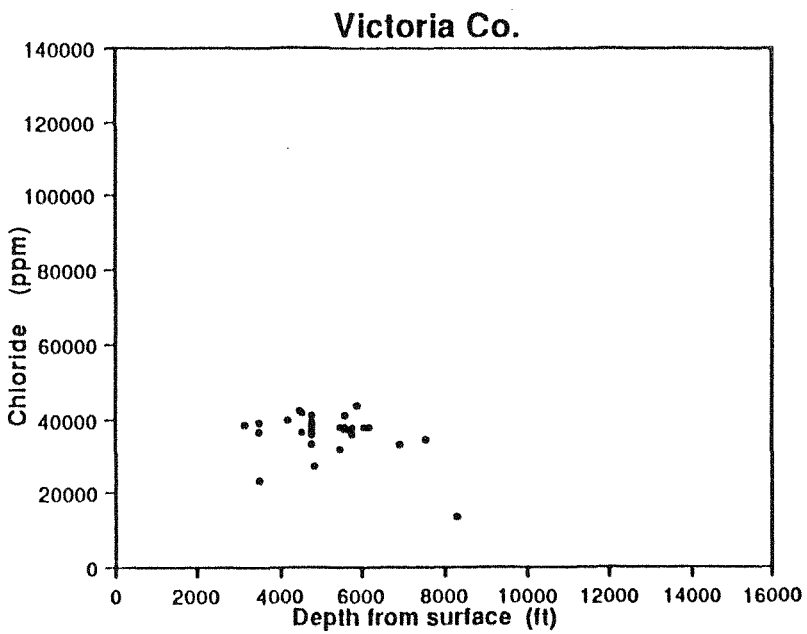
Victoria Co.
Chloride (ppm)
140000
120000
100000
80000
60000
40000
20000
0
0 2000 4000 6000 8000 10000 12000 14000 16000
Depth from surface (ft)

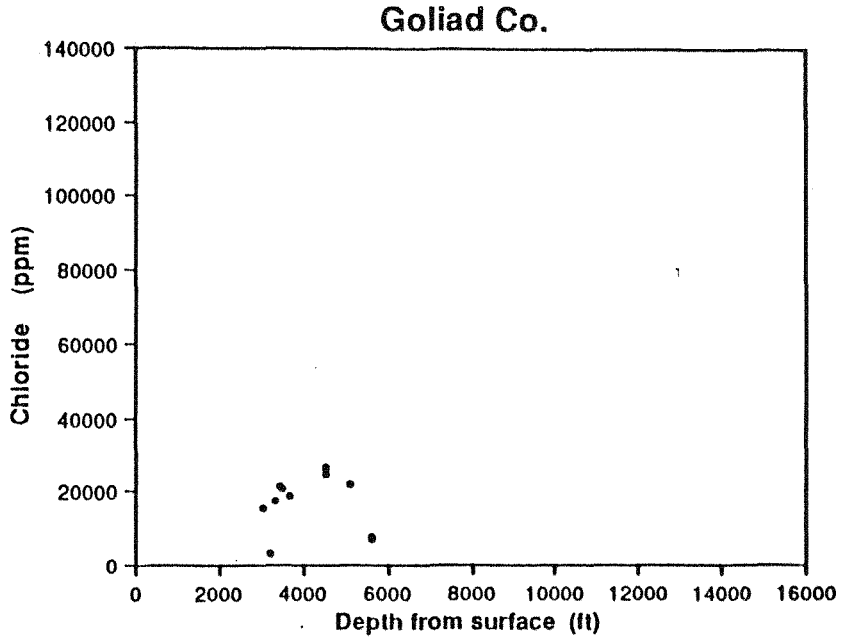
Goliad Co.
Chloride (ppm)
140000
120000
100000
80000
60000
40000
20000
0
0 2000 4000 6000 8000 10000 12000 14000 16000
Depth from surface (ft)

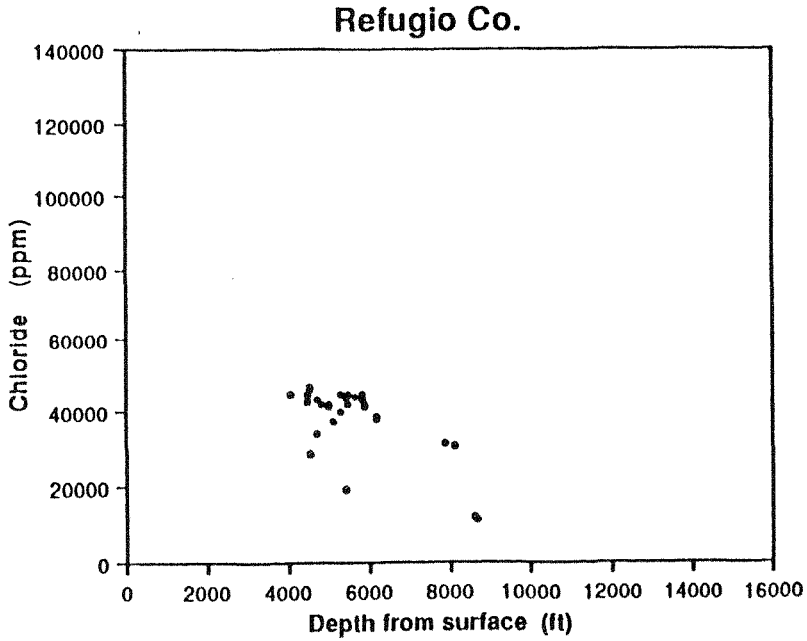
Refugio Co.
Chloride (ppm)
140000
120000
100000
80000
60000
40000
20000
0
0 2000 4000 6000 8000 10000 12000 14000 16000
Depth from surface (ft)

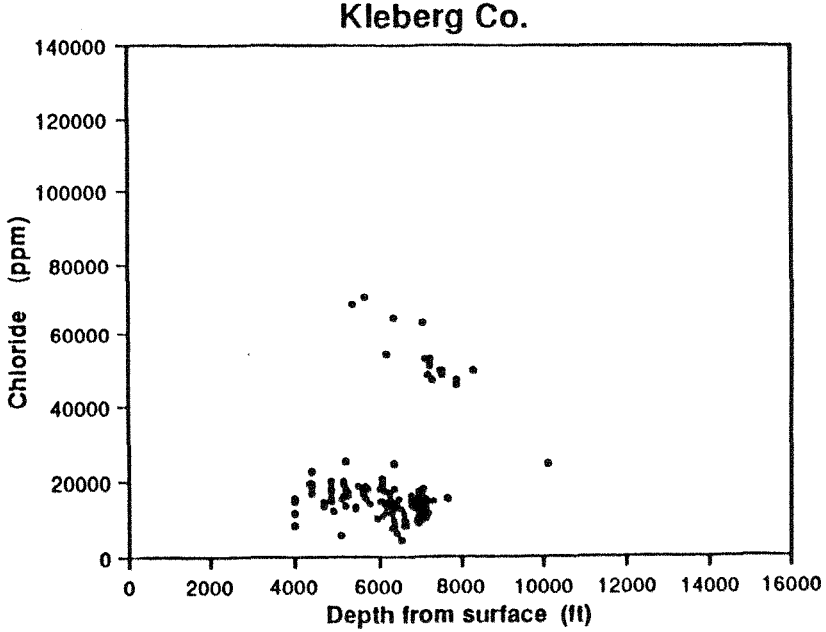
Kleberg Co.
Chloride (ppm)
140000
120000
100000
80000
60000
40000
20000
0
0 2000 4000 6000 8000 10000 12000 14000 16000
Depth from surface (ft)

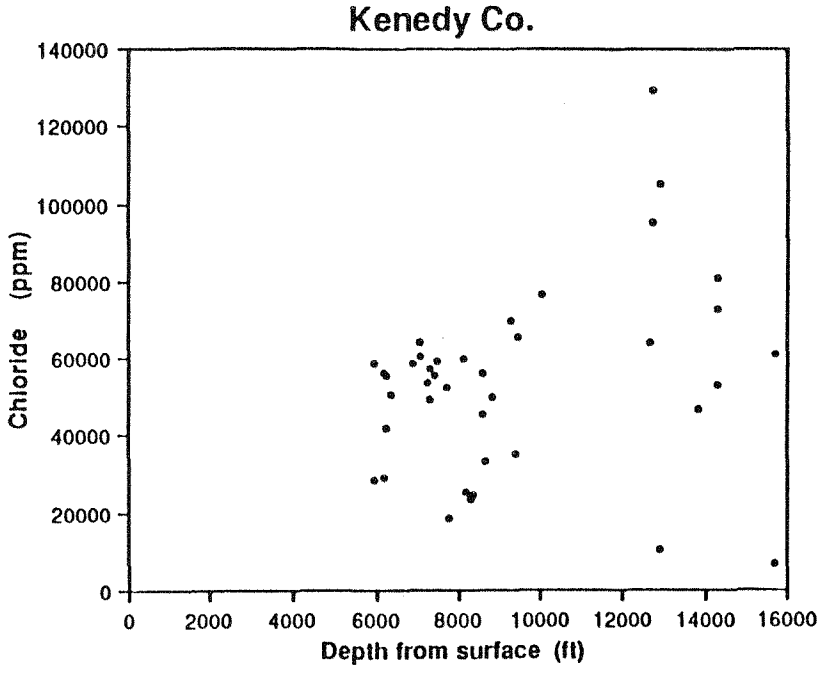
Kenedy Co.
Chloride (ppm)
140000
120000
100000
80000
60000
40000
20000
0
0 2000 4000 6000 8000 10000 12000 14000 16000
Depth from surface (ft)

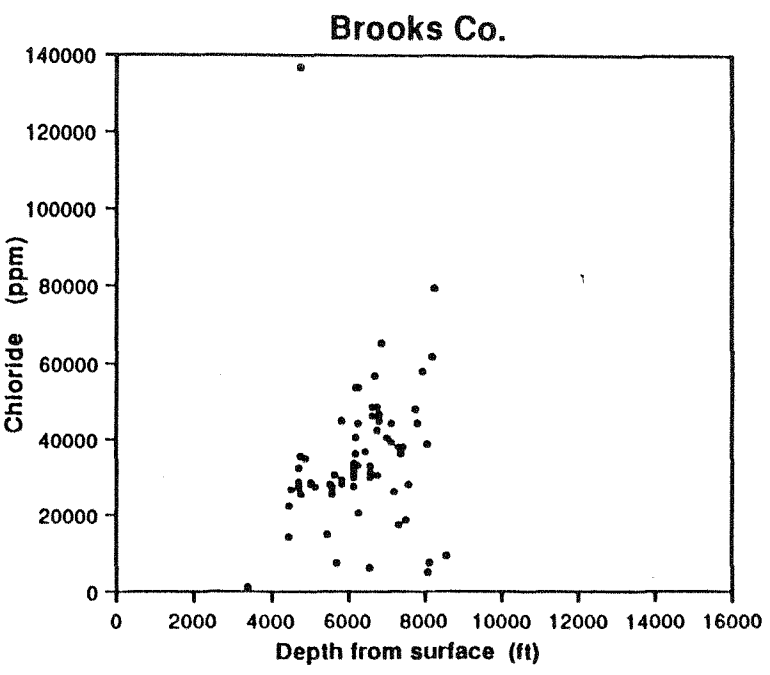
Brooks Co.
Chloride (ppm)
140000
120000
100000
80000
60000
40000
20000
0
0 2000 4000 6000 8000 10000 12000 14000 16000
Depth from surface (ft)

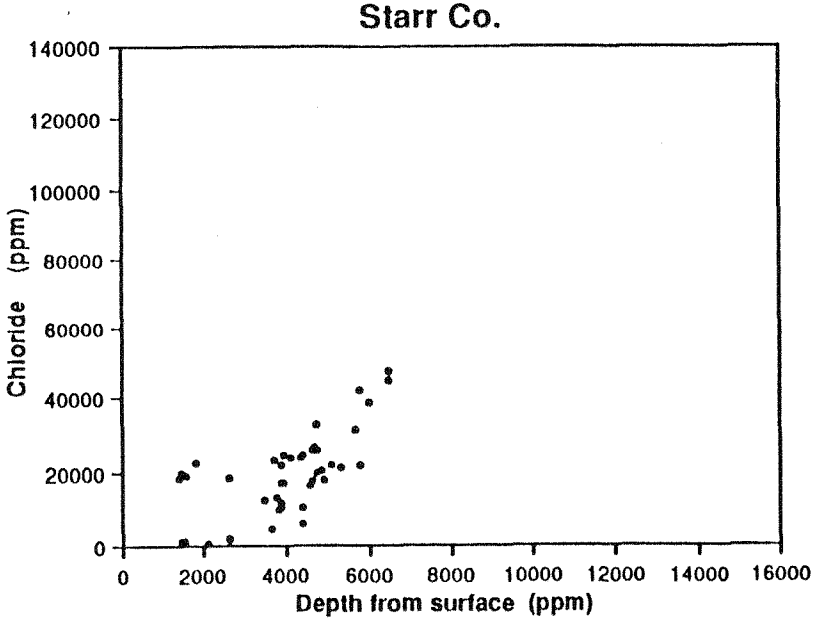
Starr Co.
Chloride (ppm)
140000
120000
100000
80000
60000
40000
20000
0
0 2000 4000 6000 8000 10000 12000 14000 16000
Depth from surface (ppm)

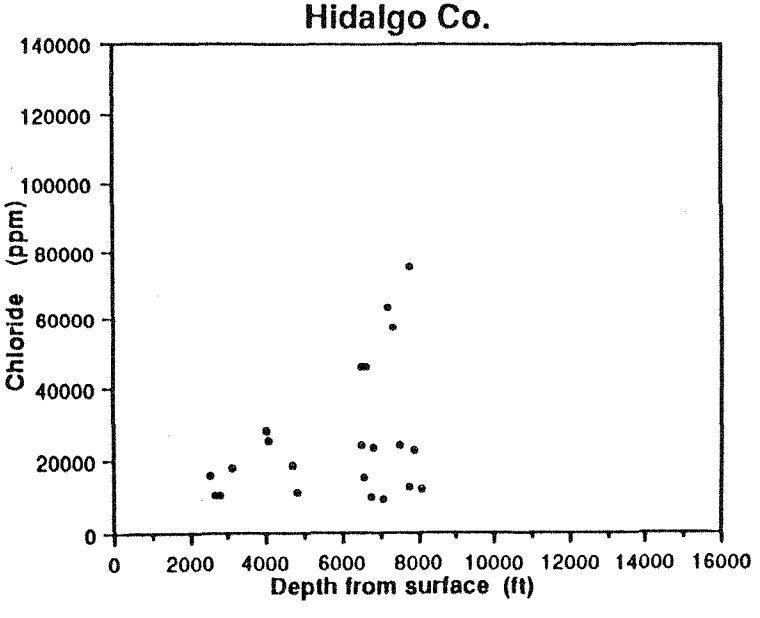
Hidalgo Co.
Chloride (ppm)
140000
120000
100000
80000
60000
40000
20000
0
0 2000 4000 6000 8000 10000 12000 14000 16000
Depth from surface (ft)